GEOLOGICAL EVOLUTION AND MAGMATIC MODELS FOR SPATIALLY AND TEMPORALLY VARIABLE MODES OF DISTRIBUTED VOLCANISM, JEJU ISLAND, REPUBLIC OF KOREA

A thesis presented in partial fulfillment of the requirements for the degree of

Doctor of Philosophy

in

Earth Science

at Massey University, Palmerston North, New Zealand.

MASSEY UNIVERSITY

Marco Brenna

2012

When the haze clears,

You see the mountain.

When you gaze at the mountain,

You see within and beyond.

Abstract

Dispersed volcanism in intraplate settings produces volcanic fields that may erupt over millions of years to produce hundreds to thousands of scoria and spatter cones, tuff cones and maars, as well as lava flows. Many aspects of this globally ubiquitous process are poorly known, ranging from the tectonic drivers to the mechanisms controlling magma accumulation and ascent. To investigate magma generation processes leading to a variety of individual eruption types at volcanic fields and to understand the spatio-temporal evolution of these whole-systems, knowledge of the geochemical and petrological properties of erupted products must be linked to the geologic and tectonic framework. This study was based on detailed stratigraphic sampling of small- (<0.01 km^3) and large-volume (>1 km^3) eruptive sequences in the Jeju Island Volcanic Field, Korea at both individual exposed eruption centres and from deep drill cores. This island is the subaerial representation of a volcanic field developed above continental crust over the last 1.8 Ma. Pyroclastic and lava samples were analysed for whole-rock major-, trace-elements and Sr-Nd-Pb isotopes, and for mineral compositions and Sr-Nd-Pb isotopes.

The Jeju magmatic system started with small-volume alkali basaltic eruptions sourced at mantle depths equivalent to c. 2.5 GPa in partially hydrous peridotite. These magmas passed through the crust and erupted rapidly, with minor modification. Intrusions and eruptions accommodated regional tectonic strain, and excess melts became stalled to fractionate toward trachyte compositions in both the lower and upper crust. Trachyte erupted sporadically, with the first episode at c. 750 ka. After this, the system started to erupt with volumetric rates two orders of magnitude higher. This accelerated magma production involved alkali basalt melts derived from greater depths/pressures (3.5 GPa) than earlier, along with subalkali basalts derived from c. 2.5 GPa. Despite prevailing extensional tectonics in the Ryukyu Volcanic Arc and strain accommodation at Jeju, further magmas accumulated and evolved to trachyte compositions at lower crustal depths and erupted in a second episode c. 25 ka ago. Small-volume eruptions of rapidly rising primitive alkali basalt also continued throughout the life of the field, and potentially interacted with shallower reservoirs of subalkali magmas to generate bimodal volcanism. Depending on magma volumes, intrusion and plumbing complexities, these generated a range from simple volcanic

structures to complex multiple-episode and/or multiple vent eruptive centres at the surface.

The geochemical data collected revealed how seemingly simple monogenetic eruptions can be fed by complex and distinct magmatic entities. The same was valid for the entire field, where magma source and evolution conditions vary over time. The variety in volcanic activity is a function of magma types influenced by prior mantle modification events, as well as local and distal tectonic stresses and strain arrangements. This study showed that it is ultimately the site and spatial pattern of melting and melt-production rate that determines the final surface morphology, elevation and spatial distribution of magma types in a volcanic field.

Acknowledgements

Many people have made valuable contributions to the completion of this work. I will endeavour to name them all, and I apologize in advance to those who will have been left out, not because I don't value their contribution, but because of the rust in my memory.

First and foremost I would like to thank wholeheartedly Shane Cronin and Ian Smith for offering me the Jeju Island project after I had unsuccessfully applied for a spot in its Auckland "younger sister" project. Their effort, as well as that of all those involved in the FRST/IIOF (Foundation for Research Science and Technology/International Investment Opportunity Fund) project provided me with an opportunity to pursue my passion for learning more about volcanic systems, and a Massey University Vice Chancellor's Doctoral Scholarship gave me a steady income.

The foundation of a sound geological investigation remains the fieldwork. I was fortunate to do this in an island where the majority of people spend their holidays. Therefore, wherever I went, I always met people with a smile on their face and a friendly word of welcome, although I couldn't understand them at the time. Even the soldier with his rifle did not consider me and my geological pick as a threat, when I suddenly stumbled out of the bush upon a military installation at the top of Dangsanbong. During the first field season I was, however, plagued by the unmovable bureaucracy of Korean car rental companies, who needed to see an international driving permit for me to get on four wheels. And I was left at the airport alone, with the prospect of doing fieldwork by bus. To be fair, however, I ought to thank the public transportation system on Jeju for its efficiency and good coverage. Eventually I did receive an international driver permit, thanks to the help of a kind receptionist at the Jeju Grand Hotel and of Dave Smith in Perth. When not alone, field work was done successfully with the logistical support and organization of several Korean colleagues. Special thanks go to Prof. Sohn (for the leadership), Mr. Kwon (for the driving), Dr. Jeon (for getting the necessary permits) and various other Korean students and academics, who enthusiastically joined me and the Massey contingent in a concerted effort to have us make the most of our Korean experience… and that's how we learnt why Korea is the "land of morning calm". Korea is also the land of delicious food, and the best is the one you taste adventurously without the guidance of the locals, and, together with Károly Németh, I will surely forever

remember the delicious, spicy, living-sea-slugs hotpot at Songaksan, or the equally peculiar though not as delicious "scraped up rice boiled in water" after a glorious black pig barbecue. And thanks go to Károly for scrambling up behind me to the summit of Mount Halla to reach the peaceful roof of Jeju, beyond the "hordes of Genghis Kahn".

After the fieldwork comes the analytical part, which, although not as adventurous is nonetheless necessary. As any good geochemist knows, sample preparation mainly consists of cleaning equipment, and all the more so at Massey, where labs are shared with uncooperative soil scientists. Precious assistance was nonetheless provided by Bob Toes, Ian Furkert, Clel Wallace and Damian Jones. Analytical work would have been impossible without the efforts of John Wilmshurst on the XRF and Ritchie Sims on the microprobe at the University of Auckland, Charlotte Allen on the LA-ICP-MS at the Australian National University in Canberra, and Ashlea Wainwright and Roland Maas in the isotope lab at the University of Melbourne.

Once the data are plotted on a chemical diagram, joining the dots and making any "real-world" sense of the images appearing on the screen was much facilitated by critical and constructive discussion with (and I'll name them in alphabetical order) Anja Möbis, Bob Stewart, Gábor Kereszturi, Gert Lube, Greg Valentine, Ian Smith, Javier Augustín-Flores, Károly Hidas, Károly Németh, Lucy McGee, Marc Bebbington, Mary Gee, Matteo Roverato, Natalia Pardo, Nicolas Le Corvec, Richard Price, Shane Cronin and Ting Wang as well as the official and unofficial reviewers of the submitted manuscripts and academics who commented on my posters at various conferences. Special thanks go to Ting Wang, who helped me to make actual mathematical sense of the data.

If one way of disseminating one's knowledge is by publishing in reputable journals, another is by attending conferences and communicating one's ideas in person. During the course of my PhD I was privileged to attend the meeting for the 250th Anniversary of the Birth of Volcán Jorullo in Morelia, Mexico in September 2009, which included the (in)famous horse ride to the feet of Paricutin, the 2009 Geological Society of South Korea annual meeting in Jeju, the 2009 Geological Society of New Zealand conference in Oamaru, and the AGU Fall Meeting 2009 (self supported) in San Francisco, where I met a particularly "gentle people", although it wasn't "summertime", and nobody had "flowers in their hair". In 2010 I attended the explosive basaltic volcanism course at Etna, Sicily organized by the AIV and the

INGV, and again the annual meeting of the Geological Society of South Korea, followed by a spectacular few days (extended by the raging waves of the East Sea hindering the ferry service) of fieldwork on Ulleung Island. 2011 was the year of the rabbit, as well as that of the IUGG General Assembly in Melbourne (self supported) and of Goldschmidt in Prague, followed by a "Central European" experience organized by Károly and his indefatigable Hungarian and Slovak friends. Finally in 2012, just before submitting this work, I attended the 4th International Maar Conference in Auckland. For all these experiences (even the self financed) I would like to thank Shane Cronin and Kate Arentsen for financial and organizational support. Finally, my thanks go to my parents, who brought me up appreciating the beauty and complexity of nature and especially of the geological world of the Swiss-Italian Alps, and later supported me in my quest for knowledge. More recently, Ting motivated and inspired me when I failed to see a higher scope in my work, and patiently supported me every other day.

I would like to dedicate this thesis to the memory of Katia and Maurice Krafft, whose effort to educate the general public on volcanic hazards fascinated me when I was a little boy, and later inspired me to pursue a career in geology and volcanology.

Table of Contents

Chapter 7:

Integration of Small- and Large-Volume Magmatic Systems 151

List of Figures

List of Tables

Chapter 1

Introduction

This chapter presents a brief review of the current understanding of distributed volcanic systems and highlights the existing knowledge gaps. It states the motivation for this study and introduces the aims and outline of the thesis.

1.1 Distributed volcanic systems

Intraplate, small-volume, distributed, monogenetic basaltic volcanism is the most widespread type of volcanic activity on Earth and occurs in all tectonic environments (Valentine & Perry, 2007). These volcanic systems are also termed continental basaltic systems (Valentine & Gregg, 2008), basaltic volcanic fields (Connor & Conway, 2000), or are grouped with continental intraplate volcanoes (Schmincke, 2004). Unlike in polygenetic calderas, stratovolcanoes or shield volcanoes, eruptions mostly occur at independent locations each time, and hence volcanic fields result in less prominent morphological features, but these are spread over a much larger area than central-vent volcanoes. The term "monogenetic" can lead to confusion as small-volume eruptions can also be associated with longer lived systems such as caldera volcanoes (Hunter, 1998), stratovolcanoes (Carn & Pyle, 2001, Dorendorf *et al.*, 2000, Schaaf *et al.*, 2005) and shield volcanoes (Porter, 1972). Similar volcanic structures can also be derived from flank (parasitic) or lateral dyke eruptions (Hunter, 1998, Nakamura, 1977).

Single eruptive centres in volcanic fields are generally active over days to a few months or years (Camp *et al.*, 1987, Kienle *et al.*, 1980, Yamamoto *et al.*, 1991). Eruptions can occur separated by intervals of several hundreds to thousands of years during a lifetime of the field of hundreds of thousands to millions of years (Connor & Conway, 2000). These timescales are longer than a human lifetime and hence memory of events is lost with subsequent generations and hazard awareness can be

low in such volcanic areas. The rarity and long intervals between events also means that few such eruptions have been observed by scientists with modern equipment. Knowledge of the eruption precursory signs is therefore poor. Generally, seismic activity related to dyke intrusion and magma ascent occurs only days to weeks before eruptive events (Camp *et al.*, 1987, Cronin & Neall, 2000, Yamamoto *et al.*, 1991, Yokoyama & de la Cruz-Reyna, 1990). Due to these characteristics, small-volume, distributed basaltic volcanic fields represent a threat to human life and infrastructure, which often exists within the confines of a field, as in the case of the cities of Auckland, New Zealand, Medinah, Saudi Arabia and Mexico City, Mexico, the city/holiday resort island of Jeju in the Republic of Korea, and other facilities such as the proposed Yucca Mountain nuclear waste repository in Nevada, USA. Moreover, where distributed eruptions are associated with polygenetic volcanoes, hazards may be perceived as originating from the centre of the main edifice and focused into valleys or rift axes radiating from the summit (e.g. Cronin *et al.*, 2004, Parra & Cepeda, 1990). Therefore occurrence of monogenetic eruptions on the flanks of larger volcanoes could pose an underestimated threat (Crisci *et al.*, 2003). Improved magmatic and genetic models are necessary for better hazard forecasting.

Due to the long-lived nature of distributed volcanism, surface vent location within a volcanic field may be controlled by the specific site(s) of mantle melting. Activity locus thus may shift over time, such as in the Springerville Volcanic Field, Arizona (Condit & Connor, 1996) possibly as a consequence of the migration of mantle melting site. In the Ojika Jima Volcanic Field, Japan, the focus of activity remained centred throughout the lifetime of the field, but eruptions expanded laterally in the first 0.5 Ma of activity, and then shrunk back to the centre during the last waning period (Sudo *et al.*, 1998). It is therefore possible that a heated path, created by successive episodes of dyke intrusion, is necessary for small-volume basaltic melts to reach the surface (Strong & Wolff, 2003). Better constraints are needed to ascertain the link between source and surface.

In addition to the source spatial control, the eruption site and morphology are ultimately influenced by near surface structures and tectonic stress fields. Volcanic vents in the Michoacán-Guanajuato Volcanic Field, Mexico, are generally aligned parallel to the relative motion vector of the subducting and overriding plates

(Hasenaka & Carmichael, 1985), whereas they appear aligned parallel to the subduction front and the associated "back arc" rift (i.e. the Taupo Volcanic Zone) in the Auckland Volcanic Field, New Zealand (Bebbington & Cronin, 2011). Interaction between more than two tectonic plates may give rise to more complex vent alignment trends, such as in the Pali Aike Volcanic Field in southern Patagonia (Mazzarini & D'Orazio, 2003). Over time, tectonic reorganization can also affect distribution of volcanism. The change in stress field due to the collision of the Izu block with Honshu (Japan) caused activity in the Higashi-Izu Volcanic Field to change from central polygenetic to distributed (Hasebe *et al.*, 2001). Clearly, plate tectonics influence the surface expression of distributed field volcanism. This link suggests that even distal tectonic events may control eruptive activity in a field.

Magma flux rates also control the interaction between magma and host-rock. Low magma supply rates and high differential stress result in independent dykes not coalescing, hence monogenetic volcanism results (Takada, 1994). Low magma flux will result in "capture" of rising magma by pre-existing crustal weaknesses such as faults and joints, hence forming alignments that are not necessarily indicative of the stress field at the time of eruption (Valentine & Gregg, 2008 and references therein). Low-flux, small-volume events are characteristic of "tectonically controlled" volcanic fields, in which magma generation, accumulation and transport are controlled by tectonic patterns resulting in a time-predictable behaviour (Valentine & Hirano, 2010, Valentine & Perry, 2007). On the other hand, high magma flux is more likely to generate fissure vents or vent alignments perpendicular to the least compressive stress (σ_3) at the time of eruption (Valentine & Gregg, 2008). High magma-flux events are characteristic of "magmatically controlled" fields, where eruptions are controlled by pressure build-up in reservoirs due to magmatic processes (e.g. accumulation, fractionation, volatile exsolution) and eruptive volume is dependent on magma flux and time interval between eruptions, hence eruptions are volume-predictable (Valentine & Perry, 2007). In young systems such as the Auckland Volcanic Field, where the last vent (Rangitoto Island) erupted in two phases with distinct compositions and volumes (Needham *et al.*, 2011) it is, however, unclear how small- and large-volume activity (low and high flux) may relate and interact, with resulting uncertainty in hazard forecast.

Due to the wide spectrum of tectonic settings, mantle sources and evolutionary processes associated with distributed volcanic fields, the composition of erupted products vary widely from subalkalic to alkali, and to potassic, and from SiO_2 poor to SiO_2 rich. Magmas can both rise rapidly (Demouchy *et al.*, 2006, Rutherford, 2008, Spera, 1984) and hence record primitive signatures and deep processes (McGee *et al.*, 2011, Smith *et al.*, 2008, Valentine & Perry, 2007), or stall at various levels on the way to the surface and record processes of fractionation and assimilation of upper mantle or crustal material, as well as mixing of multiple magmas (Erlund *et al.*, 2010, Johnson *et al.*, 2008, McBirney *et al.*, 1987, Németh *et al.*, 2003). The spatial (horizontal and vertical) distribution of melting and magma ascent is an important factor controlling melt properties and evolution. Changing lithospheric structure between adjacent volcanic fields results in magmas being sourced from different depth and undergoing different evolutionary processes (Mordick & Glazner, 2006, Wang *et al.*, 2002). Even within a single volcanic field individual eruptions can reveal heterogeneity of processes. Silica-undersaturated to alkali basalt magmas from selected localities in the East and West Eifel Volcanic Fields, Germany, erupted without residence time in crustal magma chambers (Mertes & Schmincke, 1985, Ulrich & Schmincke, 1990). At other eruption centres in this field more complex crystallization histories indicate periods of magma residence in the upper mantle to lower crust (Duda & Schmincke, 1985).

Magma chemical properties can vary temporally with the evolution of a field. Early lithospheric mantle melting followed by melting of upwelling asthenospheric mantle was proposed to explain volcanism in the Vogelsberg region of Germany, where tholeiites were erupted before alkaline lavas (Jung & Masberg, 1998). This was also hypothesised for volcanism in the Basin and Range region of the western USA, in which case, however, the early phase was dominated by silicic magmatism (Leeman & Harry, 1993, Perry *et al.*, 1988). By combining chemical and chronological data, Gray & McDougall (2009) proposed that the Newer Volcanics of southern Australia, evolved from alkaline to tholeiitic and back to alkaline in a typical Hawaiian mantle plume fashion despite no plume tracks or alignments. In the Yucca Mountain region in the USA, trace element ratios as well as some major-element concentrations and phenocryst modal-assemblages are indicative of decreasing melt fraction at greater depths with younging of the volcanic field (Fleck *et al.*, 1996).

Chemical variability can also occur during the short period of a single small-volume eruption, generally due to the involvement of different source materials. Compositional difference between early-erupted tuff/scoria and later-erupted lava shields [OIB-like (ocean island basalt) to calc-alkaline] has been attributed to different source regions rather than internal magmatic processes (Strong & Wolff, 2003). Heterogeneous sources and variable degrees of partial melting also caused bimodal volcanism in the Trans Mexican Volcanic Belt (Carrasco-Núñez *et al.*, 2005). Involvement of different mantle sources was also proposed to explain chemical variations over the lifespan of the field in the Big Pine Volcanic Field, California (Blondes *et al.*, 2008) and in other volcanic fields worldwide (Reiners, 2002). The spectrum of chemical signatures is therefore a promising aspect to explore the intricacies of the plumbing systems of distributed volcanic fields.

Monogenetic eruption types and products are a function of several magmatic and external factors such as magma chemistry, shallow crustal structures and availability of external water (Kokelaar, 1983, Roggensack *et al.*, 1997, Sohn & Park, 2005). The resulting volcanic eruptive phenomena will have a variety of impacts on the surroundings and on more distal areas. Eruptive vents are generally marked by scoria cones and small shields in dry land settings (Hasenaka & Carmichael, 1985). In addition, tuff cones, rings and maars occur when eruptions interact with groundwater, or in shallow subaqueous environments (Walker, 1993). Evolved lavas (trachyte, phonolite, rhyolite) tend to be more volatile rich compared to the more primitive end members (alkali and subalkali basalt), resulting in a greater explosivity. Their greater viscosity compared to basalts, however, means that they may alternatively form domes or short lava flows, and hence impact only locally. Interaction with groundwater or saturated sediments can nonetheless cause phreatomagmatic explosions independently of the magma type involved (Lorenz, 1987). Although there is a good understanding of the hazards associated with each eruptive style present at distributed volcanic fields, the parameters controlling magmatic evolution, and hence the magmatic factors influencing the eruption styles, are still poorly understood.

Generalized models proposed for explaining the occurrence of small-volume intraplate volcanic fields have been based on the overall chemistry of eruptive

products during the history of magmatic activity. These models include mantle-plume magmatism (e.g. Clague & Frey, 1982, Tatsumi *et al.*, 2005), intracontinental rifting (e.g. Hare *et al.*, 2005, Jung *et al.*, 2006) and backarc spreading (Mashima, 2009), or crustal delamination (Hoernle *et al.*, 2006). Subduction-related volcanic fields also occur on thick continental lithosphere (e.g. Bacon, 1990). Many monogenetic volcanic fields are located behind volcanic arcs, although they are not thought to be subduction-induced. The Auckland Volcanic Field is situated c. 400 km behind the nearest arc and Jeju Island is c. 630 km behind its closest subduction zone, while other volcanic fields in NE China (e.g. Wudalianchi) are even further away from a subduction zone. On the other hand, volcanic fields such as the Newer Volcanics, Australia or Tengchong, China are far removed from modern subduction zones. There is therefore no clear link recognized between plate boundaries, tectonic events along them and intraplate field volcanism.

1.2 Problem Statement

Fundamental open questions include the reasons for the generation of monogenetic volcanism (Valentine & Gregg, 2008) and especially how some monogenetic volcanic fields relate to the polygenetic volcanoes with which they are co-located. Magma chemistry varies within single eruptions and with age of eruption in a field (Blondes *et al.*, 2008, Sakuyama *et al.*, 2009), however it is still not certain whether this variability is dependent on the magmatic source, or on the processes affecting the magma after it has left the source. Another uncertainty relates to the site of volcanic activity; whether it is structurally controlled by shallow weaknesses in the crust, or whether it is dependent on the melting properties and spatial inhomogeneity of the source region (Nakamura, 1977, Valentine & Gregg, 2008). An even more fundamental question remains as to why small-volume intraplate volcanic fields occur where they do.

To better understand distributed basaltic field volcanism and how this relates or interacts with co-located polygenetic volcanism that may be several orders of magnitude larger in volume a new model of their development and evolution is needed. This model must integrate aspects of field petrology, structure, geochemistry,

physical volcanology and tectonic environment. This could be the basis for informing new process-constrained probabilistic forecasting of hazards, including estimation of future eruption locations, magnitudes and eruption styles.

The paucity of observational data on eruptions in monogenetic volcanic fields means that knowledge of the volcanic/magmatic characteristics of individual eruptions must be gained through the study of the remaining volcanic deposits and the geological record. This study focuses on the Jeju Island Volcanic Field in the Republic of Korea. Jeju Island consists of a small-volume (c. 0.01 km^3 per event) distributed volcanic field superposed to a large-volume (c. 500 km^3), central composite shield volcano and has been active over the past 1.8 Ma (Sohn *et al.*, 2008). Activity on Jeju began with small-volume volcanism, before large-volume primitive magma erupted to form a shield and a central volcanic dome and flow complex (Lee, 1982, Sohn & Park, 2004, Tatsumi *et al.*, 2005). As a consequence of distributed activity continuing throughout the overall volcanic activity the surface of the Island is dotted with more than 300 single-eruption vents (Hasenaka *et al.*, 1997) with many more centres buried by the large-volume lavas (Sohn & Park, 2004).

The Jeju Island Volcanic Field is suitable for a study of this type because it is long lived and it is still regarded to be active because the last eruption occurred c. 1000 years ago (Lee & Yang, 2006). In addition, detailed knowledge of the sub-surface geology has become available due to an extensive groundwater drilling program. Another benefit of studying the Jeju Island Volcanic Field is the existence of the small-volume eruptions superposed with a large-volume system; hence insights gained by studying Jeju may help understand the enigmatic and sudden increase in erupted volume in the Auckland Volcanic Field, New Zealand (Allen & Smith, 1994). It may also help in understanding other examples where large variations in magma flux occur such as in the San Francisco Volcanic Field, Arizona (Conway *et al.*, 1998) or the Black Rock Volcanic Field, Utah (Oviatt & Nash, 1989).

1.3 Hypothesis

The basic hypothesis for this research is that the evolution of a volcanic field comprising monogenetic and superposed composite shield/strato-type volcanic activity will be controlled by the site (Valentine & Hirano, 2010) and extent of melting in the mantle and mode of magma ascent (Takada, 1994). The depth and degree of melting of the source are hence paramount in influencing the chemical characteristics and the stability and evolution of the magma during ascent (e.g. Putirka *et al.*, 2009, Sakuyama *et al.*, 2009). Magma volume and flux rates, which depend on the chemistry, will control how the magma interacts with the surroundings and with other magmas during its ascent (Cañón-Tapia & Walker, 2004), and ultimately the mode of eruption. The tectonic stress (Nakamura, 1977) and strain (Valentine & Perry, 2007) regimes will also influence the mode of magma ascent by facilitating or hindering upward magma propagation. Hence, the degree of magmatic evolution is a function of tectonic stress and strain, and the magma volumes involved. Larger magma production rates coupled with low extensional strain rates are responsible for building increasingly expansive and complex volcano plumbing systems, which result in more evolved magmas.

1.4 Methodology

In order to test this working hypothesis, several chemical and petrographical techniques have been used to analyse samples collected from a range of volcanic suites representing both the small- and large-volume phases of activity on Jeju Island. Major- and trace-element chemical analyses (XRF and LA-ICP-MS) of small- and large-volume eruptive products, as well as mineral analyses (electron microprobe), were employed to gain insight into the partial melting conditions and the processes affecting the magma during ascent (fractionation ± assimilation). Isotopic analyses (MC-ICP-MS) were applied to derive fundamental information on the characteristics of the mantle source or sources involved, such as its composition and melting rates, and on the degree of interaction between such sources or the magma and its surroundings during ascent. Evaluating dates collected by $^{40}Ar/^{39}Ar$ techniques of

selected horizons in the large-volume lava pile (obtained from drill cores) helped pinpoint in time particular events in the volcanic field evolution.

1.5 Aims and Outline

Chemical and petrological investigations of small-volume volcanic deposits are expected to yield insight into the source characteristics and melting rates, and the evolution (both chemical and physical) of magma batches as they rise to the surface. A model was developed to describe the evolution of the Jeju Island Volcanic Field in a spatio-temporal framework. This allows better constraints for temporal and spatial models used for hazard forecasting in continental monogenetic volcanic fields.

This thesis consists of five sections. Chapter Two presents a review of the current understanding and knowledge of the Jeju Island Volcanic Field. Chapter three exposes the sampling and analytical methodologies. The following four chapters are presented as manuscripts, or combination of manuscripts published or submitted for publication to international journals, each dealing with a particular aspect of the Jeju Island Volcanic Field. Chapter Four presents a case study from a single, small-volume monogenetic volcano involving diverse magma batches. Data gained from the detailed sampling of the eruptive sequence was employed to model the conditions of melting and chemical evolution for the feeding magmas. Chapter Five draws cases from two publications to illustrate the chemical complexity of monogenetic eruptions, and its significance for the magma ascent modes. Chapter Six presents a focused study of small-volume monogenetic magma evolution over the lifetime of Jeju, which was used to derive a model for its temporal and spatial evolution in a tectonic framework. Chapter Seven explains also how the large-volume magmatic system on Jeju evolved over time, along with their relationship with the small-volume magmatic system. This concludes with the proposition of an integrated comprehensive magmatic model for the Jeju Island Volcanic Field. Chapter Eight presents a summary and integrated conclusions, as well as a short discussion of the relevance of this study for other intraplate volcanic areas worldwide.

Chapter 2

The Jeju Island Volcanic Field

This chapter presents a literature review of the Jeju Island Volcanic Field.

2.1 Introduction

Jeju Island (also Jeju-do, "do" meaning "island", or Cheju or Cheju-do prior to the Revised Romanisation of the Korean script in 2000) is an intraplate continental volcanic field forming a volcanic island off the coast of South Korea in the East China Sea, at the western entrance of the Korea-Tsushima Strait (Fig. 2.1). Jeju Island is one of several intraplate volcanoes in continental NE Asia that were active during the Cenozoic (Chen *et al.*, 2007). The Island consists of a composite shield central volcanic edifice with its surface and surroundings dotted by over 300 monogenetic eruptive centres, mainly scoria cones, with minor tuff rings, maars and lava domes. Many more small-volume volcanic centres are buried or submerged. The Island hosts three UNESCO World Natural Heritage Sites: Mount Halla (Hallasan), the Geomunoreum Lava Tube System and the Seongsan Ilchulbong tuff cone.

2.2 Tectonic settings and structures

Jeju Island is surrounded by c. 100 metre-deep water (Sohn & Park, 2007) on the continental shelf part of the Amurian Plate, which is the same tectonic plate as the rest of the Korean Peninsula (Hamdy *et al.*, 2004, Jin *et al.*, 2007, Zonenshain & Savostin, 1981). The base of the continental crust (the Mohorovich discontinuity) has been detected at c. 34 km depth beneath Jeju (Yoo *et al.*, 2007). Global Positioning System (GPS) deformation data indicate differential displacement of stations within the Island, with the northwestern side moving southeast and the southeastern side moving northeast at 1 to 2 millimetres per year (Hamdy *et al.*, 2004, Park *et al.*, 2001). An overall WSW-ENE compressional and NNW-SSE extensional regime exists in

the southern part of the Korean Peninsula (Jin *et al.*, 2006), and this has been suggested for Jeju in order to explain the apparent alignment of volcanic centres (Fig. 2.1d; Koh *et al.*, 2003)

Jeju Island is situated approximately 600 km behind the subduction front where the Philippine Sea Plate is subducted perpendicularly under the Eurasian/Amurian Plates (Kubo & Fukuyama, 2003; Fig. 6.1c). Approximately 800 km to the northeast of Jeju Island is the active North China plain rift system related to the Bohai Sea (Liu, 1987). The Pacific Plate, subducted under the Eurasian Plate at the Japan Trench and under the Philippine Sea Plate at the Izu-Bonin Trench, is present beneath NE China and the Korean Peninsula between the 440 and the 660 km discontinuities (Gudmundsson & Sambridge, 1998, Lei & Zhao, 2005, Li *et al.*, 2000, Zhao, 2004).

Few tectonic structures are notable on the present landscape of Jeju. Hwang *et al.* (1994) reported some fault surfaces indicating NW-SE, NE-SW and more recently ENE/WSW extensional regimes; the last being opposite to the direction reported above. The faults in this study however occurred in volcanic deposits and may be related to syn-eruptive instabilities. One of the most apparent geomorphological features of Jeju Island is that in the north, west and east, lava flows dip gently into the sea, whereas in the south the coastline generally consists of cliffs tens of metres high. Consequently several waterfalls are present in the southern part of the Island, but none elsewhere. However, the tectonic significance of this morphology contrast has not been previously addressed. Seismic profiles of the sea bed to the south of Jeju Island (Lee *et al.*, 1997) also show no evidence for major faulting. Neo-tectonic movements are however suggested by the outcropping of the Seoguipo Formation. It is composed of marine deposits which are exposed over tens of metres in cliffs to the west of Seoguipo Harbour, but they are in the subsurface to the east of the harbor, a few hundred of metres away. Everywhere elase they are below the Island. On these exposures of the Seoguipo Formation there are small (<1 m) normal faults trend which trend E-W.

Bathymetric maps of the sea to the south of Jeju Island show a topographic high (40 to 60 m below sea level compared with the normally c. 100 m deep shelf) oriented ENE parallel to the long axis of Jeju Island (e.g. Suk, 1989, Xie *et al.*, 2002)

suggesting the presence of a seamount to the south of Jeju Island. Seismic profiles of the seafloor up to 15 km offshore to the south of Jeju Island, however, failed to reveal any topographic features other than a gently southward-dipping seafloor (Lee *et al.*, 1997).

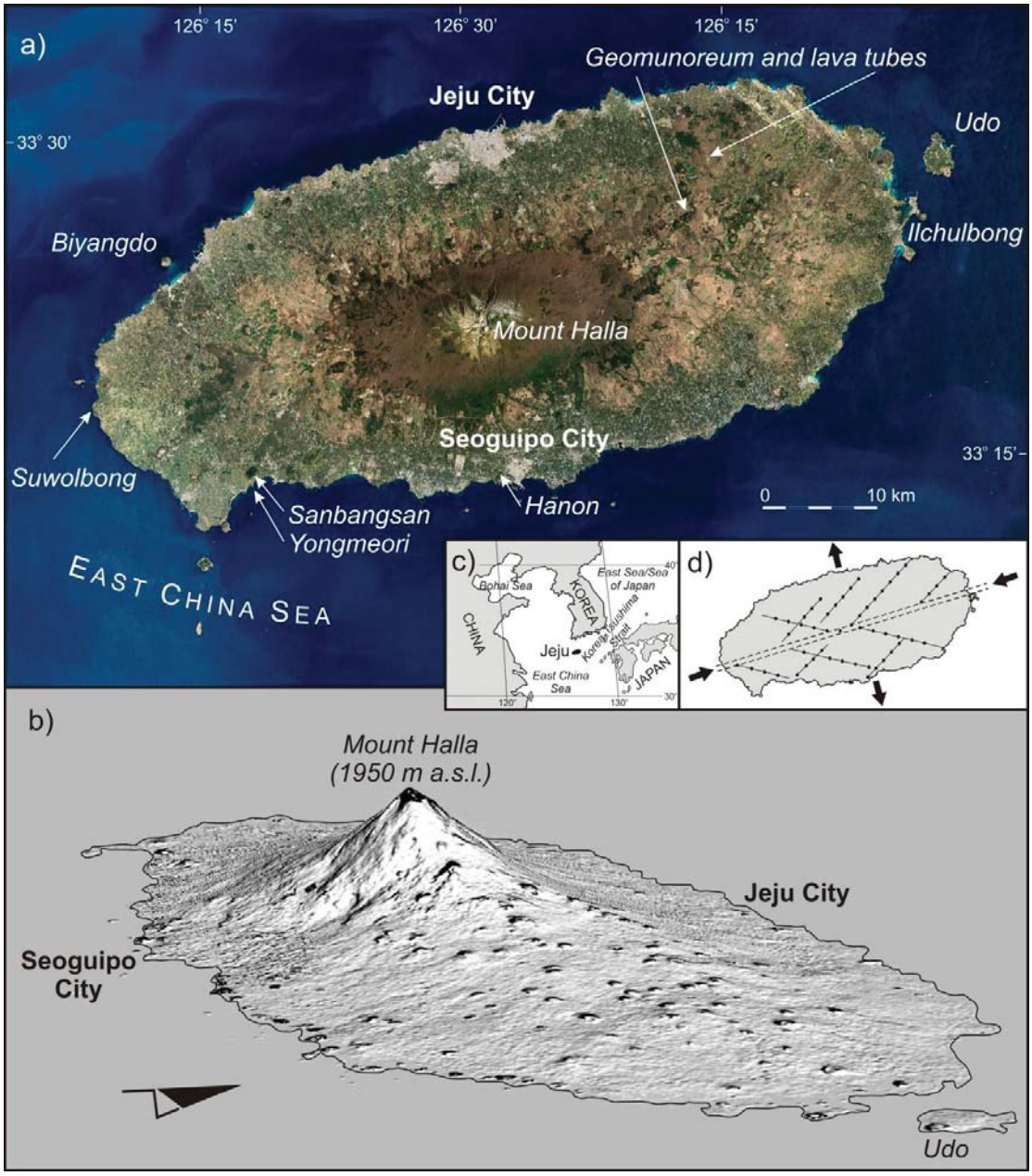

Figure 2.1: *a) Satellite image of Jeju Island. Image source: NASA Earth Observatory, b) Bird eye view of Jeju towards the west with visible dispersed centres, vertically exaggerated 5 times, c) General location of Jeju Island, d) Stress field influence on volcanic vent alignments from Koh et al. (2003).*

2.3 Sedimentary and volcanic stratigraphy

Following the study of Lee (1982), the overall stratigraphy of Jeju was subdivided into four stages: the first stage includes the Seoguipo Formation and a so called "basal basalt"; the second is the "lava plateau" stage that built the shallow-dipping outskirts of the Island; the third is the "shield stage" that built Mt Halla and formed the main bulk of the Island; and finally the "scoria cone" stage generated the distributed small-volume vents seen on the surface. A thorough understanding of the subsurface geology of the Island, gained from thousands of groundwater bores drilled over the past fifty years however suggests a wider interplay between small-volume (<<1 km^3) and large-volume (>1 km^3) eruptions (Fig. 2.2; Sohn & Park, 2004, Sohn & Park, 2007), and hence Lee's interpretation needs reviewing.

2.3.1 Basement geology

The basement of Jeju Island consists of granitic and felsic volcanic rocks. K-Ar dating of granitic rocks gave both Cretaceous and Jurassic ages, and these were interpreted as correlating with the Ogcheon (Okchon) Fold Belt in the Korean Peninsula (Kim *et al.*, 2002 and references therein). This is a NE-SW trending fold-and-thrust belt consisting of metasedimentary and metavolcanic rocks spanning ages from Proterozoic to Jurassic (Chough *et al.*, 2000b), which was subsequently affected by granitic intrusions during the Daebo Orogeny in the Jurassic (Chough *et al.*, 2000a, Kim *et al.*, 2002). The fold belt is bound by the Precambrian high grade gneisses and schists of the Kyonggi Massif to the northwest and by the Yongnam Massif to the southeast (Chough *et al.*, 2000a).

The basement granite is overlain by Late Cretaceous/Early Tertiary rhyolitic welded tuff in the eastern part of the Island (Lee *et al.*, 1994), and despite both granite and tuff not being exposed anywhere on the Island there is evidence of them as xenoliths in the erupted basaltic lavas or as accidental fragments in tuffs. These are reworked and can be found on beach deposits around the Island.

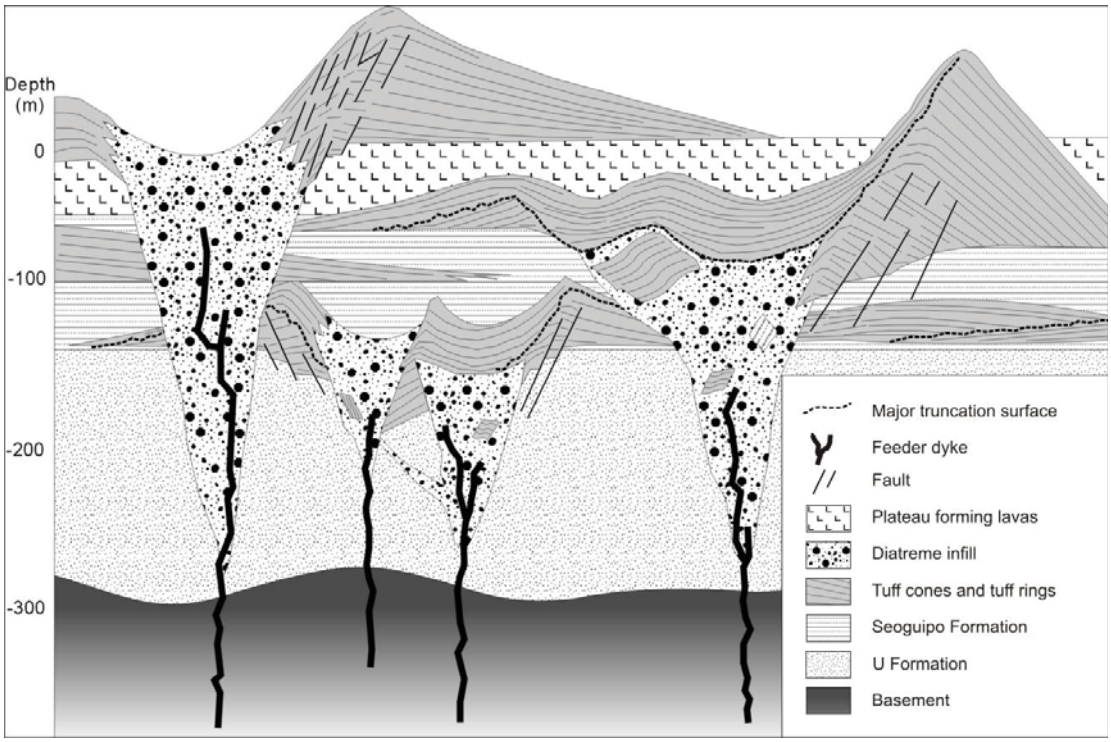

Figure 2.2: *Schematic stratigraphy of a section through part of Jeju Island (after Sohn & Park, 2004).*

2.3.2 U and Seoguipo Formations

The basement is overlain by 70 to 250 m thick submarine and subaerially emplaced unconsolidated quartzose sandy and muddy sediments, named the U Formation. These were deposited on the continental shelf prior to the onset of volcanism (Sohn & Park, 2004, Sohn & Park, 2007, Sohn *et al.*, 2008).

The commencement of Jeju-centred volcanism is recorded in the c. 100 m thick Seoguipo (Seogwipo) Formation, which is composed of primary and reworked, subaerial and submarine, Early to Middle Pleistocene (1.8 to 0.8-0.4 Ma) hydrovolcanic/phreatomagmatic deposits and intercalated marine and non marine fossiliferous sedimentary sequences (Fig. 2.3) and soil horizons (Kang, 2003, Li *et al.*, 1999, Sohn & Park, 2004, Sohn *et al.*, 2008). Facies and erosional surfaces within the Seoguipo Formation can not be correlated laterally even over very short distances (few hundred metres), and subaerial and submarine facies associations are intercalated randomly (Sohn *et al.*, 2008). This was interpreted to indicate episodic explosive volcanic/hydrovolcanic activity during Quaternary glacial-interglacial sea

level fluctuation rather than tectonically controlled uplift and subsidence (Sohn *et al.*, 2008). In the exposed section of the Seoguipo Formation, near Seoguipo Harbour, the deposits have been interpreted to represent the result of settling pyroclastic density currents that flowed over water (Sohn & Yoon, 2010).

Figure 2.3: *a), b) and c) exposures of Seoguipo Formation near Seoguipo Harbour and d) is the equivalent sedimentary formation in drill core. a) volcaniclastic/epiclastic deposits, b) fallen blocks, width of view 1 m in the foreground, c) shelly horizon seen from above bedding surface. d) primary tuff, photograph by Shane Cronin.*

Surveys of numerous deep diamond cores also revealed that the upper surface of the Seoguipo Formation is irregularly distributed throughout the Island. It is generally more elevated in the central part of the Island (between 50 m below and 50 m above sea level), and it becomes deeper in the eastern and western sides (up to 100 m below seal level; Won *et al.*, 2006). This irregular surface can partly be attributed to early phreatomagmatic volcanoes (pre-"lava shield" stage) capping the Seoguipo Formation in parts (Sohn & Park, 2007; Fig. 2.2).

2.3.3 Lava outskirts and composite shield

Subalkali lava flows forming the outskirts of the Island's volcanic shield are c. 50-150 m thick in coastal regions (Sohn *et al.*, 2008). The Pyosunri (Pyoseolli) Basalt, which forms the eastern low-lying parts of the Island (Lee, 1982, Tatsumi *et al.*, 2005) was interpreted to be erupted in the early stages of magmatism (i.e. it is the stratigraphically lowest lava-flow unit) and was followed by the alkaline lavas (Lee, 1982, Tatsumi *et al.*, 2005). However dates of subalkali to transitional lava flows in core samples in both eastern and western parts of Jeju are <300 ka and overlie alkali and trachytic lavas (Koh & Park, 2010a, Koh & Park, 2010b, Koh *et al.*, 2008). This implies that the previous genetic model (Lee, 1982) is flawed because eruption did not occur in stages but was a continuous process.

Trachyte and trachyandesite lava flows are also intercalated within the subalkali to transitional lava succession, which was then overlain by the volcanic rocks that form the Halla composite shield volcano as well as by c. 300 scoria cones. Several lava tubes, some of which have been designated as UNESCO World Natural Heritage Sites, are present throughout the low flanks of the Island, mainly in the subalkali shield lavas. These lava flows are generally <3 m thick and are inter-layered with associated rubbly flow breccia (clinker, often confused for pyroclastic material), ash and tuff associated with eruptive episodes, and soil horizons developed during inter-eruptive periods (Won *et al.*, 2006). Additionally, based on rock cores, Kim *et al.* (2006) described pillow lavas from Jeju.

A break in slope occurs at c. 500-700 m above sea level. The slope is gentle (2-5%) in the lower flanks but steeper (12-25% on average) on the upper flanks (Fig. 2.4a).

Figure 2.4: *a) view of Mount Halla from the eastern lower flanks, note the break in slope of the central edifice, b) Mount Halla summit trachyte lava dome seen from the west.*

Mount Halla consists of a trachyte lava dome (Fig. 2.4b; Koh *et al.*, 2003), and valleys incised in its upper flanks reveals trachytic flows several hundreds of metres thick extending from the summit region. The break in slope is therefore likely indicative of this event of more viscous lava extrusion. These trachyte flows, as well as the summit dome, are, however covered by younger trachybasaltic flows (Koh *et al.*, 2003), which smoothed the slopes (Fig. 2.4a).

2.3.4 Small-volume distributed volcanism

As mentioned previously, monogenetic volcanism generating distributed small-volume centres has affected Jeju Island throughout its history, and at present c. 300 eruptive centres are exposed at its surface. These mainly consist of scoria cones with minor hydrovolcanic centres (tuff cones and rings) near the shoreline (Fig. 2.5). No dominant arrangement is apparent and centres occur scattered throughout the Island, although generally more concentrated along its long axis, where some vent groups form local alignments (Fig. 6.1a).

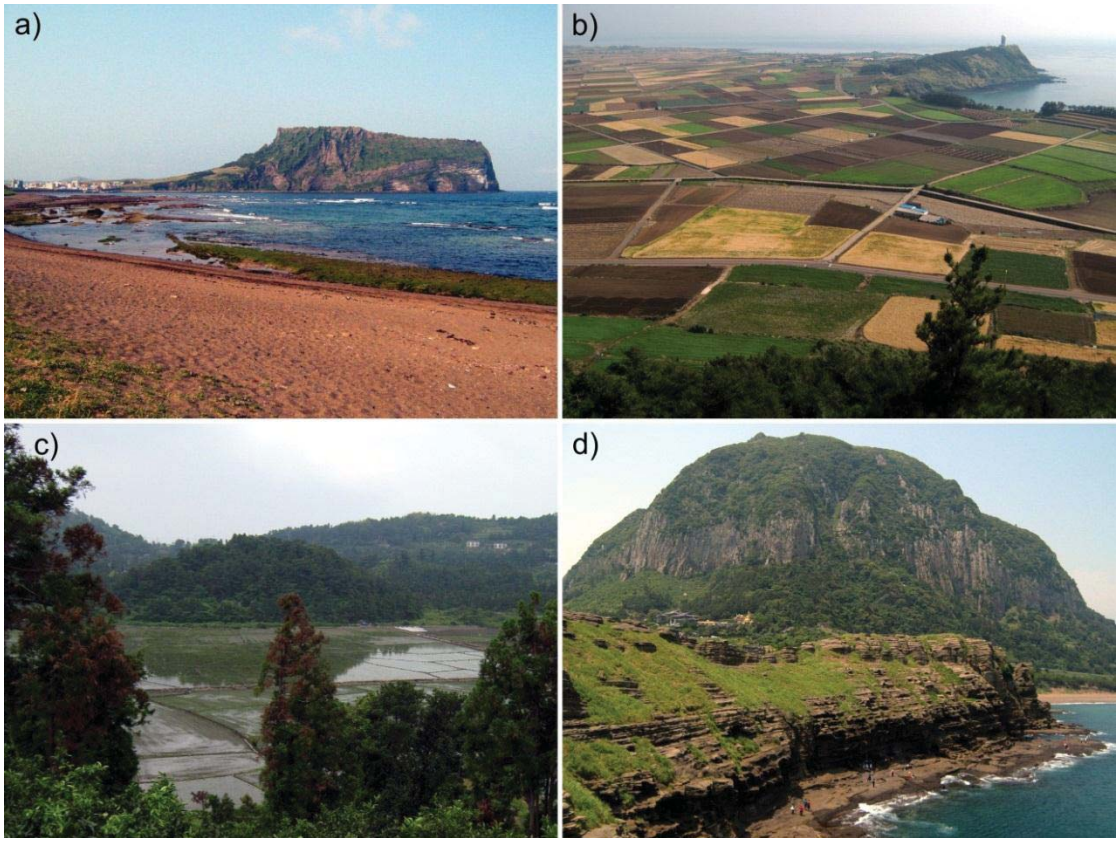

Figure 2.5: *Variety of eruptive morphologies on Jeju Island. a) Ilchulbong tuff cone, b) Suwolbong tuff ring, c) Hanon maar with nested spatter cone and the only rice fields on Jeju Island, d) Sanbangsan trachyte dome with the Yongmeori tuff ring in the foreground.*

Early to Middle Pleistocene hydrovolcanic centres developed multiple superposed tuff rings and cones as a consequence of vent collapse and migration due to the instability of the unconsolidated sedimentary substrate (U and Seoguipo Formations;

Sohn & Park, 2005). In contrast, Holocene phreatomagmatic centres formed over plateau-forming lavas and have more stable morphologies (Sohn & Park, 2005).

Sanbangsan (Mount Sanbang), in the southwestern part of Jeju Island, is a standalone trachyte dome (Fig. 2.5d). Other spatially distinct trachytic domes and lava flows occur in the area (Lee *et al.*, 1994) but are covered by later lava flows. These trachytic centres are volumetrically larger compared to the scoria and phreatomagmatic cones, but given that they are erupted at independent location they may also be considered distributed monogenetic.

It is important to note that small-volume eruptions forming scoria cones and hydrovolcanic centres have occurred throughout the volcanic history of Jeju Island, and are therefore not solely a surface and recent expression of volcanism (Sohn *et al.*, 2002) as previously interpreted (Lee, 1982).

2.3.5 Volcanic chronology

Records relating to historical volcanic activity on Jeju Island refer to a 5 day-long eruption during the 5th year of the reign of king Mok-jong (1002 AD, possibly on Biyangdo (Biyang Island; Fig. 2.1a); Hulbert, 1962, Woo & Kim, 2005 and references therein). Other possible eruptions may have occurred in 1007 and 1570 AD (Kim *et al.*, 2002, Ogawa, 1982), and two "catastrophic eruptions and earthquakes" are reported from 1455 and 1670 AD (IAEA, 1967). No indication of eruption sites, eyewitness reports or any information source was given by these authors. Authors referring to specific Korean historical records report an effusive eruption lasting five days in July 1002 AD from Mount Halla ("red water erupted from four orifices in Mount Tamra (Halla). All the red water turned into bricks and stones") closely followed by another eruption lasting seven days in October 1007 AD ("an island arose above the sea near Cheju Island with thunder like tremors for 7 days") supposedly forming Biyangdo (see appendices in Lee & Yang, 2006, and references therein). Visual inspection of volcanic deposits on Biyangdo, however, did not reveal any evidence for magma/lava-water interaction. Given that sea level has not changed significantly in the last 1000 years, Biyangdo is not likely to be the site

of the 1007 AD eruption. The relatively fresh morphological features of the Island suggest that the eruption occurred recently during a period of low sea stand, possibly during the last glaciation.

The majority of reported K/Ar and $^{40}Ar/^{39}Ar$ ages for the volcanic rocks of the Island are ≤1.2 Ma, with only one date around 2.2 Ma (Kim *et al.*, 2002, Sohn, 1996, Sohn & Park, 2004). The age frequency reported by Kim *et al.* (2002) shows two peaks between 0.7 and 0.4 Ma and from 0.1 Ma to present but this may be biased by sampling methodologies and is likely not representative of both surface and buried lavas. Ages of some small-volume volcanic centres gained either through direct measurement or based on sedimentary formations surrounding the volcanic vents or field relationships between deposits from adjacent eruptive centres are reported in Table 2.1.

Table 2.1. *Available ages of specific small-volume volcanic centres on Jeju Island.*

Location	Age	Method	Reference
Ilchulbong tuff cone	c. 5 ka	^{14}C of shells in sedimentary formation containing reworked tuff	(Sohn *et al.*, 2002) (Kim *et al.*, 1999)
Songaksan tuff ring	7.0 ± 0.3 ka	OSL, reworked material from the tuff ring dated at 4 ka by ^{14}C	(Cheong *et al.*, 2007) (Sohn *et al.*, 2002)
Suwolbong tuff ring	18.3 ± 0.7 and 18.6 ± 0.9 ka	OSL	(Cheong *et al.*, 2007)
Hanon maar	34 ka	AMS^{14}C	(Yoon *et al.*, 2006)
Udo lava shield	114 ka	K/Ar	(Koh *et al.*, 2005)
Dangsanbong	Middle Pleistocene	Field relationships	(Sohn & Park, 2005)
Dansan tuff ring	Younger than Dansan 1	Field relationships	(Sohn & Park, 2005)
Dansan tuff cone	Early/Middle Pleistocene	Coeval to Seoguipo Formation	(Sohn & Park, 2005) (Sohn *et al.*, 2008)
Yeongmori	> c. 800 ka	Covered by Sanbangsan trachyte dome (733 ± 56 ka)	(Won *et al.*, 1986) (Sohn & Park, 2005)
Seoguipo Formation and deep core tuffs	> c. 1 Ma	Older than onset of voluminous lava effusion	(Kim *et al.*, 2002)

OSL = optically stimulated luminescence ; AMS = accelerator mass spectrometry

Possible tephra layers, described as sand-rich layers in the Hanon crater lake sediments (Lee *et al.*, 2008) suggest further explosive eruptions occurred in nearby areas c. 6.3, 13, 14.3 and 17 ka before present. The low level wind direction on Jeju Island is very seasonal with prevalent NW winds in spring, SW-SE winds in summer E-NE winds in autumn, and N winds in winter (Carmichael *et al.*, 1997). As a

consequence, and assuming wind patterns to have been similar during the last glaciation, not having details of the seasonal occurrence of the sandy layers, there is no indication of where on the Island an eruption may have occurred, although they were likely within 10 km of Hanon, based on typical fall dispersals from magmas of these compositions (e.g. Cronin & Neall, 2000).

Chronological interpretation of stratigraphically complex volcanic areas can be hindered by the impracticability of collecting enough data points. Nevertheless chemical signatures can be matched with eruption stages to determine any correlation such as has been carried out for the Newer Volcanic Province in Australia (Gray & McDougall, 2009). One advantage on Jeju Island is the presence of numerous rock cores, which allow a three-dimensional correlation, as done for instance by Koh *et al.* (2008).

2.4 Chemistry and petrology

2.4.1 Geochemistry

Lavas from Jeju Island, as well as from other Pliocene to Quaternary centres in Korea have characteristics of alkaline (sodic) intraplate basalts with enriched LILE and LREE, depleted HFSE and HREE and moderate positive Nb and Ti anomalies, sourced deeper in the mantle than 60 to 80 km and with residual garnet (Pouclet *et al.*, 1995) and generally unaffected by modern subduction fluids (Nakamura *et al.*, 1989). Isotopic ratios tend to remain constant with increasing SiO_2 (chemical evolution) indicating that crustal contamination is a minor factor in the evolution of the Jeju magmatic system (Tatsumi *et al.*, 2005).

Surface geology on Jeju Island consists mainly of trachybasalt and basalt lava flows, trachyte lava domes, several scoria cones and minor tuff, and sedimentary rocks (Park *et al.*, 2006). The volcanic rocks can be subdivided mainly into alkali and subalkali (tholeiitic) and minor transitional fields (Fig. 2.6), with the alkali rocks spanning the whole spectrum from olivine alkali basalt to trachytes and the subalkali being mainly tholeiitic basalt to tholeiitic andesites (Park *et al.*, 1999, Tatsumi *et al.*, 2005).

Classification schemes have been introduced by various workers. Beside the four-stage volcanic activity model (Lee, 1982), Park & Kwon (1993a, 1993b) introduced a classification based on whole-rock P_2O_5/K_2O ratio (High PK = P_2O_5/K_2O >0.3 and Low PK = P_2O_5/K_2O <0.3) although this is applicable to primitive alkaline rocks only, whereas Tatsumi *et al.* (2005) distinguished a high-Al and low-Al alkali suites (Fig. 2.6). All workers also recognize tholeiitic or subalkali basalts as a different lava suites. Koh *et al.* (2008) moreover defines a transitional basaltic suite. From their spatial distribution, transitional basalts appear only in the lower reaches of the eastern part of Jeju, but this distribution may be due to sampling bias.

A further classification scheme is based on two episodes of trachytic magmatism (Chang *et al.*, 2006, Won *et al.*, 1986). The earlier trachytic episode is defined as the Sanbangsan Group and occurs mainly on the southern reaches of the Island, whereas the second episode defined as the Baengnokdam Group occurs around the summit of Mount Halla (Fig. 2.6; Chang *et al.*, 2006). The two groups are interpreted to have evolved from different alkali basalt parent magmas, because the Sanbangsan Group has distinctly higher $^{87}Sr/^{86}Sr$ (0.704727 to 0.704934) and different trace element concentrations compared to the Baengnokdam Group (0.704089 to 0.704229; Chang *et al.*, 2006). The Sanbangsan Group erupted between c. 0.94 and 0.73 Ma ago and the Baengnokdam Group between 0.25 and 0.07 Ma ago based on K/Ar dates reported in Kim *et al.* (2002 and references therein). Won *et al.* (1986) gives palaeomagnetic average ages of 0.733 ± 0.056 and 0.025 ± 0.008 Ma for the two trachytic episodes respectively.

2.4.2 Petrology and mineralogy

Alkali basalt lavas have phenocryst content between 10 and 15% and are poorly vesicular (Lee, 1982). Common phenocrysts include olivine (<10%) often with spinel inclusions, clinopyroxene (<5%) and plagioclase feldspar (~20%), with minor amphiboles, potassic feldspar, Fe-Ti oxides and apatite (Park & Kwon, 1993b, Tatsumi *et al.*, 2005). Subalkali lavas are generally olivine microphyric (<10%) in an

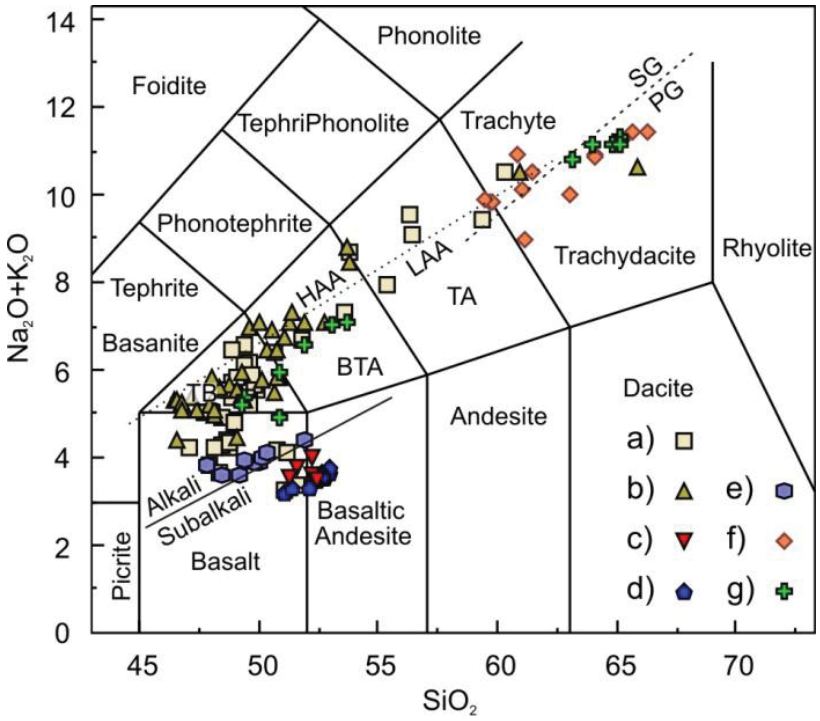

Figure 2.6: *Selected published whole-rock chemical data (oxide wt%) of Jeju Island, including both large- and small-volume volcanism. a) overall Jeju, Tatsumi et al. (2005), b) lavas from northern part of Jeju, Park and Kwon (1993b), c) Jeju tholeiites, Park and Kwon (1996), d) Udo Volcano lava shield, Koh et al. (2005), e) lavas in the Ilchulbong area, Koh et al. (2007), f) Jeju trachytes, Chang et al. (2006), g) Mount Halla summit area, Koh et al. (2003). Nomenclature after LeBas et al. (1986). Note the limited chemical variation of transitional and subalkali data. TB is trachybasalt, BTA is basaltic trachyandesite and TA is trachyandesite. HAA (high-Al alkali) and LAA (low-Al alkali) are after classification of Tatsumi et al. (2005) and SG (Sanbangsan trachytes) and PG (Baengnokdam trachytes) are after Chang et al. (2006). Alkali/subalkali boundary is after Miyashiro (1978).*

intergranular plagioclase + clinopyroxene ± Fe-Ti oxides groundmass (Koh *et al.*, 2005, Park & Kwon, 1996). At the more evolved chemical end, the Sanbangsan Group lavas are generally aphyric with antirapakivi feldspars and titanomagnetite, whereas the trachytes of Mount Halla contain alkali feldspar + pyroxene + olivine phenocrysts, sometimes glomerocrystic, and titanomagnetite and ilmenite (Chang *et al.*, 2006, Lee, 1982).

Studying phenocryst chemistry in the large-volume lavas Park and Kwon (1993c) concluded that High PK magmas fractionated at deeper levels compared to Low PK magmas. They also mention that olivine phenocrysts in the hawaiites samples they measured (as opposed to other magma types) are generally not in equilibrium with their host magma, indicating a different genetic history. The small-volume Songaksan magma was also interpreted to have chemically evolved through clinopyroxene fractionation at depth (Sohn *et al.*, 2002). No quantitative approach to determine P-T conditions of crystallization was, however, used in either works.

2.4.3 Peridotite xenoliths

Ultramafic xenoliths, mostly spinel lherzolite with minor spinel harzburgite and pyroxenite, occur in the alkali basalts of Jeju Island. These can be found in a variatey of textures from protogranular through porphyroclastic and mylonitic (Yu *et al.*, 2010). Their whole-rock chemistry suggests that they are refractory residues after partial melting and metasomatism of a heterogeneous mantle source (Choi *et al.*, 2002, Yang *et al.*, 2010). On the basis of Sr, Nd, Pb and Hf isotopes, Choi *et al.* (2006) defined the mantle beneath Jeju as having characteristics of both depleted mantle (DMM) and enriched mantle (EMII) domains. The xenoliths' isotopic compositions, however, differs from that of their host basalt (Choi *et al.*, 2002), suggesting that they were incorporated in the magma during its ascent. Spinel-lherzolite xenoliths in alkali basalts from eastern Jeju were interpreted to have been derived from the upper mantle at pressures of 18 kbar (1.8 GPa) and temperatures of 1023 to 1038 ˚C (Yun *et al.*, 1998). This is consistent with the geothermal gradient under Jeju from 13 kbar (1.3 GPa) at 880°C to 26 kbar (2.6 GPa) at 1040°C as established by Choi *et al.* (2001) on mineral compositions in spinel peridotites. No garnet has been reported in peridotite xenoliths from Jeju.

2.5 Tectonomagmatic models

Based on P_2O_5, K_2O and trace elements systematics of the lava succession Park and Kwon (1993a, 1993b) suggested that large-volume Jeju lavas are not primary melts,

but are derived from an overall homogeneous mantle source that melted to different degrees and at different depths.

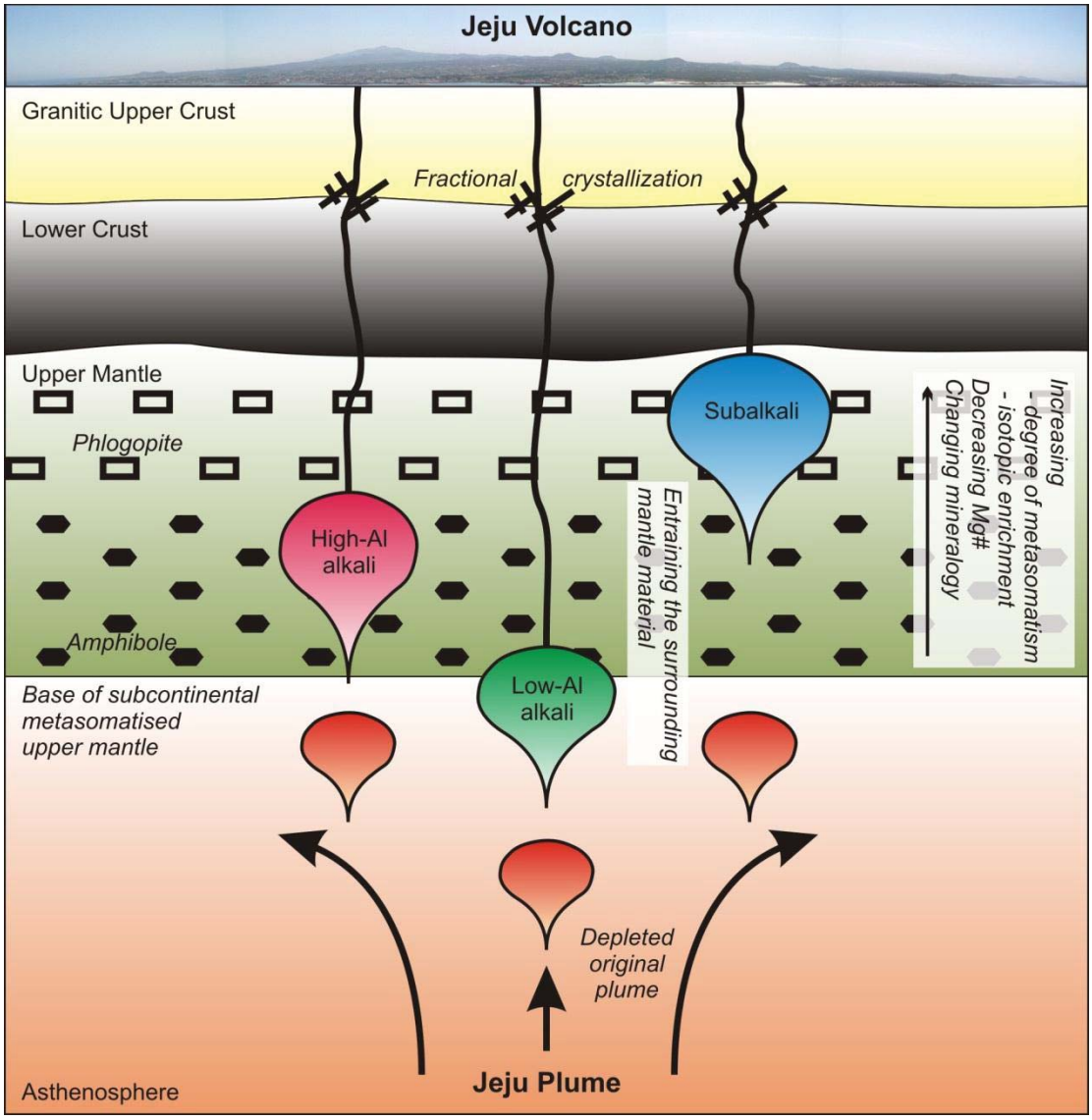

Figure 2.7: *Model summarising the Jeju plume redrawn after Tatsumi et al. (2005).*

Tatsumi *et al.* (2005) argued for the existence of a mantle plume beneath Jeju Island, based on major and trace element geochemistry and mineralogy (Fig. 2.7). In their model, originally depleted material from an asthenospheric mantle plume reaches the base of the subcontinental (lithospheric) upper-mantle, which had previously been metasomatized. The degree of metasomatic and isotopic enrichment increases with decreasing depth, and with it, the source region hydrous mineralogy changed from deeper amphibole to shallower phlogopite. Different degrees of melting at different

depths therefore resulted in the three magma types introduced earlier (Tatsumi *et al.*, 2005):

i) larger partial melting degree, subalkaline magma formed in the shallower upper mantle with phlogopite in the source,
ii) low partial melting degree, high-Al alkali magma formed in the lower upper-mantle with amphibole in the source and,
iii) moderate partial melting degree, low-Al alkali magma formed at the base of the upper-mantle.

Choi *et al.* (2006) argued against a thermo/mechanical mantle plume as the source of volcanism in South Korea based on its distribution, which lacks evidence for any hot-spot track. Instead its distribution tends to be related to pre-existing crustal weaknesses, and is indicative of being sourced from a heterogeneous asthenospheric mantle. This heterogeneity may be the result of lateral mantle extrusion following the continental collision of India and Eurasia coupled with subduction of the Pacific and Philippine Sea Plates under Eurasia (Choi *et al.*, 2006, Liu *et al.*, 2004 and references therein).

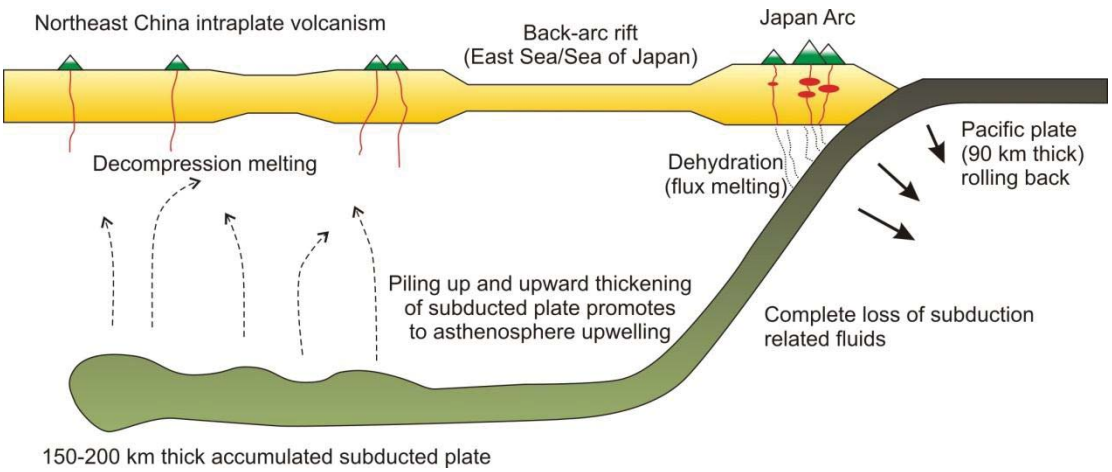

Figure 2.8: *Model of asthenospheric upwelling caused by piling up of subducted Pacific Plate redrawn after Zou et al. (2008).*

Lei & Zhao (2005) suggest that the reason for extensive magmatic activity in NE China is related to asthenospheric upwelling and circulation under the region due to subduction at the Japan/Ryukyu volcanic arcs. Zou *et al.* (2008) reviewed and

improved this argument by suggesting that piling-up and upward thickening of the subducted Pacific slab underneath NE China may cause upwelling in the asthenosphere and induce decompression melting (Fig. 2.8). Indeed, mantle upwelling centeres under the East China Sea, and causing lateral mantle movement was modeled by Toh & Honma (2008) using magnetovariational anomalies and on tomographic images (Li *et al.*, 2000) Jeju appears to lie above a relatively warmer window of mantle. However, the presence of the subducted Pacific Plate between the 440 and 660 km discontinuities beneath NE Asia forms a mechanical boundary that would obstruct any lower mantle plume from causing melting in the upper mantle.

Volcanism on Jeju occurs on a central volcano and numerous monogenetic centres surrounding it, and is volumetrically larger than other centres in NE China (e.g. Wudalianchi), that may be associated with small lava fields, but not to large-volume lava effusion forming composite central shields. This may suggest that there is some tectonic or source control on the magmatic plumbing system that directs output to the Jeju Island region, or generates larger melt volumes in the core of the system. The existence of a (or several?) magma chamber(s) or storage and evolution area(s) beneath Jeju Island has been suggested by Eom *et al.* (2007) based on the presence of gabbroic and pyroxene + plagioclase cumulate xenoliths in erupted alkali basalts. A low resistivity anomaly in the generally more resistive basement was detected at depths of up to 10 km under Mount Halla and interpreted to represent either a volcanic plumbing system or a region of fracturing filled with seawater/hydrothermal fluids (Lee *et al.*, 2009).

Chapter 3

Methodology

This chapter presents the sampling and analytical methodologies used throughout this study.

3.1 Sampling

3.1.1 Field techniques

A number of small-volume (<0.1 km^3) monogenetic eruptions within the Jeju Island Volcanic Field were selected for detailed sampling, based on the quality and availability of outcrop in order to examine the fullest-possible stratigraphic sequence of each eruption. Juvenile material was selected in the field based on density, vesicularity, morphology and preservation characteristics. Primary magmatic lapilli have higher vesicularity compared to accidental fragments of lava derived from the basement, consequently they are lighter and often less competent and easily fragmented. They also show outer textures and particle shapes consistent with primary late stage expansion, travel through the air or impact on the ground. Carful examination in the laboratory excluded any coated or armoured particles (i.e., recycled) from analysis. Juvenile clasts have black, glassy groundmass and microvesicularity, in contrast to crystalline lava clasts, which are generally paler grey coloured and are dense, with few smooth rounded macro-vesicles. Coarse juvenile lapilli and bombs have cauliflower shapes, and sub-rounded or angular particles were avoided as possible reworked or country rock clasts. Bombs within bomb-sags also indicate direct provenance from the eruption rather than reworking on the flanks of the volcano. Intensely mud-coated lapilli were not collected as this indicates within-vent recycling, or post-depositional reworking. Lapilli with visibly different textural domains (colour and crystallinity) were also sampled and noted in the field, unless insufficient material for either domains was available, as in the case of coated lapilli.

Where it is not specifically indicate, samples are numbered in stratigraphic order (from lower to higher).

Drill core lavas, surface lava flows and domes were sampled by breaking c. 1 kg rock samples with a geological hammer or sledgehammer. The sample was then reduced in size to remove surface contaminant (e.g. soil, oxidized surfaces) or vegetation (e.g. lichens, moss). Samples were securely stored in zipable plastic bags and shipped to New Zealand. Samples are generally numbered in inverse stratigraphic order (from surface to bottom).

3.1.2 Laboratory techniques

Coarse lapilli and bomb fragments were cleaned with a brush and repeatedly washed in an ultrasonic bath in weak HCl solution followed by distilled water. Fine lapilli were further discriminated by hand-picking based on colour, vesicularity and surface texture. Samples where more than one textural type was found were divided and both types were prepared for analysis. Fine lapilli were subsequently washed in an ultrasonic bath in weak HCl solution followed by distilled water.

Lava samples or large bomb fragments were cut with a diamond saw to remove surface contaminants. Specimens were subsequently crushed using a steel crusher and chips free of saw-blade or crusher-plate marks were handpicked and 20 to 50 g aliquots milled in a tungsten carbide ring grinder for 3x20 seconds. Both crusher and ring grinder were thoroughly cleaned with compressed air and acetone between samples. The resulting powders were stored in airtight 50 cl cups.

Feldspar separates for isotopic analyses were hand picked from crushed and sieved material (<2mm).

3.2 XRF analytical procedure

H_2O and LOI were measured by heating ~4 g of powdered sample for 12 hours at 105 ºC and 1000 ºC respectively. 2 g of dried sample powder were weighed together with

6 g of SPECTRACHEM 12-22 flux and the mixture fused in Pt crucibles and cooled to a glass disc. Major element concentrations were measured by X-ray fluorescence (XRF; Siemens SR3000 spectrometer) at the University of Auckland using standard techniques. Major and minor elements (Si, Ti, Al, Fe, Mn, Mg, Ca, Na, K, P,) were determined as oxide components using methods similar to those described by Norrish & Hutton (1969). In general, precision for each major or minor element is better than ±1% (1σ) of the reported value. Where Fe is reported as both Fe_2O_3 and FeO, the oxides were calculated based on the total molar amount of Fe based on the total Fe_2O_3 given in the raw data (raw data in Appendix O).

XRF trace element (V, Cr, Ni, Cu, Zn, Rb, Sr, Zr, Nb, Ba) measurements used the glass discs used for major element determination. A suite of 36 international standards were used for calibration, and Siemens SPECTRA 3000 software was used for data reduction. The Compton scatter of X-ray tube RhKb1 emission was used to correct for mass attenuation, and appropriate corrections were used for those elements analysed at energies below the Fe absorption edge. Theoretical detection limits are of 1-2 ppm. Reproducibility is <5% (2σ) for all elements except Ba.

3.3 LA-ICP-MS analytical procedure

Laser-Ablation Inductively-Coupled-Plasma Mass-Spectrometry (LA-ICP-MS) analysis for a larger group of trace elements was carried out at the Research School of Earth Sciences, Australian National University (ANU), using Excimer LPX120 laser (193 nm) and Agilent 7500 series mass spectrometer following the method of Eggins *et al.* (1998). For this work, the same fused glass discs as for XRF were prepared as a multi sample polished mount. Samples were run in batches of 15 using NST612 glass standard at the beginning and end of each run to calibrate. Standard BCR-2 was also run with each batch to monitor analytical performance. The average of 59 repeat analyses of standard BCR-2 (Table 3.1) as well as duplicate analysis of a tephra sample (Electronic Appendix I) indicate precision of <4% (RSD) and accuracy better than 5% at the 95% confidence level for most elements. Comparison of USGS standard values (Wilson, 1997) and ANU internal values for BCR-2 reveals the variability in element concentrations analysed by different laboratories and different

techniques. By increasing the number of repeated analyses, the average concentration is likely to converge towards the standard value, and standard deviation (σ) will decrease.

Table 3.1. *Comparison of measured BCR-2 standard data with reference values from USGS (Wilson, 1997) and ANU internal values.*

Element	Average of 59 analyses	Standard deviation (±)	USGS standard values	Standard deviation (±)	ANU internal standard
Be	2.08	0.18			
Sc	54.18	0.05	33	2	
V	418.29	9.32	416	14	429
Cr	18.22	0.58	18	2	
Co	37.76	1.07	37	3	
Ni	13.52	0.75			13.3
Cu	18.35	0.33	19	2	34.1
Zn	134.35	23.24	127	9	129
Ga	21.56	0.29	23	2	21.9
Rb	45.44	2.31	48	2	48.1
Sr	329.06	13.79	346	14	335
Y	32.89	1.74	37	2	39.4
Zr	171.48	9.85	188	16	201
Nb	12.28	0.17			13.1
Cs	1.08	0.07	1.1	0.1	1.18
Ba	662.48	14.88	683	28	672
La	25.26	0.82	25	1	24.4
Ce	52.71	1.07	53	2	51.9
Pr	6.70	0.19	6.8	0.3	6.48
Nd	29.13	1.13	28	2	28.4
Sm	6.43	0.15	6.7	0.3	6.58
Eu	1.90	0.06	2.0	0.1	1.98
Gd	6.65	0.25	6.8	0.3	6.67
Tb	1.00	0.04	1.07	0.04	1.06
Dy	6.32	0.32			6.33
Ho	1.27	0.07			1.32
Er	3.59	0.16			3.73
Tm	0.51	0.03			
Yb	3.41	0.18	3.5	0.2	3.34
Lu	0.50	0.03	0.51	0.02	0.5
Hf	4.61	0.26	4.8	0.2	4.9
Ta	0.80	0.04			0.81
Pb	11.00	0.83	11	2	10.3
Th	5.94	0.26	6.2	0.7	6.03
U	1.65	0.03	1.69	0.19	1.62

3.3.1 Comparison of analytical techniques

There is a very close correlation (r^2 mostly >0.95, Electronic Appendix I) between those trace element abundances determined by XRF and those by LA-ICP-MS. Additionally, most elements correlations have intercept near 0. This comparison provides a check on the analytical process. LA-ICP-MS was the preferred analytical

technique for trace element measurement rather than Dissolution ICP-MS (e.g. Jenner et al., 1990) because of the large number of collected samples. LA-ICP-MS allows quicker analytical work, yet retaining high data reliability (Table 3.1).

When the data is used in a comparative fashion and to identify trends, the minor discrepancies present between the XRF and LA-ICP-MS dataset do not influence data interpretation. For quantitative modeling, the LA-ICP-MS data is preferred to the XRF data because of the lower detection limits, more comprehensive element suite and better precision of the technique (Table 3.1).

3.4 Microscopy and electron microprobe analyses

3.4.1 Thin section preparation and microscopy

Lava and lapilli samples were cut into c. 1 cm thick blocks to fit 27x46 mm petrographic slides using a coarse rock saw. Progressively finer silicon carbide grits (200-400-600 grit) were used to grind the basal surface of the rock sample and a 200 grit to roughen one surface of the petrographic slide. A two component epoxy (EpoTek) was used to impregnate porous samples, which, once dried, were re-ground with 200-400-600 grit. The same two component epoxy was then used to glue the basal surface of the blocks to the pre-roughened petrographic slide surface. After 24 hours the blocks were cut close to the slide and the thin-section was ground to c. 50 μm thickness using varying sizes of silicon carbide. For use on the electron microprobe thin-sections were polished using a Struers Planopol-3 and increasingly finer grades of diamond paste (6, 3 and 1 μm).

Thin-sections were observed with a Nikon Eclipse E600 POL microscope fitted with a Nikon DS-U1 digital camera and the captured images were elaborated with NIS-Elements version 3.22.00. Reported mineral and vesicles modal abundances are made from visual estimation.

3.4.2 EMP analyses

Mineral analyses were obtained by electron microprobe. The instrument used was a JEOL JXA-840A at the University of Auckland using LINK systems LZ5 detector, QX2000 pulse processor and ZAF-4/FLS matrix correction software. Standard operating conditions were an accelerating voltage of 15 kV, beam current of 0.5 nA, beam diameter of 5 μm and a live count time of 100 s. Analytical precision was estimated by replicate analyses of mineral standards as (σ) ≤3% for elements present in abundances >1 wt%. A complete set of mineral analyses is provided in Electronic Appendix N.

Calibration of silicate mineral analyses used a suite of Astimex™ mineral standards (selected analyses are reported in Table 3.2). Oxide analyses were standardised using Astimex™ magnetite standards. A calibration factor for oxide analyses was employed to correct FeO (total) and this factor was assumed to be constant throughout the analyses period (R. Sims personal communication 2009). As part of an inter-laboratory EMP project (64 participating laboratories) basaltic glass was analysed with deviation from its accepted composition listed in Table 3.3. Precision for electron microprobe analyses are given in Table 3.4.

Table 3.2. *Average measurements of Astimex™ mineral standards (number of analyses in brackets) and comparison with Detection limit of element oxides measured at the Electron Microprobe (University of Auckland).*

Mineral	SiO_2	Al_2O_3	FeO	MnO	MgO	CaO	Na_2O	K_2O
Albite (24)	68.23	19.32				0.18	11.52	0.23
Astimex™ Albite	68.52	19.54				0.13	11.59	0.22
Olivine (12)	41.80		7.22	0.10	50.50			
Astimex™ Olivine	41.58		7.51	0.10	50.43			
Almandine (2)	39.79	22.45	23.33	0.47	10.6	4.08		
Astimex™ Almandine	39.19	22.05	23.27	0.59	10.7	4.2		
Sanidine (1)	64.01	18.36	0.24				2.93	12.23
Astimex™ Sanidine	64.67	18.76	0.18				3.01	12.11

Table 3.3. *Deviation of basaltic glass composition from accepted values.*

SiO_2	TiO_2	Al_2O_3	FeO	MnO	MgO	CaO	Na_2O	K_2O	P_2O_5
-0.18	0.12	-0.05	-0.04	-0.01	0.17	-0.02	0.05	0.02	0.01

Table 3.4. *Precision of element oxides measured at the Electron Microprobe (University of Auckland).*

Precision	SiO_2	TiO_2	Al_2O_3	FeO	MnO	MgO	CaO	Na_2O	K_2O	P_2O_5	Cr_2O_3	NiO
1σ (wt%)	0.11	0.08	0.06	0.07	0.07	0.07	0.04	0.11	0.03	0.07	0.06	0.10
3σ (wt%)	0.32	0.23	0.18	0.20	0.20	0.21	0.13	0.32	0.10	0.20	0.17	0.30

Some analyses have relatively high totals due to non-linear SiO_2 calibration; however this does not affect the quantitative analysis and relative concentration of major oxides (R. Sims personal communication 2012). The number of cations per formula unit (Electronic Appendix N) mostly fall within 0.02 of the expected number, providing a test for the analytical method and the oxide concentrations. Very few analyses have cations sums more or less than ±0.5 of the expected whole digit, and these are generally from resorbed/altered/rim crystal analyses. The analyses chosen for geochemical modeling are within the majority of crystal compositions from the particular magmatic stage that is investigated, and are therefore considered reliable.

3.5 Sr-Nd-Pb isotopes analytical procedure

Sr-Nd-Pb isotopic compositions were acquired at the University of Melbourne, using procedures similar to those described in Maas *et al.* (2005). All analyses were carried out on carefully handpicked 1-2 mm chips free of visible alteration; a few samples were also analysed as powders (see procedure above). After acid leaching (6M HCl, 100^{o}C, 60 min), the samples were dissolved in closed Savillex beakers on a hotplate (2 ml of 3:1 HF-HNO_3 for 2 days at 110^{o}C and 6M HCl for 1 day). Pb, Nd and Sr were extracted using a combination of anion exchange (AG1-X8, 100-200 mesh, HBr-HCl) and EICHROM RE, LN and SR resin chromatography (Manhes *et al.*, 1978; Pin *et al.*, 1994; Pin & Santos-Zalduegui, 1997). Total analytical blanks (<100 pg) were negligible relative to the amounts of analyte material available (e.g. >100 ng Pb in all cases).

Isotopic analyses were carried out on a NU Instruments 'Plasma' multi-collector ICP-MS coupled to a CETAC Aridus desolvation unit; samples were aspirated using a Glass Expansion 'Opalmist' teflon nebuliser (40 μl/min uptake rate), which produced sensitivities in the range of 50-60 V/ppm Sr, Nd or Pb. Data were acquired for 300-

600 sec, for typical signals of ~8 V total Sr, 13-21 V total Nd and 7-12 V total Pb produced from 100-160 ppb analyte solutions. Instrumental mass bias for Sr and Nd was corrected by internal normalization to $^{86}Sr/^{88}Sr=0.1194$ and $^{146}Nd/^{145}Nd=2.0719425$ (equivalent to $^{146}Nd/^{144}Nd = 0.7219$, Vance & Thirlwall, 2002), using the exponential law. Typical internal precisions (2σ) were ≤0.000020 for $^{87}Sr/^{86}Sr$ and ±0.000010 for $^{143}Nd/^{144}Nd$; external precisions (2σ of multiple analyses) are ≤0.000040 (Sr) and 0.000020 (Nd). Data are reported relative to SRM987 = 0.710230 and La Jolla Nd = 0.511860. The results for secondary standards (JNd-1, BCR-2, BHVO-2, MSS - modern seawater Sr) obtained in the course of this work are identical within errors to their reference ratios as determined by TIMS (see Table 3.5). eNd describes the deviation (in parts of 1 in 10000) of $^{143}Nd/^{144}Nd$ from modern chondritic Bulk Earth (CHUR, 0.512638).

Table 3.5. *Analyses of standard data and comparison with reference values (in bold).*

Sample	$^{87}Sr/^{86}Sr \pm 2\sigma$	$^{143}Nd/^{144}Nd \pm 2\sigma$	$^{206}Pb/^{204}Pb$	$^{207}Pb/^{204}Pb$	$^{208}Pb/^{204}Pb$
BCR2	0.704995 ± 18	0.512647 ± 12	18.760	15.620	38.721
BCR2	0.704980 ± 11	0.512636 ± 10	18.761	15.624	38.738
BCR2	0.704974 ± 14		18.757	15.615	39.713
BCR2	0.705013 ± 14		18.764	15.623	38.740
BCR2 reference	**0.704958**[a]	**0.512633**[a]	**18.750**[b]	**15.615**[b]	**38.691**[b]
BCR2 reference			**18.758**[c]	**15.628**[c]	**38.752**[c]
BCR2 reference			**18.765**[d]	**15.628**[d]	**38.752**[d]
BHVO2	0.703457 ± 16	0.512983 ± 08	19.628	15.524	38.213
BHVO2	0.703471 ± 14				
BHVO2 reference	**0.703435**[a]	**0.512957**[a]	**18.641**[b]	**15.538**[b]	**38.228**[b]
BHVO2 reference	**0.703455**[c]		**18.652**[c]	**15.539**[c]	**38.245**[c]
BHVO2 reference			**18.649**[d]	**15.540**[d]	**38.249**[d]
EN-1	0.709170 ± 15				
EN-1 reference	**0.709160**[e]				
JNd-1		0.512130 ± 09			
JNd-1		0.512114 ± 15			
JNd-1		0.512108 ± 08			
JNd-1 reference		**0.512117**[f]			

[a]Raczek *et al.* (2003)
[b]Woodhead & Hergt, (2000)
[c]Elburg *et al.* (2005)
[d]Baker *et al.* (2004)
[e]McArthur *et al.* (2006)
[f]Tanaka *et al.* (2000)

Instrumental mass bias observed during Pb isotope runs was corrected using the thallium-doping technique of Woodhead (2002). Mass bias factors for each Pb isotope ratio were derived from Pb-Tl mass bias correlation lines based on results from >200 runs of SRM981 carried out over several years. $^{205}Tl/^{203}Tl$ in the running solution is assumed to be 2.3871, while SRM981 is assumed to have the following Pb isotope ratios: $^{206}Pb/^{204}Pb$ 16.935, $^{207}Pb/^{204}Pb$ 15.489, $^{208}Pb/^{204}Pb$ 36.701. The use of a mass bias line based on long-term rather than 'within-session' standard data allows the SRM981 results obtained in each session to be used as independent quality checks. External precisions for mass bias-corrected $^{206}Pb/^{204}Pb$, $^{207}Pb/^{204}Pb$ and $^{208}Pb/^{204}Pb$ ratios are ~0.025-0.05% (2σ); this is confirmed by the results for 12 runs of SRM981 and by multiple runs for several samples (Table 3.6). BCR-2 and BHVO-2 yield results consistent with reference data from double spike TIMS and MC-ICPMS (see Table 3.5).

Table 3.6. *Comparison of duplicate chips and powder analyses for selected samples.*

Sample	$^{87}Sr/^{86}Sr \pm 2\sigma$	$^{143}Nd/^{144}Nd \pm 2\sigma$	$^{206}Pb/^{204}Pb$	$^{207}Pb/^{204}Pb$	$^{208}Pb/^{204}Pb$
U1-23	0.704403 ± 14	0.512801 ± 10	18.942	15.644	39.523
U1-23 duplicate		0.512809 ± 10	18.935	15.636	39.496
U1-23 powder	0.704409 ± 19	0.512800 ± 08	18.948	15.645	39.538
YM10	0.704605 ± 15	0.512805 ± 09	19.008	15.639	39.513
YM10 duplicate		0.512808 ± 08			
YM10 powder	0.704640 ± 13	0.512784 ± 10	19.012	15.639	39.516
BY04	0.704102 ± 18	0.512826 ± 07	19.008	15.640	39.600
BY04 duplicate	0.704098 ± 14				
SK05	0.704074 ± 14	0.512814 ± 11	19.061	15.642	39.654
SK05 duplicate	0.704145 ± 09				
SK09	0.704062 ± 14	0.512832 ± 10	19.057	15.641	39.650
SK09 duplicate	0.704107 ± 14				
SK26	0.704240 ± 15	0.512796 ± 09	19.036	15.653	39.637
SK26 duplicate	0.704266 ± 14		19.033	15.650	39.628
SK26 powder	0.704300 ± 17	0.512808 ± 10	19.032	15.654	39.633

Three samples were analysed as both chips and powders (U123, YM10, SK26, all samples acid-leached prior to dissolution). In all cases, measured isotope ratios in chips and powders were the same within errors, indicating negligible sample

heterogeneity at the sampled level, and an absence of detectable contamination during milling (Table 3.6).

The ratios measured in a single run of BHVO-2 (18.628, 15,524, 38.213) are somewhat lower than reference values (Table 3.5). Several studies have reported significant Pb isotopic variation in BHVO-2, suggesting some intrinsic Pb isotope heterogeneity in this standard (e.g. Elburg *et al.*, 2005): this would suggest that BHVO-2 is unsuitable for testing of Pb isotope procedures.

Table 3.7. *Original and repeated analyses for selected samples.*

	original		repeats	
Sample	$^{87}Sr/^{86}Sr \pm 2\sigma$	$^{143}Nd/^{144}Nd \pm 2\sigma$	$^{87}Sr/^{86}Sr \pm 2\sigma$	$^{143}Nd/^{144}Nd \pm 2\sigma$
DB10	0.704858 ± 15	0.512761 ± 08	0.704891 ± 15	0.512771 ± 06
U1-25	0.704442 ± 14	0.512796 ± 07	0.704445 ± 17	0.512805 ± 09
YM04	0.704627 ± 15	0.512792 ± 10	0.704621 ± 15	0.512808 ± 11
EP28	0.704559 ± 19	0.512733 ± 07	0.704542 ± 13	0.512738 ± 10
E33	0.704642 ± 15	0.512709 ± 09	0.704653 ± 16	0.512739 ± 07
E36	0.704899 ± 17	0.512711 ± 12	0.704908 ± 17	0.512734 ± 08

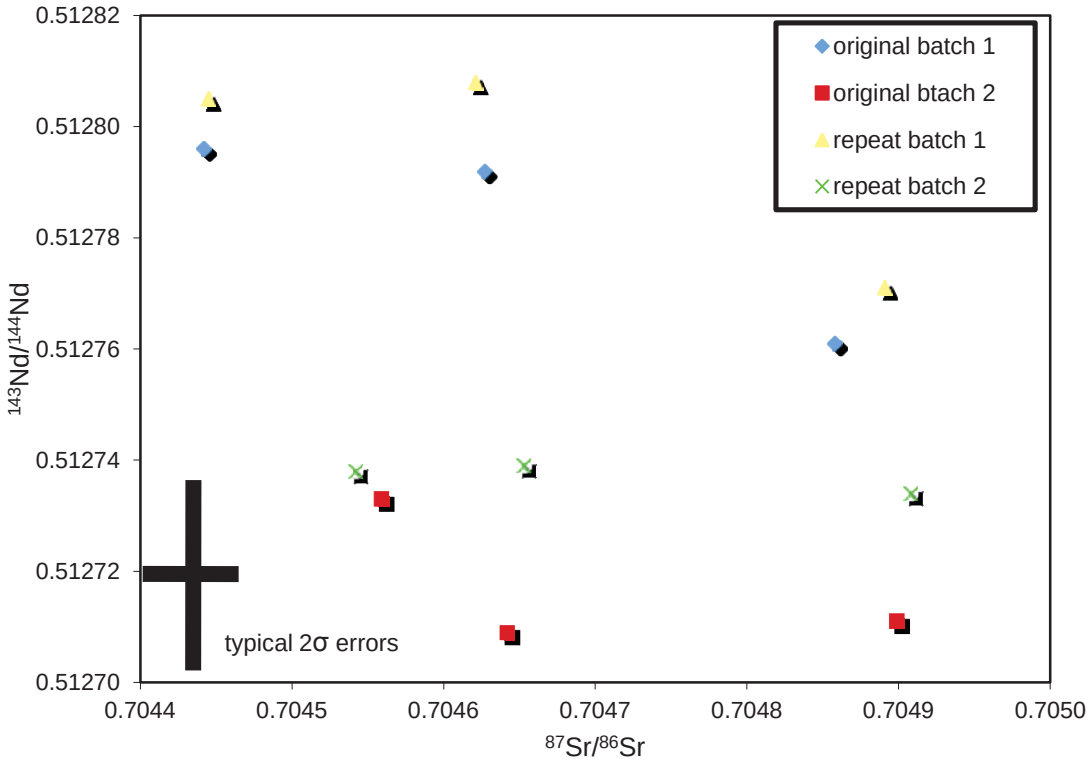

Figure 3.1: *Comparison of repeat analyses for batch 1 (small volume eruptions) and batch 2 (large volume lavas).*

Sr-Nd-Pb isotopes were analysed in two batches. The first batch included samples from small volume eruptive centres and was completed in July 2010. The second batch was analysed in March 2011 and included samples from large volume lavas. Following the observation of a shift towards lower $^{143}Nd/^{144}Nd$, three samples from each batch were reanalysed to investigate analytical reproducibility. The results are reported in Table 3.7 and plotted in Figure 3.1. The repeat analyses confirm that the shift is not due to analytical uncertainty.

Chapter 4:

Petrogenesis and Evolution of a Single Monogenetic Vent

This chapter presents and discusses the chemical evolution of a single monogenetic vent within the Jeju Island Volcanic Field. Detailed chemical sampling reveals two chemical stages with different compositions, each of which had independent internal controlling factors (P, T, X). The termination of the eruption of the first stage magma was linked to, or facilitated initiation of the second stage magma eruption.

4.1 Introduction

Monogenetic eruptions are relatively short-lived (days/years) volcanic events that occur separated by hundreds to thousands of years, over the lifetime of a volcanic field that may be millions of years long. Due to the scarcity of direct observation of such events, understanding of the factors controlling them must be sought in the resulting volcanic deposits. Detailed sampling of pyroclastic successions for the purpose of chemical analysis has the potential to yield precious information on the chemical evolution of magma batches that feed monogenetic eruptions. In this and the next two chapters, three different approaches were followed to gain a comprehensive picture of the behaviour and controlling factors of monogenetic eruptions.

This chapter consists of the manuscript "*Mechanisms driving polymagmatic activity at a monogenetic volcano, Udo, Jeju Island, South Korea*" by: Marco Brenna, Shane J. Cronin, Ian E. M. Smith, Young Kwan Sohn and Karoly Németh, published in *Contributions to Mineralogy and Petrology* (160, 931-950, April 2010; DOI 10.1007/s00410-010-0515-1). A copy of the published article is attached to this thesis as Electronic Appendix A and the supplementary data file is attached as Electronic Appendix B. This manuscript is devoted to the investigation of a single eruption within the Jeju Island Volcanic Field, the Udo Volcano. The study of this single but complex eruption reveals characteristics of the mantle under Jeju, in which the

magma feeding the eruption was sourced. It also reveals the within-batch evolutionary processes that lead to chemical variability

The contributions of each author to the study were as follows:

Marco Brenna:	Principal investigator:	
	Carried out:	Field investigations and sampling
		Petrographic observations
		Electron microprobe analyses
		Chemical data interpretation and modelling
		Manuscript preparation and writing
Shane J. Cronin:	Chief advisor:	
	Aided the study by:	Assisting in the field and sampling
		Editing and discussion of the manuscript
Ian E. M. Smith:	Advisor:	
	Aided the study by:	Assisting in the field and sampling
		Providing chemistry data
		Discussion of results and modelling
		Editing and discussion of the manuscript
Young Kwan Sohn, Karoly Németh:		
	Advisors:	
	Aided the study by:	Assisting in the field and sampling
		Editing and discussion of the manuscript

4.2 Mechanisms driving polymagmatic activity at a monogenetic volcano, Udo, Jeju Island, South Korea

Marco Brenna[1], Shane J. Cronin[1], Ian E. M. Smith[2], Young Kwan Sohn[3], Karoly Németh[1]

[1]*Volcanic Risk Solutions, Massey University, Palmerston North, New Zealand*
[2]*School of Geography, Geology and Environmental Science, The University of Auckland, Auckland, New Zealand*
[3]*Department of Earth & Environmental Sciences, Gyeongsang National University, Jinju, South Korea*

4.2.1 Abstract

High-resolution, stratigraphically-ordered samples of the Udo tuff cone and lava shield offshore of Jeju Island, South Korea, show complex geochemical variation in the basaltic magmas that fed the eruption sequence. The eruption began explosively, producing phreatomagmatic deposits with relatively evolved alkali magma. The magma became more primitive over the course of the eruption, but the last magma to be explosively erupted had shifted back to a relatively evolved composition. A separate subalkali magma batch was subsequently effusively erupted to form a lava shield. Absence of weathering and only minor reworking between the tuff and overlying lava implies that there was no significant time break between the eruption of the two magma batches. Modelling of the alkali magma suggests that it was generated from a parent melt in garnet peridotite at c. 3 to 3.5 GPa and underwent mainly clinopyroxene + olivine ± spinel fractionation at c. 1.5 to 2 GPa. The subalkali magma was, by contrast, generated from a chemically different peridotite with residual garnet at c. 2.5 GPa and evolved through olivine fractionation at a shallower level compared to its alkali contemporary. The continuous chemostratigraphic trend in the tuff cone, from relatively evolved to primitive and back to evolved, is interpreted to have resulted from a magma batch having risen through a single dyke and erupted the batch's head, core and margins respectively. The alkali magma acted as a path opener for the subalkali magma. The occurrence of the two distinct batches

suggests that different magmatic systems in the Jeju Island Volcanic Field have interacted throughout its history. The polymagmatic nature of this monogenetic eruption has important implications for hazard forecasting and for our understanding of basaltic field volcanism.

4.3 Introduction

Basaltic volcanic fields are typically dominated by monogenetic volcanoes that have a lifespan of months to decades and that record spatially and temporally distributed volcanism (Walker, 1993). Such systems may display widely differing magma flux and eruption frequencies (Valentine & Perry 2007). Individual monogenetic (*sensu stricto*) volcanoes within fields are regarded as being geochemically and volcanologically simple, at least in comparison to long-lived polygenetic centres where greater degrees of magma evolution are expected.

Detailed chemical investigation of individual monogenetic volcanoes can yield insights into the generation of magma in the mantle and the processes affecting the magma during ascent. The typically low magma volumes reach the surface with little fractionation or interaction with the crust (Blondes *et al.*, 2008, Németh *et al.*, 2003, Reiners, 2002, Smith *et al.*, 2008, Strong & Wolff, 2003, Valentine & Perry, 2007) due to relatively fast ascent rates (Demouchy *et al.*, 2006, Spera, 1984), and over relatively short periods of time, hence lending themselves to small-scale investigations. By sampling eruptive sequences in great detail it is possible to observe magmatic evolution over the short period of a monogenetic eruption, such as in the Auckland Volcanic Field, New Zealand (Smith *et al.*, 2008), in the Big Pine Volcanic Field, California (Blondes *et al.*, 2008) and at Parícutin and Jorullo volcanoes, Mexico (Erlund *et al.*, 2010, Luhr, 2001, Luhr & Carmichael 1985, McBirney *et al.*, 1987). These studies have shown that single eruptive centres can be fed by magma batches that display varying degrees of chemical evolution resulting from processes within the source and conduit/plumbing system. Conversely, other centres do not display significant chemical variability during consecutive eruption stages despite varying eruption styles, such as Lathorp Wells, Nevada (Valentine *et al.*, 2007). At Crater Flat, Nevada, separate cones and lava fields with relatively constant chemical

composition and originally interpreted as derived from polygenetic activity (Bradshaw & Smith, 1994), were subsequently re-interpreted, based on field relationships, to have erupted over relatively short time spans (Valentine *et al.*, 2006).

Other types of magmatic variation in monogenetic volcanoes have been noted by Strong & Wolff (2003), who, in the southern Cascade arc, found that the chemical composition of scoria cones may differ from their related and subsequently erupted lava shields, and hence related the variation to different source compositions. Chemical variability in other intraplate basaltic centres (Reiners, 2002) has been attributed to mixing of different magmas derived from distinct sources. Mixing of similar magmas at various stages of evolution may also give rise to chemical variability. For example, bimodal magmatism in the Waipiata Volcanic Field, New Zealand, and the Miocene-Pliocene volcanic fields in the Pannonian Basin, western Hungary, was proposed to be controlled by fractionation and mixing processes (Németh *et al.*, 2003). In these cases initial eruption of tephrite was interpreted to have derived from stalling and fractionation of early-formed basanitic magma, which subsequently intersected with, and mixed with, ascending basanite that initiated eruption of the fractionated magma. Chemical variability of monogenetic centres in the Trans-Mexican Volcanic Belt instead suggests a greater involvement of the continental crust, and could be linked to the early stage evolution of composite volcano growth (Siebe *et al.*, 2004).

These studies provide evidence for chemical complexities in monogenetic (*sensu lato*) volcanoes, given that eruptions may be fed by magma batches derived from different sources. They also suggest that a detailed investigation of an individual volcano within a monogenetic field might provide high-resolution information on the nature of magma generation, evolution and mixing processes that characterise the behaviour in the field as a whole. If more than one magma type is involved, it is moreover important to determine how these may interact and behave at depth, which will ultimately control the resulting eruption and final volcanic landform. Involvement of different magmas erupted from a single vent over a relatively short time interval may have repercussions on the way we perceive volcanic hazards, given that the physical behaviour of the volcano may change through the course of the eruption.

In this paper we present a high-resolution, stratigraphically controlled geochemical investigation of the Udo tuff cone and lava shield, Jeju Island, South Korea, which is a monogenetic volcano displaying complex chemical behaviour. This reveals insights into magma generation in the c. 1700 km^2 Jeju Island Volcanic Field, which comprises over 300 distributed monogenetic centres, plateau lavas and a concurrent central composite volcano.

4.4 Geological setting and field relationships

Jeju Island is situated on continental crust c. 35 km thick (Yoo *et al.*, 2007) and is approximately 600 km behind the subduction front, where the Philippine Sea Plate is subducted perpendicularly to the front under the Eurasian/Amurian plates (Kubo & Fukuyama, 2003) and generates the Ryukyu arc (Fig. 4.1). However, the Jeju Island Volcanic Field is unrelated to modern subduction, although its mantle sources are metasomatised by Mesozoic subduction-derived fluids (Kim *et al.*, 2005, Tatsumi *et al.*, 2005). Commencement of distributed, small-volume volcanic activity is recorded in the volcaniclastic Seoguipo Formation in the subsurface (Sohn *et al.*, 2008) and most recent activity occurred in 1002 and 1005 AD (Lee & Yang, 2006). Paleontological and magnetostratigraphic studies of the Seoguipo Formation suggest that the Plio-Pleistocene boundary is intercalated within the lowermost part of the Formation (Kang, 2003, Kim & Lee 2000, Yi *et al.*, 1998). Magmatic activity on Jeju has therefore been active during the past c. 1.8 Ma. The chemical compositions of magmas erupted in the field as a whole varies widely from alkali to subalkali basalt, trachyandesite and trachyte (e.g. Tatsumi *et al.*, 2005).

Udo Volcano is an example of a single vent system within the Jeju Island Volcanic Field. Udo Volcano forms an island, c. 3 x 4 km across, c. 3 km off the east coast of Jeju, consisting of a tuff cone, spatter mound and a lava shield (Fig. 4.1), allowing the investigation of different eruptive products unambiguously derived from a single vent. It was targeted for detailed study because the tuff cone is well exposed by wave action, making it possible to sample material representing the majority of the eruption

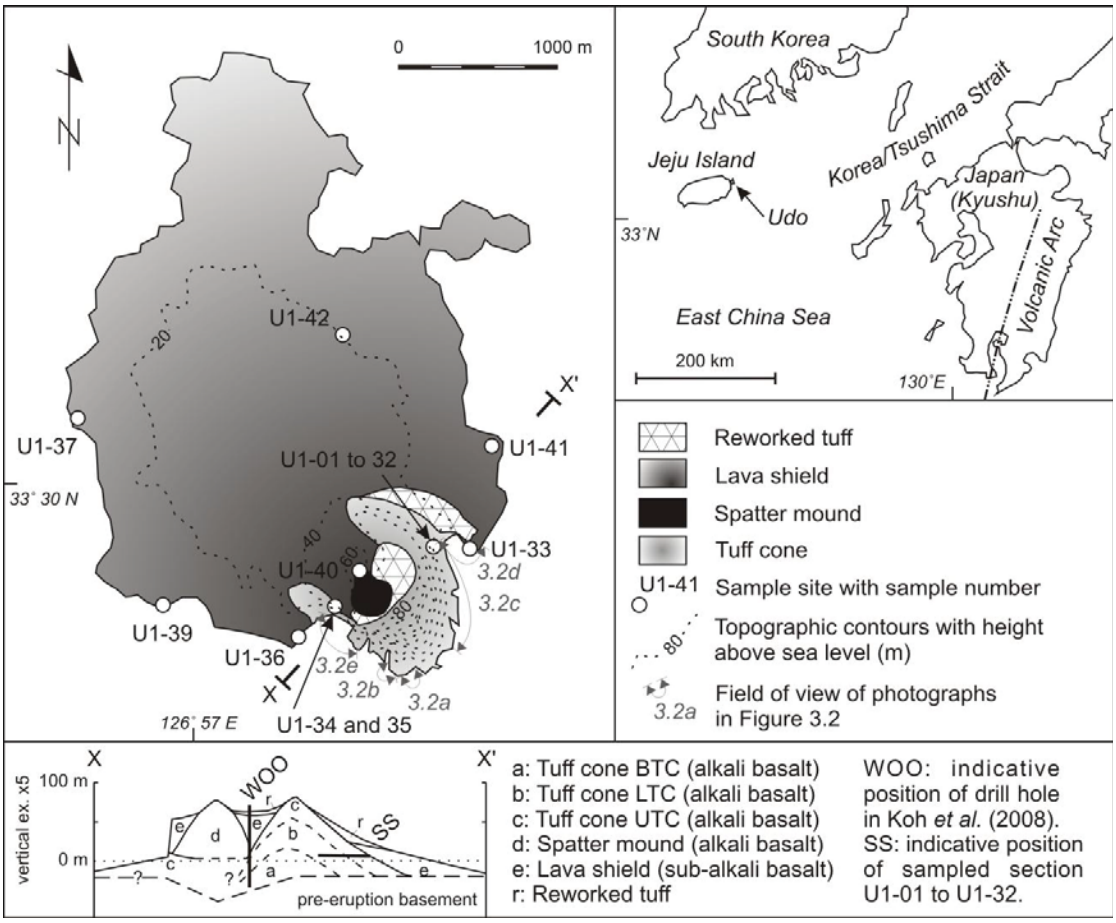

Figure 4.1: *Geology of Udo Volcano after Sohn & Chough (1993), cross section based on drill hole data in Koh et al. (2008) showing indicative sampled sequence (SS), see Figure 4.2 for more detailed position of tuff cone samples. BTC: basal tuff cone, LTC: lower tuff cone, UTC: upper tuff cone. Cross section is x5 vertically exaggerated.*

sequence. Udo Volcano has a single main vent situated in the southeastern part of the Island (Fig. 4.1). A horseshoe-shaped tuff cone open towards the northwest contains a nested, rounded spatter mound and is partially filled by ponded lava. A series of flows form a lava shield to the northwest of the vent. Dating of the lava shield rocks gave a K-Ar age of 114 ± 3 ka (Koh *et al.*, 2005), whereas dates of core samples gave $^{40}Ar/^{39}Ar$ ages of 102 ± 69 ka for a tholeiitic andesite lava flow at an elevation of 25.5 m a.s.l. and 86 ± 10 ka for an alkali basalt 7.5 m a.s.l. part of the spatter mound or associated lava (cf. cross section in Figure 4.1; Koh *et al.*, 2008). An apron of reworked tephra from the tuff cone overlies the lava shield to the northeast of the tuff cone and inside it (Fig. 4.1). An estimate of the eruptive volumes, taking into account the height and topographic surface of the Island, is c. 0.06 km^3 for the tuff stage and c. 0.65 km^3 for the lava shield stage. Note that these are minimum volume estimates, as

they do not take into account tephra distributed in eruption plumes and magma frozen in the plumbing system. Despite the imprecision inherent in defining the actual thickness of all units, it is fair to assume that the volume of the lava shield stage was one order of magnitude larger than that of the tuff cone stage of this eruption.

Older basaltic lava flows from the Jeju plateau lava stage (c. 100 m thick), unconsolidated silty sediments (c. 150 m thick), as well as felsic ignimbrite and lava units underlie the volcanic complex (Sohn & Chough, 1993). A depth of c. 23 m below sea level to the basal contact of the tuff in drill core (Koh *et al.*, 2008) is probably an overestimate given that the core was taken within the tuff cone crater, and hence may comprise part of the diatreme. A depth to basement of c. 15 m below sea level is more consistent with water depth around Udo Island.

The tuff cone generally comprises steeply inclined (20-30˚) beds of lapilli tuff and tuff that dip radially away from the vent. A detailed sedimentological study of the tuff cone revealed that it formed by a Surtseyan-type eruption, which became drier toward the end of the eruption (Sohn & Chough, 1993). The deposition was mostly accomplished by grain flows of lapilli and blocks in addition to airfall of finer-grained tephra. Absence of marine-reworked deposits suggests that the majority of the tuff cone was constructed subaerially, although the part below the current low tide level may have formed underwater. Common inclusion of acidic volcanic rock fragments (rhyolite and welded tuff) that were most likely derived from the Cretaceous volcanic basement rocks in the eastern Jeju area suggests that the level of hydrovolcanic explosions and the depth of country-rock excavation reached more than 300 m below the present sea level (Sohn, 1996).

Recent observations of the whole tuff cone deposits aboard a boat revealed that the deposits can be divided into three stratigraphic packages that are bounded by distinct truncation surfaces or discontinuities (Fig. 4.2). A basal tuff cone (BTC), exposed only on an inaccessible seacliff exposure (Fig. 4.2a) is interpreted to represent the outward-dipping rim deposit of an early tuff cone on the basis of its bed attitude and geometry and represents c. 15% of the volume of the tuff cone. A lower tuff cone (LTC), exposed extensively but only locally accessible overlies the BTC either conformably or with local truncation. The steeply inclined truncation surface between

BTC and LTC (Fig. 4.2a) is interpreted to have formed by collapse of the inner rim deposit toward the vent associated with gravitational instability of the rim deposit because of differential loading or enlargement of the volcanic conduit (cf. Sohn & Park, 2005) indicating that a stable conduit had not been established yet, resulting in considerable recycling. Due to the mechanism of emplacement during Surtseyan eruptions (Kokelaar, 1983, Németh *et al.*, 2006) it is also likely that deposits more proximal to the vent consist of a greater amount of recycled material (Houghton & Smith, 1993). Therefore sampling of the BTC may not yield significant data. For this reason, and given that the BTC represents a minor portion of the total volume of the tuff cone, lack of samples from this section should not cause a significant drawback for interpreting the chemical history of the volcano. A significant break in time or in eruptive activity is not inferred to have occurred between BTC and LTC because the truncation surface passes laterally into a conformable surface without any signs of erosion (Fig. 4.2a).

The contact between the LTC and the upper tuff cone (UTC) is overall conformable and difficult to identify along the whole tuff cone exposures. The contact is conspicuous only at one locality where the top of the LTC consists of a chaotic deposit of contorted and brecciated strata, suggesting slumping of steep tuff cone deposits by gravitational instability (Sohn & Chough, 1993) and is overlain by the well-bedded deposits of the UTC (Fig. 4.2d). Except for this locality, LTC and UTC can be distinguished only by subtle contrasts in deposit characteristics, the former consisting mainly of planar-bedded lapilli tuff whereas the latter consisting of the alternations of thin-bedded tuff and discontinuous lapilli layers (Sohn & Chough, 1993). A significant break in time or in eruptive activity is hence not inferred to have occurred between LTC and UTC either.

At the eastern end of the tuff cone along the beach (Fig. 4.1, 4.2d, f), the stratigraphic relationship between the tuff cone deposits and the shield-forming lavas could be identified. The tuff cone deposits here are overlain by reworked volcaniclastic deposits with near-horizontal bed attitudes (Fig. 4.2d, f). The reworked deposits are massive to cross-stratified and scour-and-fill-bedded, suggesting emplacement by debris flows and stream or rill flows after the cessation of the tuff cone-forming

Figure 4.2: *Field relationships and tuff cone sampling site. a) shows the sharp discordant contact changing laterally into a conformable one between basal tuff cone (BTC) and lower tuff cone (LTC) and conformable contact with the upper tuff cone (UTC), also seen in b), height of cliff c. 60 m. c) contact between LTC and UTC highlighted to the sampled site, with sample numbers, height to tuff cone rim c. 80 m. d) UTC sampled site and relationship with the overlying lava flow and reworked tuff cone deposits, height of cliff c. 40 m, detail in f) with 1 m for scale. e) Ponded lava inside tuff cone, height of cliff c. 80 m. Note that only*

initial and final sample number for each section is indicated for clarity. Photograph positions indicated in Figure 4.1.

eruption (Sohn & Chough, 1992). Such reworking processes (surface run-off and gully formation) are known to begin almost simultaneously with the cessation of eruption and prior to consolidation of the pyroclastic deposits and, in some cases, during the eruption in tropical or rainy regions (Ferrucci *et al.*, 2005, Németh & Cronin, 2007). The lava flow here is intercalated between the primary tuff cone deposits and the overlying reworked volcaniclastic deposits. Only a minor part of the reworked volcaniclastic deposits are sandwiched between the tuff cone deposits and the lava flow in a wedge-form (Fig. 4.2d, f). This stratigraphic relationship suggests that the lava here was emplaced within days to weeks after the end of the tuff cone-forming eruption. Intra-crater, ponded lava flows are visible on the eroded western side of the tuff cone (Fig. 4.2e). The whole volcanic deposits of the Udo Volcano can thus be considered monogenetic in that it resulted from a small-volume, short lived single eruption without a significant break in eruptive activity.

The term monogenetic has long been used for eruptions generating scoria cones, pyroclastic cones and small lava shields (Wood, 1979 and references therein). The final products of such eruptions (Valentine & Perry, 2007, Verwoerd & Chevallier, 1987, White, 1991) are comparable in geometry and volume to the products of the Udo eruption, which can hence be considered monogenetic. These are relatively short-lived, small-volume eruptions; however, a clear definition of the chemical meaning of "monogenetic" is still lacking, and as will be discussed below, chemical variability may be complex.

4.5 Petrography

Continuous, stratigraphically controlled sampling could be carried out only at the eastern margin of the tuff cone in outward-dipping flank deposits, where the accessible outcrops of the upper part of the LTC and whole UTC are available (Fig. 4.2c, d). Samples were collected at regular intervals of generally 1 to 3 m from lapilli- or bomb-rich beds (Fig. 4.2). A description of bed characteristics and interpreted

emplacement mechanism for each sampled bed is reported in Table B2 in Electronic Appendix B. Juvenile material was selected in the field, based on surface characteristics and density. Coarse lapilli and bombs were selected having cauliflower texture rather than subrounded or angular edges and intensely mud-coated lapilli were removed. Basaltic clasts with black glassy groundmass and microvesicularity were preferred, which made them less dense compared to crystalline lava clasts (which also generally have well formed macro vesicles). For fine lapilli layers, further discrimination and hand picking were carried out in the laboratory after sample cleaning. Samples were collected from the lava shield at different localities (Fig. 4.1); the coordinates are reported in Table B1 in Electronic Appendix B.

Rock textures and mineralogy were observed in thin-sections and mineral identifications were confirmed using an electron microprobe (Electronic Appendix N). The petrography of the sample suite from Udo Volcano varies throughout the succession. In the lower tuff sequence the mineral assemblage is dominated by olivine phenocrysts (3-5%) and plagioclase microphenocrysts (7-8%) in a glassy groundmass. Vesicles (25-40%) are rounded and spherical to elliptical with minor coalescence. Weak flow banding, where present, is defined by plagioclase and elliptical vesicle alignment. Olivine crystals show skeletal form, indicative of rapid growth, and some occur as polycrystalline aggregates. Olivine also occurs with intergrown chrome spinel indicating a xenocrystic origin. Microprobe data indicate that the olivine crystal cores have MgO/FeO ratios similar for most of the olivine in tuff stage samples (ratios of c. 2.5 with some cores >3), whereas rims have MgO/FeO <2. Plagioclase needles have swallow tails form indicating rapid growth.

The phenocryst assemblage in the upper tuff sequence consists of olivine (3-4%), clinopyroxene (<2%) and orthopyroxene (<1%). Plagioclase occurs as microphenocrysts (1-5%) in a glassy groundmass and is rarest in the middle to upper part of the sequence. Vesicles (20-50%) are subrounded to subangular, subspherical and show variable degrees of coalescence. Clinopyroxene occurs as glomerocrysts and as overgrowths surrounding orthopyroxene. It shows twinning and oscillatory and sector zoning. Less often it exhibits greenish cores with colourless overgrowths. Clinopyroxene also forms rims around resorbed and sieve textured cores. Olivine is skeletal. Orthopyroxene is rare and not observed in all samples.

The lava shield mineral assemblage consists of variable amounts of olivine (<5%), Ca-rich and Ca-poor clinopyroxenes (<1%), orthopyroxene (<2%) and plagioclase (<2%) phenocrysts to microphenocrysts in a plagioclase/clinopyroxene/oxide intergranular groundmass (cf. Koh *et al.*, 2005). Olivine shows skeletal growth and weak alteration to orange iddingsite. Orthopyroxene has good cleavage, for which it can easily be distinguished from clinopyroxene, and which makes it similar to orthopyroxene from mantle xenoliths observed in basalts from other eruptive centres on Jeju and described elsewhere (e.g. Yang, 2004). Clinopyroxene crystals show lamellar twinning and also form thin rims around olivine in some cases. Plagioclase phenocrysts are normally zoned and groundmass plagioclase typically shows albite twinning. Minor (<5%) vesicles occur and are generally diktytaxitic (having angular shapes defined by crystal faces) due to the surrounding holocrystalline texture. Fe-Ti oxides in the groundmass occur as dendritic needles. Koh *et al.* (2005) found that in the lava shield, plagioclase in both groundmass and microphenocrysts consists of labradorite (An_{70-50}) with rims generally less anorthitic compared to the core. Their olivine compositions are Fo_{80-77} and the opaque phases are mainly ilmenite.

4.6 Whole rock chemical compositions

Mineral analyses were by electron microprobe. The instrument used was a JEOL JX-5A using a LINK systems LZ5 detector, QX-2000 pulse processor and ZAF-4/FLS matrix correction software. Standard operating conditions were an accelerating voltage of 15 kV, beam current of 0.5 nA, beam diameter of 5 μm and a live count time of 100 s for all mineral analyses. Analytical precision was estimated by replicate analyses of mineral standards as (σ) ≤3% for elements present in abundances >1% wt. The complete list of microprobe analyses is provided in Electronic Appendix N.

For the whole rock analytical work, clean rock fragments were crushed between tungsten carbide plates and a 100 g aliquot ground to <200 mesh in a tungsten carbide ring grinder. Major and trace element concentrations were measured by X-ray fluorescence (Siemens SRS3000 spectrometer) using standard techniques on glass

Table 4.1: *Representative chemical data of Udo samples. Fe_2O_3 and FeO calculated from Fe_2O_3tot assuming Fe_2O_3/FeO = 0.2. bdl: below detection limit. Major elements and V measured by XRF, trace elements by LA-ICPMS. Major elements in wt%, trace elements in ppm. Totals are from XRF with total Fe as Fe_2O_3 and include XRF measured trace elements. LTC: lower tuff cone, UTC: upper tuff cone, LS: lava shield.*

Sample	U1-1	U1-8	U1-11	U1-16	U1-17	U1-23	U1-32	U1-33	U1-39
Stage	LTC	LTC	LTC	LTC	UTC	UTC	UTC	LS	LS
SiO_2	47.91	49.9	48.06	48.04	47.91	46.55	47.15	52.46	51.06
TiO_2	2.47	2.11	2.47	2.47	2.43	2.41	2.45	1.8	2.1
Al_2O_3	14.6	14.08	14.58	14.58	14.13	13.53	14.19	14.24	14.75
Fe_2O_3	1.86	1.84	1.85	1.87	1.89	1.90	1.89	1.83	1.91
FeO	9.31	9.20	9.27	9.35	9.44	9.49	9.45	9.14	9.54
MnO	0.161	0.155	0.159	0.16	0.165	0.17	0.167	0.15	0.157
MgO	8.06	8.51	7.85	8.03	8.95	10.05	9	6.95	6.81
CaO	8.49	8.77	8.66	8.55	8.49	9.66	9.17	8.45	8.66
Na_2O	3.35	2.92	3.25	3.26	2.87	2.89	2.97	2.98	3.13
K_2O	1.74	1.03	1.74	1.73	1.6	1.5	1.58	0.65	0.45
P_2O_5	0.600	0.358	0.583	0.589	0.534	0.453	0.533	0.233	0.264
Total	99.82	100.08	99.72	99.88	99.66	99.86	99.81	100.03	100.01
Mg#	54.5	56.1	53.9	54.3	56.7	59.4	56.8	53.5	51.9
B	1.44	1.05	1.53	1.34	1.27	1.20	1.33	0.72	0.88
Cs	0.50	0.29	0.42	0.48	0.37	bdl	0.43	bdl	bdl
Ba	444	272	438	422	432	405	421	156	161
Rb	40.0	21.6	39.0	37.9	37.0	33.2	36.5	15.0	7.1
Sr	605	417	575	562	560	505	551	286	299
Pb	3.44	3.79	4.02	3.07	5.60	1.44	5.26	4.36	5.74
Th	6.36	3.40	6.05	5.97	6.06	4.91	5.72	2.26	2.43
U	1.34	0.64	1.26	1.19	1.16	0.95	1.13	0.45	0.49
Zr	234	157	230	229	224	195	218	117	141
Nb	51.7	27.9	50.3	48.5	47.4	43.2	47.1	13.7	16.4
Hf	5.63	4.23	5.75	5.63	5.42	4.59	5.32	3.18	3.65
Ta	3.46	1.75	3.31	3.17	3.05	2.76	3.21	0.90	1.10
Y	23.0	21.2	22.6	22.5	22.9	22.8	24.1	20.6	23.0
Sc	22.8	24.1	23.1	22.9	25.0	29.7	27.3	22.9	24.2
V	187	172	191	190	187	225	213	158	167
Cr	265	356	259	241	307	393	330	294	260
Co	75.7	52.4	74.2	55.9	58.8	65.5	64.8	49.9	47.9
Ni	190	177	130	140	183	194	183	159	153
Cu	46.5	37.3	41.8	38.6	50.8	41.3	43.8	50.6	50.9
Zn	124	111	106	100	115	81	118	110	124
Ga	20.6	18.1	20.1	19.3	20.1	18.5	19.8	18.6	18.8
La	38.8	22.0	37.0	36.9	36.0	32.2	35.5	12.3	13.7
Ce	73.8	41.9	71.0	70.4	68.2	61.8	67.8	25.0	28.9
Pr	9.04	5.28	8.59	8.42	8.37	7.35	8.16	3.35	3.91
Nd	37.6	23.5	35.5	35.6	35.6	31.7	34.7	16.1	18.6
Sm	7.16	5.47	7.14	7.16	7.25	6.62	7.22	4.51	5.25
Eu	2.41	1.87	2.39	2.27	2.17	2.18	2.23	1.55	1.74
Gd	6.91	5.61	6.76	6.62	6.68	6.34	7.13	4.82	5.53
Tb	0.94	0.83	0.91	0.92	0.93	0.86	1.02	0.74	0.88
Dy	5.09	4.76	5.18	5.08	5.40	5.10	5.23	4.59	5.00
Ho	0.89	0.87	0.91	0.92	0.90	0.91	0.97	0.84	0.87
Er	2.26	2.16	2.25	2.27	2.32	2.29	2.54	2.21	2.51
Tm	0.33	0.28	0.28	0.29	0.30	0.29	0.28	0.28	0.31
Yb	1.86	1.82	1.83	1.60	1.66	1.87	2.10	1.70	1.90
Lu	0.22	0.21	0.22	0.24	0.22	0.28	0.27	0.23	0.27

fusion discs prepared with SPECTRACHEM 12–22 flux. For the trace elements a suite of 36 international standards was used for calibration and Siemens SPECTRA

3000 software was used for data reduction. The Compton scatter of X-ray tube line RhKb1 was used to correct for mass attenuation and appropriate corrections were used for those elements analysed at energies below the Fe absorption edge. One-sigma relative error for V is 1-3% and detection limit is 2-5 ppm. Trace elements (apart for V) were analyzed by LA-ICP-MS at the Research School of Earth Sciences, Australian National University, using an Excimer LPX120 laser and Agilent 7500 series mass spectrometer. For this work the same fused glass discs as for XRF were used. Detection limits are <1 ppb and analytical errors <1% relative.

Three distinct chemostratigraphic groups can be distinguished in the eruption products of Udo Volcano (Fig. 4.3, 4.4, 4.5). In stratigraphic order, from oldest to youngest and consistent with the above field classification, these are the lower tuff cone (LTC), the upper tuff cone (UTC) including the spatter mound, and the lava shield (LS). Representative wholerock chemical analyses (which include all phenocrysts) are tabulated in Table 4.1 and the complete set is available in Table B1 in Electronic Appendix B.

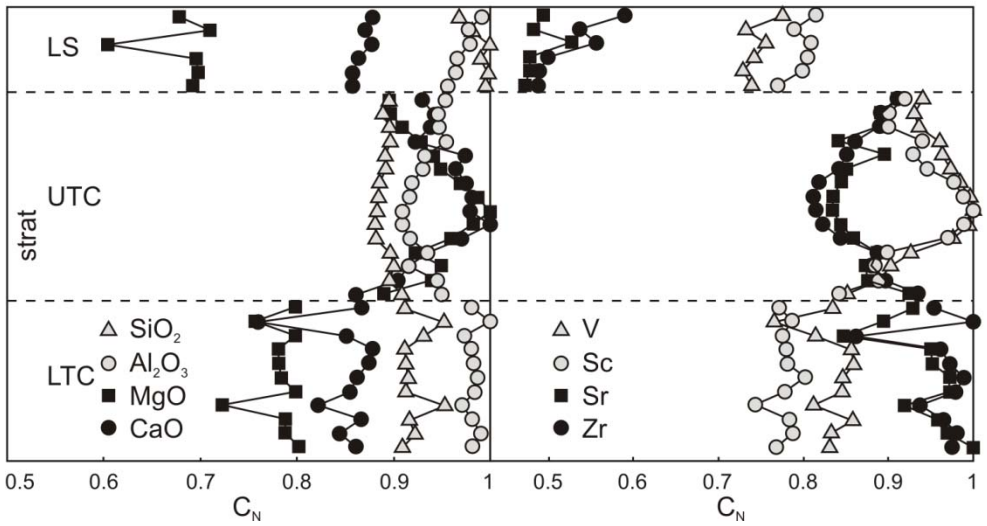

Figure 4.3: *Chemical variation with relative stratigraphic position (strat). LTC: lower tuff cone, UTC: upper tuff cone, LS: lava shield, C_N: concentration normalized to the maximum value for each element. The two samples with intermediate composition between the three stages are omitted for clarity. Note that there is no relative stratigraphic control for the LS samples.*

4.6.1 Major elements

The majority of samples from the stratigraphically lowest series (LTC, U1-1 to U1-16; Fig. 4.4, Table 4.1) have a restricted MgO range between 8 and 7 wt% and do not show any systematic trends with position in the sequence (Fig. 4.3). They show narrow abundance ranges for all major elements except for Na_2O, which has wide variability. The clustering on variation diagrams is good, apart for samples U1-5 and U1-14 which have lower MgO, and samples U1-8 and U1-15 that have characteristics intermediate between the three groups (see particularly the K_2O, TiO_2 and P_2O_5 v MgO graphs in Fig. 4.4).

Samples from the stratigraphically intermediate series (UTC, U1-17 to U1-32 and U1-40; Fig. 4.4, Table 4.1) are relatively primitive compared to the LTC, with MgO ranging between c. 10 and c. 9 wt%. An evolutionary trend is present within the cluster from lower MgO (U1-17, 8.95 wt%) to higher MgO (U1-23, 10.05 wt%) and back to lower MgO (U1-32, 9.00 wt%) upward through the sequence (Fig. 4.3). This trend is mirrored in increasing and then decreasing CaO, decreasing and then increasing Al_2O_3, SiO_2, and to a lesser extent K_2O, TiO_2 and P_2O_5. Fe_2O_3 remains constant whereas Na_2O is scattered and shows only weak negative correlation with MgO. The spatter mound (U1-40) has 9.47 wt% MgO, and is hence slightly more primitive than the stratigraphically youngest samples of the tuffaceous sequence.

The stratigraphically younger series (LS, U1-33 to U1-39 and U1-41 and U1-42; Fig. 4.4, Table 4.1) has a MgO range from c. 7.5 to c. 6 wt%. Major element trends are of increasing SiO_2, K_2O, Na_2O and TiO_2 (slightly) and decreasing Fe_2O_3 with decreasing MgO; CaO and P_2O_5 remain constant. Only a single gap occurs in the data between c. 6.2 and c. 6.7 wt% MgO (in both our data and Koh *et al.* (2005) data). This gap is not correlated with the geographical distribution of samples.

Based on CIPW normative criteria the LTC and UTC stage samples are nepheline to olivine normative alkali basalts whereas the LS stage samples are quartz normative tholeiites.

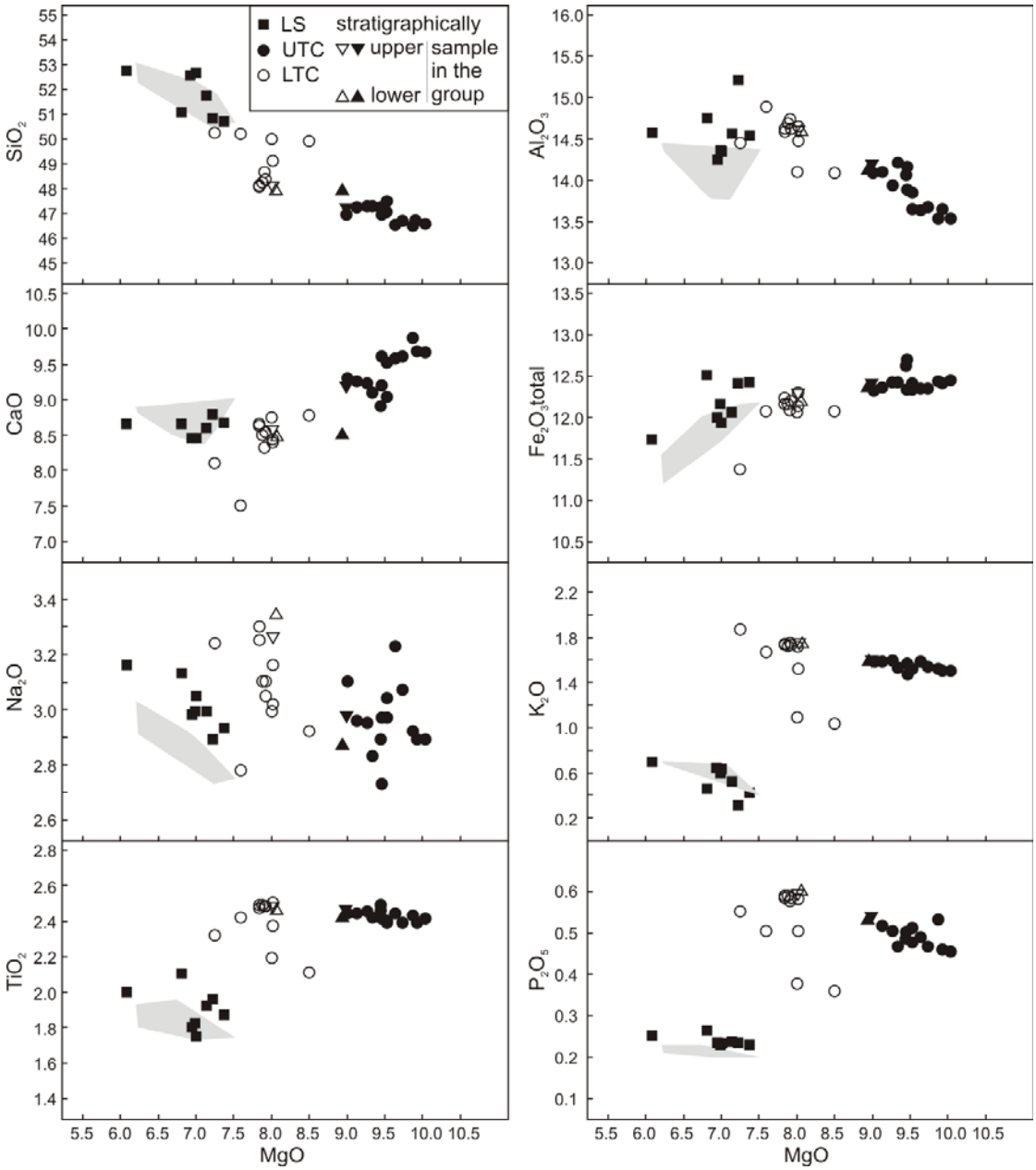

Figure 4.4: *Major element variation diagrams of Udo Volcano (wt% oxides). LTC: lower tuff cone, UTC: upper tuff cone, LS: lava shield; grey field data is lava shield from Koh et al. (2005). XRF data.*

4.6.2 Trace elements

The groups defined by major element variation are also consistently defined in trace element space (Fig. 4.5, Table 4.1). The LS stage has lower Zr compared to the tuff cone stages, which also shows greater compositional continuity than in major element

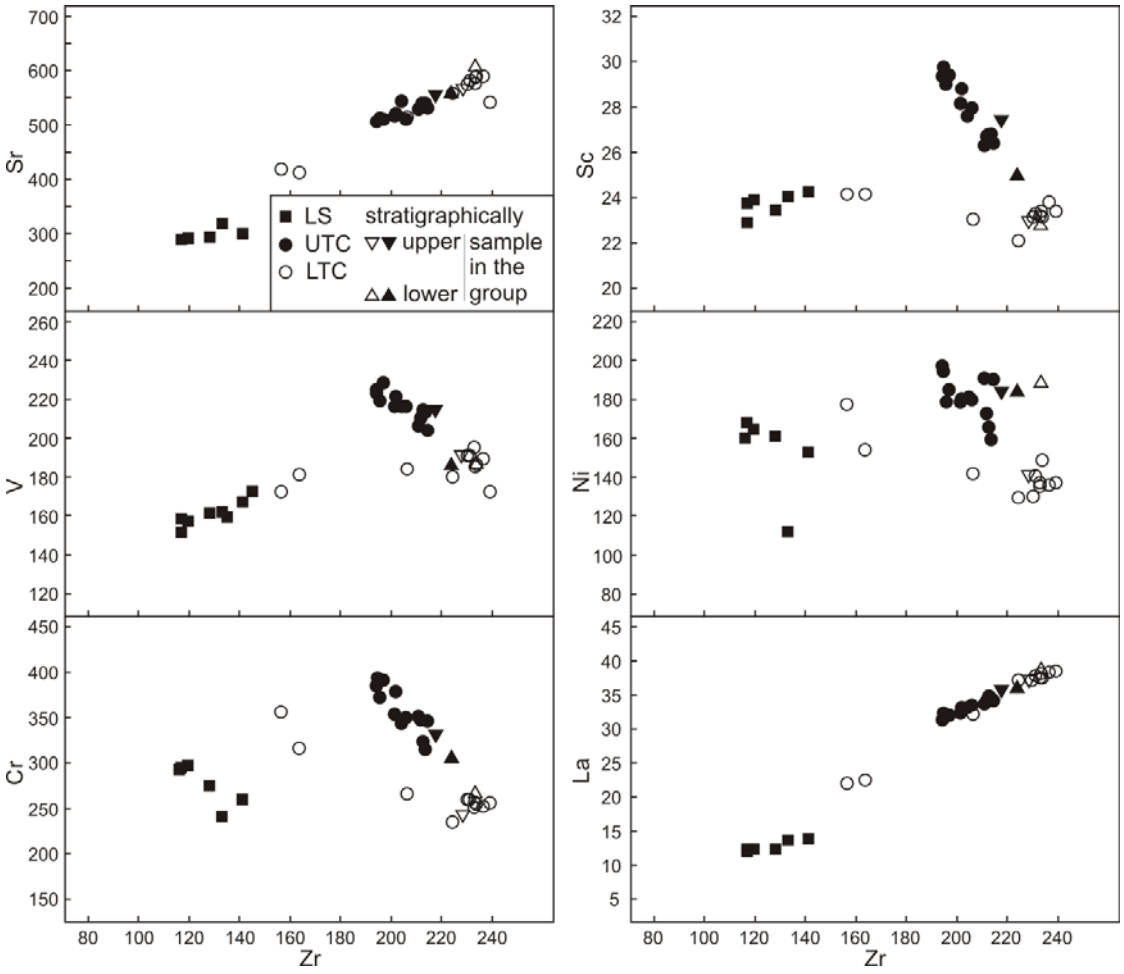

Figure 4.5: *Trace element (ppm) variation diagrams of Udo Volcano. ICP-MS data, apart V is XRF.*

composition (no gap occurs between LTC and UTC). The trend in the UTC from relatively evolved to primitive and back to evolved compositions is also seen (Fig. 4.3). In the tuff cone stages, Sc and V decrease with increasing evolution. Cr and, to a certain extent Ni also decrease with evolution. In the lava shield, Sc and V remain constant or increase slightly, whereas Cr and Ni decrease. Sr increases with increasing evolution during all stages (Fig. 4.5). The contrasting chemistry of the tuff cone and the lava shield stages is also apparent using trace element ratios. On a primitive mantle normalized diagram the tuff cone stage is more enriched in incompatible elements compared to the lava shield stage (Fig. 4.6). The tuff cone clasts have a slight Hf negative anomaly and peaks at Ta and Nb that are subdued in the lava shield stage. The main difference is the positive Pb anomaly in the lava shield stage as opposed to a negative, or no anomaly in the tuff cone stage (Fig. 4.6).

Cs is also notably depleted in the tuff cone stage magma and was below detection limit in the lava shield magma.

The stratigraphic variation through the Udo eruptive sequence is well illustrated in the plots of normalized concentration against relative stratigraphic position (Fig. 4.3). The constant chemistry of the LTC contrasts with the variability of the UTC compositions and is markedly different from the LS stage compositions.

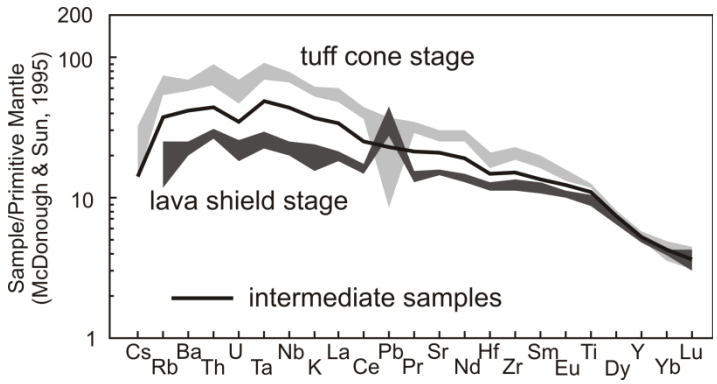

Figure 4.6: *Primitive mantle normalized (McDonough & Sun, 1995) diagram for the Udo samples.*

4.7 Interpretation of chemistry

The magmas forming the tuff cone stage and the lava shield stage can not be related through fractionation of common mineral phases in basaltic magmas. No model using the phenocryst phases observed in the rocks can reproduce a c. threefold depletion in K_2O and P_2O_5 from the tuff to the lava shield stages (Table 4.1, Fig. 4.4). For instance, MgO depletion and SiO_2 enrichment may be a result of olivine fractionation; however this would cause enrichment of K_2O and P_2O_5 rather than the observed depletion. Conversely, crustal contamination is also not a viable model to explain the SiO_2 enrichment from the tuff cone stage to the lava shield stage, because this would also result in K_2O and P_2O_5 enrichment. Modelling of crystal fractionation within each stage, using observed or reasonable phenocryst phases for each of the two magmatic stages separately, is presented in the following discussion. Discussion of the source characteristics that may give rise to the observed chemical difference is in the following section.

4.7.1 Tuff cone stage

The chemical variability in the UTC can not be the result of the mixing of two different primary magmas because of the continuity of the trend of depletion, followed by enrichment, of incompatible trace elements (Fig. 4.3). It also can not be the result of mixing between the tuff primary magma and the lava shield primary magma; this is clear because the evolutionary trend from the most primitive sample of the tuff cone stage (U1-23) does not extend towards the LS stage composition. Trace element trends, such as decreasing Ni, Cr, V, Sc with increasing magmatic evolution, suggest fractionation of olivine + clinopyroxene ± spinel ± orthopyroxene. Spinel appears a more likely fractionating aluminous phase than plagioclase, because Sr is enriched with evolution in this suite. Orthopyroxene is present only in trace amounts as a phenocryst phase in the UTC samples and is generally rimmed by clinopyroxene, suggesting that it was not an equilibrium phase in the fractionating assemblage. TiO_2 is not depleted with evolution, indicating the absence of a Fe-Ti oxide phase in the fractionation assemblage.

Crystal fractionation within the tuff cone compositions is modelled, with the aim of investigating the fractionating assemblages introduced above, using U1-23 as the most primitive sample and U1-11 as the most evolved one based on MgO and Zr concentrations (Table 4.1). We used the least squares mass balance (Stormer & Nicholls, 1978) option in the software PETROGRAPH (Petrelli *et al.*, 2005) with ten components (SiO_2, TiO_2, Al_2O_3, FeO_{tot}, MnO, MgO, CaO, Na_2O, K_2O and P_2O_5) and three to four fractionating phases (olivine + clinopyroxene ± aluminous spinel ± orthopyroxene) with compositions reported in Table 4.2. Representative olivine and clinopyroxene cores in sample U1-23 were chosen based on calculated partition of FeO and MgO between crystal and liquid equal to c. 0.30 and c. 0.32 respectively, in agreement with Roeder & Emslie (1970) and Takahashi & Kushiro (1983), indicative of them being in equilibrium with the most primitive erupted magma composition at Udo. Crystal core compositions were used to approximate deep fractionating composition, in order to distinguish it from late crystallizing rims, as discussed later. The composition of olivine, clinopyroxene and orthopyroxene is from microprobe

data on the tuff stage lapilli, whereas the spinel composition is from aluminous spinel in spinel peridotite xenoliths found in lavas in the northeastern part of Jeju Island (Kil *et al.*, 2008) and is used to approximate fractionating spinel in upper mantle conditions beneath Jeju.

The modelling assumes constant composition of the fractionating phases and is hence independent of factors such as temperature, pressure and oxygen fugacity. Although these calculations do not give a unique solution, they nevertheless allow semi-quantitative evaluation of the fractionation process, especially when the sum of the residual squared is <2 (Stormer & Nicholls, 1978). The mass balance calculations result in three assemblages with the sum of the residuals squared <1 (Table 4.3). These are assemblages of ol + cpx + opx, ol + cpx + sp and ol + cpx + opx +sp and these will be discussed further below.

Table 4.2: *Mineral compositions used for mass balance calculations. Spinel composition is from Kil et al. (2008). Recalculated to 100% totals.*

	olivine	clinopyroxene	spinel	orthopyroxene
SiO_2	40.06	51.67	0.06	53.73
TiO_2	0	1.03	0.1	0.3
Al_2O_3	0	2.99	63.73	3.01
FeO_{tot}	14.94	5.75	12.63	14.06
MnO	0.17	0.04	0.01	0.2
MgO	44.55	16.11	23.4	26.81
CaO	0.25	21.63	0.03	1.71
Na_2O	0.01	0.53	0.01	0.1
K_2O	0.03	0.12	0.02	0.08
P_2O_5	0	0.13	0	0
total	100	100	100	100

Table 4.3: *Results of the mass balance calculation for investigation of the fractionating assemblages. See text for discussion.*

Assemblage	subtracted amount as wt% of initial magma	added amount as wt% of initial magma	sum of the squares of the residuals
ol + cpx	5.0 ol, 5.8 cpx		2.4
ol + cpx + opx	11.7 ol, 7.2 cpx	13.2 opx	0.4
ol + cpx + sp	3.6 ol, 10.6 cpx, 2.2 sp		0.8
ol + cpx +opx + sp	11.2 ol, 7.4 cpx, 0.1 sp	12.5 opx	0.4

Modelling of the behaviour of Cr suggests that no, or only minor spinel was involved in the fractionation process contrasting to the model above. By using the variation of

P as an indicator of evolution by assuming a bulk $^{P}K_D$ of 0 (that is, P is not partitioned in any crystallizing phases), the Cr depletion trend can be modelled with a bulk $^{Cr}K_D$ of c. 2.5 (Fig. 4.7), which is too low if chromian spinel is involved other than in trace amounts (McKenzie & O'Nions, 1991). This $^{Cr}K_D$ value is more consistent with clinopyroxene + olivine fractionation with c. 24% crystals removal. Al_2O_3 is enriched with evolution, suggesting the absence of a strongly aluminous phase (such as aluminous spinel) in the fractionation assemblage other than in trace amounts. Magmatic aluminous spinel is also not observed petrographically.

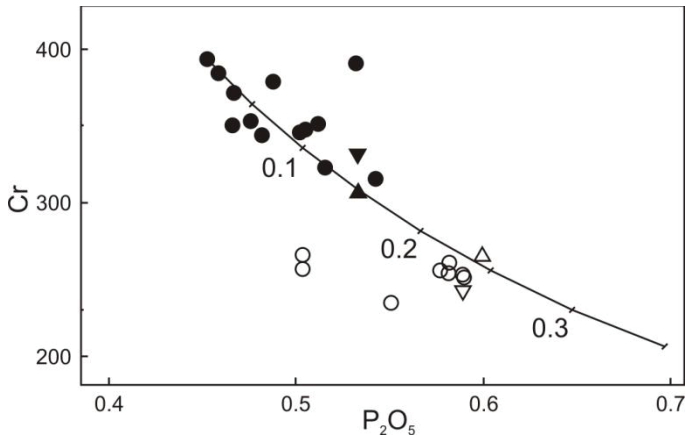

Figure 4.7: *Modelling fractionation of Cr (ppm) using $^{P}K_D$ = 0 results in bulk $^{Cr}K_D$ = c. 2.5 and removal of c. 24 % crystal fraction. Symbols as in Figure 4.4. P_2O_5 in wt% oxide.*

Ni is less well correlated with P, however, modelling suggests a bulk $^{Ni}K_D$ of c. 2.5. Comparing this to the value calculated by Smith *et al.* (2008), Ni appears slightly more compatible in the fractionating assemblage, suggesting the presence of olivine rather than orthopyroxene. Further discrimination between olivine and orthopyroxene is difficult. However, SiO_2 is enriched with evolution (decreasing MgO). Microprobe data (Table 4.2), as well as representative analyses (Deer *et al.*, 1992), indicate that both clinopyroxene and orthopyroxene have SiO_2 contents similar to or higher than the starting composition (U1-23). As spinel was fractionating in very limited amounts (if at all), olivine is the only suitable phase that could generate SiO_2 enrichment with fractionation.

The preferred fractionating assemblage is therefore clinopyroxene + olivine ± spinel. Orthopyroxene is present as phenocrysts, however, it does not fit crystal fractionation

models and has calculated partition of FeO and MgO between crystal and liquid >0.4, which is too high for equilibrium orthopyroxene (Beattie *et al.*, 1991). We suggest that orthopyroxene is xenocrystic, being derived from the mantle and entrained in various amounts in the fractionating magma. The presence of mainly olivine phenocrysts and plagioclase microphenocrysts in the eruptive products can be explained as in the case of Crater Hill (Smith *et al.*, 2008), with these phases undergoing low pressure crystallization during magma ascent in the upper plumbing system. The relatively greater abundance of plagioclase microphenocrysts observed in the LTC compared to the UTC suggests heterogeneous nucleation of this phase in the rising magma column. Plagioclase was however not being fractionated given that Al_2O_3 and Sr are not depleted with evolution, and hence all crystallizing plagioclase was retained in the rising magma. The presence of intergrown chromian spinel in some olivine crystals suggests that these are residual cores from upper-mantle olivine, with overgrown magmatic rims with lower MgO/FeO ratios. Clinopyroxene is present as a phenocryst phase just in the UTC. The absence of clinopyroxene in the LTC suggests that this phase had settled out of the upper part of the fractionating magma column, but was carried to the surface by the ascent of the lower column.

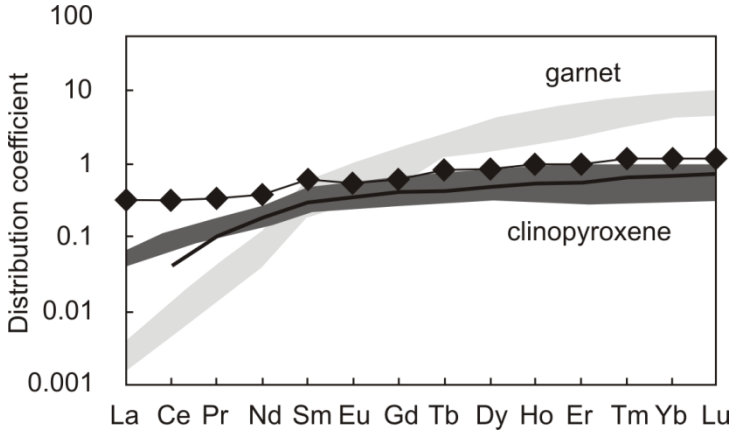

Figure 4.8: *Calculated REE bulk partition coefficients into the fractionating assemblage in the tuff sequence of Udo. Garnet and clinopyroxene fields are after Smith et al. (2008) and references therein and the solid line is their calculation for Crater Hill. Diamonds are the Udo data.*

By determining partition coefficients of REE by comparing them to that of P, with $^{P}K_D$ assumed to be 0, the plotted pattern (Fig. 4.8) resembles that determined by Smith *et al.* (2008) using the same method. This can be attributed to the fractionation

of clinopyroxene. However, the LREEs appear to have been more compatible in the Udo fractionating assemblage, compared to a distribution coefficient involving just clinopyroxene. This may be due to buffering by residual amphibole in the upper mantle at the site of fractionation. Slightly higher $^{Sm}K_D$ compared to $^{Nd}K_D$ and $^{Eu}K_D$ also supports the presence of amphibole (Rollinson, 1993 and references therein). Presence of amphibole in the upper mantle below Jeju has been suggested by Tatsumi *et al.* (2005) and resorbed kaersutite was described as a xenocryst in Jeju basalts by Eom *et al.* (2007). This may have crystallized following metasomatism by silicic, low Mg# fluids (Tiepolo *et al.*, 2001), which affected the mantle beneath Jeju, as found in mantle xenolith inclusions (Yu *et al.*, 2009).

Older basaltic lava flows underlie Udo Volcano (Sohn & Chough, 1993), and the chemical variation of samples with intermediate composition may be due to contamination from such rocks. Alternatively, given that the intermediate samples always plot between the tuff cone stage and the lava shield stage compositions (Fig. 4.4, 4.5), mixing of approximately equal amounts of the two magma batches could also produce these intermediate compositions.

4.7.2 Lava shield stage

Modelling evolutionary processes in the lava shield stage is more challenging because fewer samples are available and the chemical ranges are narrower. Magma in this stage of the eruption was subalkali and there was less enrichment of trace elements, lower MgO and higher SiO_2 contents compared to the tuff stage (Fig. 4.4, 4.5, 4.6). Notable differences compared to the tuff stage trends are enrichment (rather than depletion) of CaO, Sc and V with evolution (decreasing MgO), which counts against any clinopyroxene fractionation in this stage. Cr does not show the same depletion trend as the tuff stage samples, suggesting that spinel is also not involved in the fractionation assemblage. Major and trace element variations are instead more consistent with olivine fractionation. Enrichment of K and Rb precludes involvement of residual phlogopite in the mantle at the site of fractionation, despite this phase being proposed as a residual metasomatic phase in the source of Jeju subalkaline magmas by Tatsumi *et al.* (2005). The fractionation depth would, however, be

shallower for the LS stage compared to the tuff cone stage as indicated by the lack of a clinopyroxene influence in the observed chemical trends (e.g. Elthon & Scarfe, 1984).

Chemical variation from basanite to olivine tholeiite has previously been recorded for the 1730-1736 eruption of Lanzarote (Carracedo & Rodriguez Badiola, 1993, Carracedo *et al.*, 1992), however in that case the transition was continuous, whereas in the case of Udo, the transition between alkali and subalkali basalts is clearly a sudden step-change.

4.8 Source characteristics

In the previous section we showed that the two magmatic stages of Udo evolved through different fractionation processes. Next we will investigate the chemical heterogeneity of the source in order to determine whether more than one source type was involved in magma generation and approximate a depth of magma sourcing.

The tuff cone stage, and to a lesser extent the lava shield stage samples have La/Nb less than primitive mantle (Sun & McDonough, 1989), and, given that the upper mantle (N-MORB source) or the continental crust are generally Nb depleted (Fitton *et al.*, 1997), it follows that the source for the Udo tuff is Nb enriched. La also appears enriched as La/Zr and La/P are higher than primitive mantle for both stages.

Trace element systematics suggest the involvement of two different mantle sources in the generation of the Udo magmas. Notably Pb is depleted in the tuff cone stage magma, whereas it is enriched in the lava shield magma (Fig. 4.6). Different trace element ratios also suggest that different mantle sources were involved in the generation of the Udo magmas rather than different degrees of partial melting of a single source (Reiners, 2002, Zhi *et al.*, 1990).

Modelling was carried out for bulk melting and aggregated fractional melting (Albarède, 1995) using four different source lithologies. These are mantle peridotite (McDonough & Sun, 1995), garnet pyroxenite (using 30 averaged analyses reported

by Zeng *et al.*, 2009), eclogite (Xu *et al.*, 2009) and spinel lherzolite averaged from three mantle xenolith compositions in Jeju basalts (Choi *et al.*, 2005). Distribution coefficients are from Salters & Longhi (1999), Fujimaki *et al.* (1983), Elkins *et al.* (2008) and Klemme *et al.* (2002). The parameters used are summarized in Table 4.4 and the results are illustrated in Figure 4.9.

Table 4.4: *Mineral/melt distribution coefficients used for modelling of bulk partial melting of different sources.*

phase	cpx[a]	opx[a]	gt[a]	ol[b]	cpx[a]	opx[a]	gt[a]	sp[c]	cpx[d]	gt[d]
P (GPa)	2.8	2.8	2.8	NA	2.4	2.4	2.4	2.5	3	3
Nb K_D	0.0073	0.001	0.0179	0	0.01	0.0033	0.01	0.0006	0.021	0.008
Zr K_D	0.038	0.022	0.555	0.011	0.051	0.019	0.656	0.0081	0.093	0.40
Hf K_D	0.06	0.048	0.588	0.011	0.085	0.0328	0.68	0.003	0.17	0.31

source	PM[e] 2.8 GPa	PM[e] 2.4 GPa	gt pyroxenite[f]	eclogite[g]	sp lherzolite[h]
ol	65	65	20	-	60
cpx	5	5	37	70	10
opx	25	25	35	-	25
gt	5	5	8	30	-
sp	-	-	-	-	5
Nb $^{B}K_D$	0.0035	0.00382	0.0048	0.0171	0.00186
Zr $^{B}K_D$	0.07355	0.0855	0.06836	0.1851	0.01686
Hf $^{B}K_D$	0.08775	0.0981	0.08824	0.212	0.02345

The 2.4 GPa clinopyroxene K_D was interpolated with a power regression from 1.5, 1.9 and 2.8 GPa K_Ds of Salters & Longhi (1999). Bulk distribution coefficients used in the calculations are based on modal proportions for the different source compositions. Garnet pyroxenite calculated with 2.8 GPa K_Ds, spinel lherzolite calculated with 2.4 GPa K_Ds and eclogite calculated with 3 GPa K_Ds. cpx: clinopyroxene, opx: orthopyroxene, gt: garnet, ol: olivine, sp: spinel, PM: primitive mantle (garnet peridotite), $^{B}K_D$: bulk distribution coefficient

[a]Salters & Longhi (1999)
[b]Fujimaki *et al.* (1983)
[c]Elkins *et al.* (2008)
[d]Klemme *et al.* (2002)
[e]McDonough & Sun (1995)
[f]Zeng *et al.* (2009)
[g]Xu *et al.* (2009)
[h]Choi *et al.* (2005)

The only source material that can reasonably reproduce the trace element ratios in the Udo samples is mantle peridotite with residual garnet (Fig. 4.9). According to the bulk partial melting model, the tuff cone stage magma would have been derived from between 1 and 2% partial melting of peridotite at c. 2.8 GPa. By contrast the lava shield magma results derived from c. 5 to 7% partial melting of peridotite at c. 2.4 GPa. The slight enrichment of Nb compared to primitive mantle, as discussed above, may support a shifting of the source (and the model) to a higher Nb/Zr ratio, thereby increasing the amount of partial melting required to generate the magma. Given that

observed fractionation trends are towards lower Zr/Hf, and the magmas plotted in Figure 4.9 are not primary, it is likely that the Zr/Hf ratio of the source is also higher than primitive mantle. The aggregated fractional melting model for garnet peridotite (Fig. 4.9) gives a similar degree of partial melting for the tuff cone stage, but a lower degree (between 3 and 4%) of partial melting for the lava shield stage. Such degree of partial melting is very low for generation of subalkali magma (Frey *et al.*, 1978) and hence the bulk partial melting model is preferred.

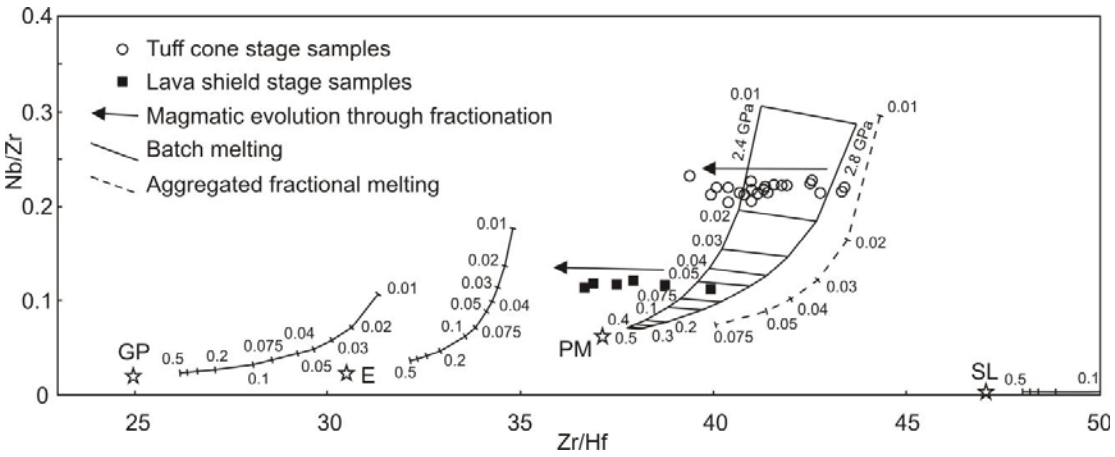

Figure 4.9: *Bulk melting models. See Table 4.4 for list of parameters and references and text for discussion. PM is primitive mantle (mantle peridotite), GP is garnet pyroxenite, E is eclogite, SL is spinel lherzolite.*

Garnet pyroxenite and eclogite have lower Zr/Hf ratios (e.g. Xu *et al.*, 2009) and modelling of partial melting of these materials using K_Ds from Elkins *et al.* (2008) for garnet pyroxenite and from Klemme *et al.* (2002) for eclogite, results in curves with Zr/Hf substantially lower than those of the Udo magma (Fig. 4.9). Fractionation decreased Zr/Hf, hence it is likely that neither garnet pyroxenite nor eclogite was involved in the melting process. Spinel lherzolite from mantle xenoliths found in Jeju basalts (Choi *et al.*, 2005) has very low Nb content, and modelling using K_D for spinel determined experimentally by Elkins *et al.* (2008) could not reproduce a melting curve fitting the data (Fig. 4.9, note that the curve at degrees of partial melting <10% has been omitted, to minimize distortion of the x axis, however it is horizontal down to 1% partial melting).

Without claiming these models to be precise, it is nevertheless apparent from their results that the tuff cone stage magma was generated by a lesser degree of partial melting compared to the lava shield stage magma, and both stages were generated in garnet peridotite.

4.8.1 Depth of magma generation

Samples from the tuff cone stage have Mg# 53-60 and show a linear correlation in their major element correlations. Measured rock compositions are linearly extrapolated to Mg# 70 (Table 4.5), which is assumed for melts in equilibrium with lherzolite with olivine composition Fo_{90} (Ulmer, 1989, Wood, 2004) and similar to olivine compositions measured in Jeju mantle xenoliths (Kil *et al.*, 2008). Based on CaO and Al_2O_3 composition, an extrapolated primary melt would be in equilibrium with lherzolite at c. 3.2 GPa (Herzberg, 1995). Based on the total FeO and SiO_2 content of the primary melts, equilibrium pressure should be between 2.5 and 3.5 GPa (Hirose & Kushiro, 1993).

For the lava shield stage, the equilibrium pressures based on the extrapolated CaO and Al_2O_3 composition is 2.9 GPa (Herzberg, 1995), and between 1.7 and 2.7 GPa based on extrapolated total FeO and SiO_2 (Hirose & Kushiro, 1993). Due to the weak linear correlation within the sample group (Table 4.5) these should be treated as qualitative only.

The negative gradient of the normalized HREE patterns suggests the involvement of residual garnet in the source of both the tuff cone and the lava shield stages, which would indicate a minimum source pressure of c. 2.5 GPa (e.g. Walter, 1998). Involvement of garnet peridotite rather than spinel peridotite, garnet pyroxenite or eclogite in the source is also supported by the modelling above.

Immobile incompatible trace element ratios can be useful for investigating melting conditions and magmatic contaminants. The use of Ti/Yb and Th/Yb v. Nb/Yb plots was introduced by Pearce & Peate (1995) and further elaborated by Pearce (2008). On the basis of greater $^{Yb}K_D$ than $^{Ti}K_D$ and $^{Nb}K_D$ in garnet compared to spinel (Halliday *et*

al., 1995, McKenzie & O'Nions, 1991), TiO_2/Yb and Nb/Yb can be used as proxies for melting depth (Pearce, 2008). Thorium is highly incompatible in crustal material and hence it would be enriched with respect to Yb in basaltic magma interacting with the continental crust (Nicholson *et al.*, 1991), or by fluids derived from subducted crustal recycling (Pearce, 2008, Pearce & Peate, 1995). The Udo samples plot along the MORB-OIB array with a slight shift towards high Th/Yb, indicative of an enriched source, or of a small degree of crustal contamination (Pearce, 2008; Fig. 4.10a). Based on Sr and Nd isotope ratios remaining constant with increasing SiO_2, Tatsumi *et al.* (2005) however concluded that crustal contamination was not an important process in the evolution of Jeju magmas, and hence the Th signature is more likely to indicate an enriched source. Both groups of alkaline and subalkaline magmas have characteristics consistent with an OIB source with residual garnet (Fig. 4.10b).

Table 4.5: *Linear regression parameters and calculated primary magma compositions of alkali batch (tuff cone) and subalkali batch (lava shield) with Mg# = 70.*

	R^2	Slope	Intercept	$Mg\#_{70}$
tuff stage				
SiO_2	0.81	-0.30	65.2	44.0
TiO_2	0.67	-0.01	3.3	2.3
Al_2O_3	0.80	-0.19	25.3	12.0
FeO	0.43	0.03	8.3	10.6
Fe_2O_3	0.43	0.01	1.7	2.1
MnO	0.75	0.00	0.1	0.2
MgO	0.82	0.36	-12.3	13.0
CaO	0.89	0.24	-4.8	11.7
Na_2O	0.28	-0.04	5.3	2.6
K_2O	0.75	-0.04	4.0	1.2
P_2O_5	0.78	-0.02	1.8	0.3
Mg#	1.00	1.00	0.0	70.0
lava shield stage				
SiO_2	0.32	-0.16	61.1	49.6
TiO_2	0.51	-0.05	4.7	1.0
Al_2O_3	0.23	-0.05	17.1	13.6
FeO	0.59	0.08	6.0	11.3
Fe_2O_3	0.59	0.02	1.2	2.3
MnO	0.69	0.00	0.1	0.2
MgO	0.98	0.31	-9.8	12.1
CaO	0.46	-0.04	10.9	7.8
Na_2O	0.77	-0.05	5.6	2.2
K_2O	0.50	-0.03	2.4	0.0
P_2O_5	0.73	-0.01	0.6	0.1
Mg#	1.00	1.00	0.0	70.0

The Udo tuff cone samples plot very close to samples from the Auckland Volcanic Field (Smith *et al.*, 2008) on the trace element-ratio plots (Pearce, 2008; Fig. 4.10), suggesting that they are derived from a similar depth and degree of partial melting. The lower Th/Yb ratio of the Auckland samples, however, suggests that their source was not enriched as the Udo source is, or that there was a lesser degree of crustal interaction.

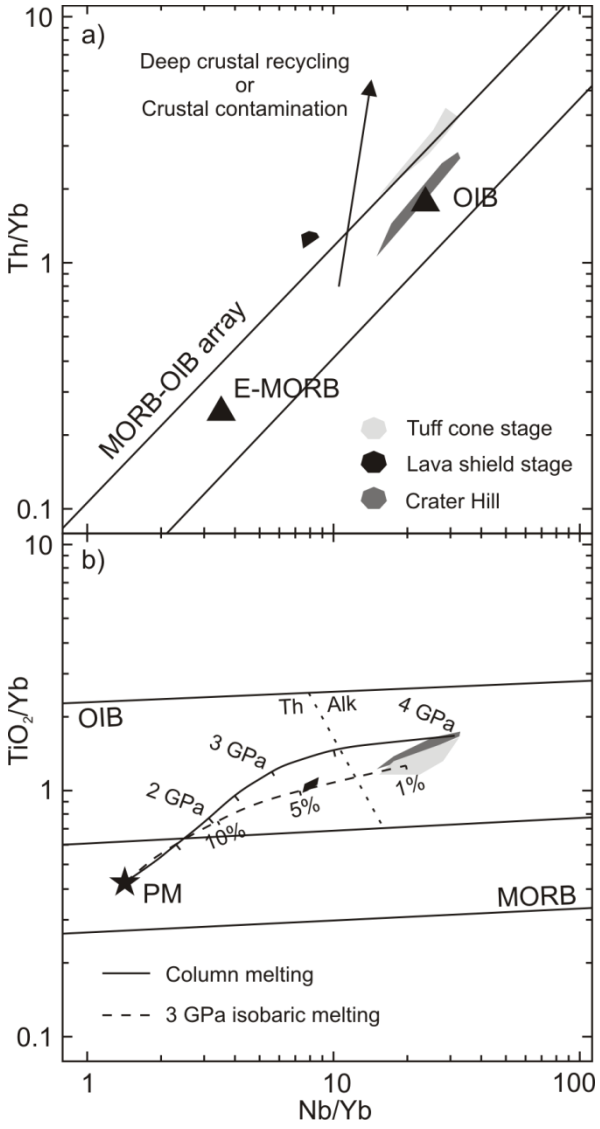

Figure 4.10: *Trace elements ratio plots with regions and partial melting models after Pearce (2008) and Crater Hill field from Smith et al. (2008).*

By applying the partial melting trajectories of Pearce (2008; Fig. 4.10b), the alkali magma would be generated at 4GPa in a melting column. However, as we have seen

above, slightly enriched Nb would increase the Nb/Yb ratio and shift the path to the right, which would decrease the modelled depth of melting and would fit the subalkali batch to the curve too. For the modelled 3 GPa isobaric melting (Fig. 4.10b) a similar shift would increase the melt fraction.

We therefore suggest that the source for the two magmatic stages of Udo had slight chemical differences that can not be attributed only to varying degrees of partial melting. The alkali magma source was possibly metasomatized garnet peridotite with slight Nb and Zr enrichment and Pb and Hf depletion to various degrees at c. 3 to 3.5 GPa, whereas the subalkali magma source was Pb enriched garnet peridotite mantle at c. 2.5 GPa.

4.9 Model of conduit and magma batch interaction

The model of deep clinopyroxene fractionation during magma ascent generating a trend towards more primitive magma composition as eruption proceeded for the Auckland centre of Crater Hill (Smith *et al.*, 2008) may be applicable in the case of Udo because the first erupted magma was the most evolved, and it became more primitive as the eruption proceeded. However, at Udo, the LTC stage does not show evidence for significant internal crystal fractionation, although it does have the most evolved compositions. In addition, the UTC has an evolutionary trend from relatively evolved to primitive and back to the initial level of evolution involving olivine as well as clinopyroxene. This complex pattern was not observed at Crater Hill where the chemistry followed a constant shift towards more primitive composition during the eruption (Smith *et al.*, 2008). Furthermore at Udo there is evidence for two magma batches erupted from the same vent within a short time span. The model proposed here is summarised in Figure 4.11.

The Crater Hill model of fractionation by flow crystallization on dyke walls (Irving, 1980, Smith *et al.*, 2008) could be reconciled with the Udo eruptive sequence if the LTC stage represents a magma batch that was fractionating at depth and subsequently erupted without time for further within-batch fractionation. The trend in the second batch, forming the UTC, is more complex. The return to greater degrees of evolution,

after the trend towards more primitive composition, might represent magma that was stalled in a dyke system being squeezed out at the end of the eruption. Magmatic flow in a dyke is generally considered to be laminar (Rubin, 1995), indicating that the core of the dyke rises faster than its margins, and hence leaving more time for magma near the margins to fractionate by crystallizing on the dyke walls (Irving, 1980, Smith *et al.*, 2008). Reducing magma pressure from the source may have led to the conduit walls compressing due to pressure from the country rock (Valentine & Gregg, 2008, Valentine & Krogh, 2006), and hence squeezing out the liquid portion of the crystal mush close to the margins of the dyke in a process akin to filter pressing (Anderson *et al.*, 1984, Sinigoi *et al.*, 1983). That the subsequent lava shield stage erupted immediately afterward at the same location, suggests that the eruptive conduit/dyke was still active, at least in its upper part, above the level of the shallower-fractionating subalkali magma.

The upper part of the UTC has low modal proportion of plagioclase microphenocrysts and higher vesicularity (+ microvesicularity) compared to the LTC or the lower part of the UTC. This may be interpreted as indicating that the last erupted tuff magma did not have time to crystallize plagioclase (it did not spend as much time in the plagioclase stability field) or degas in the upper conduit, hence rose from the fractionation site and erupted more quickly. This is plausible given that the early-rising magma batch would have opened a path for the later batch that could therefore rise more freely. Also, the presence of clinopyroxene phenocrysts only in the upper part of the sequence may suggest that the initial batch rose slower, allowing settling out of clinopyroxene, which was subsequently carried to the surface by faster rising magma forming the UTC.

The chemo-stratigraphic continuity (Fig. 4.3), especially in the UTC, suggests that the alkali magma was erupted from one single dyke/conduit. Such a trend could not have been easily achieved by a combination of several dykes carrying discrete magma batches to the surface. A single large dyke would also be associated with greater heat retention due to its smaller surface to volume ratio compared to several thin dykes, allowing the eruption of the late relatively evolved alkali magma, rather than this freezing *in situ* in a distributed plumbing system.

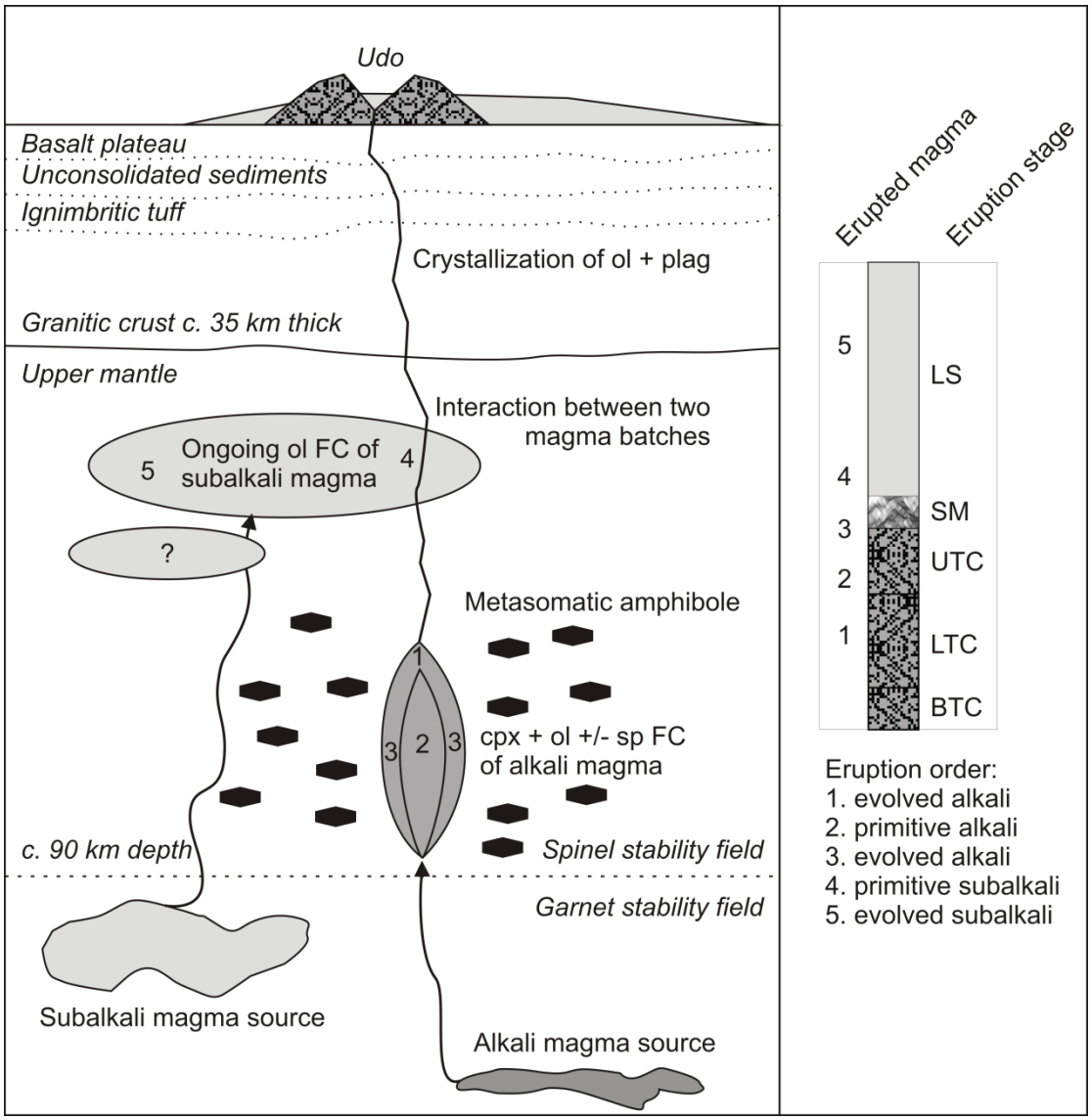

Figure 4.11: *Model of the evolution of the Udo plumbing system. ol: olivine, plag: plagioclase, cpx: clinopyroxene, sp: spinel, FC: fractional crystallization. Diagram not to scale. Relative stratigraphic column showing order of erupted magmas not to scale. BTC: basalt tuff cone, LTC: lower tuff cone, UTC: upper tuff cone, SM: spatter mound, LS: lava shield.*

The presence of very small quantities of fassaitic (Fe-rich) green clinopyroxene cores (analyses 6609-6620 in Electronic Appendix N) suggests that more evolved alkali magma was present, possibly as small stalled bodies near the site of crystal fractionation or shallower, and that minor interaction between the erupted alkali magma and these bodies took place (c.f. Duda & Schmincke, 1985). These may represent earlier, smaller magma batches that did not have enough energy to reach the

surface and erupt as occurred up to several years prior to monogenetic eruptions (Okada & Yamamoto, 1991, Ukawa & Tsukahara, 1996). Shallow crustal sills have been described in the exposed basement of small-volume basaltic volcanic fields (Diez *et al.*, 2009, Valentine & Krogh, 2006). Such features have been interpreted as having stored magma during the eruption of Parícutin resulting in greater crustal contamination of late erupted magmas (Erlund *et al.*, 2010). However, at Udo, the lack of indicators of major crustal contamination throughout the eruption sequence suggests that if these shallow storage units exist, they did not play a major role in the eruption evolution, and might have just solidified as they were intruded.

The most primitive samples of the LS stage were collected from the eastern part of Udo Island similar to the pattern observed by Koh *et al.* (2005). This suggests that the initial lava flowed northward then eastward down slope from the tuff cone. This probably created a rampart that directed subsequent, more evolved flows to the north and the west. The observed sequence and fractionation trends are hence consistent with sequential eruption from a magma chamber that was undergoing olivine fractionation.

Initial interaction between the two batches is suggested by the presence in the LTC stage of samples with chemical compositions intermediate between the tuff and lava shield magmas. Further, more thorough mixing was possibly avoided because of chemistry/viscosity contrasts and high flux rates of the alkali magma that can reach >1 and up to 6 ms^{-1} (Demouchy *et al.*, 2006, Rutherford, 2008). A temperature difference due to derivation form different depths may also have created a temporary chilled boundary between the two magmas.

According to the Jeju mantle plume chemical genetic model of Tatsumi *et al.* (2005), the lava shield would correspond to the subalkalic series whereas the tuff stage would correspond to the low-Al alkalic series. In their model the subalkalic magma is thought to be derived from a shallower portion of the mantle compared to the alkalic magma. This is also supported by our data. This would indicate that the magma forming the tuff cone had to transit through the lava shield magma, and possibly opened a path for it to follow. The tuff cone magma was derived from a relatively lower degree of partial melting compared to the lava shield magma, therefore it was

probably richer in volatiles (Moore, 1970), as suggested also by the greater CO_2 content in alkali magmas compared to subalkali magmas (Holloway & Blank, 1994). This would have resulted in higher propagation energy for the dyke tip to open a path to the surface (Rubin, 1995). Once the vent was opened and the initial source exhausted, the subalkali magma could have exploited the upper section of the alkali magma's plumbing system to reach the surface.

This raises the question of whether fertile mantle sources, giving rise to subalkali magma under Jeju, are continuously generating magma, which only has the possibility to erupt once a path is opened by a more active alkali magma possibly triggered by a mechanism such as that proposed by Valentine & Hirano (2010). The converse does not necessarily have to occur, given that the subalkali magma is derived from a shallower depth compared to the alkali magma, and hence it can erupt without disturbing the latter. Particularly in the case of Jeju Island a spectrum of alkali and subalkali magmas has occurred intercalated throughout the existence of the volcanic field. This may represent a combination of the time and volume predictability suggested by Valentine & Perry (2007). In the Udo case, the small-volume alkali magmas may relate to tectonically-controlled, time-predictable events, whereas the larger-volume, subalkali magmas may represent magmatically-controlled, volume-predictable events (Valentine & Perry, 2007). The two magmatic systems however do not necessarily have to be acting independently or in a mutually exclusive fashion. Such behaviour, if true, has important implications for hazard prediction, because the magma flux involved in the initial eruption may not be indicative of the final eruptive volume but instead give a gross underestimate.

4.10 Conclusions

Detailed geochemical sampling of the small-volume basaltic eruption sequence of Udo Volcano has shed light on magmatic processes in the upper mantle beneath Jeju Island, Republic of Korea, and parts of its plumbing system.

Two distinct magmas, derived from separate sources at different depths in the mantle were involved in the eruption sequence. The first magma to be erupted is concluded

to have been a small-volume alkali basalt magma derived from metasomatized peridotite with residual garnet at c. 3 to 3.5 GPa. This alkali magma underwent clinopyroxene + olivine ± spinel fractionation at c. 1.5 to 2 GPa in the upper mantle and was buffered by metasomatic amphibole. Shallow crystallized plagioclase + olivine were retained in the magma as phenocrysts. During ascent the alkali magma intersected a larger ponded subalkali basalt magma batch that was fractionating olivine and derived from a chemically distinct mantle and shallower source at c. 2.5 GPa. Emptying of the deeper alkali source region caused the closure of the conduit/dyke system where fractionation had been taking place causing a subsequent squeezing out of the residual magma that had a more evolved composition, despite lower levels of shallow crystallization of olivine and plagioclase. The eruption conduit was exploited in the final stages of this polymagmatic eruption by the subalkali magma, which erupted to form the lava shield.

These results led us to suggest that deeply-derived, small-volume alkali basaltic magma may act as a trigger or path-opener for eruption of shallower-derived, larger-volume subalkali basaltic magma and that the two magmatic systems are not mutually exclusive. Moreover the two magmas used the same, single-dyke plumbing system; it is possible that this is a precondition for eruption of two magma types at a monogenetic volcano.

The contrasting nature of the two magma batches involved in the monogenetic eruption of Udo Volcano shows how chemically and petrologically diverse a seemingly simple monogenetic volcano can be. It demonstrates that a high-resolution or comprehensive sample set is necessary to characterize the range in eruption chemistry and nature of eruption models for individual monogenetic vents.

From a hazard perspective the findings of this study indicate that the course and final developments of a volcanic eruption in a monogenetic basaltic field can not be solely predicted on the basis of the initial style of volcanism and the characteristics of the magma type involved.

4.11 Acknowledgments

Appreciation is expressed to Bob Stewart, Richard Price, Greg Valentine, Ting Wang and Mary Gee for constructive discussion and comments and to Chang Woo Kwon for able assistance in the field. Thorough review by Greg Valentine, Amanda Hintz and an anonymous reviewer greatly improved the manuscript. This project was supported by the Foundation for Research, Science and Technology International Investment Opportunities Fund Project MAUX0808 to SJC "Facing the challenge of Auckland volcanism", by the Basic Science Research Program to YKS (2009-0079427) through the National Research Foundation of Korea funded by the Ministry of Education, Science and Technology and by a Massey University Vice-Chancellor's Scholarship to MB.

Chapter 5:

Geochemical signature of plumbing complexity in monogenetic eruptions

This chapter investigates the detailed chemo-stratigraphy of four monogenetic volcanic centres on Jeju Island and attempts to explain the different chemical trends observed. Deeply derived and possibly multiple-sourced, independently evolving magma bodies may erupt sequentially from the same vent through a clear plumbing system to form generally uninterrupted depositional sequences with continuous chemical trends, such as described in Chapter 4. Alternatively, magma bodies may rise independently through congested plumbing systems composed of dyke complexes and multiple vents, resulting in interrupted eruptions and vent instability, which are reflected by breccia horizons and truncation surfaces in depositional sequences, correlated with stepped and mixed chemical trends.

This chapter is based on work published in two separate manuscripts. The main conclusions were drawn from the manuscript "The influence of magma plumbing complexity on monogenetic eruptions, Jeju Island, Korea" *by Marco Brenna, Shane J. Cronin, Károly Németh, Ian E. M. Smith and Young Kwan Sohn, published in* Terra Nova *(23, 70-75, 2011; DOI 10.1111/j.1365-3121.2010.00985.x), which deals with chemical variability and its significance for the plumbing system of Udo, Suwolbong and Songaksan Volcanoes. This article and its supplementary data file are attached to this thesis as Electronic Appendix C and D respectively. Chemical variability and its significance for the plumbing system of the Ilchulbong Volcano was published in the manuscript* "Ilchulbong tuff cone, Jeju Island, Korea, revisited: A compound monogenetic volcano involving multiple magma pulses, shifting vents, and discrete eruptive phases" *by Young Kwan Sohn, Shane J. Cronin, Marco Brenna, Ian E. M. Smith, Károly Németh, James D. L. White, Rachel M. Murtagh, Yeong Mun Jeon and Chang Woo Kwon, published within the* Geological Society of America Bulletin *(124, 259-274, 2012; DOI 10.1130/B30447.1). This article is attached to this thesis as Electronic Appendix E.*

The author of this thesis was the principal investigator dealing with the interpretation of the geochemistry data and the link with the stratigraphic record in both manuscripts. This geochemical aspect forms the basis for this chapter and the model proposed in its conclusion. Co-authors provided assistance in the field, chemical data and comments on the Terra Nova manuscript, while Sohn and Cronin led the sedimentological work that forms the basis of the GSA Bulletin manuscript.

5.1 Introduction

Monogenetic volcanic eruptions occur in single, generally uninterrupted eruptive events lasting days (Camp *et al.*, 1987, Kienle *et al.*, 1980) to a few years (Foshag & Gonzáles, 1956), which may be interspersed with periods of relative quiescence. Once a monogenetic eruption has ceased, it will not re-start at the same location. Although the term monogenetic suggests a singular and possibly simple eruptive history, a range of different eruption styles and variability in the composition of erupted magmas can occur in eruptive phases separated by small time intervals (Fisher & Schmincke, 1984).

Very few monogenetic eruptions have been observed, hence interpretations are made from the sedimentary record (e.g. Lorenz, 1986, Pioli *et al.*, 2008, Riggs & Duffield, 2008, Sohn, 1996, Sohn & Park, 2005, Valentine *et al.*, 2005), or petrology and geochemistry [e.g. Blondes *et al.*, 2008, Brenna *et al.*, 2010 (Chapter 4), Erlund *et al.*, 2010, Johnson *et al.*, 2008, Luhr, 2001, Smith *et al.*, 2008]. Until now, however, integration between chemical transitions observed within eruptive sequences and the physical/depositional manifestation of these has been lacking for monogenetic events.

Here the relationships between chemical transitions and physical eruption mechanisms are described, as recorded by changes in the physical nature of erupted deposits. The significance of these for interpreting deeper magma pocket assembly and rise processes is also assessed. The study is based on four monogenetic eruptive centres in the Jeju Island Volcanic Field, Korea (Fig. 5.1a, b), and for each, chemical variability is correlated to indicators of changes in the eruption dynamics as

evidenced by truncation surfaces in stratigraphic sections and volcano-sedimentological transitions.

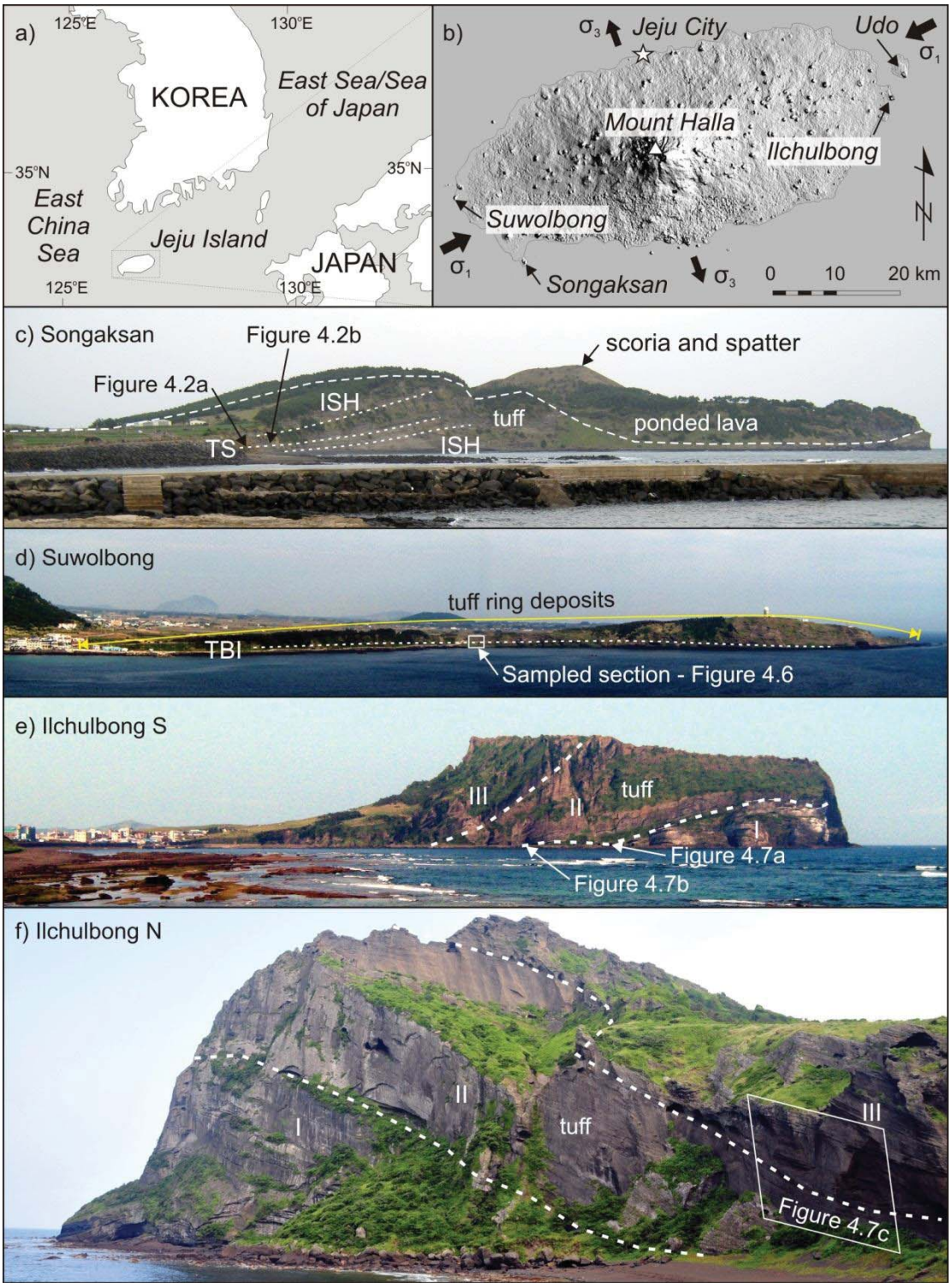

Figure 5.1: *a) Regional setting of Jeju Island, Republic of Korea. b) Digital elevation model of Jeju showing the locations of the four eruption centres discussed in this manuscript. The ENE-WSW compressional*

(σ_1) and NNW-SSE extensional (σ_3) stress fields are from GPS deformation data (Hamdy et al. 2005) and are likely to have been similar at the times of eruptions. c) View of Songaksan Volcano from the west. Truncation surface (TS) and impact sag horizons (ISH) as in Fig. 5.2 d) View of Suwolbong Volcano from the west. TBI is the tuff breccias horizon in Fig. 5.4d and 5.6. Note the asymmetry of the deposit thickness (thicker on the right than on the left, not due to differential erosion). TB disappears at the base of the southern exposure, but subsequent deposits are thicker in the south than in the north. The sampled section corresponds to section N3 of Sohn & Chough (1989). e) View of Ilchulbong tuff cone seen from the south and f) from the north (photograph by Yong Kwan Sohn). Note the three eruptive units.

5.2 Stratigraphic and chemical record

Four monogenetic eruptive centres were selected for detailed investigation based on their excellent exposure: Udo tuff cone and lava shield (Chapter 4); Songaksan tuff ring (Fig. 5.1c) and lavas; Suwolbong tuff ring (Fig. 5.1d); Ilchulbong tuff cone (Fig. 5.1e, f). Udo was described in Chapter 4 and hence only a summary of the stratigraphy is given below. Based upon observed outcrops all four centres had single eruptions with no enduring breaks associated with soil formation. Truncation surfaces are generally localized and sub-parallel to bedding suggesting that eruptions occurred over periods of a few days to weeks, and hence can be considered monogenetic. Sampling methodology for juvenile pyroclasts and lavas, along with analytical procedures, are described in Chapter 3. Whole-rock selected major (XRF) and trace element (LA-ICP-MS) analyses, as well as descriptions of sampled beds and locations are provided as Electronic Appendix F.

5.2.1 Udo tuff cone and lava shield

A comprehensive description of the tuff and lava shield and their field relationships, as well as the interpretation of their chemical variation was given in Chapter 4.

Briefly, the alkali basalt Udo tuff cone consists of three pyroclastic units separated by partial discontinuities and breccia horizons (Fig. 5.1). Subalkali basaltic lava lies directly over the tuff, with no evidence for erosion or soil formation, and is ponded inside the tuff cone as well as forming a surrounding shield. The alkali magma fractionated olivine + clinopyroxene at depth (c. 1.5 GPa) prior to eruption, whereas the subalkali magma fractionated olivine at a shallower level without obvious crustal interaction as described in Chapter 4 and investigated further in Chapter 6. The chemical variation within the tuff cone is smooth and continuous.

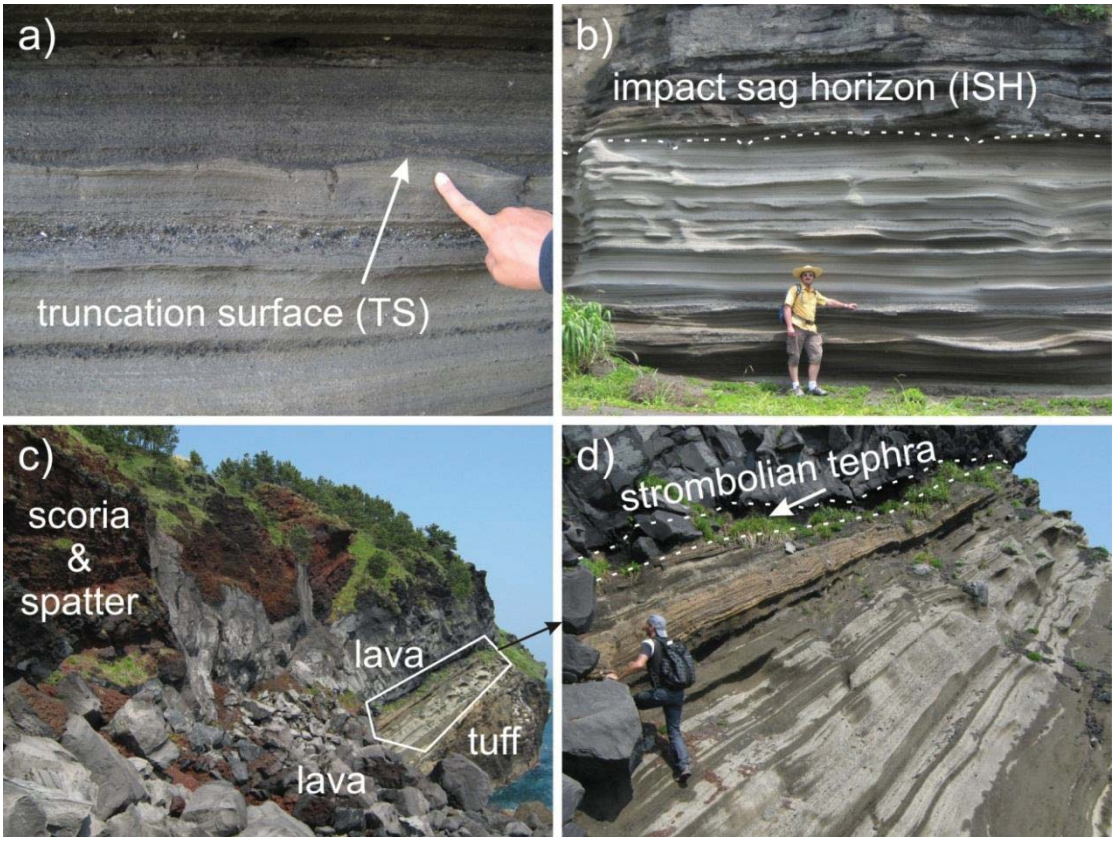

Figure 5.2: *Songaksan tuff ring. a) Truncation surface in the distal deposits. b) Characteristic bomb impact sag rich horizon. Note the deposit colour difference above and below the horizons in a) and b). c) Tuff overlain by lava and scoria and spatter complex. Also, note the lava fingers intruding the scoria sequence. d) Detail of the eruptive sequence with the strombolian tephra between the tuff and the lava.*

5.2.2 Songaksan tuff ring and lavas

Songaksan (Fig. 5.1b, c) consists of a phreatomagmatic tuff ring overlain by intra-crater ponded lava and a scoria cone and spatter complex. The succession is estimated at c. 7 ka in age (Cheong *et al.*, 2007). The ring comprises thin bedded and gently dipping lapilli tuff, tuff with high concentrations of accidental clasts and minor tuff breccia (Chough & Sohn, 1990). A local truncation surface in the distal deposits (Fig. 5.2a) is at the same stratigraphic level as volcanic bomb rich beds (Fig. 5.2b) separates finer and pale-coloured from coarser and darker pyroclastic deposits. The transition between phreatomagmatic and lava effusion is marked in the deposits by a c. 1 m thick strombolian tephra layer (Fig. 5.2c, d). The lava and scoria are olivine + clinopyroxene phyric basalts and contain locally abundant peridotite and pyroxenite mantle xenoliths together with felsic crustal xenoliths. Magma evolved through olivine + clinopyroxene fractionation at a deep level, before rapid ascent and eruption (Sohn *et al.*, 2002).

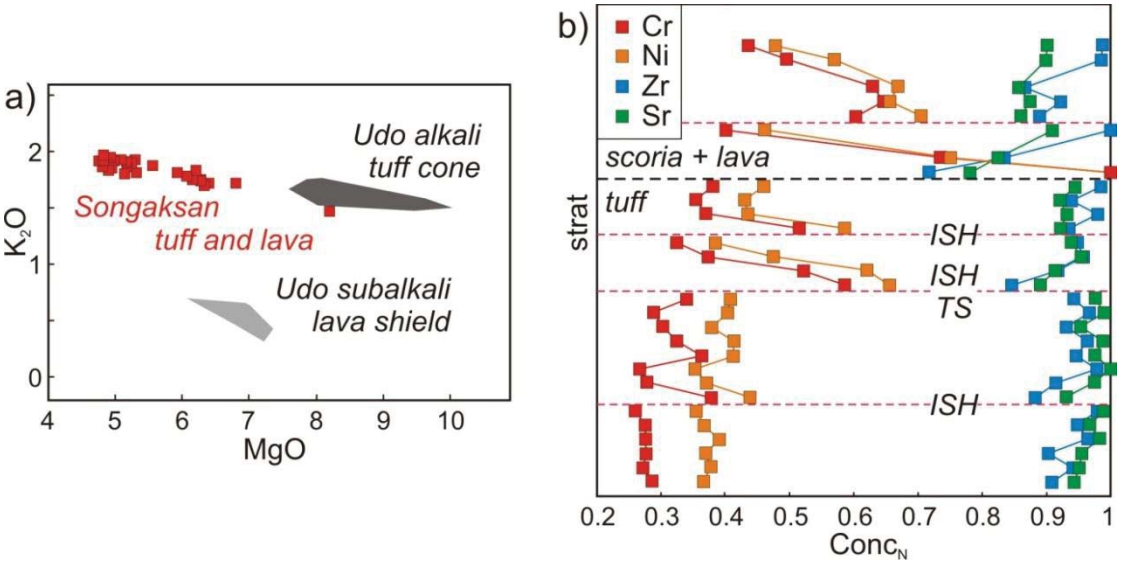

Figure 5.3: *a) Comparison of the chemical compositions of the Songaksan field with the Udo alkali and subalkali fields (wt% oxides). b) Chemostratigraphy and position of impact sag horizon (ISH) rich beds and truncation surface (TS). Note the stepped trends.*

The Songaksan magma was similar overall to the alkali magma that fed the Udo eruption (Chapter 4), but was generally more evolved (lower MgO, Fig. 5.3a). A

more thorough investigation of the physical conditions of magma fractionation and evolution at Songaksan are integrated into the discussion of small-volume centres presented in Chapter 6, however the overall similarity with the Udo alkali magma, and the presence of peridotite xenoliths suggests derivation from similar mantle depths. The greater degree of evolution (lower MgO) may however suggest a longer residence time in mantle or crustal dyke complexes. Chemically the Songaksan eruption can be subdivided into six different magma pulses (Fig. 5.3b): four within the tuff ring deposits and two within the lava and scoria field. The lowest two magma pulses in the tuff ring have relatively constant composition, whereas the others have considerable chemical variation within them, ranging from relatively primitive (compatible element enriched) to evolved (incompatible element enriched) compositions (Fig. 5.3b). This variation is likely due to mixing of magma at different stages of evolution, as will be investigated in more detail in Chapter 6.

5.2.3 Suwolbong tuff ring

The Suwolbong tuff ring (Fig. 5.1b, d) was formed c. 1 km off the present shore line (Sohn & Chough, 1989), during the last glacial maximum c. 18.5 ka ago (Cheong *et al.*, 2007). The marginal pyroclastic deposits overlie a distinctive paleosol topping a lava flow (Fig. 5.4a) and are dominated by breccias and lapilli tuff (Fig. 5.4) emplaced by pyroclastic fallouts and dry pyroclastic surges (Sohn & Chough, 1989). A tuff breccia layer (TBI in Fig. 5.4d and 5.6) c. 2 m above the basement in the northern deposits, tapers out and disappears at the base of the southern tuff sequence. The southern tuff sequence is thicker compared to the northern sequence (Fig. 5.1d), although it is much finer and hence represents distal tuff deposition compared to the coarser and more proximal deposits of the northern exposure (Fig. 5.4). The lithofacies variations hence indicate that the eruption was not radially symmetrical and pyroclastic surges with different physical properties were emplaced in different sectors of the tuff ring. Fluidal bomb sags in the fine tuff layers underlying breccia horizons indicate that the entire sequence was rapidly emplaced (Fig. 5.4c, d).

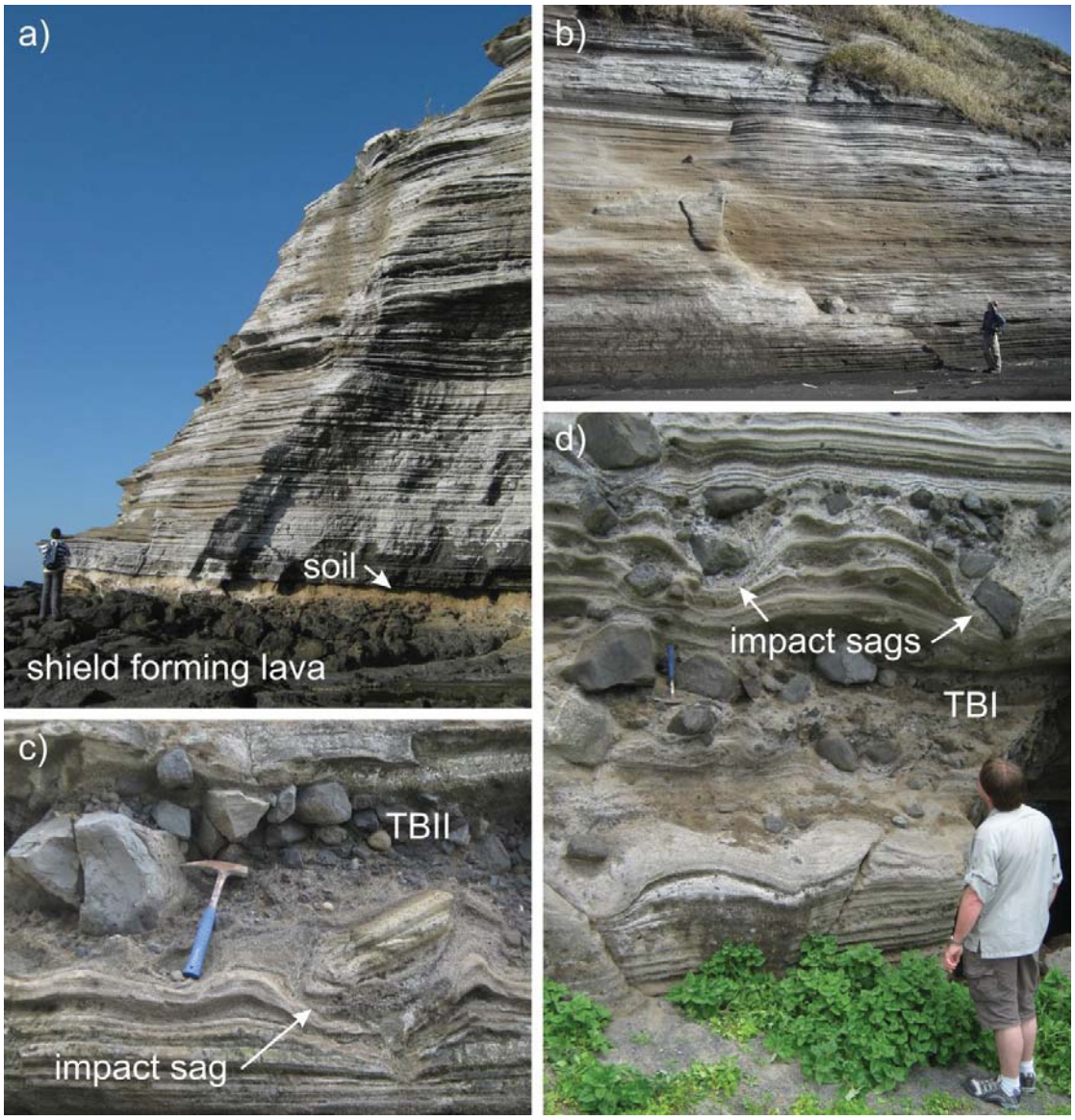

Figure 5.4: *Suwolbong tuff ring. a) and b) distal surge deposits in the southern cliff exposure. Note the soil horizon underlying the tuff sequence. b) Photograph by Károly Németh. c) and d) Exposure in the northern section of the tuff ring with tuff breccia layers TBII in c) and TBI in d). Note the fluidal impact sags indicative of rapid deposition of the eruptive sequence.*

Juvenile pyroclasts have olivine ± pyroxene phenocrysts in a glassy vesicular basaltic groundmass, but include a spectrum of alkali to mildly subalkali magmas intermediate between the end member compositions of Udo (Fig. 5.5), suggesting some mixing. Chemical trend similarity of the Suwolbong alkali samples with the Udo alkali magmas (Fig. 5.5), however, suggests a similar (i.e. deep) fractionation

regime for this magma types. The eruptive sequence can be chemically and stratigraphically subdivided into five different packages. The transition between these correlates with tuff breccia horizons as well as deposit style and colour changes (Fig. 5.6). The possibility of mixing between alkali and subalkali magmas, results in the chemical composition within individual packages, or magma pulses, not varying consistently, and hence making for a somewhat hazy distinction. However, changes in direction of chemical variation, as well as stepped resetting of chemical ratios are apparent (Fig. 5.6) and correlate with stratigraphic boundaries and marker beds.

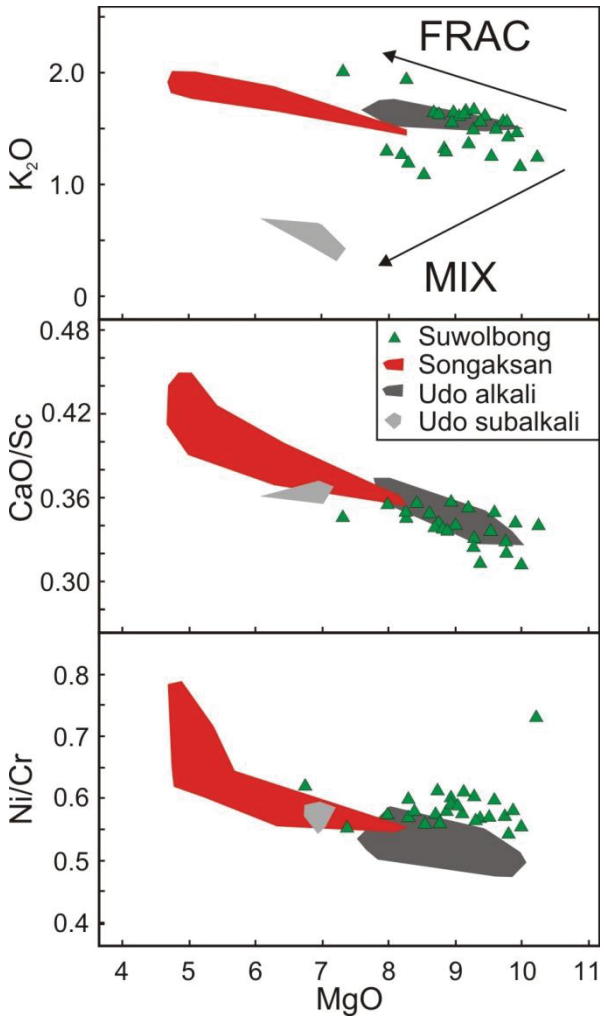

Figure 5.5: *Suwolbong chemical data show partially mixed (MIX) compositions intermediate between the two end member of Udo (alkali and subalkali). Partial mixing is visible in most major and trace elements, hence, element ratios similar in both alkali and subalkali magmas (e.g. CaO/Sc and Ni/Cr), but affected by fractionation (FRAC) are considered for the purpose of showing new magma influx.*

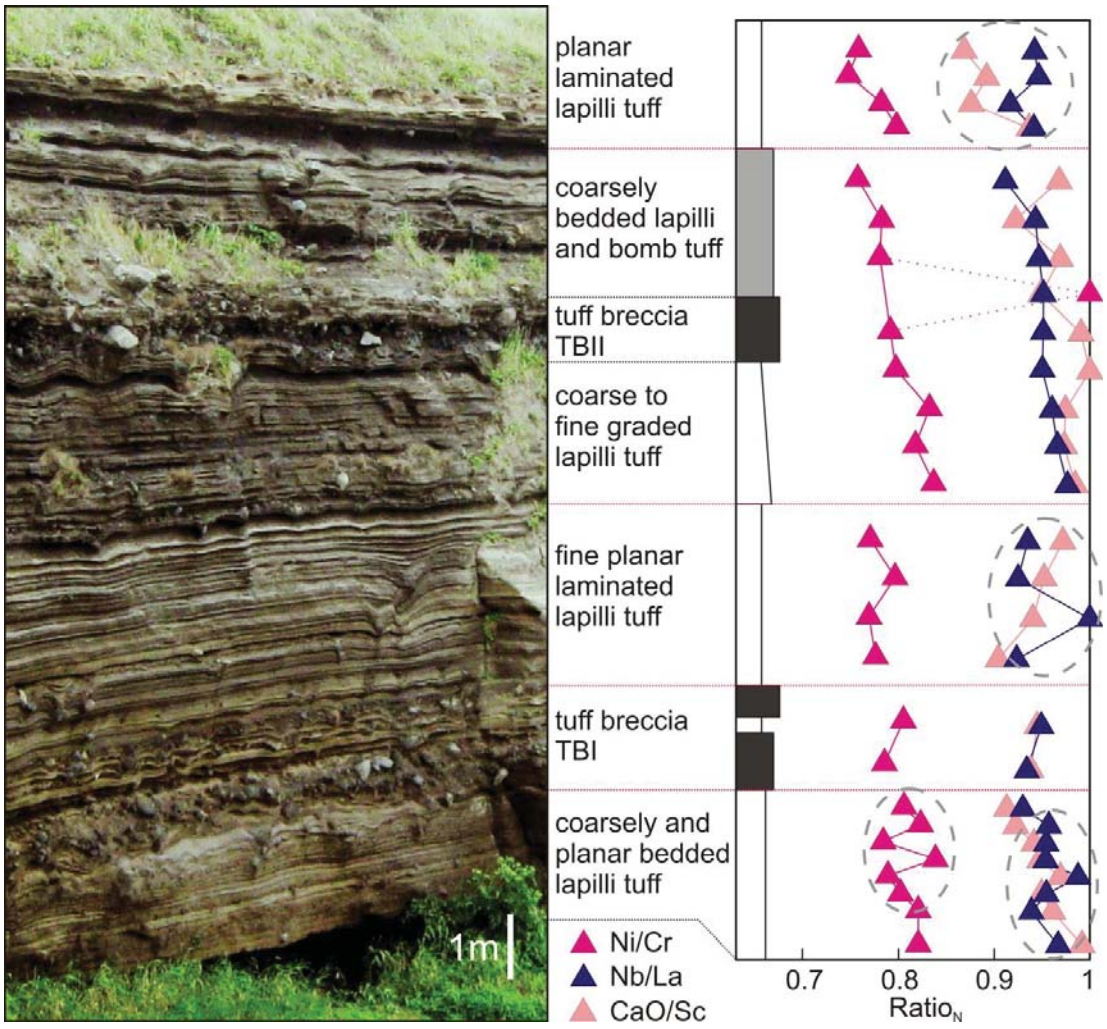

Figure 5.6: *Eruptive sequence at Suwolbong with subdivision into stratigraphic packages and correlation to chemostratigraphy. Height of cliff c. 15 m. Note the oscillating trend (dashed grey circles) possibly due to the alkali/subalkali mixing effect. Ratio$_N$ is the element ratio normalized to the maximum ratio value for each element pair.*

5.2.4 Ilchulbong tuff cone

The Ilchulbong tuff cone (Fig. 5.1b, e, f) was erupted in the middle Holocene, as the sea level was close to that at present (Cheong *et al.*, 2006, Sohn *et al.*, 2012). The eruption in shallow seawater generated wet tephra jets, which built a partially unstable tuff cone leading to sliding and slumping (Sohn & Chough, 1992). Three remarkable slumping horizons are associated with localized and volcano-wide

truncation surfaces and coarser breccia horizons (Fig. 5.7) and define separate eruptive units (I, II, III). Postdepositional faulting in the lower eruptive unit, which does not continue in the overlying deposits, and bed geometry suggest a vent shift occurred between the first and second eruptive phases (Sohn *et al.*, 2012). No deep runoff gullies are associated with the erosional surfaces on the steeper cone facies, suggesting that the cone was produced by a short-lived eruption.

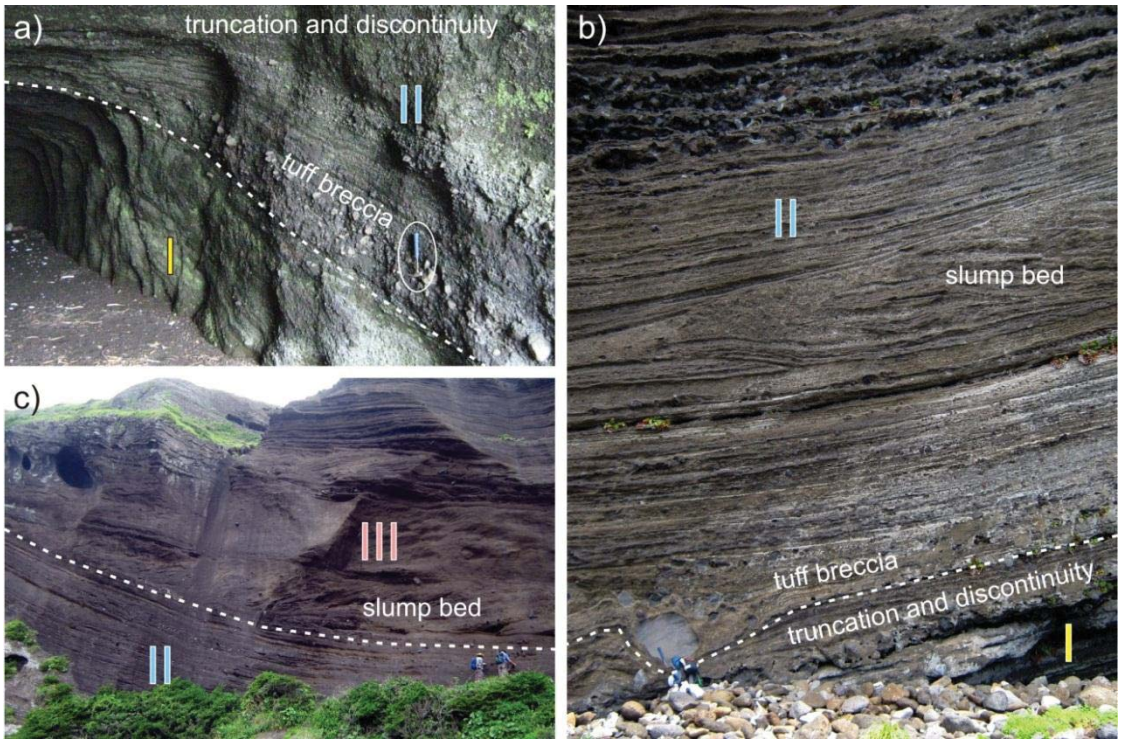

Figure 5.7: *Ilchulbong tuff cone. a) and b) Boundary between eruptive units I and II highlighted by discontinuous surfaces and truncations, also associated with breccia and reworked material. Geological hammer (circled in a) for scale. c) Boundary between eruptive units II and III highlighted by a prominent slump bed.*

Juvenile lapilli samples are homogenously olivine + clinopyroxene ± plagioclase phyric and microphyric in a vesiculated tachylite glass groundmass with olivine and plagioclase microlites. Samples from the second eruptive phase contain sparse olivine and clinopyroxene phenocrysts with sieve-textured cores and are also poorer in plagioclase, which if present, occurs as microlites in the groundmass.

Up to three alkali basalt magma pulses can be distinguished on the basis of a range of major and trace element abundances (Fig. 5.8) and the stepping chemostratigraphy (Fig. 5.9). The three phases have overlapping SiO_2 concentrations but can be distinguished on the basis of their MgO, Fe_2O_3, TiO_2, Cr, Sr and REEs and trace elements content together with evolutionary trends. Magmas 1 (phase I) and 2 (phase II) initially erupted with a relatively primitive composition of c. 8.5 to 9.5 wt% MgO, and evolved to c. 7.5 to 8 wt% MgO, whereas Magma 3 (phase III) has consistently lower MgO contents (c. 8 to c. 7 wt%). Magma 2 is distinct from Magmas 1 and 3 in having lower Fe_2O_3, TiO_2 and Sr concentrations for comparable MgO contents. The three magma batches/pulses were erupted consecutively with no apparent mixing or interaction, forming a stepped chemical stratigraphy similar to that of the Songaksan tuff ring.

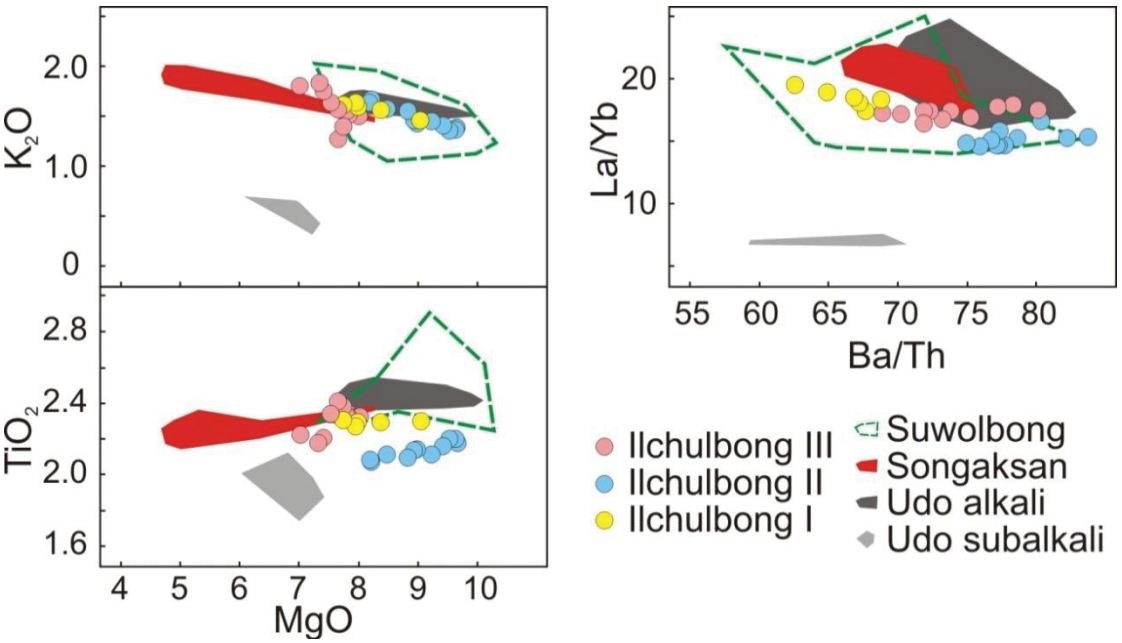

Figure 5.8: *Chemical discrimination of three magma batches (wt% oxides) feeding the Ilchulbong three eruptive units. Note that phases I and III are more similar to each other compared to phase II.*

5.3 Linking composition and stratigraphy

Geochemistry is useful for deciphering the magmatic history of an eruption. The generally small volumes involved in monogenetic systems (Valentine *et al.*, 2006)

together with the fast ascent rates (Rutherford, 2008) mean that magma can reach the surface with little interaction with its surroundings. Therefore erupted products of small-scale basaltic systems commonly preserve fine chemical variations indicative of internal petrogenetic processes [Blondes *et al.*, 2008; Brenna *et al.*, 2010 (Chapter 4); Smith *et al.*, 2008]. Small basaltic magma batches appear to rise so quickly in

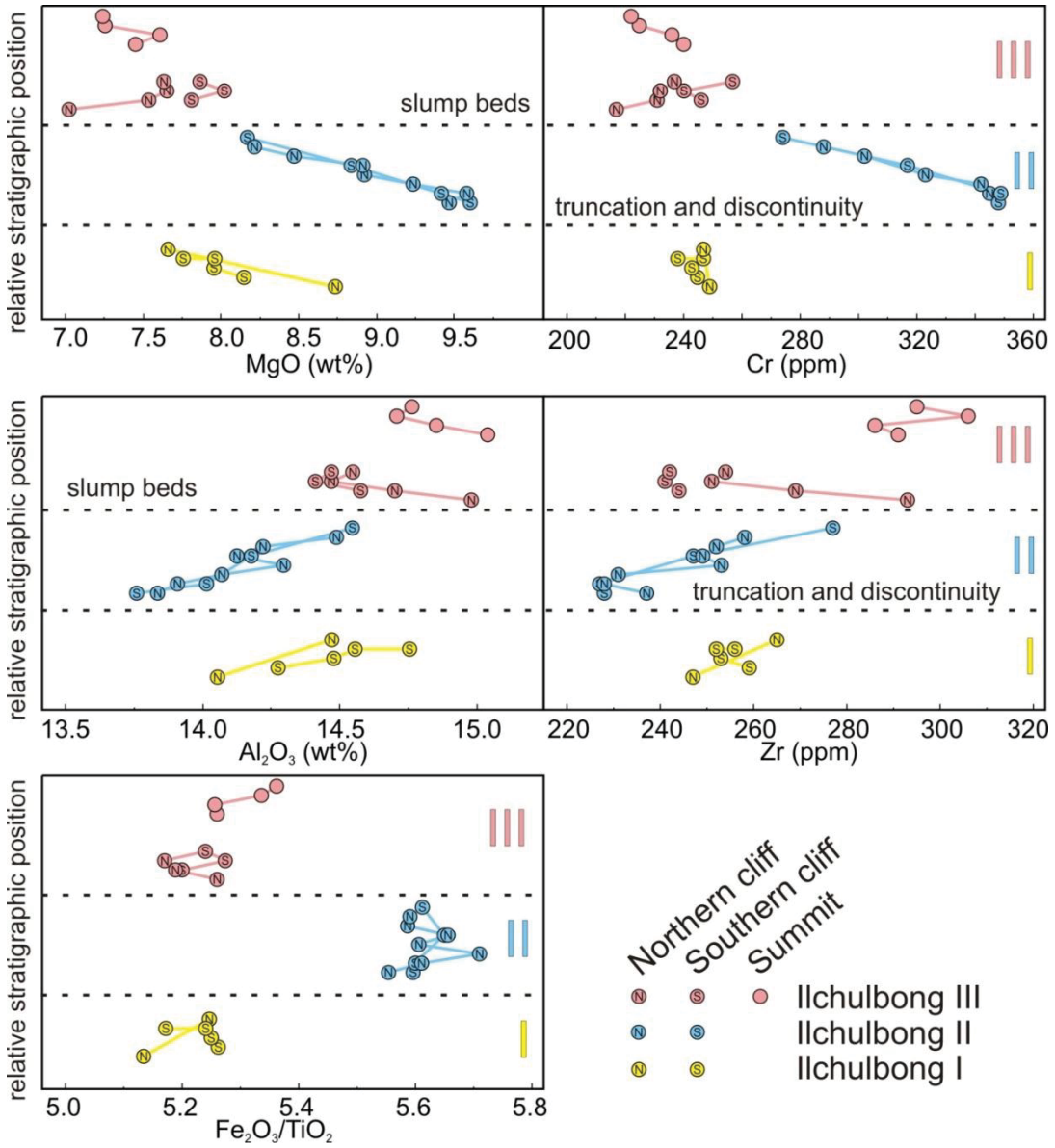

Figure 5.9: *Chemical discrimination of three magma batches feeding the three eruptive units. The three batches are clearly identifiable in a plot of chemical stratigraphy. Due to their greater chemical similarity, phases I and III may be related to each other. Note the pattern similarity between samples collected in the northern (N) and southern (S) sides of the tuff cone at comparable stratigraphic positions.*

confined conduits that there is little opportunity to homogenize any chemical variations that may be inherited from melting and fractionation processes at or near the source. Hence, even very small magma batches, each with a characteristic range in compositions can be identified in the chemical record of the eruption. The transition between these batches could then be mirrored in overall eruption sequence and deposit sedimentology.

The greatest chemical variation was observed at Udo, from an alkali magma batch forming the tuff cone to a subalkali magma to form the subsequent lavas (Chapter 4). A more subtle transition is also observed within the tuff cone succession. There, a breccia horizon associated with a minor discontinuous surface divides the tuff cone into a lower tuff cone and an upper tuff cone. The breccia horizon correlates with a transition from relatively constantly evolved chemical composition to onset of primitive magma that subsequently reverts back to evolved compositions (Fig. 4.3). This chemical shift is not an abrupt step between magmas. In this case rather than having two magma batches that evolved and erupted independently it is more likely that the two stages represent eruption of different parts of the same batch and that the breccia horizon indicates a vent shift with conduit clearing to a depth of 300 m (Sohn, 1996).

In the Songaksan tuff ring a truncation surface (Fig. 5.2a) correlates with a chemical shift (Fig. 5.3). Magma with relatively constant composition marks the beginning of the eruption. This is replaced by eruption of a series of rapidly evolving magma batches, following a short eruptive pause marked by a subtle truncation surface in distal pyroclastic deposits. This boundary also corresponds to a change in deposit colour and a bomb-sag rich bed (Fig. 5.2b). Two further distinct magma batches formed the lava and scoria field, the onset of which is marked by a c. 1 m thick strombolian lapilli fall bed that has the most primitive composition found at Songaksan (Fig. 5.2d, 5.3).

Truncation surfaces and related slump and tuff breccia horizons are also associated with the Ilchulbong eruption (Fig. 5.7). This was generated by at least two, and probably three, independent magma bodies with different genetic and evolutionary histories. Magma 1 erupted first during phase I, followed by the arrival of Magma 2

to initiate phase II. Magma 3 subsequently erupted in phase III and may be genetically related to Magma 1 due to its similarity in REE characteristics and TiO_2 concentration (Fig. 5.8, 5.9).

The stepped chemostratigraphic profile at Ilchulbong is parallel for duplicate sets of samples taken in each of northern and southern sampled sections (Fig. 5.9). One-to-one correlation of each bed in the tuff is not possible, however the thickness of phase II is similar in both northern and southern exposures, and hence samples can be correlated based on their position within the eruptive unit. The systematic compositional changes preserved in both northern and southern directions show that the eruption was symmetrical around a central vent during each phase.

Unconformities or truncation surfaces do not accompany every chemical variation. Several magma batches at the Suwolbong tuff ring are separated only by conformable breccia horizons, or by transitions in eruptive style from surges- to fall-dominated sequences, causing also a colour change of the deposit (Fig. 5.4c, d, 5.6). This suggests that separate magma batches may reach the surface with only a very short pause in eruption. Colour changes may not always be reliable indicators of relative chemical concentrations because these are also influenced by degree of fragmentation, oxidation state and diagenesis.

The stepped chemostratigraphy at Songaksan, Ilchulbong and Suwolbong indicates that these eruptions were formed by several distinct magma batches. At Suwolbong new vents were likely opened at new locations, also generating the asymmetry in the deposits, similar to Ukinrek, Alaska (Kienle *et al.*, 1980). The same occurred in the Ilchulbong eruption, with the first phase being erupted from a location to the east of the present volcanic edifice, which is where phases II and III were centred (Sohn *et al.*, 2012). In contrast, the lack of notable country rock-rich breccia units in the Songaksan deposits as well as the relatively concentric eruptive deposits centred in the core of the tuff ring imply that each ascending magma batch followed a single and stable shallow conduit to erupt from the same location.

5.4 Significance for the plumbing system

Different types of behaviours are recorded in the chemical evolution and deposition record of the four monogenetic volcanoes in the Jeju Field (Fig. 5.10). At Udo the continuity of the chemical trend suggest continuous ascent of magma in a single open plumbing system. By contrast at Suwolbong there is the stepped and oscillating trend, which is indicative of different magma batches ascending independently along different pathways, producing an asymmetric structure due to eruption from different vents. The compositional trends at Suwolbong are intermediate between the two end members (alkali and subalkali) of Udo, indicating that interaction (and mixing) between two magma sources occurred. This may be due to magma ascent being obstructed by the plumbing geometry, which is indicative of a congested system. Songaksan did not erupt a subalkali magma but involved a relatively open conduit that facilitated eruption of the initial batch with minor chemical modification. This was followed by pulses of independently ascending, chemically changing and erupting magma. Possibly the opening of a dyke at depth for one batch to rise, temporarily stalled the subsequent batches, and the closing of the dyke after the first batch's eruption changed the local stress field, allowing subsequent batches to ascend. The rapid chemical variation may be due to mixing of magmas at different stages of evolution (as detailed in Chapter 6). This suggests that magma stalled in dykes also interacted with later ascending (more primitive) magma pulses. The Ilchulbong eruption did not involve a subalkali magma. Magma erupted at the start of phase III was at a similar stage of evolution compared to the magma erupted during the last part of phase I, and both had similar chemical characteristics (Fig. 5.8, 5.9). This suggests that Magmas 1 and 3 were related by a common parental melt that became separated at depth andascended through different paths. These magmas, however, did not erupt sequentially because of the interruption caused by the ascent and eruption of Magma 2. Here too, interaction of ascending magmas in dykes may have influenced the eruption order of each magma pulse.

Regarding the near-source part of the plumbing system, Valentine & Hirano (2010) proposed that magma accumulates in porous and permeable shear zones (Fig. 5.10) extending laterally for several kilometres in the mantle, and that ascent would be initiated by magma overpressure/buoyancy. In their model this would generate a

series of deep dyke complexes (Fig. 5.10) where initial fractionation may occur, before final ascent to the surface. High deformation rates within the mantle have been

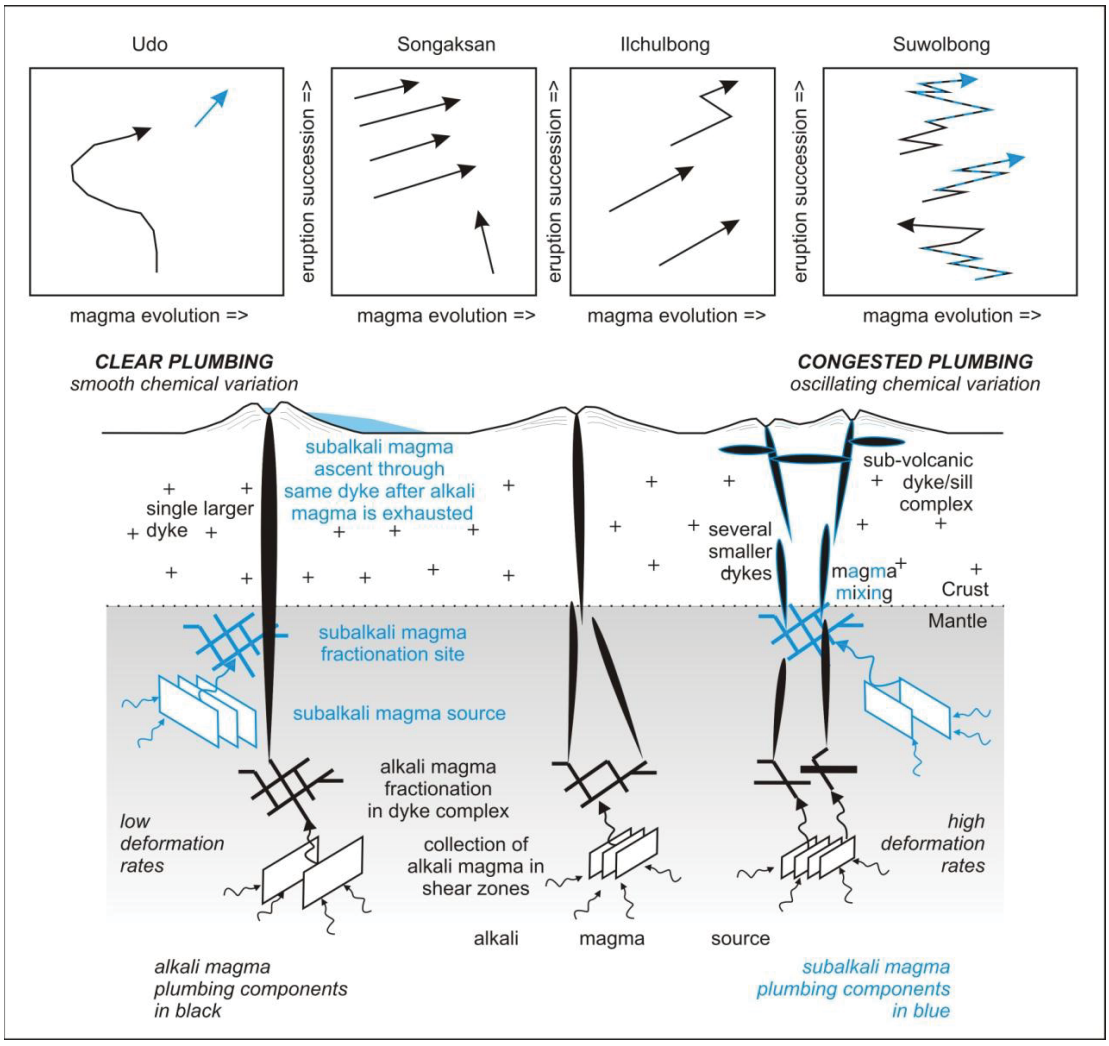

Figure 5.10: *Plumbing models described in the text. Diagram not to scale. The four schematic chemical-evolution diagrams at the top are indicative of the type of chemical variability observed in each case. Magma collects in shear zones near the source and evolves in overlying dyke complexes (Valentine & Hirano, 2010) before rising to the surface. The lack of a sub-alkali component in the Songaksan and Ilchulbong eruptions may be due to the lack of shallower magma reservoirs along the path of the alkali magma ascent. The single dyke in the Udo model does not imply a plumbing system open from source to surface, but rather that the eruption was fed by a single main dyke. At Suwolbong, dykes' volumes are smaller and hence, coalescence is limited (Ito & Martel, 2002).*

modelled to generate many small magma batches with highly variable chemical signatures reflecting mantle compositions (Bons *et al.*, 2004). Hence not only the shallow conduit character influences the final eruption characteristics, but also deeper mantle dynamics need to be considered.

This ultimately leads to the question of what controls the rise of magma and the number of eruptive phases in monogenetic eruptions. It is here proposed that generation of distinct magma batches is the result of magma accumulation processes occurring in several discrete reservoirs in the mantle. Interaction of these batches in the resulting dyke complexes during ascent can be variable and possibly depends on the overall magma volumes involved and horizontal dyke separation (Ito & Martel, 2002). Hence an integration of strain rate and magma generation rates will control the complexity of the plumbing system and resulting monogenetic eruption.

5.5 Conclusions

The widely accepted concept of a monogenetic volcano is that it represents the essentially continuous eruption of a single magma. However, detailed study of the geochemistry and volcanological evolution of four monogenetic volcanoes in the Jeju Island Volcanic Field shows complexities that can only be explained by the successive eruption of discrete magma batches and pulses. A hierarchy of increasingly complex plumbing systems is defined, which are independently linked to different source scenarios. Smooth within-batch chemical trends are indicative of sustained magma supply in an open plumbing system, whereas oscillating and stepped trends are suggestive of congestion. Open plumbing systems result in eruptions from a single vent, whereas magma in congested systems ascends through distinct dykes that have to fracture the basement each time. This results in truncation surfaces and tuff breccia horizons associated with the renewal of magma supply and activity and opening of new vents forming asymmetrical deposits. These findings illustrate the potential complexities that can be found in apparently simple monogenetic basaltic systems and which are only revealed by detailed studies of both the geochemistry and volcanology of the erupted deposits. The concepts may potentially be applied in real eruption scenarios in monogenetic volcanic fields. Live

monitoring of magma chemistry may give an indication of whether the eruption is likely to continue from the same vent or whether the eruption locus could shift overtime. Finally, the exposed complexity highlights the need for further investigation into the factors resulting in multiple eruptive phases in monogenetic volcanoes.

Chapter 6:

Development of the Small-Volume Magmatic System

This chapter presents and investigates the chemical variation and geological evolution of the small-volume basaltic magmatic system of Jeju based on detailed sampling of selected eruptions. The mantle source evolved spatially and chemically, and generated different magma compositions occurring in temporally distinct periods. A model for the tectonic control of the magmatic system is proposed.

6.1 Introduction

Intraplate volcanic fields consist of distinct eruptive centres that are relatively independent of each other, but which are related by spatial and temporal constraints. These constraints however do not have to remain constant and hence the characteristics of magmatic activity can vary throughout the life of the field. In the preceding two chapters, eruptive centres have been investigated on a singular basis. In this chapter, those eruptions will be integrated with other eruptions spanning the lifetime of the field to construction of a timeline of activity.

This chapter consists of the manuscript "*How small-volume basaltic magmatic systems develop: A case study from the Jeju Island Volcanic Field, Korea*" by: Marco Brenna, Shane J. Cronin, Ian E. M. Smith, Roland Maas and Young Kwan Sohn, published in *Journal of Petrology* (53, 985-1018, 2012; DOI 10.1093/petrology/egs007). This manuscript is devoted to the investigation of small-volume eruptions in the Jeju Island Volcanic Field. The study reveals a switch in the predominant magma generation mechanism c. 700 ka ago. It reviews the currently accepted genetic model for Jeju, and proposes a tectonic model for the control of the mechanisms leading to the initiation of magma generation. The article and its supplementary data files are attached to this thesis as Electronic Appendix G, H and I respectively.

The contributions of each author to the study were as follows:

Marco Brenna:	Principal investigator:	
	Carried out:	Field investigations and sampling
		Petrographic observations
		Electron microprobe analyses
		Sample preparation and chemical analysis
		Chemical data interpretation and modelling
		Manuscript preparation and writing
Shane J. Cronin:	Chief advisor:	
	Aided the study by:	Assisting in the field and sampling
		Editing and discussion of the manuscript
Ian E. M. Smith:	Advisor:	
	Aided the study by:	Assisting in the field and sampling
		Providing chemistry data
		Discussion of results and modelling
		Editing and discussion of the manuscript
Roland Maas:	Collaborator:	
	Aided the study by:	Providing Sr-Nd-Pb isotope data
		Editing and discussion of the manuscript
Young Kwan Sohn:		
	Advisors:	
	Aided the study by:	Assisting in the field and sampling
		Editing and discussion of the manuscript

6.2 How small-volume basaltic magmatic systems develop: A case study from the Jeju Island Volcanic Field, Korea

Marco Brenna[1], Shane J. Cronin[1], Ian E. M. Smith[2], Roland Maas[3], Young Kwan Sohn[4]

[1]*Volcanic Risk Solutions, Massey University, Palmerston North, New Zealand*
[2]*School of Environment, University of Auckland, Auckland, New Zealand*
[3]*School of Earth Sciences, The University of Melbourne, Parkville, Australia*
[4]*Department of Earth & Environmental Sciences, Gyeongsang National University, Jinju, South Korea*

6.2.1 Abstract

Jeju is a volcanic field that has erupted from around 1.8 Ma up to c. 1 ka ago. Eruptive activity began with distributed, basaltic, monogenetic, phreatomagmatic volcanism. Continuing monogenetic volcanism was later joined by more voluminous lava effusion events building a central composite shield. Samples from older (>0.7 Ma) and younger (<0.2 Ma) monogenetic centres were analysed for whole-rock major elements, trace elements and Sr-Nd-Pb isotopic compositions. Pyroclastic products of monogenetic centres are dominantly alkali basalt to trachybasalt, whereas the more voluminous lava flows and domes of the central edifice consist of subalkali basalt and alkali basalt to trachyte. Lavas from Early Pleistocene monogenetic centres are depleted in MgO, Cr and Ni, reflecting considerable olivine fractionation. By contrast, Late Pleistocene/Holocene monogenetic magmas fractionated clinopyroxene + olivine at deeper levels. Isotopic compositions show little variation across the suite but the Late Pleistocene/Holocene monogenetic centres have generally lower $^{87}Sr/^{86}Sr$ and $^{208}Pb/^{204}Pb$ and higher $^{143}Nd/^{144}Nd$ than the older centres and subalkali lavas. Major and trace element and isotope data suggest a common, shallower source for high-Al alkali and subalkali lavas, in contrast to a deeper source for low-Al alkali magmas. We propose that mantle melting was initiated in partially hydrous conditions at a pressure of near 2.5 GPa, followed by drier conditions and extension of the melting zone to 3-3.5 GPa, with a concomitant increase in the volume of melt derived

from the shallower part of the system to produce subalkali magma. Increasing melt production at shallow depths may be related to accelerated heat transfer resulting from deepening of the melting zone, or increased mantle upwelling. Shear zones-bound mantle lenses were uplifted probably lubricated by the shear zones created during the opening of the Sea of Japan/East Sea c. 15 Ma ago, and reactivated during rotation of the Philippine Sea Plate direction of subduction at around 2 Ma ago. This is the first hypothesised link between subduction processes and intraplate volcanism at Jeju.

6.3 Introduction

Small-volume magmatic systems are characterised by distributed plumbing systems and, at the Earth's surface, are expressed as fields of small volcanoes (Takada, 1994). These are usually basaltic but can display a wide range of chemical compositions and, importantly, petrological evolution can occur both within individual eruption sequences as well as over longer timescales that encompass the lifespan of the field. Although many studies have investigated the chemical evolution and compositional variability within single eruption sequences, relatively few studies have attempted to integrate the evolution of a series of eruptions within a volcanic field over time to understand the development of the field as a whole (e.g. Blondes *et al.*, 2008, Putirka *et al.*, 2009, Sakuyama *et al.*, 2009, Valentine & Perry, 2007) through its magmatic footprints (Valentine & Perry, 2006). Identifying, quantifying and modelling changes over differing timescales provides the key to understanding the way that magmas are generated in the mantle and how they rise toward the Earth's surface in small-volume magmatic systems.

Magmas of small-volume systems ascend relatively fast (Rutherford, 2008) and reach the surface without significant modification, therefore deep processes can be interpreted through the study of their chemical variation (McGee *et al.*, 2011, Smith *et al.*, 2008). By specifically targeting chemical variability within individual eruption sequences spaced out through the lifespan of the volcanic field, insight can be gained to the dynamic conditions of melt generation during the onset of activity, as well as changes during subsequent volcanism. In addition, investigation of single eruptions

can provide information on the nature of mixing and crystal fractionation processes that affect magmas prior to eruption.

Small-volume intraplate volcanic fields occur in all tectonic settings and on all continents, therefore factors controlling their genesis are likely to be as varied as their tectonic occurrence. Their existence has been related to mantle plume activity (Ritter *et al.*, 2001, Tatsumi *et al.*, 2005), lower crustal gravitational instabilities (Hoernle *et al.*, 2006, Timm *et al.*, 2010), lithospheric stretching (Mashima, 2009), asthenospheric upwelling unrelated to plumes (Faccenna *et al.*, 2010, Zou *et al.*, 2008), or modification of the stress field in a pre-existing polygenetic volcanic area (Hasebe *et al.*, 2001). The magmatic development of a volcanic field may also give insights into the underlying tectonics controlling the spatial distribution of activity.

Here we introduce a new dataset of small-volume basaltic eruptions from the Jeju Island Volcanic Field, Korea (Fig. 6.1), with the aim of developing a more general tectonic and magmatic model for the evolution of continental volcanic fields. We collected a series of samples from older (>0.7 Ma) and younger (<0.2 Ma) monogenetic, small-volume eruptive events in order to integrate the investigation of the chemical evolution with the temporal evolution of the distributed volcanism. Finally, we propose a tectonic model to explain the occurrence and location of the Jeju Island volcanic field. This study follows on from detailed studies of individual volcanoes by Brenna *et al.* (2010; Chapter 4), Brenna *et al.* (2011) and Sohn *et al.* (2011; Chapter 5).

6.4 Geological background and sampling localities

The Jeju Island volcanic system lies on the continental shelf off the south coast of the Korean Peninsula and consists of a large (c. 70 x 30 km), elliptical (elongate in an ENE-WSW direction) and symmetrical composite shield volcano (Mount Halla; Fig. 6.1). It is situated on continental crust and the volcanic pile is underlain by unconsolidated, muddy-to-sandy continental shelf sediments mapped as

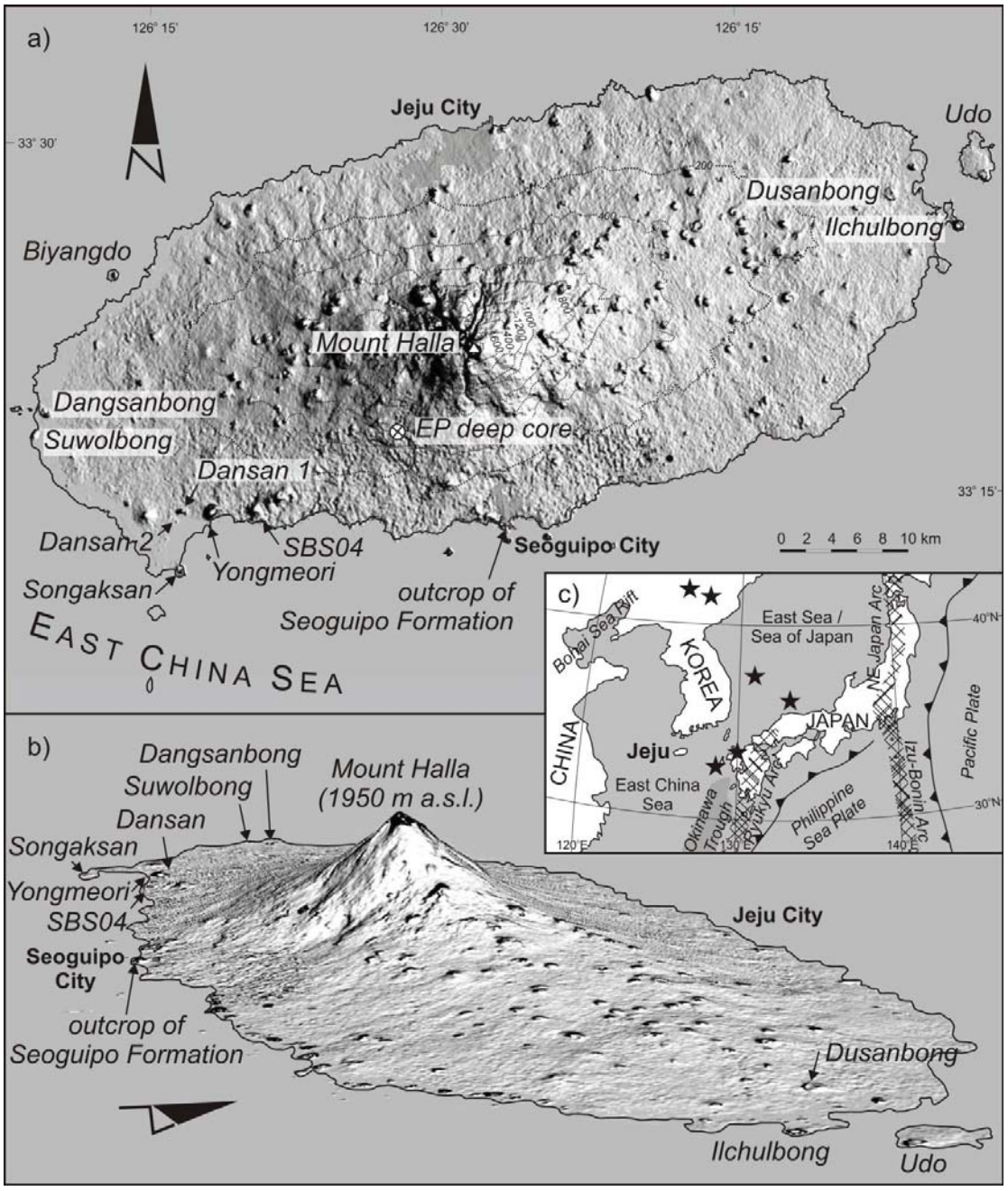

Figure 6.1: *Geological setting of Jeju Island and studied locations. a) and b) digital elevation model (DEM) based on ASTER satellite data acquired on 11 March 2002 and 19 May 2007. b) is an oblique view from the east, with vertical exaggeration of x5. c) Regional setting with the major tectonic features of the region. Stars indicate other locations of major Quaternary intraplate volcanic activity.*

the U Formation. Lava compositions span alkali basalt to trachyte and subalkali basalt to andesite (Park *et al.*, 1999). A distributed, small-volume, mainly alkali-basaltic volcanic field is superposed on the main volcanic edifice. This field contains over 300

monogenetic scoria and phreatomagmatic cones and rings scattered within and above the flanks of the central edifice, and these are the subject of this study.

Lee (1982) defined four stages of magmatic activity on Jeju Island and this subdivision has persisted in the literature until recently (Tatsumi *et al.*, 2005, Yang *et al.*, 2010). The first stage includes the Seoguipo Formation and a so called "basal basalt", the second is a "lava plateau" stage, the third is the "shield" stage that built Mt Halla and formed the main bulk of the Island, and the final "scoria cone" stage generated the distributed small-volume vents seen on the surface (Lee, 1982).

A different perspective on the evolution of the Jeju Island volcanic system was introduced by Sohn & Park (2004). A thorough study of the subsurface of Jeju Island, made possible by thousands of diamond-core wells drilled throughout the Island for groundwater research and exploitation, revealed that the onset of volcanism was expressed in small-volume phreatomagmatic eruptions c. 1.8 Ma ago in a shallow marine setting represented by part of the sedimentary Seoguipo Formation (Sohn & Park, 2004, Sohn *et al.*, 2008, Sohn & Yoon, 2010). Small-volume volcanism subsequently continued throughout the history of the magmatic system, intercalated with periods of larger-volume lava effusion that generated the central volcanic edifice (Mt. Halla). Some of the small-volume volcanoes that generated the phreatomagmatic successions and scoria cones are also temporally associated with these generally larger-volume lava flows (Brenna *et al.*, 2010; Chapter 4).

These two models have very different genetic implications. Our aim in this paper is to investigate the development of the Jeju field based on the evolution of the small-volume centres. These generally encompass the most primitive magmas erupted on Jeju, and as such preserve the most information on the origin of the magmas.

6.4.1 Sampled sites

The geographical distribution of sampled volcanic centres is shown in Figure 6.1 with available relative and absolute ages summarised in Table 6.1. Yongmeori tuff ring is one of the oldest volcanic centres exposed on the surface of the Island and was

described in detail by Sohn & Park (2005). For this study juvenile lapilli samples were collected from the tuff sequence and samples representing the onset of volcanic activity in the Early Pleistocene on Jeju were collected from the Seoguipo Formation near Seoguipo City, the Yongmeori tuff ring, and from tuff in EP deep core (equivalent to the buried Seoguipo Formation).

Table 6.1: *Published ages of studied volcanic centres on Jeju Island and subdivision into three time periods.*

Period	Location	Age	Method	Reference
Late Pleistocene/ Holocene	Ilchulbong tuff cone	c. 5 ka	^{14}C of shells in sedimentary formation containing reworked tuff	Sohn *et al.* (2002), Kim *et al.* (1999)
	Songaksan tuff ring	7.0 ± 0.3 ka	OSL + reworked material from the tuff ring dated at 4 ka by ^{14}C	Cheong *et al.* (2007), Sohn *et al.* (2002)
	Suwolbong tuff ring	18.3 ± 0.7 and 18.6 ± 0.9 ka	OSL	Cheong *et al. (*2007)
	Udo tuff and lava	114 ka	K/Ar	Koh *et al.* (2005),
	Dusanbong tuff cone and lava	< c. 160 ka	K/Ar age of rocks in nearby cores	Koh *et al. (*2008)
Middle Pleistocene	Dangsanbong tuff cone	Middle Pleistocene	Field relationships	Sohn & Park (2005)
	Dansan tuff ring 2	Younger than Dansan 1	Field relationships	Sohn & Park (2005)
	Dansan tuff cone 1	Early/Middle Pleistocene	Coeval with Seoguipo Formation	Sohn & Park (2005), Sohn *et al.* (2008)
Early Pleistocene	Yongmeori tuff ring	> c. 800 ka	Covered by Sanbangsan trachyte dome (733 ± 56 ka)	Won *et al.* (1986), Sohn & Park (2005)
	Seoguipo Formation and deep cores tuffs	> c. 1 Ma	Onset of small-volume phreatomagmatic volcanism, older than onset of voluminous lava effusion	Kim *et al. (*2002), Sohn *et al.* (2008)

OSL = optically stimulated luminescence

Centres from the second period of volcanic activity (Middle Pleistocene) on Jeju (the ages are relative; Table 6.1), include the Dansan cone and ring structures and the Dangsanbong tuff cone (Sohn & Park, 2005; Fig. 6.1). There too, juvenile lapilli samples were collected from the tuff sequences.

Late Pleistocene/Holocene centres include the Udo tuff cone and lava shield [Brenna *et al.*, 2010 (Chapter 4), Sohn & Chough, 1993], the Songaksan tuff ring and lava [Brenna *et al.*, 2011, Sohn *et al.*, 2002 (Chapter 5)], the Suwolbong tuff ring [Brenna *et al.*, 2011 (Chapter 5), Sohn & Chough, 1989], the Ilchulbong tuff cone [Sohn & Chough, 1992, Sohn *et al.*, 2012 (Chapter 5)], the Dusanbong tuff cone and lava, and Biyangdo, an island consisting of a scoria cone and associated lava flows (Fig. 6.1, Table 6.1). No direct age information is available for the Dusanbong and Biyangdo eruptions, however, these are grouped with the Late Pleistocene/Holocene centres

based on their preservation and geomorphic characteristics, and $^{40}Ar/^{39}Ar$ ages of rocks in a core near Dusanbong (<160 ka; Koh *et al.*, 2008). At each location juvenile lapilli, scoria and lava samples were collected.

Juvenile material was selected in the field based on density, vesicularity, morphology and preservation characteristics. Detailed location of the selected samples can be found in Electronic Appendix H, in Brenna *et al.* (2010) for Udo (Electronic Appendix B), in Brenna *et al.* (2011) for Suwolbong and Songaksan, and in Sohn *et al.* (2012) for Ilchulbong (Electronic Appendix F).

6.5 Whole rock geochemistry

6.5.1 Analytical procedures

Clean rock specimens were crushed using a steel crusher and chips free of saw-blade or crusher-plate marks were handpicked and milled in a tungsten carbide ring grinder. H_2O and LOI were measured by heating ~4 g of sample for 12 hours at 105 ºC and 1000 ºC respectively. 2 g of dried sample powder were weighed together with 6 g of SPECTRACHEM 12-22 flux and the mixture fused in Pt crucibles and cooled to a glass disc. Major element concentrations were measured by X-ray fluorescence (XRF; Siemens SR3000 spectrometer) at the University of Auckland using standard techniques. Major and minor elements (Si, Ti, Al, Fe, Mn, Mg, Ca, Na, K, P,) were determined as oxide components using methods similar to those described by Norrish & Hutton (1969).

In general, precision for each major or minor element is better than ±1% (1σ) of the reported value. Fe was measured as total Fe_2O_3 and analyses were recalculated to 100% volatile free and total FeO. Representative Major element analyses are reported in Table 6.2 and the whole dataset is available as Electronic Appendix I.

Table 6.2: *Major elements (XRF; normalized oxide wt%) and CIPW normative compositions of representative samples from small-volume centres in the Jeju Island Volcanic Field.*

Sample	YM03	YM04	YM10	YM12	S011	EP36b	SBS-04
Period	EP	EP	EP	EP	EP	EP	EP
Suite	HAA	HAA	HAA	HAA	HAA	HAA	HAA
SiO_2	50.5	49.34	48.76	50.49	44.71	44.67	44.56
TiO_2	2.35	2.44	2.58	2.37	3.49	3.13	3.26
Al_2O_3	17.42	17.52	18.2	17.43	16.17	16.18	14.90
FeO_{tot}	10.09	10.4	10.98	10.22	13.76	11.79	12.14
MnO	0.22	0.22	0.23	0.22	0.18	0.21	0.19
MgO	3.12	3.44	3.54	3.21	8.00	7.04	8.83
CaO	8.39	8.88	9.03	8.28	9.96	11.01	10.72
Na_2O	3.98	3.86	3.49	3.88	2.00	3.01	4.03
K_2O	2.82	2.71	2.07	2.82	0.69	1.96	0.78
P_2O_5	1.09	1.18	1.12	1.06	1.05	1.00	0.58
Total	100.00	100.00	100.00	100.00	100.00	100.00	100.00
LOI	0.02	1.30	1.64	0.22	2.72	0.41	-0.01
Mg#	35.55	37.07	36.52	35.93	50.90	51.56	56.45
Apatite	2.59	2.79	2.64	2.52	2.48	2.36	1.37
Ilmenite	4.47	4.64	4.90	4.51	6.63	5.94	6.20
Orthoclase	16.65	16.00	12.24	16.66	4.09	11.58	4.62
Albite	27.50	24.04	26.98	27.78	16.88	8.36	10.72
Anorthite	21.34	22.48	27.87	21.8	33.13	24.87	20.23
Diopside	11.47	12.11	8.54	10.79	8.08	19.53	24.23
Hyperstene	-	-	-	-	9.39	-	-
Olivine	12.73	13.39	15.58	13.31	19.41	18.21	20.02
Nepheline	3.36	4.69	1.39	2.75	-	9.25	12.68

Sample	DA-3	DA-7	DA-10A	DA-24	DB01	DB10	DS2
Period	MP	MP	MP	MP	MP	MP	LPH
Suite	LAA	LAA	LAA	LAA	LAA	LAA	LAA
SiO_2	48.02	49.46	48.73	48.43	49.29	47.88	48.44
TiO_2	3.10	2.64	2.81	2.51	2.50	2.36	2.51
Al_2O_3	16.21	14.65	14.88	15.10	14.76	13.73	14.93
FeO_{tot}	12.09	11.38	11.51	11.47	10.70	11.32	11.51
MnO	0.15	0.17	0.16	0.17	0.16	0.17	0.16
MgO	8.40	7.70	7.96	9.00	8.08	10.34	8.77
CaO	8.76	9.38	8.94	8.83	8.38	9.48	8.58
Na_2O	2.22	2.60	3.07	2.89	3.52	2.82	2.97
K_2O	0.62	1.53	1.41	1.06	1.91	1.43	1.61
P_2O_5	0.43	0.48	0.53	0.54	0.70	0.48	0.51
Total	100.00	100.00	100.00	100.00	100.00	100.00	100.00
LOI	2.53	2.07	-0.34	0.22	1.26	-0.10	0.36
Mg#	55.34	54.69	55.21	58.32	57.36	61.94	57.60
Apatite	1.02	1.14	1.25	1.27	1.66	1.13	1.20
Ilmenite	5.89	5.02	5.34	4.76	4.74	4.47	4.76
Orthoclase	3.66	9.07	8.34	6.24	11.27	8.46	9.54
Albite	18.74	22.02	25.82	24.48	24.82	19.11	23.51
Anorthite	32.45	23.75	22.68	25.08	18.82	20.56	22.63
Diopside	7.01	16.71	15.23	12.71	15.24	19.30	13.85
Hyperstene	21.57	7.63	-	3.96	-	-	-
Olivine	9.73	14.80	21.35	21.56	20.83	24.44	23.67
Nepheline	-	-	0.06	-	2.70	2.58	0.90

Trace elements were measured by both XRF (V, Cr, Ni, Cu, Zn, Rb, Sr, Zr, Nb, Ba) and laser-ablation inductively-coupled-plasma mass-spectrometry (LA-ICP-MS). XRF trace element measurements used the glass discs used for major element

Table 6.2 *(cont.)*

Sample	DS3	DS6	BY04	BY06	SK04	SK05	SK09
Period	LPH	LPH	LPH	LPH	LPH	LPH	LPH
Suite	SA	LAA	LAA	LAA	LAA	LAA	LAA
SiO_2	52.66	49.17	50.28	50.56	51.23	50.94	50.71
TiO_2	2.07	2.58	2.47	2.42	2.29	2.32	2.37
Al_2O_3	14.73	15.23	15.57	15.40	16.91	16.9	16.49
FeO_{tot}	10.35	11.29	11.32	11.20	10.38	10.43	10.69
MnO	0.15	0.16	0.16	0.16	0.15	0.15	0.16
MgO	7.03	7.87	6.08	6.14	4.91	5.04	5.39
CaO	7.86	8.28	7.97	7.93	7.37	7.46	7.7
Na_2O	3.46	3.15	3.78	3.80	4.19	4.22	4.02
K_2O	1.32	1.63	1.71	1.75	1.91	1.88	1.84
P_2O_5	0.37	0.64	0.65	0.63	0.66	0.65	0.64
Total	100.00	100.00	100.00	100.00	100.00	100.00	100.00
LOI	-0.35	0.49	-0.68	-0.95	-0.60	-0.17	-0.67
Mg#	54.78	55.43	48.90	49.41	45.75	46.30	47.35
Apatite	0.89	1.51	1.54	1.49	1.56	1.55	1.52
Ilmenite	3.93	4.90	4.68	4.61	4.36	4.40	4.51
Orthoclase	7.79	9.65	10.13	10.31	11.27	11.10	10.85
Albite	29.24	26.62	31.04	31.48	34.25	33.16	32.26
Anorthite	20.78	22.61	20.44	19.79	21.70	21.63	21.54
Diopside	13.18	11.99	12.58	13.05	9.08	9.53	10.61
Hyperstene	16.95	1.63	-	-	-	-	-
Olivine	7.30	21.16	19.13	18.95	17.22	17.33	17.87
Nepheline	-	-	0.53	0.38	0.65	1.37	0.93

Sample	SK11	SK20	SK22	SK26	SK27	SK31	SK34
Period	LPH	LPH	LPH	LPH	LPH	LPH	LPH
Suite	LAA	LAA	LAA	LAA	LAA	LAA	LAA
SiO_2	51.22	51.70	52.93	49.37	51.42	50.74	51.73
TiO_2	2.28	2.27	2.17	2.41	2.26	2.30	2.22
Al_2O_3	17.00	16.67	16.28	14.77	16.45	15.90	16.45
FeO_{tot}	10.29	10.27	10.00	11.02	10.39	10.59	10.29
MnO	0.15	0.15	0.14	0.16	0.15	0.15	0.15
MgO	4.8	5.00	5.06	8.33	5.28	6.46	5.34
CaO	7.33	7.32	7.10	8.6	7.41	7.85	7.3
Na_2O	4.36	4.03	3.82	3.39	4.06	3.71	3.97
K_2O	1.93	1.96	1.92	1.48	1.94	1.73	1.94
P_2O_5	0.65	0.63	0.59	0.48	0.62	0.57	0.61
Total	100.00	100.00	100.00	100.00	100.00	100.00	100.00
LOI	0.50	0.11	-0.17	-0.55	-0.83	-0.37	-0.09
Mg#	45.43	46.49	47.41	57.4	47.54	52.09	48.08
Apatite	1.54	1.50	1.41	1.13	1.48	1.35	1.45
Ilmenite	4.33	4.31	4.12	4.57	4.30	4.37	4.21
Orthoclase	11.38	11.60	11.33	8.76	11.49	10.20	11.44
Albite	33.84	34.08	32.28	26.19	34.12	31.42	33.61
Anorthite	21.15	21.61	21.63	20.70	20.90	21.63	21.35
Diopside	9.40	9.09	8.32	15.67	10.07	11.49	9.29
Hyperstene	-	2.46	13.84	-	-	0.92	3.28
Olivine	16.8	15.44	7.14	21.69	17.58	18.70	15.46
Nepheline	1.64	-	-	1.35	0.15	-	-

Total Fe as FeO. Oxides recalculated to 100% volatiles free.
Samples: YM is Yongmeori, SO and SBS are Seoguipo Formation, EP is deep core, DA is Dansan, DB is Dangsanbong, DS is Dusanbong, BY is Biyangdo, SK is Songaksan.
Period: EP is Early Pleistocene, MPC is Middle Pleistocene, LPH is Late Pleistocene/Holocene.
Suite: LAA is low-Al alkali, HAA is high-Al alkali, SA is subalkali

Table 6.3: *Trace elements (LA-ICP-MS; ppm) compositions of representative samples from small-volume centres in the Jeju Island Volcanic Field.*

Sample	YM03	YM04	YM10	YM12	S011	EP36b	SBS-04	DA-3
Period	EP	EP	EP	EP	EP	EP	EP	MP
Suite	HAA	HAA	HAA	HAA	HAA	HAA	HAA	LAA
Cs	0.15	0.16	0.21	0.36	0.22	0.46	0.5	0.12
Ba	640.9	683.68	660.31	626.2	544.79	588.89	549.06	477.03
Rb	44.63	27.5	24.87	53.25	10.26	45.71	11.5	8.31
Sr	894.33	930.87	1008.68	918.18	790.3	804.25	695.18	738.38
Pb	6.09	5.8	7.31	4.45	6.55	4.36	4.26	3.97
Th	7.84	7.2	7.83	7.92	8.16	8.13	7.46	6.52
U	1.26	0.97	0.93	1.37	1.4	1.85	1.51	0.52
Zr	338.78	335.77	349.7	358.91	337.74	328.76	276	288.17
Nb	69.88	69.78	72.75	71.1	70.6	66.42	60.89	59.62
Hf	8.06	8.01	8.64	8.25	8.45	7.79	6.74	6.77
Ta	4.95	4.75	5.17	4.97	5	4.99	4.39	4.27
Y	34.68	34.31	37.51	36.54	28.22	33.48	30.19	19.99
Sc	-	-	-	-	31.68	-	39.06	-
V	138.8	145.43	153.76	138.71	309.6	309.32	333.41	218.76
Cr	7.95	5.31	5.91	11.85	78.55	90.99	253.61	303.49
Co	29.37	26.08	34.48	34.7	46.24	67.12	68.34	57.07
Ni	5.91	23.46	79.41	14.18	64.13	71.37	95.01	160.46
Cu	8.12	15.34	21.51	10.38	29.48	30.43	55.41	25.71
Zn	99.91	95.29	106.34	97.98	122.81	98.27	106.45	81.95
Ga	22.92	22.16	22.83	22.7	21.46	21.68	20.18	19.97
La	58.9	58.85	60.29	59.42	42.15	57.51	48.88	23.11
Ce	117.17	113.13	117.37	115.08	88.42	108.5	91.38	47.38
Pr	14.03	13.3	14.19	13.77	10.52	12.67	10.99	5.95
Nd	57.35	55.64	59.95	57.82	43.58	51.72	44.48	26.71
Sm	10.85	10.73	11.41	10.96	8.85	9.74	8.88	5.88
Eu	3.27	3.17	3.36	3.2	2.72	2.97	2.6	2.1
Gd	9.4	9.62	10.27	9.84	7.97	8.68	8.26	5.3
Tb	1.3	1.27	1.37	1.35	1.1	1.24	1.12	0.75
Dy	7.64	7.32	7.99	7.7	6.28	7.12	6.51	4.38
Ho	1.39	1.38	1.51	1.42	1.16	1.3	1.19	0.8
Er	3.66	3.55	3.88	3.85	3.07	3.48	3.19	2.14
Tm	0.5	0.49	0.55	0.53	0.42	0.48	0.43	0.28
Yb	3.1	3.05	3.25	3.33	2.42	3.14	2.59	1.73
Lu	0.46	0.44	0.46	0.47	0.35	0.42	0.35	0.25

determination, a suite of 36 international standards were used for calibration, and Siemens SPECTRA 3000 software was used for data reduction. The Compton scatter of X-ray tube RhKb1 emission was used to correct for mass attenuation, and appropriate corrections were used for those elements analysed at energies below the Fe absorption edge. LA-ICP-MS analysis for a larger group of trace elements was carried out at the Research School of Earth Sciences, Australian National University, using Excimer LPX120 laser (193 nm) and Agilent 7500 series mass spectrometer following the method of Eggins *et al.* (1998). For this work, the same fused glass discs as for XRF were prepared as a multi sample polished mount. Samples were run in batches of 15 using NST612 glass standard at the beginning and end of each run to calibrate. Standard BCR-2 was also run with each batch to monitor analytical performance. 15 repeat analyses of standard BCR-2 as well as duplicate analysis of a tephra sample (Electronic Appendix I) indicate precision of <4% (RSD) and accuracy better than 5% at the 95% confidence level for most elements.

Table 6.3 *(cont.)*

Sample	DA-7	DA-10A	DA-24	DB01	DB10	DS2	DS3	DS6
Period	MP	MP	MP	MP	MP	LPH	LPH	LPH
Suite	LAA	LAA	LAA	LAA	LAA	LAA	SA	LAA
Cs	0.18	0.36	0.31	0.07	0.13	0.3	0.38	0.46
Ba	537.47	383.34	428.73	620.2	464.77	433.76	310.96	440.85
Rb	17.86	30.64	21.03	25.75	17.71	35.12	29.78	38.32
Sr	1641.79	606.33	583.68	777.6	549.32	515.22	396.17	610.89
Pb	3.88	7.05	3.74	15.05	5.72	6.13	6.5	7.08
Th	6	4.84	5.29	9.04	5.3	5.67	4.13	5.94
U	0.69	0.98	0.87	1.08	1.09	1.12	0.89	1.26
Zr	251.55	200.99	215.51	349.18	217.91	218.44	213.15	240.24
Nb	53.09	41.5	43.17	67.94	46.08	44.31	32.51	49.08
Hf	6.04	4.88	5.32	8	5.28	5.24	5.02	5.66
Ta	3.77	3.7	3.3	5.25	3.43	3.1	2.4	3.48
Y	23.84	22.74	25.13	27.13	23.74	25.68	22.18	23.79
Sc	-	-	-	-	-	-	-	-
V	226.91	226.43	209.29	209.22	236.63	222.2	163	199.27
Cr	253.01	273.93	363.84	481.03	582.34	420.51	284.5	277.82
Co	54.6	94.06	62.47	78	70.71	54.66	58.03	57.89
Ni	126.95	149.81	187.32	214.71	266.2	201.43	155.78	152.36
Cu	29.29	38.6	41.45	46.31	50.72	38.99	40.86	41.89
Zn	83.3	92.93	88.03	111.1	82.84	102.35	95.26	100.72
Ga	18.22	19.4	20.08	20.97	18.2	19.75	19.54	20.54
La	32.74	31.12	33.63	53.95	33.99	38.22	25.02	37.34
Ce	64.67	60.37	64.01	99.5	65.46	65.13	47.5	69.26
Pr	7.66	7.29	7.81	11.66	7.89	7.91	5.68	8.34
Nd	32.63	31.49	34.18	47.57	33.52	34.02	25.2	35.21
Sm	6.73	6.77	7.51	9.17	6.98	7.13	5.94	7.23
Eu	2.19	2.18	2.34	2.76	2.18	2.25	1.92	2.33
Gd	6.26	6.3	7.05	7.91	6.56	7	5.86	7.14
Tb	0.88	0.86	0.99	1.09	0.93	0.94	0.86	0.93
Dy	5.23	5.15	5.49	6.15	5.18	5.43	4.81	5.28
Ho	0.94	0.87	1.01	1.09	0.95	1	0.87	0.92
Er	2.5	2.29	2.51	2.78	2.52	2.48	2.16	2.31
Tm	0.35	0.3	0.34	0.36	0.32	0.34	0.29	0.29
Yb	2.08	1.87	2.07	2.18	2.03	1.91	1.8	1.77
Lu	0.31	0.24	0.27	0.3	0.26	0.27	0.23	0.22

There is a very close correlation (r^2 mostly >0.95, Electronic Appendix I) between those trace element abundances determined by XRF and those by LA-ICP-MS and this also provided a check on the analytical process. We have used the abundances determined by ICP because of the lower detection limits, more comprehensive element suite and better precision of the technique. Representative trace element concentrations are reported in Table 6.3 (LA-ICP-MS only) and the complete dataset (including XRF) is available as Electronic Appendix I.

Mineral analyses were obtained by electron microprobe. The instrument used was a JEOL JXA-840A using LINK systems LZ5 detector, QX2000 pulse processor and ZAF-4/FLS matrix correction software. Standard operating conditions were an accelerating voltage of 15 kV, beam current of 0.5 nA, beam diameter of 5 μm and a live count time of 100 s. Analytical precision was estimated by replicate analyses of mineral standards as (σ) ≤3% for elements present in abundances >1 wt%. A complete set of mineral analyses is provided in Electronic Appendix N.

Table 6.3 *(cont.)*

Sample	BY04	BY06	CH07	CH11M	CH13	SK04	SK05	SK09
Period	LPH	LPH	LPH	LPH	LPH	LPH	LPH	LPH
Suite	LAA	LAA	LAA	LAA	LAA	LAA	LAA	LAA
Cs	0.34	0.15	0.47	0.44	0.38	0.58	0.55	0.51
Ba	435.03	437.48	463.63	421.35	399.32	491.84	483.57	475.93
Rb	37.70	37.45	37.63	37.34	32.4	46.43	44.22	44.15
Sr	547.70	532.22	459.82	538.1	466.7	654.48	653.58	636.44
Pb	2.61	4.71	4.85	4.61	4.48	8.75	7.64	4.43
Th	5.72	5.89	5.99	6.26	5.17	7.03	6.64	6.42
U	1.20	1.2	1.17	1.19	1.01	1.49	1.44	1.39
Zr	261.19	265.66	270.75	261.69	235.2	277.17	265.79	259.7
Nb	46.94	47.71	42.67	44.14	39.26	52.47	51.37	51.28
Hf	6.27	6.22	6.47	6.26	5.74	6.52	6.21	6.03
Ta	3.56	3.5	3.7	3.66	3.18	4.12	4.33	4.07
Y	28.40	28.15	26.47	25.38	24.95	25.83	24.86	25.3
Sc	-	-	-	-	-	16.49	16.41	17.99
V	170.66	171.49	196.51	196.22	208.73	165.87	166.22	176.62
Cr	186.26	191.91	339.61	297.46	410.82	86.07	87.49	119.44
Co	58.84	57.23	77.92	70.62	69.44	65.73	79.65	67.43
Ni	103.55	101.15	162.55	244.81	220.2	65.97	64.73	76.51
Cu	28.13	30.73	38.93	121.99	44.31	32.99	30.7	33.45
Zn	98.45	101.02	91.99	88.8	87.62	114.63	101.78	102.49
Ga	21.73	21.36	19.64	20.12	19.04	23.43	23.42	22.87
La	37.80	37.71				42.14	40.68	39.76
Ce	71.00	71.22				79.65	77.96	76.25
Pr	8.60	8.58				9.16	8.95	8.76
Nd	37.79	37.41				39.01	36.92	36.97
Sm	8.05	8.23				8.01	7.69	7.87
Eu	2.55	2.56				2.58	2.58	2.56
Gd	8.12	8.11				7.27	7.19	7.1
Tb	1.09	1.08				1	0.98	0.97
Dy	6.44	6.38				5.74	5.62	5.6
Ho	1.13	1.14				1.02	0.94	1.02
Er	2.84	2.84				2.49	2.44	2.4
Tm	0.37	0.36				0.32	0.33	0.34
Yb	2.20	2.2				2.03	1.91	1.93
Lu	0.31	0.3				0.28	0.25	0.25

Sr-Nd-Pb isotopic compositions were acquired at the University of Melbourne (e.g. Maas *et al.*, 2005). Acid-leached chips (6M HCl, 100 ºC, 60 min), were dissolved (2 ml of 3:1 HF-HNO_3 for 2 days at 110 ºC and 6M HCl for 1 day) on a hotplate, followed by sequential extraction of Pb, Sr and Nd using a combination of anion exchange and EICHROM RE, LN and SR resin chromatography. Blanks were <100 pg and negligible. Isotopic analyses were carried out on a NU Plasma multicollector ICP-MS (MC-ICP-MS). Sr and Nd isotope ratios were normalised to $^{86}Sr/^{88}Sr=0.1194$ and $^{146}Nd/^{145}Nd=2.0719425$ (equivalent to $^{146}Nd/^{144}Nd = 0.7219$, Vance & Thirlwall, 2002), respectively, using the exponential law, and are reported relative to SRM987 = 0.710230 and La Jolla Nd = 0.511860. External precision (2σ) is ≤0.000040 for $^{87}Sr/^{86}Sr$ and ≤0.000020 for $^{143}Nd/^{144}Nd$. The results for international standards (BCR-2, BHVO-2, JNd-1) obtained in the course of this work (see Table 6.4) are consistent with reference data (e.g Elburg *et al.*, 2005, Raczek *et al.*, 2003, Tanaka *et al.*, 2000, Weis *et al.*, 2006). Pb mass bias was corrected using the thallium-doping technique (Woodhead, 2002), which is expected to produce

external precisions of 0.025-0.05% (2σ). High accuracy and precision are confirmed by the results for SRM981 and BCR-2 (see Table 6.4) and by repeated analyses of samples (not listed).

Table 6.3 *(cont.)*

Sample	SK11	SK20	SK22	SK26	SK27	SK31	SK34
Period	LPH	LPH	LPH	LPH	LPH	LPH	LPH
Suite	LAA	LAA	LAA	LAA	LAA	LAA	LAA
Cs	0.56	0.64	0.62	0.4	0.42	0.52	0.56
Ba	496.43	509.8	509.96	388.2	496.08	465.34	502.96
Rb	45.11	48.18	48.12	33.7	46.22	42.39	49.28
Sr	684.26	643.86	637.63	534.66	622.1	599.33	616.85
Pb	4.8	9.96	8.13	14.48	11.14	7.71	8.73
Th	7.34	7.33	7.66	5.14	7.34	6.76	7.56
U	1.46	1.54	1.55	1.08	1.53	1.34	1.61
Zr	288	279	288.39	211.66	294.24	271.55	290.72
Nb	53.02	52.61	51.77	41.05	52.33	49.12	53.38
Hf	6.77	6.4	7.02	5.25	6.83	6.61	6.98
Ta	4.11	4.47	4.76	3.51	3.94	4.6	4.41
Y	26.57	24.93	25.9	23.31	26.8	26.69	26.26
Sc	17.03	16.97	17.88	23.77	18.31	20.96	17.86
V	162.33	164.44	163.22	213.18	165.18	187.64	159.85
Cr	84.54	102.62	116.75	316.13	127.05	204.98	137.58
Co	58.09	67.34	88.78	81.5	51.34	88.64	71.51
Ni	61.97	67.29	76.23	174.54	80.65	114.89	83.52
Cu	31.15	34.71	35.52	43.74	39.9	36.16	35.98
Zn	103.95	115.86	105.06	99.78	106.67	107.56	120.03
Ga	23.14	22.73	22.6	20.85	22.76	22.44	23.41
La	43.29	42.61	43.07	31.43	43.17	39.7	43.04
Ce	79.78	80.7	80.41	61.58	79.88	74.44	82.69
Pr	9.41	9.28	9.41	7.35	9.46	8.96	9.44
Nd	39.45	38.43	38.94	31.19	38.71	36.19	38.62
Sm	8.31	8.02	8.13	6.92	8.14	7.83	8.13
Eu	2.72	2.6	2.51	2.24	2.62	2.52	2.54
Gd	7.59	7.02	7.58	6.42	7.4	7.7	7.69
Tb	1.01	0.98	1	0.9	1.03	1.05	1.02
Dy	5.97	5.89	5.92	5.12	5.94	5.83	5.87
Ho	1.04	1.02	1.01	0.89	1.06	1.07	1.03
Er	2.64	2.35	2.68	2.3	2.57	2.65	2.66
Tm	0.34	0.34	0.34	0.31	0.34	0.34	0.36
Yb	1.93	2.03	2.06	1.83	2.02	2.01	2.06
Lu	0.25	0.26	0.27	0.25	0.29	0.28	0.26

Samples: YM is Yongmeori, SO and SBS are Seoguipo Formation, EP is deep core, DA is Dansan, DB is Dangsanbong, DS is Dusanbong, BY is Biyangdo, CH is Ilchulbong, SK is Songaksan.
Period: EP is Early Pleistocene, MPC is Middle Pleistocene, LPH is Late Pleistocene/Holocene.
Suite: LAA is low-Al alkali, HAA is high-Al alkali, SA is sub-alkali

6.5.2 Major elements

The majority of analysed samples can be classified as alkali basalt to basaltic trachyandesite with a few being picrobasalt to basanite and subalkali basalt to basaltic andesite (Fig. 6.2a). The alkali basalt suite, including the picrobasalt and basanite samples, can be further subdivided into two sub-suites. One has generally higher Al_2O_3, and lower MgO than the other at comparable SiO_2 concentrations (Fig. 6.2b, c). For the sake of consistency these will be hereafter referred to as high-Al alkali and

low-Al alkali respectively, following the nomenclature of Tatsumi *et al.* (2005). SiO_2, Al_2O_3, Na_2O, K_2O and P_2O_5 are generally negatively correlated with MgO, whereas FeO is positively correlated with MgO in all suites (Fig. 6.3). CaO is

Table 6.4: *Isotope data for the small-volume centres of the Jeju Island Volcanic Field.*

Sample	$^{87}Sr/^{86}Sr \pm 2\sigma$	$^{143}Nd/^{144}Nd \pm 2\sigma$	$^{206}Pb/^{204}Pb$	$^{207}Pb/^{204}Pb$	$^{208}Pb/^{204}Pb$
U106	0.704311 ± 16	0.512789 ± 16	19.048	15.641	39.618
U115	0.704352 ± 14	0.512790 ± 12	19.011	15.643	39.583
U123	0.704403 ± 14	0.512801 ± 10	18.942	15.644	39.523
U125	0.704442 ± 14	0.512796 ± 7	18.932	15.648	39.527
U129	0.704446 ± 12	0.512777 ± 10	18.958	15.650	39.550
U132	0.704503 ± 16	0.512803 ± 8	18.958	15.655	39.555
U136	0.704625 ± 14	0.512765 ± 10	18.708	15.650	39.273
U137	0.704713 ± 14	0.512762 ± 14	18.759	15.656	39.355
YM03	0.704713 ± 16	0.512808 ± 10	18.859	15.642	39.363
YM04	0.704627± 16	0.512792 ± 10	19.031	15.642	39.542
YM10	0.704605 ± 15	0.512805 ± 9	19.008	15.639	39.513
YM12	0.704716 ± 16	0.512786 ± 11	18.970	15.648	39.502
BY04	0.704102 ± 18	0.512826 ± 7	19.008	15.640	39.600
BY06	0.704204 ± 14	0.512787 ± 7	18.987	15.633	39.557
DB01	0.704511 ± 14	0.512758 ± 10	19.240	15.667	39.965
DB10	0.704858 ± 15	0.512761 ± 8	18.930	15.644	39.464
DS2	0.704368 ± 15	0.512809 ± 8	18.979	15.643	39.602
DS3	0.704316 ± 15	0.512818 ± 8	18.968	15.642	39.549
CH07	0.704304 ± 16	0.512807 ± 8	18.930	15.638	39.515
CH11M	0.704186 ± 16	0.512829 ± 6	19.037	15.642	39.633
CH13	0.704254 ± 13	0.512824 ± 9	18.947	15.636	39.522
SK05	0.704074 ± 14	0.512814 ± 11	19.061	15.642	39.654
SK09	0.704062 ± 14	0.512832 ± 10	19.057	15.641	39.650
SK20	0.704244 ± 15	0.512805 ± 7	19.024	15.649	39.624
SK22	0.704238 ± 16	0.512810 ± 8	19.018	15.654	39.607
SK26	0.704240 ± 15	0.512796 ± 9	19.036	15.653	39.637
SK27	0.704210 ± 12	0.512815 ± 6	19.070	15.646	39.653
SK31	0.704338 ± 16	0.512811 ± 9	19.061	15.652	39.666
Standards					
BCR2	0.704995 ± 18	0.512647 ± 12	18.761	15.624	38.738
BCR2	0.704980 ± 11	0.512636 ± 10	18.757	15.615	38.713
BCR2			18.760	15.620	38.721
BHVO2	0.703457 ± 16	0.512983 ± 8			
BHVO2	0.703471 ± 14				
JNd-1		0.512130 ± 9			
JNd-1		0.512114 ± 15			

$^{87}Sr/^{86}Sr$ normalized to $^{88}Sr/^{86}Sr = 8.37521$ and reported relative to SRM987 = 0.710230; external precision (2σ) is ≤0.000040. $^{143}Nd/^{144}Nd$ normalized to $^{146}Nd/^{145}Nd=2.0719425$ (equivalent to $^{146}Nd/^{144}Nd = 0.7219$) and reported relative to La Jolla = 0.511860; external precision (2σ) is ≤0.000020. Pb mass bias corrected using thallium doping. Fifteen runs of SRM981 (not used to construct the Tl-Pb mass bias correlations) average 16.936±0.005, 15.489±0.009 and 36.701±0.024, consistent with the nominal composition adopted for this standard in Woodhead (2002).
Major and trace element data for the U1 series samples are reported in Brenna *et al.* (2010; Chapter 4) and for the CH series samples are reported in Sohn *et al.* (2012; Chapter 5).

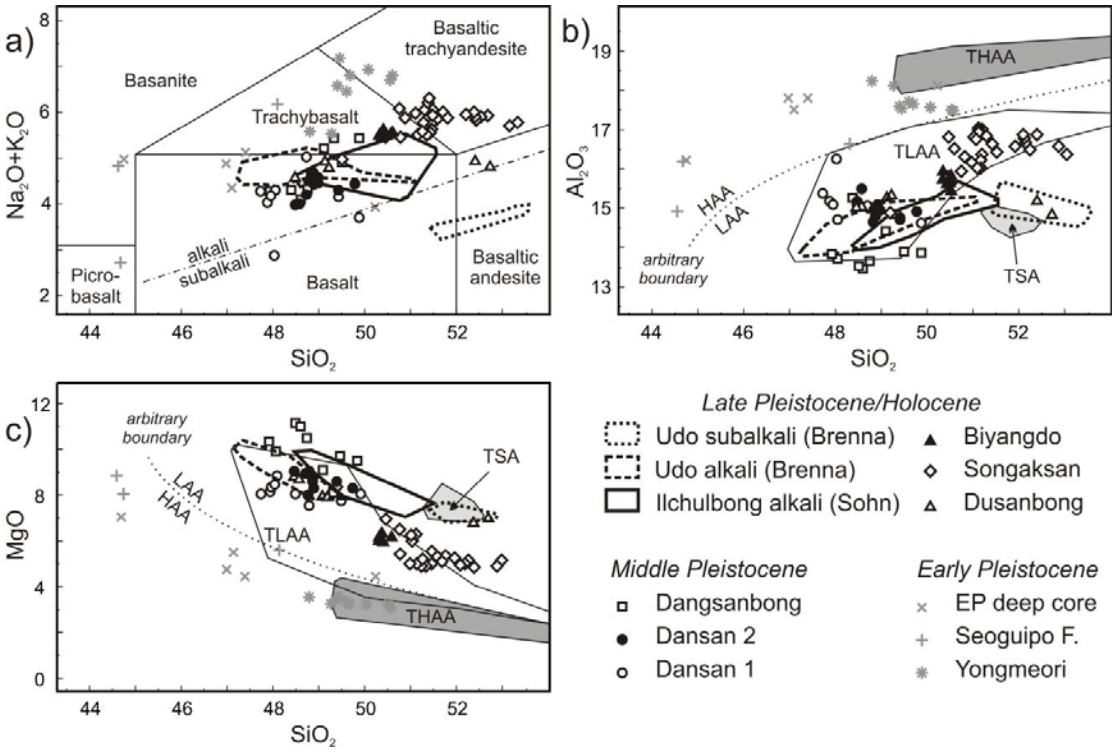

Figure 6.2: *a) TAS diagram (after LeBas et al., 1986) for samples from Jeju Island small-volume volcanoes. The boundary between alkali and subalkali is after Miyashiro (1978). b) and c) Distinction of samples from Jeju Island small-volume volcanoes based on the classification of Tatsumi et al. (2005). The alkali suite is separated into high-Al alkali (HAA) and low-Al alkali (LAA) with a dotted arbitrary boundary. THAA, TLAA and TSA are respectively the high-Al alkali, low-Al alkali and subalkali fields of Tatsumi et al. (2005). The Udo alkali and subalkali fields are from Brenna et al. (2010; Chapter 4) and the Ilchulbong alkali field is from Sohn et al. (2012; Chapter 5). wt% oxides.*

positively correlated with MgO in the alkali suites, but it is less clearly correlated in the subalkali suite. The behaviour of TiO_2 is variable within suites, on a scale of single eruptive sequences. It is both negatively (Udo, Dangsanbong) and positively (Songaksan, Ilchulbong, Yongmeori) correlated with MgO in the alkali suites. MnO is relatively positively well correlated with MgO in the low-Al alkali suite, whereas its concentration is variable in the high-Al alkali suite (Fig. 6.3). Samples of the high-Al alkali suite have lower SiO_2 and higher TiO_2, FeO_{tot} and CaO at comparable MgO concentrations compared to the low-Al alkali suite (Fig. 6.3). A minor chemical gap is apparent between c. $SiO_2 < 45$ and c. $SiO_2 > 47$ in the high-Al alkali suite (Fig. 6.2). Three samples with lower SiO_2 form a relatively different slope than the samples with higher SiO_2.

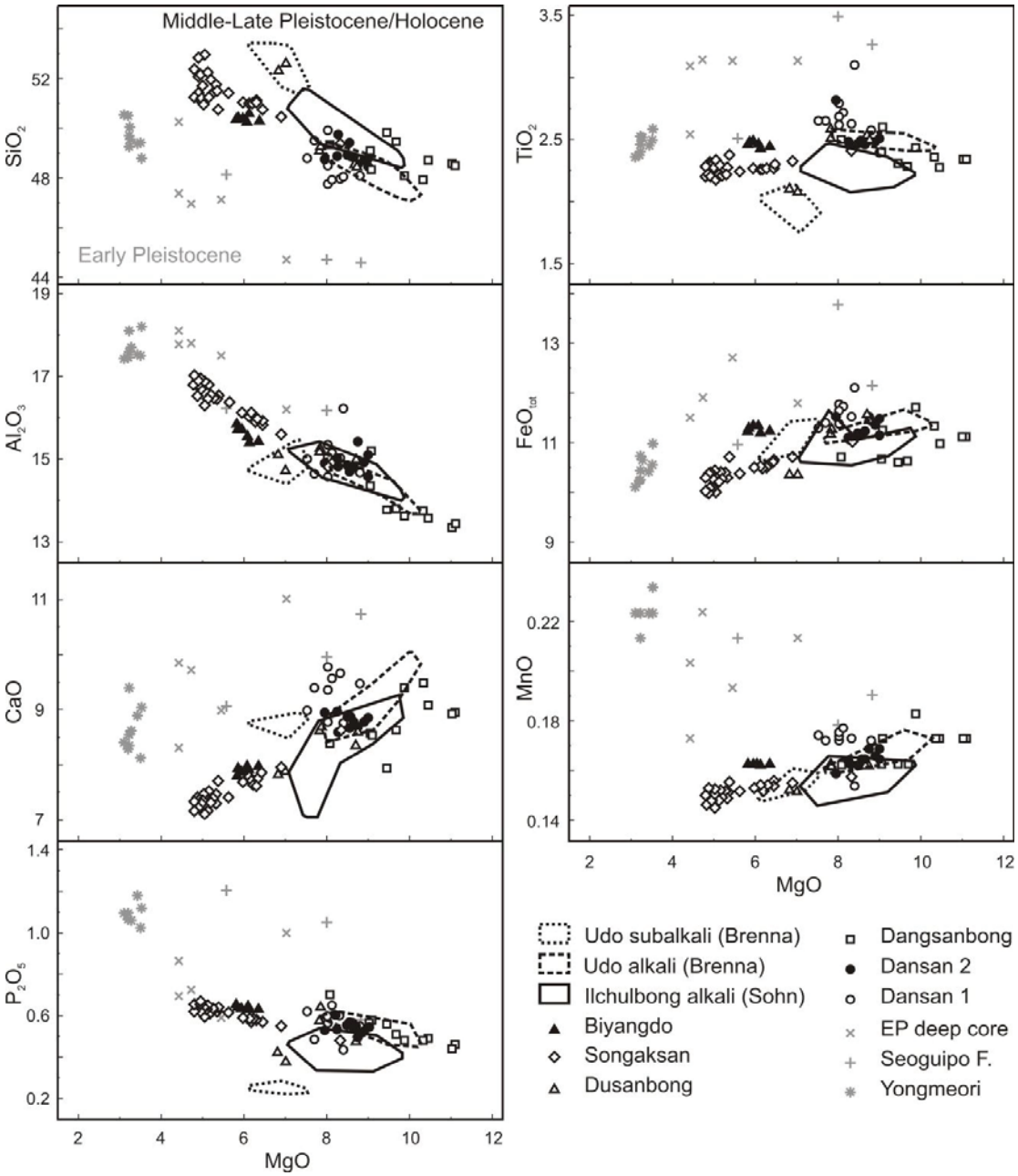

Figure 6.3: *Variation diagrams of major element data (in oxide wt%) of small-volume centres on Jeju Island, split into Early Pleistocene high-Al alkali (HAA) suite (grey) and Middle-Late Pleistocene to Holocene low-Al alkali (LAA) and subalkali suites (black). Plotted for comparison are the Udo alkali and subalkali fields of Brenna et al. (2010; Chapter 4) and the Ilchulbong alkali field of Sohn et al. (2012; Chapter 5). Note that the Ilchulbong field is broader compared to the Udo alkali field as a result of different magma batches being involved in the Ilchulbong eruption (Sohn et al., 2012).*

Two samples collected from scoriaceous agglutinate in a tuff complex near Yongmeori (SBS04) and lapilli in reworked volcaniclastic deposits in the Seoguipo Formation (SO11; Sohn & Yoon, 2010) have compositions similar to the Yongmeori tuff ring and to samples in the EP deep core (Fig. 6.2, 6.3). Dusanbong samples are both alkali (from the tuff cone) and tend towards mildly subalkali (from lava flows; Fig 6.2a). The Dansan suite is subdivided into Dansan 1 and Dansan 2. These correspond to vent 1 and vent 2 respectively in the description of Sohn & Park (2005), with Dansan 1 being older than Dansan 2.

There is considerable compositional variation among the small-volume centres. Some have single compositional trends, whereas others show multiple trends. Most analyses fall outside previously defined compositional fields [Brenna *et al.*, 2010 (Chapter 4), Sohn *et al.*, 2012 (Chapter 5), Tatsumi *et al.*, 2005], especially the high-Al alkali field of Tatsumi *et al.* (2005), where they extend to more primitive compositions (lower SiO_2; Fig. 6.2).

6.5.3 Trace elements

The classification into three different suites based on major elements is also applicable to trace elements (Fig. 6.3, 6.4). Samples in the alkali suites generally have higher abundances of trace element compared to the subalkali lavas (Fig. 6.4, Table 6.3). Trace elements compatible in mafic mineral phases (Cr, Ni, V) generally decrease with decreasing MgO concentration (Fig. 6.4). At Yongmeori, Cr and Ni are strongly depleted. The high-Al alkali suite is richer in V at similar MgO concentration compared to the low-Al alkali suite (Fig. 6.4).

Incompatible elements are generally enriched in all suites, but they are present in variable amounts. Samples from the high-Al alkali suite are generally richer in Sr compared to other suites, consistent with the results of Tatsumi *et al.* (2005). Some samples at Dansan 1 have anomalously high Sr concentrations (>1200 ppm). Given that these are not correlated to other LILE (Large Ion Lithophile Element) concentrations (Fig. 6.4) and that Dansan 1 is the only centre to show such an

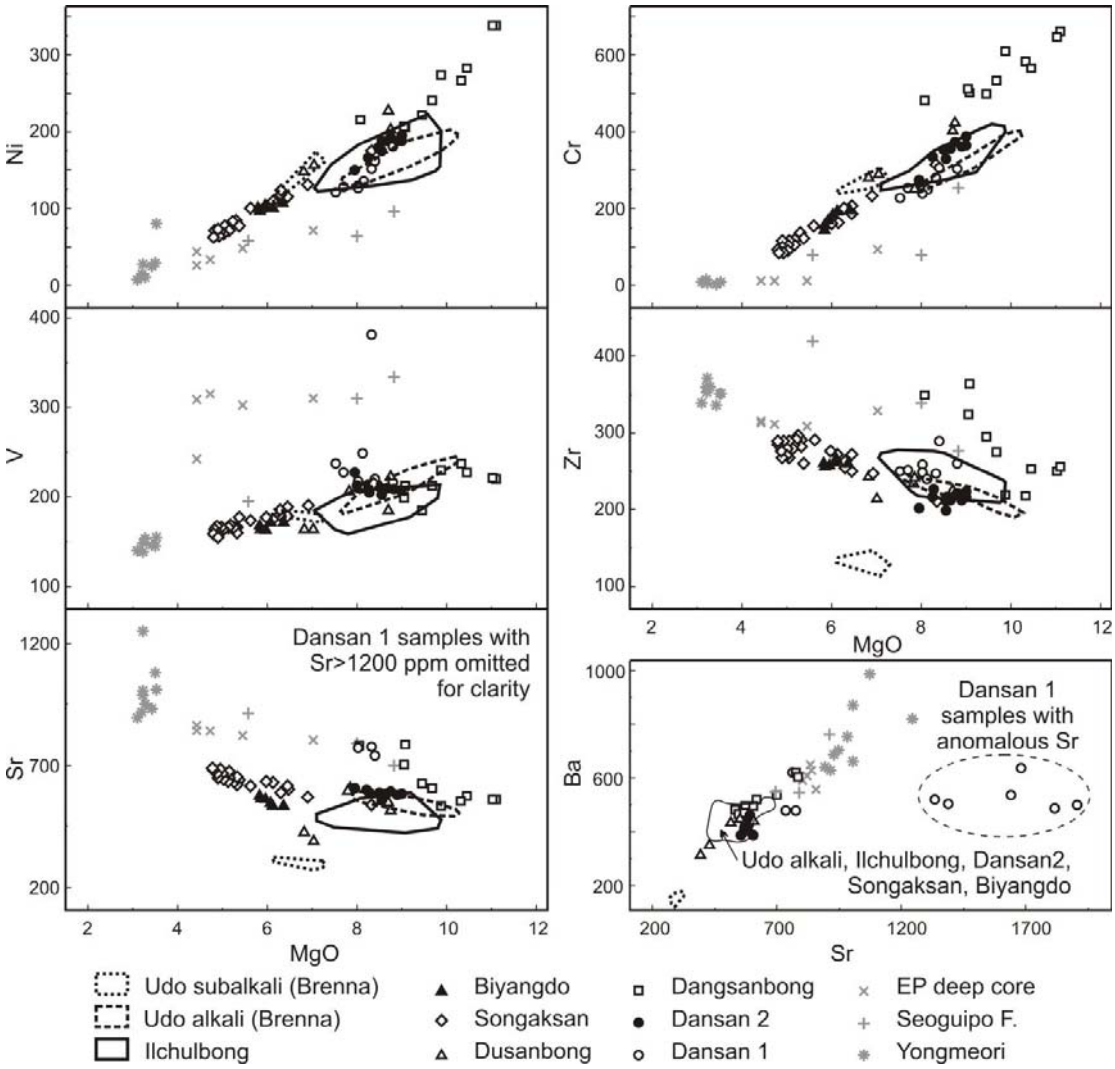

Figure 6.4: *Variation diagrams of trace element data (in ppm) of small-volume centres on Jeju Island. Distinction into Early Pleistocene high-Al alkali (HAA) suite (grey) and Middle-Late Pleistocene to Holocene low-Al alkali (LAA) and subalkali suites (black). Plotted for comparison are the Udo alkali and subalkali fields of Brenna et al. (2010; Chapter 4). Note that the Ilchulbong field is broader compared to the Udo alkali field as a result of different magma batches being involved in the Ilchulbong eruption (Sohn et al., 2012). Note the Dansan 1 samples with anomalous Sr concentrations not correlated with other LILEs (e.g. Ba).*

enrichment, this may be due to diagenetic processes rather than reflecting primary magma characteristics. As a result Dansan 1 data will not be considered hereafter. Samples from Dangsanbong are also richer in Sr, HFSEs (High Field Strength Elements) and REEs (Rare Earth Elements) than the low-Al alkali suite at comparable MgO concentrations.

Incompatible trace elements generally show enrichment factors of 1.1 to 1.3 from the most primitive (high MgO) to the most evolved (low MgO) samples in each volcano suite. However, Dangsanbong and Songaksan have considerably higher incompatible element enrichment factors (up to 1.6; Fig. 6.4, Table 6.3).

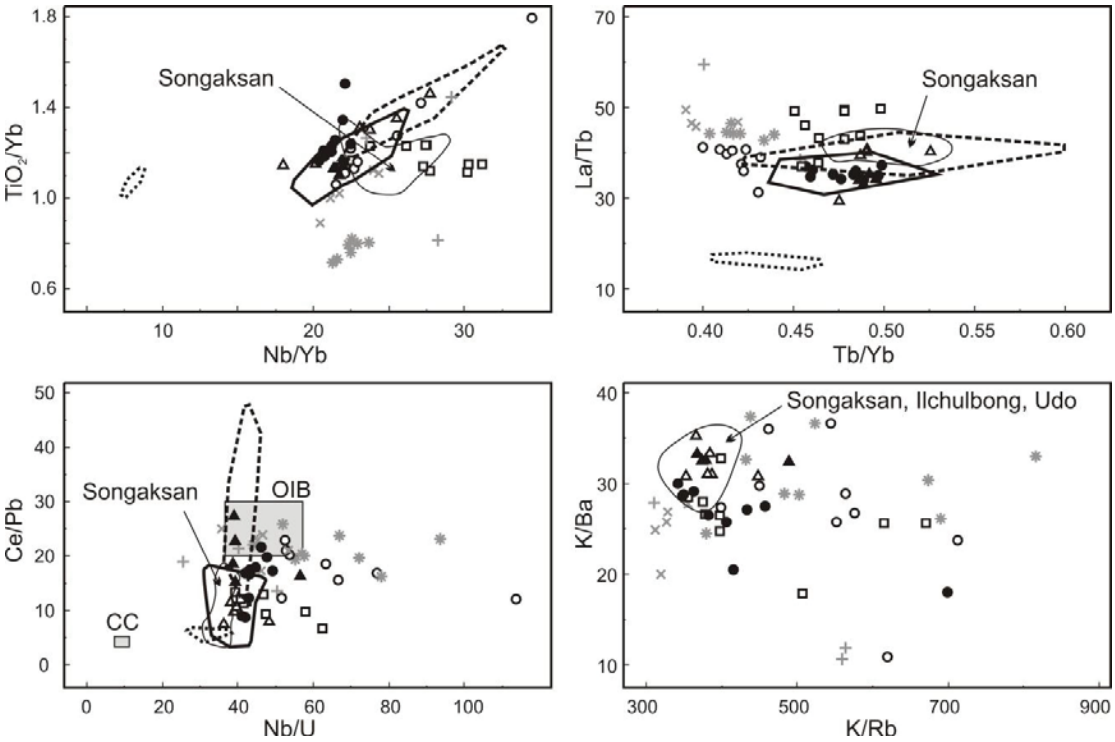

Figure 6.5: *Selected trace element ratios discriminating between the three chemical suites of Jeju small-volume eruptions. Symbols as in Figure 6.4. Note the general positive correlation in TiO_2/Yb vs. Nb/Yb apart for the Dangsanbong and Songaksan samples, which show negative correlation. In the Ce/Pb vs. Nb/U diagram the fields of Ocean Island Basalt (OIB) and Continental Crust (CC) are from Hofmann et al. (1986).*

The three chemical suites can be distinguished by a variety of trace element ratios and individual eruptions often have distinct ratios (Fig. 6.5). High-Al alkali samples have lower Tb/Yb and TiO_2/Yb than low-Al alkali samples, comparable to the subalkali suite (Fig. 6.5). The variability of K/Ba and K/Rb is much larger in the high-Al alkali suite and in samples from the Middle Pleistocene (Dansan and Dangsanbong) compared to the Late Pleistocene/Holocene samples. Despite some overlap, the latter have generally higher K/Ba and lower K/Rb compared to the former (Fig. 6.5).

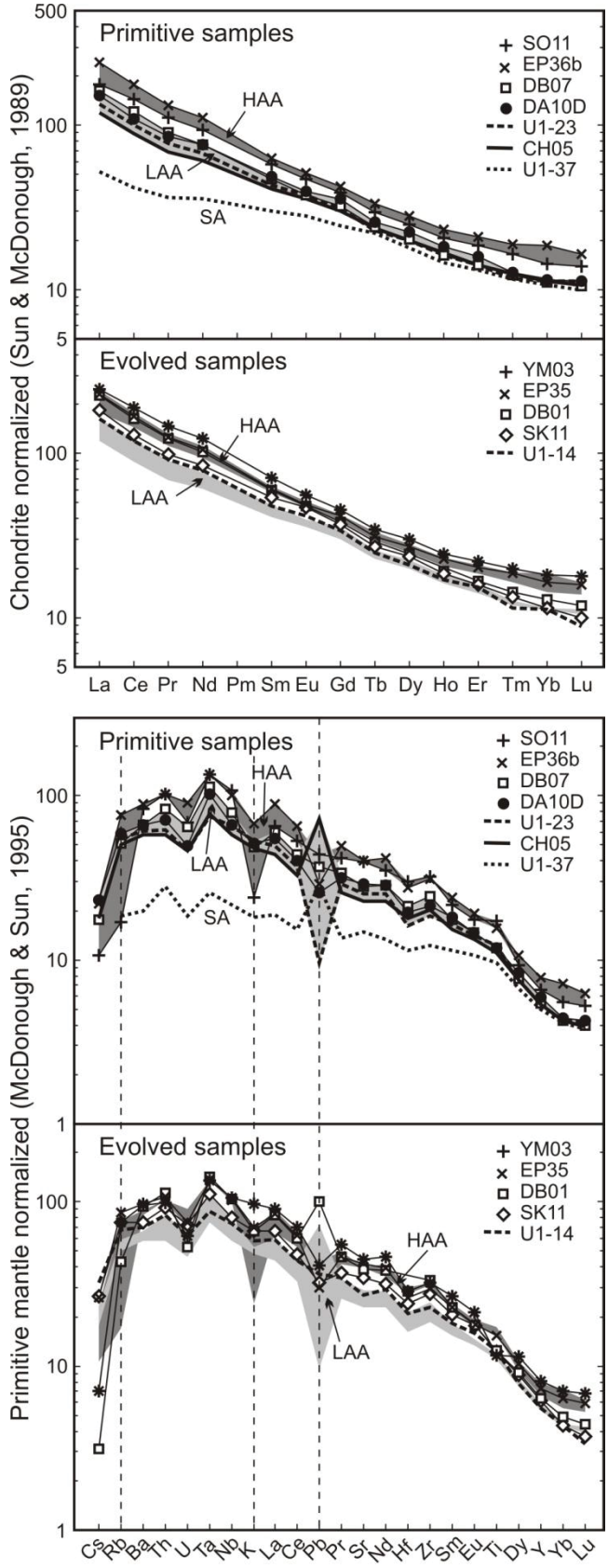

Figure 6.6: *Chondrite normalized (Sun & McDonough, 1989) REE and primitive mantle normalized (McDonough & Sun, 1995) trace element plots for the High-Al alkali (HAA), Low-Al alkali (LAA) and subalkali (SA)*

suites of small-volume eruptions on Jeju Island. Note the comparison between primitive (high MgO) and evolved (low MgO) samples, with the latter being consistently enriched. Samples U1 are from Udo (Brenna et al., 2010; Chapter 4) and REEs data for sample CH05 are from Sohn et al. (2012; Chapter 5).

Chondrite normalized REE patterns (Sun & McDonough, 1989) are similar for the two alkali suites, but the high-Al alkali suite shows greatest enrichment in REEs (Fig. 6.6). The subalkali suite has a similar pattern of HREE (heavy REE) depletion, but shows less enrichment of LREE (light REE) than the alkali suites. Chemically evolved samples (low MgO) have consistently higher REE concentrations compared to the more primitive samples (high MgO; Fig. 6.6). On a primitive mantle normalized diagram (McDonough & Sun, 1995) the patterns of the two alkali suites are also similar overall, and the high-Al alkali samples are generally more enriched compared to the low-Al alkali samples (Fig. 6.6), whereas the subalkali suite is the least enriched. Notable differences between the two alkali suites are the marked negative K and Rb anomalies in the high-Al alkali suite and Dangsanbong, features not observed in the low-Al alkali and subalkali suites. Note also the variable Pb anomaly in the low-Al alkali suite.

Overall, eruptions from the Middle Pleistocene period have major element concentrations akin to the low-Al alkali suite, however they often have trace element characteristics transitional between the two alkali suites.

6.5.4 Sr-Nd-Pb isotopes

Measured isotope ratios show very limited variability and all plot within the mantle domain (Fig. 6.7a, b). $^{87}Sr/^{86}Sr$ ranges from 0.70406 to 0.70486 and is negatively correlated with $^{143}Nd/^{144}/Nd$, which ranges from 0.51276 to 0.51283. Lead isotope ratio variability is also small with $^{206}Pb/^{204}Pb$ ranging from 18.708 to 19.240, $^{207}Pb/^{204}Pb$ ranging from 15.633 to 15.667 and $^{208}Pb/^{204}Pb$ ranging from 39.273 to 39.965. $^{206}Pb/^{204}Pb$ and $^{208}Pb/^{204}Pb$ are positively correlated whereas $^{207}Pb/^{204}Pb$ is not correlated with the other Pb isotopes but it is weakly correlated with $^{87}Sr/^{86}Sr$. All

ratios remain relatively constant when plotted against SiO_2 (Fig. 6.7c), as well as Sr, Nd and Pb concentrations.

The Early/Middle Pleistocene alkali centres (Dangsanbong, Yongmeori) tend to have more radiogenic $^{87}Sr/^{86}Sr$ (≥0.7045), similar to Udo subalkali magma, compared to the Late Pleistocene/Holocene alkali centres (Udo alkali, Songaksan, Dusanbong, Biyangdo, Ilchulbong; ≤0.7045, Fig. 6.7a). A less clear distinction between older centres and subalkali lavas, and younger centres can also be made on the basis of Pb and Nd isotopes. $^{143}Nd/^{144}Nd$ and Pb isotope ratios tend to be slightly lower in older centres. The two Dangsanbong samples have very different Pb isotope ratios ($^{206}Pb/^{204}Pb$ of 18.93 and 19.24, and $^{208}Pb/^{204}Pb$ of 39.46 and 39.97), compared to the limited variability seen at other centres.

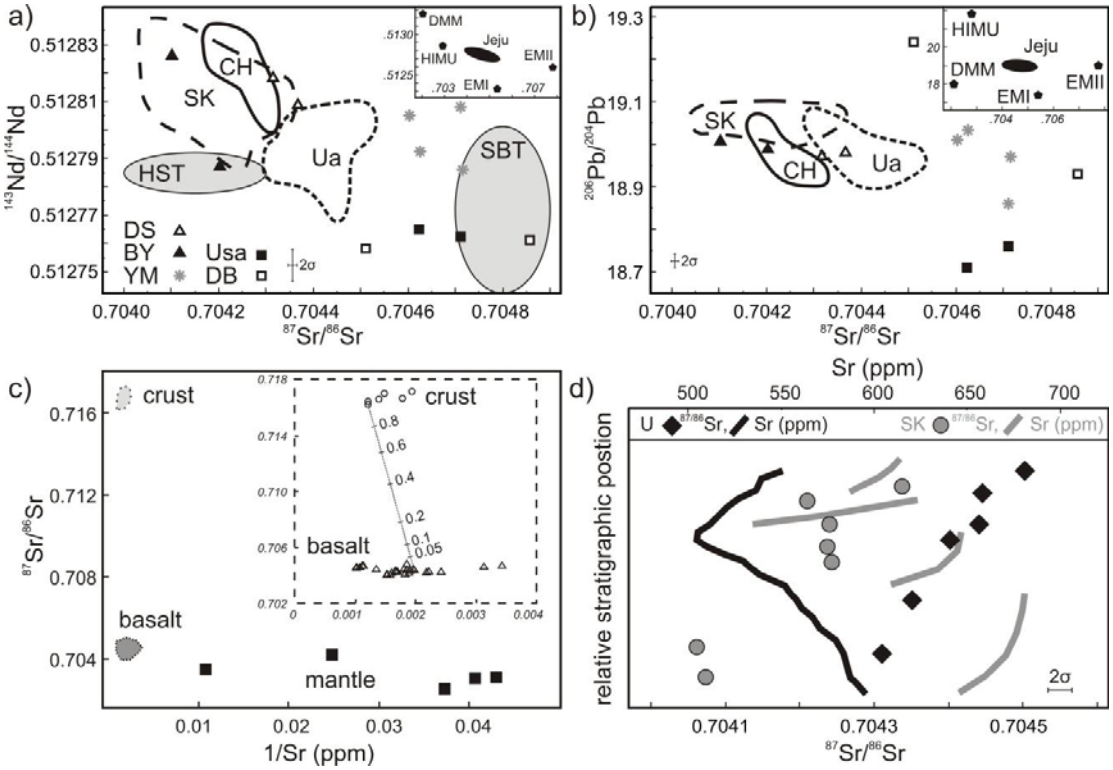

Figure 6.7: *a) and b) Sr, Nd and Pb isotope variation, Jeju sample fields are drawn taking into account 2σ error, CH is Ilchulbong, SK is Songaksan, YM is Yongmeori, Ua is Udo alkali, Usa is Udo subalkali, DB is Dangsanbong, DS is Dusanbong and BY is Biyangdo. Mantle end members are from Hart et al. (1992). HST and SBT are the fields for the Hallasan (Mount Halla) Trachyte and Sanbangsan Trachytes of Chang et al. (2006). c) Comparison of Jeju basalts (open triangles and dark grey field) with Jeju mantle xenoliths (full squares; Choi et al.,*

2005) and mixing line with mixing fractions of Jeju granitic rocks (open circles and light grey field; Kim et al., 2002). d) Comparison of Sr concentration [patterns after Brenna et al., 2010 (Chapter 4), Brenna et al., 2011 (Chapter 5)] and $^{87}Sr/^{86}Sr$ ratio against stratigraphic position. Note the lack of correlation between composition (ppm; upper horizontal axis) and isotope ratios (lower horizontal axis) at Udo (U), and the stepping $^{87}Sr/^{86}Sr$ corresponding to the stepped concentration pattern at Songaksan (SK; Brenna et al., 2011; Chapter 5).

The relatively young age of the Early Pleistocene centres (maximum 1.8 Ma) and the generally low Rb/Sr ratios (<0.1) mean that age corrections are negligible, and therefore the isotope ratio difference between Early and Late Pleistocene centres, and the distinct signature of each eruption are a true reflection of the source signature or of magmatic processes.

Sr element concentrations and isotope ratios are plotted versus stratigraphic position (Fig. 6.7d). The marked inflection in Sr concentration shown by Udo is not reflected in the $^{87}Sr/^{86}Sr$, which increase up-stratigraphy. In contrast at Songkasan the identification of different magma pulses (Brenna *et al.*, 2011; Chapter 5) is supported by the presence of three fields with distinct $^{87}Sr/^{86}Sr$ values (Fig. 6.7d).

6.6 Petrography

6.6.1 Tephra and lapilli

Samples from the Early Pleistocene high-Al alkali basalt Yongmeori tuff ring have almost no mafic mineral phases, either as phenocrysts or groundmass, but consist of relatively homogeneous, flow-aligned plagioclase (plag) microcrysts (Fig. 6.8a). Primitive samples from the high-Al alkali suite however contain olivine (ol) microphenocyrsts but rare clinopyroxene (cpx) or groundmass plagioclase.

Samples from Middle Pleistocene to Holocene alkali centres consist mainly of ol ± cpx microphenocrysts in a glassy to ol + cpx ± plag microcrystalline vesicular groundmass (Fig. 6.8b). Crystals are generally subhedral and often skeletal, indicating

fast growth rates (e.g. Vernon, 2004). Apart from the green-cored clinopyroxene noted by Brenna *et al.* (2010; Chapter 4) in the Udo alkali basalt, crystals rarely show zoning or overgrowths. Glomerocrysts of olivine or clinopyroxene, within which single crystals are generally <2 mm in size, are also observed.

At Songaksan and Dangsanbong lapilli often consist of domains of different basaltic textures (Fig. 6.8c, d). At Songaksan ol + plag phenocrysts in a glassy, black, vesiculated groundmass with disseminated oxides are mingled with domains with olivine phenocrysts in a microcrystalline, dusty plag + cpx, oxide-poor groundmass (Fig. 6.8d).

Forsterite (Fo#) content in olivine phenocrysts varies from 88 to 66 (Fig. 6.9a) and the most forsteritic occur in the low-Al alkali suite. Fo# is generally unimodally distributed in individual eruptions, but the Songaksan eruption shows bimodal distribution (Fig. 6.9a). Clinopyroxene tend to be more diopsidic in the high-Al alkali magma suite and more augitic in the low-Al alkali magma suite (Fig. 6.9b). In the alkali suites clinopyroxene cores tend to have higher Al^{VI}/Al^{IV} than rims and groundmass clinopyroxene (Fig. 6.9c). Representative olivine and clinopyroxene analyses are reported in Table 6.5. Groundmass plagioclase has anorthite (An) content varying from 80 to 88.

6.6.2 Lavas

Lava flows associated with the monogenetic small-volume centres are alkali at Songaksan (Sohn *et al.*, 2002) and Biyangdo, and subalkali at Udo (Brenna *et al.*, 2010; Chapter 4) and Dusanbong. Subalkali lavas are generally olivine-phyric in a fine grained plag + cpx ± Fe-Ti oxide groundmass (Fig. 6.8e). Olivine phenocrysts are Fo_{70-80}. Clinopyroxene from the Udo lava shield is augite with variable Ca content that is lower than the alkali magma clinopyroxenes (Fig. 6.9b). Plagioclase is An_{80-85}.

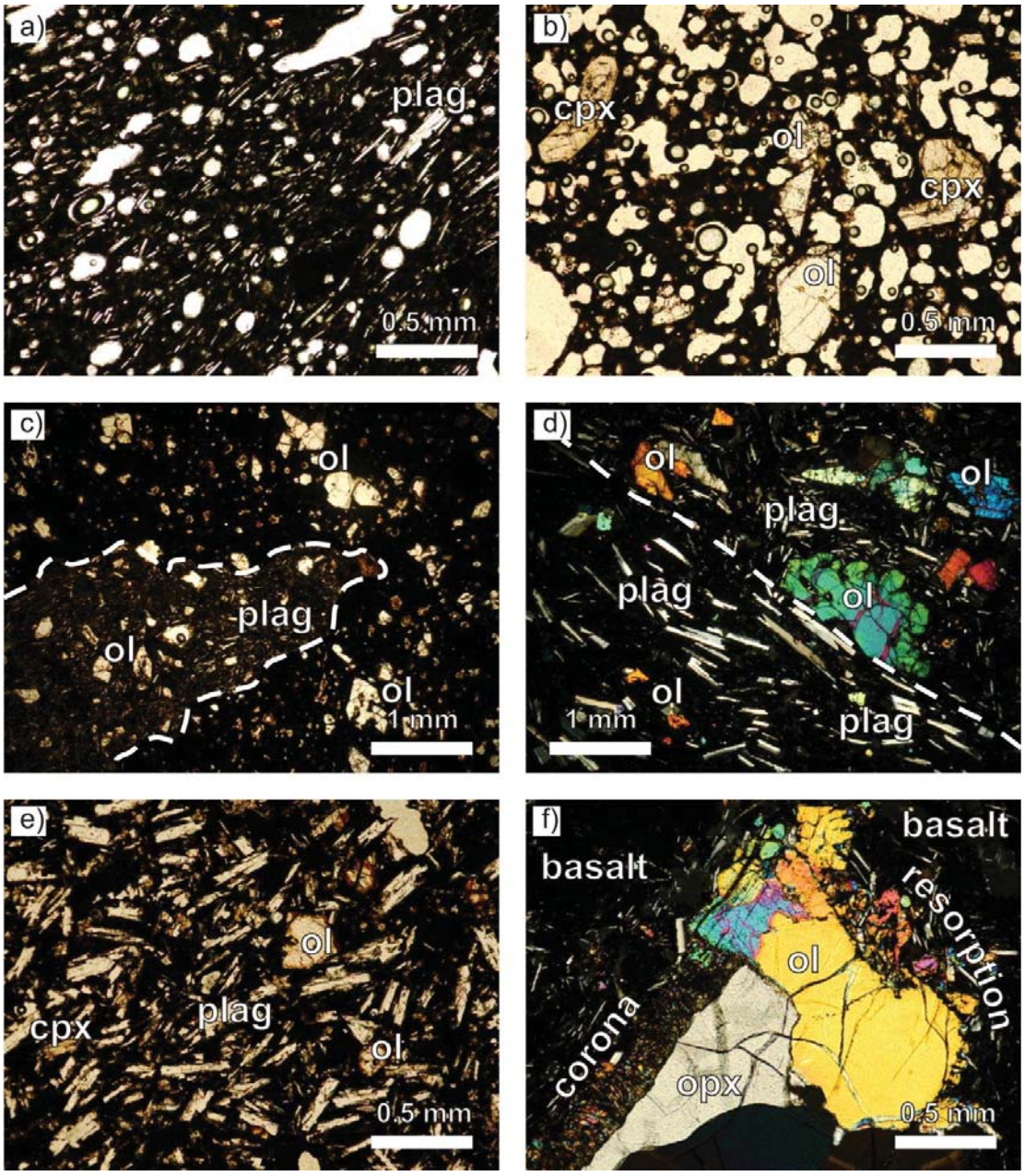

Figure 6.8: *Photomicrographs of Jeju rocks. a) Yongmeori high-Al alkali magma, note the paucity of mafic phases and the aligned plagioclase (plag) microlites with some larger plagioclase microphenocrysts; b) Udo low-Al alkali magma, clinopyroxene (cpx) and olivine (ol) phenocrysts in a vesiculated, plagioclase poor groundmass; c) Dangsanbong, mingling between two different magma domains, note the irregular contact indicating that mingling occurred as both magmas were of sufficient low viscosity; d) Songaksan, mingling between two different magma domains with contact diagonal from upper left to lower right, note the different plagioclase populations; e) Udo subalkali magma, note the intersertal plag + cpx groundmass; f) Songaksan mantle xenolith, note the ol + cpx corona at the contact between orthopyroxene (opx) and melt, and the resorption of olivine.*

Table 6.5: *Representative electron microprobe analyses of olivine (ol) and clinopyroxene (cpx) in Jeju rocks. Totals are original totals from microprobe analysis.*

Sample	EP36	YM03	DB01	DB10	SK04	SK26	SK27	EP36b	DB10	YM03	SK26
Mineral	ol	ol	ol	ol	ol	ol	ol	cpx	cpx	cpx	cpx
SiO_2	40.64	39.24	39.36	40.86	40.05	39.12	38.63	45.64	50.44	46.43	52.09
TiO_2	0.07	0.08	0.18	0.03	0.01	0.08	nd	3.15	1.50	2.14	0.52
Al_2O_3	nd	0.16	0.07	0.12	nd	0.07	0.04	7.29	3.31	8.18	1.93
FeO_{tot}	19.11	21.60	17.76	14.03	14.05	17.83	22.27	8.35	7.23	6.73	6.09
MnO	0.40	0.34	0.37	0.16	0.14	0.15	0.33	0.17	0.08	nd	0.20
MgO	42.31	40.00	41.60	45.28	45.40	42.05	38.71	13.07	15.24	13.40	18.33
CaO	0.27	0.19	0.26	0.23	0.14	0.29	0.17	21.77	21.04	21.57	18.20
Na_2O	0.01	nd	nd	nd	nd	nd	nd	0.37	0.33	0.60	0.38
K_2O	nd	0.01	0.09	0.12	nd	0.04	0.05	0.13	0.09	0.10	0.11
tot	102.94	101.46	100.03	101.12	100.05	99.78	100.20	100.16	99.92	99.39	98.93
Fo#	79.8	76.7	80.7	85.2	85.2	80.8	75.6				
En								39	44	41	53
Fs								14	12	12	10
Wo								47	44	47	38

nd: not detected

6.6.3 Xenoliths

Felsic xenoliths in Songaksan basalts have sharp to diffuse boundaries with the hosting basalt, and have brown basaltic glass containing clinopyroxene and plagioclase microlites injected into cracks.

Spinel and plagioclase lherzolite xenoliths, also in the Songaksan basalt, contain rare phlogopite near the boundaries, suggesting that this might be secondary. At the xenolith margin olivine is sometimes fragmented without showing reaction features with the basaltic liquid, or shows resorption (Fig. 6.8f). In contrast orthopyroxene is usually rimmed by a corona of fanning cpx + ol microlites (Fig. 6.8f).

Rare xenocrysts (both mafic and felsic) are also observed. These are generally partially or almost completely resorbed. Orthopyroxene xenocrysts are generally rimmed by a corona of ol + cpx similar to those in lherzolite xenoliths (Fig. 6.8f).

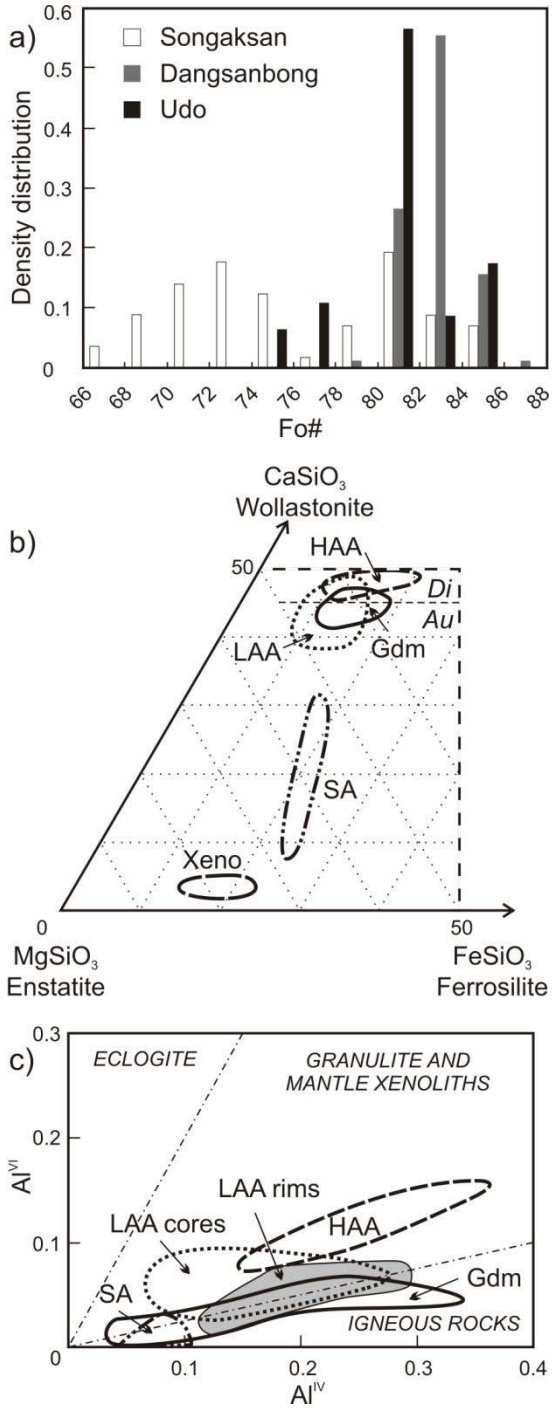

Figure 6.9: *a) Density distribution of Fo# of olivine crystals in rocks from Songaksan, Dangsanbong and Udo Volcanoes. Note the bimodal distribution of Songaksan olivines. b) and c) Chemical properties of clinopyroxene in the Jeju rocks. The separation into different fields in c) is from Aoki & Kushiro (1968). Dashed line is diopside (Di)-augite (Au) boundary. HAA is High-Al alkali, LAA is Low-Al alkali, Gdm is groundmass, SA is subalkali, Xeno is mantle xenolith.*

6.7 Discussion

Interpretation of the new data presented here is subdivided into three parts. The first section will deal with magmatic processes affecting chemical variability in individual eruptions above the magma source region, the second section will investigate the source region and primary magma characteristics and the third will integrate the interpretations of dynamic conditions of magmatic generation and evolution within a tectonic framework in order to formulate a model for the evolution of the Jeju small-volume volcanic system.

6.7.1 Volcano-scale magmatic evolution

Chemical evolution on individual volcano scale at Jeju was described for the low-Al alkali magma suite for Udo Volcano (Brenna *et al.*, 2010; Chapter 4), Songaksan and Suwolbong Volcanoes (Brenna *et al.*, 2011; Chapter 5), and for Ilchulbong Volcano (Sohn *et al.*, 2012; Chapter 5). The data from additional eruptive centres, as well as new LA-ICP-MS trace element data for the Ilchulbong eruption allow an integrated interpretation of the alkali magma suites. A comprehensive sample suite for the subalkali magma is available mainly from Udo Volcano, and has been discussed previously by Brenna *et al.* (2010; Chapter 4). They modelled this magma to have been derived by 5-7% partial melting of a peridotite source with residual garnet at c. 2.5 GPa near the garnet-spinel transition, and it evolved by mainly olivine fractionation. These results are in agreement with data from a similar eruption (Rangitoto) involving both alkali and subalkali magmas in the Auckland Volcanic Field, New Zealand (McGee *et al.*, 2011).

6.7.1.1 Crustal contamination

Jeju lies on c. 35 km thick (Yoo *et al.*, 2007) felsic crust comprising granites of Jurassic to Cretaceous age within a Proterozoic fold belt (Kim *et al.*, 2002). Crustal contamination can alter the primary signature of mantle-derived basaltic magmas, and the presence of felsic xenoliths requires an assessment of this process before the chemical data can be interpreted in term of magmatic processes. The main evidence

against crustal interaction is the relative lack of variation in isotopic ratios, particularly Sr, despite the observed range in SiO_2 and considerable ranges in Sr, Nd and Pb concentrations, even within single eruptive sequences (Fig. 6.7c). Modern Sr, Nd and Pb isotope ratios in granites from the Jeju basement (Kim *et al.*, 2002, Tatsumi *et al.*, 2005) are distinct from the restricted range found in the volcanic rocks, and mixing lines (Fig. 6.7c) clearly show that crustal material has had a negligible effect on isotopic ratio variation.

Spinel lherzolite xenoliths (Choi *et al.*, 2005) have isotopic ratios slightly less radiogenic than their host basalts on Jeju (Fig. 6.7c). However, the spinel lherzolite does not strictly represent the source material and the measured rock isotope ratios fall well within the recognized mantle domains (Zindler & Hart, 1986). Indeed, the mantle beneath the southern end of the Korean Peninsula and Jeju Island most likely comprises depleted mantle (DMM) and enriched mantle (EMII; Choi *et al.*, 2005, Choi *et al.*, 2006).

The large variability of Pb concentrations in Jeju magmas gives rise to a wide range of Ce/Pb ratios (c. 5 to 45, Fig. 6.5). Low Ce/Pb is generally interpreted as indicating crustal contamination (Hofmann *et al.*, 1986). Clinopyroxene in spinel lherzolite and peridotite xenoliths in Jeju basalts have Ce/Pb ranging from as low as 2 to as high as 90 and 126 in clinopyroxene from clinopyroxenite xenoliths and mylonitised spinel peridotite (Choi *et al.*, 2005, Yang *et al.*, 2010, Yu *et al.*, 2010). At very low degrees of partial melting (<2%) clinopyroxene is one of the first phases to melt (Walter, 1998), and compositional heterogeneity derived from partial melting of clinopyroxene with a wide range of Ce and Pb concentrations would be transferred to the resulting melt. Due to the very high Ce/Pb variability of mantle material, even the low whole-rock Ce/Pb is therefore not interpreted as indicating crustal contamination. In addition, other trace element ratios (e.g. Nb/U; Fig. 6.5; Nb/Th 6-10, Nb/La > 1) are typical of mantle derived melts and higher than continental crust ratios (Hofmann *et al.*, 1986, Weaver, 1991).

In summary, crustal contamination is not considered to have appreciably affected the Jeju small-volume magmas. Therefore, the chemical variability discussed hereafter is considered as primary magmatic.

6.7.1.2 High-Al alkali (Early Pleistocene) magma fractionation

Early Pleistocene magmas (Yongmeori, Seoguipo Formation and EP deep core samples) are high-Al alkali basalts. This magma type is found only in the Early Pleistocene centres, suggesting that early melt generation in the small-volume magmatic system occurred under different conditions compared to the later activity. Except from Yongmeori and the EP deep core, samples from the high-Al alkali suite can not be related to individual eruptions. They are nevertheless treated as a cogenetic suite because they were erupted during the same activity period and have similar trace element characteristics, distinct from the later low-Al alkali magmas. The more primitive (high MgO) samples in the high-Al alkali suite have relatively low SiO_2 (c. 44 wt%), and at comparable SiO_2 concentrations to the most primitive samples of the low-Al alkali suite (i.e. c. 48 wt%) they have very low MgO (c. 5 wt%; Fig. 6.2). Trace elements are also distinctly different from the Late Pleistocene eruptive centres, particularly in their LILE and REE relative and absolute abundances (Figs. 6.4, 6.5, 5.6). This suggests that the high-Al alkali suite was derived from a distinctly different parent melt and evolved by a different fractionation path from to the low-Al alkali suite, implying a change in the petrologic development of the field through time. The switch between high-Al and low-Al alkali magmatism occurs approximately between the eruptions of Yongmeori and Dansan. However the Middle Pleistocene centres (Dansan and Dangsanbong) still retain some chemical characteristics in common with oldest centres (Sr, Nd, Pb isotopes and trace elements; Figs. 6.4, 6.5, 6.7).

The most primitive samples in the high-Al alkali suite have MgO < 9 wt% and Ni c. 100 ppm, which are too low for primary magmas derived from the mantle. They must have therefore evolved by fractionation from a parent melt. Although early fractionation depleted magmas in MgO, as well as Ni and Cr, CaO, FeO_{tot} and V are richer at comparable MgO than in the low-Al alkali suite. It is therefore likely that early fractionation in the high-Al alkali suite involved mainly olivine ± Cr spinel and no clinopyroxene. Nonetheless CaO, FeO_{tot} and V are also positively correlated with MgO (Fig. 6.3, 6.4) and at SiO_2 > 47, Al_2O_3 is negatively correlated with SiO_2, indicating the fractionation of a phase incorporating them (i.e. clinopyroxene + plagioclase). The high-Al alkali suite was therefore affected by two different fractionation stages with different mineral assemblages.

Table 6.6: *Approximation of a primary magma composition for the high-Al alkali suite by addition of equilibrium olivine. The olivine composition EP36 (898) measured by electron microprobe has been normalized.*

	SBS04	Add olivine in EP36 (898)	ADD_{05}	Add 0.05 olivine	ADD_{10}	Add 0.05 olivine	**ADD_{15}**	Add 0.05 olivine	ADD_{20}	Add 0.035 olivine	**$ADD_{23.5}$**
SiO_2	44.56	39.43	44.30	39.94	44.09	40.50	43.91	40.80	43.75	41.00	43.66
TiO_2	3.26	0.06	3.10	0.04	2.95	0.03	2.80	0.02	2.66	0.01	2.57
Al_2O_3	14.90	0.05	14.16	-	13.45	-	12.78	-	12.14	-	11.71
FeO_{tot}	12.14	17.93	12.43	15.80	12.60	14.15	12.68	12.70	12.68	11.70	12.65
MnO	0.19	0.32	0.20	0.30	0.20	0.20	0.20	0.15	0.20	0.10	0.20
MgO	8.83	41.94	10.49	43.70	12.15	44.97	13.79	46.25	15.41	47.14	16.52
CaO	10.72	0.26	10.20	0.22	9.70	0.15	9.22	0.08	8.76	0.05	8.46
Na_2O	4.03	-	3.83	-	3.64	-	3.46	-	3.29	-	3.17
K_2O	0.78	-	0.74	-	0.71	-	0.67	-	0.64	-	0.62
P_2O_5	0.58	-	0.55	-	0.52	0	0.49	-	0.47	-	0.45
TOT	100.00	100.00	100.00	100.00	100.00	100.00	100.00	100.00	100.00	100.00	100.00
Mg# *(Fo#)*	56.4	*(0.81)*	60.1	*(0.83)*	63.2	*(0.85)*	66.0	*(0.87)*	68.4	*(0.88)*	70.0
R&E eq	0.31		0.30		0.30		0.30		0.30		
Ni (ppm)	95.01		146.2		224.9		346.1		532.4		819.2

R&E eq is the Fe-Mg exchange equilibrium of Roeder & Emslie (1970).

Given the major and trace element constraints on the first stage of fractionation, we can approximate the fractionation path and hence potential primary magma compositions (ADD_{15} and $ADD_{23.5}$) by addition of equilibrium olivine (Table 6.6). The discussion of the likely primary magma composition and its implications is remanded to the following section on source characteristics.

Quantitative modelling of the second stage of fractionation, which resulted in the low-MgO lavas of Yongmeori, is carried out by mass balance calculations (Petrelli *et al.*, 2005, Stormer & Nicholls, 1978). The model is based on the chemical variation from sample EP34 to sample YM03, and mineral compositions hosted in these end member samples or in more primitive samples, representative of crystallizing phases responsible for the fractionation trends. Input compositions and results are summarised in Table 6.7. The chemical variation can be modelled by removal of c. 9% clinopyroxene, c. 3% olivine, c. 20% plagioclase and c. 7% Fe-Ti oxide, with a sum of the squared residual (SSR) of 0.17.

Table 6.7: *Input data and results of the mass balance modeling (Petrelli et al., 2005) of the second stage fractionation of high-Al alkali magma.*

	start EP34	end YM03	YM03 cpx	YM03 ol	EP36 Plag	EP36 usp	BComp	ODiff	CDiff	Res
SiO_2	49.73	54.83	50.36	38.81	52.23	0.15	41.66	5.10	5.04	0.06
TiO_2	3.32	2.55	1.32	0.04	0.23	18.50	3.66	-0.77	-0.43	-0.35
Al_2O_3	18.83	18.92	5.34	nd	31.84	5.82	18.80	0.09	0.05	0.04
FeO_{tot}	12.59	10.95	6.42	21.33	0.98	69.06	15.69	-1.64	-1.82	0.18
MnO	0.24	0.24	0.05	0.27	nd	0.59	0.14	0.01	0.04	-0.04
MgO	5.01	3.39	15.46	39.37	0.19	5.67	7.63	-1.62	-1.62	-0.00
CaO	10.28	9.11	21.04	0.18	14.53	0.21	12.42	-1.16	-1.27	0.10
TOT	100.00	100.00	100.00	100.00	100.00	100.00				0.00
SSR										0.17
Wt% phase removed			8.76	2.92	19.90	6.70				

nd: not detected. Start and end compositions and mineral phases employed are recalculated to 100%. BComp is the bulk composition of material removed, ODiff is the observed difference between initial and final magmas, CDiff is calculated difference between initial and final magma, Res is the residual, SSR is the sum of the squared residuals. cpx is clinopyroxene, ol is olivine, plag is plagioclase and usp is ulvöspinel.

From the trace element constraints for the first stage and the model for the second stage of fractionation we can see that the initial olivine-dominated fractionation is replaced by a cpx + ol + plag + Fe-Ti oxide fractionating assemblage. This transition

may indicate that magma was fractionating at increasingly shallow depths and lower temperatures up to crustal levels (Bartels *et al.*, 1991, Bultitude & Green, 1971, Elthon & Scarfe, 1984).

6.7.1.3 Low-Al alkali (Late Pleistocene/Holocene) magma fractionation

A fractionation model involving mostly deep clinopyroxene fractionation for the low-Al alkali magma was presented for the Udo Volcano by Brenna *et al.* (2010; Chapter 4). Given the overall similarity of chemical trends in the suite (Figs. 6.2, 6.3, 6.4), it is likely that the same process produced the observed variation in the majority of the low-Al alkali suite, or at least of the more primitive magmas. Clinopyroxene and clinopyroxenite xenoliths with isotope signatures similar to host basalts in the Jeju system also indicate that clinopyroxene crystallized from magmas at mantle depths in the plumbing system of Jeju small-volume centres (Choi *et al.*, 2005). Clinopyroxene phenocryst cores in the Jeju magmas tend to have Al^{VI}/Al^{IV} akin to clinopyroxene from granulite and mantle xenoliths, rather than eclogite or igneous rocks, and are therefore likely to represent crystallization at mantle depths (Aoki & Kushiro, 1968; Fig. 6.9c). Groundmass clinopyroxene, as well as pyroxene rims were likely crystallized late and at shallower depth (Fig. 6.9c). In order to assess the possible influence of garnet and amphibole, in addition to clinopyroxene, on the observed fractionation trends, we examine La/Yb variability. In these minerals the partition coefficient of HREE is higher than for LREE and may cause some differential fractionation of La and Yb and change the La/Yb ratio. When compared with other trace elements fractionated preferentially by these phases, it appears that clinopyroxene is predominantly responsible for the observed variability (Fig. 6.10).

Some volcanoes, however, (e.g. Songaksan, Dangsanbong) show contrasting and contradicting evidence from compatible and incompatible elements regarding evolutionary processes, suggesting a more complex process than simple fractional crystallization. For example, qualitative Rayleigh fractional crystallization modelling suggests that only approximately 10% by volume of cpx and olivine would be required to reproduce the major element variation. However, the observed enrichment of Zr from 200 to 300 ppm (enrichment factor 1.5) corresponds to a c. 33% decrease

in the original magma volume. Clearly there is discordance between compatible and incompatible elements depletion/enrichment signals.

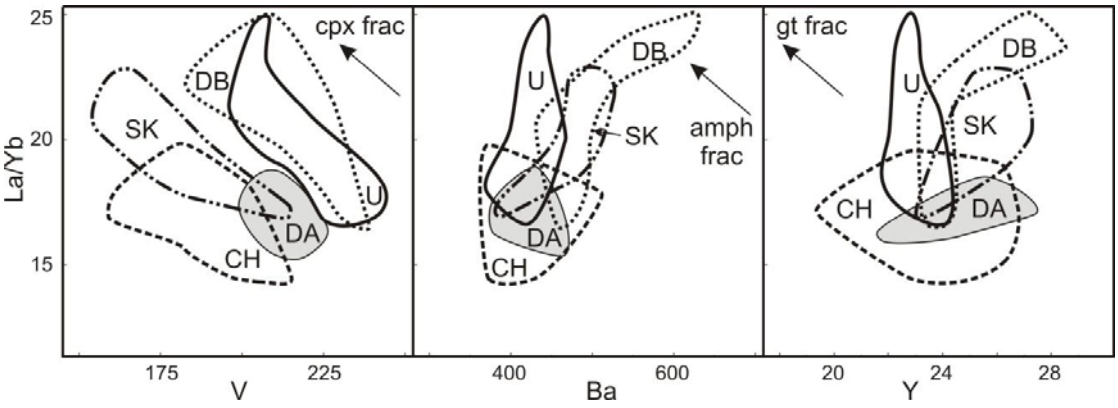

Figure 6.10: *Comparison of La/Yb versus trace elements (ppm) fractionated preferentially into clinopyroxene (V), amphibole (Ba) and garnet (Y). A negative correlation is indicative of fractionation effect. Note that only the eruptions for which a detailed sample set is available were plotted. U is Udo, DB is Dangsanbong, DA is Dansan 2, SK is Songaksan, CH is Ilchulbong.*

Crustal interaction has been ruled out on the basis of isotope and trace element evidence. Discordance between compatible and incompatible elements has previously been attributed to in-situ crystallization (Langmuir, 1989). In-situ crystallization on the dyke walls, followed by filter pressing of evolved magma out of the crystal mush may explain the great range in incompatible elements, and the discordance in estimated fractionation models. However, results of in-situ crystallization modelling yielded under-depletion in compatible elements (Langmuir, 1989), contrary to what we observe at Songaksan. The variation is also unlikely to reflect variable amounts of phenocrysts in the analysed samples because the modal amounts of phases present and their low variability are insufficient to account for the chemical variation amongst the most primitive (SK26) and the more evolved samples.

Following, we discuss the possible influence of magma mixing giving rise to the contrasting chemical signature and Songaksan and Dangsanbong.

6.7.1.4 Magma mixing

The large variability in trace elements might be interpreted as resulting from mixing of different magmas (Kamber & Collerson, 2000, Reiners, 2002). This may apply in some cases such as Suwolbong, where alkali and subalkali magmas were mixed in the eruption products (Brenna *et al.*, 2011; Chapter 5). However, the chemical continuity of the Udo alkali magma (Brenna *et al.*, 2010; Fig. 4.3), the systematic rejuvenating of magmatic signature in the eruptive pulses at Ilchulbong (Sohn *et al.*, 2012; Fig. 5.9), as well as the relatively small magma volumes in which such changes occur, suggest mixing of two different magmas is unlikely to be responsible for the majority of the observed range of chemical compositions within the suite. Moreover the isotopic signature of the rocks is not always coupled to their trace element variability (Fig. 6.7d). The seemingly simple magmatic history recorded in the phenocrysts and microphenocrysts observed in Jeju alkali basalts, which do not generally show evidence for disequilibrium such as resorption, zoning, overgrowths etc., is further evidence that discounts mixing of magmas at different stages of chemical evolution as a major contributor to chemical variability. Nonetheless, magma mixing may have played a part at Songaksan and Dangsanbong.

Magma mixing for the Dangsanbong eruption is suggested by the negative correlation of TiO_2/Yb and Nb/Yb (Fig. 6.5), which contrasts with the positive correlation of other eruptions, despite TiO_2 not being fractionated at Dangsanbong (Fig. 6.3). Note also the distinct ratio of the subalkali magma (Fig. 6.5), indicating the lack of mixing between this and the alkali magma.

The mingling of magmas with different textures (Fig. 6.8c, d) seen at Dangsanbong and Songaksan also suggest mixing of different magmas or cogenetic magmas at different stages of evolution. However, even where petrographic and geochemical evidence suggests mixing of different magmas, these may still have a common evolutionary history. At Dangsanbong, despite the large variation in trace elements (Fig. 6.4) and Sr, Nd and Pb isotope ratios (Fig. 6.7a, b), olivine crystals analysed across the texture boundary and in different samples have a unimodal distribution in their Fo# (Fig. 6.9a), similar to olivines from the Udo alkali magma. In contrast, at Songaksan the Fo# of olivine crystals is bimodally distributed (Fig. 6.9a) suggesting

interaction of magmas at different stages of evolution. A model of TiO_2 variability also suggests the mixing of a primitive magma and an evolved magma that had fractionated a titaniferous phase (Fig. 6.11). The evolved magma fed the onset of the eruption unmixed, but as activity continued contribution of the primitive component increased. This, in addition to the isotopic heterogeneity across pulses (Fig. 6.7d), supports the interpretation of Brenna *et al.* (2011; Chapter 5) that the Songaksan eruption was fed by discrete pulses, which evolved in independent dykes possibly at different depths, before becoming mingled in the main plumbing dyke that fed the eruption.

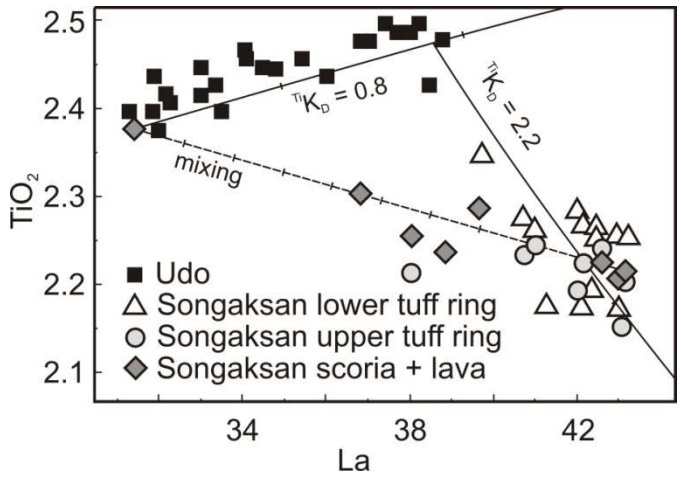

Figure 6.11: *Model of crystal fractionation and mixing of magmas feeding the Songaksan eruption. The Udo samples (Brenna et al., 2010; Chapter 4) are plotted to compare a low-Al alkali eruptive suite trend in which TiO_2 (wt% oxides) is relatively incompatible (La is ppm). Marks on model lines are 0.1 volume fractions of fractionation and mixing. Models were produced using the program PetroGraph (Petrelli et al., 2005) and the bulk Ti distribution coefficient ($^{Ti}K_D$) is selected to best fit the data. The $^{La}K_D$ is 0 for both fractionation models.*

In summary, based on crystal phase diagrams (Bartels *et al.*,1991, Bultitude & Green, 1971, Elthon & Scarfe, 1984), fractionation of olivine in the high-Al alkali suite is substituted by cpx + ol + plag as the P-T conditions of the system are lowered. In the low-Al alkali suite cpx + ol + spinel dominated fractionation occurred at comparatively greater depths than the olivine-only fractionation of the high-Al alkali suite, but was also followed in some eruptions by shallower fractionation involving plagioclase. Hence, in both suites we have crystallization and fractionation occurring

at various depths from the upper mantle to the crust, but generally deepening in the Middle/Late Pleistocene and Holocene.

6.7.2 Field-scale magmatic evolution

6.7.2.1 Source characteristics

Detailed accounts of the mineralogy and geochemistry of the mantle beneath Jeju Island have been presented by Choi *et al.* (2005), Choi *et al.* (2006), Tatsumi *et al.* (2005) and Yang *et al.* (2010). The mantle beneath Jeju Island is believed to comprise domains of DMM and EMII (Choi *et al.*, 2005, Choi *et al.*, 2006; Fig. 6.7a, b after Hart *et al.*, 1992). Rather than focusing on a detailed characterization of the mantle domains in the source, here we will discuss the characteristics and relationships between the source domains of individual volcanic centres and the changes that occurred over the life of the volcano field.

Independent of the mantle domains involved in the generation of the various magmas that fed the Jeju volcanic field, individual eruptive centres can be distinguished on the basis of their isotope ratios (Fig. 6.7a, b). The Early and Middle Pleistocene Yongmeori and Dangsanbong Volcanoes have relatively higher $^{87}Sr/^{86}Sr$ and lower $^{143}Nd/^{144}Nd$, similar to the Udo subalkali magma and trachytes of the Middle Pleistocene Sanbangsan suite (Chang *et al.*, 2006). The Late Pleistocene and Holocene alkali centres such as Ilchulbong, Songaksan and the Udo alkali magma (Fig. 6.7a) instead have $^{87}Sr/^{86}Sr$ and $^{143}Nd/^{144}Nd$ akin to Late Pleistocene trachytes of Mt. Halla (Chang *et al.*, 2006). Even single eruptions within either high-Al or low-Al alkali suites do not always have overlapping Sr, Nd and Pb isotope ratios, and are therefore likely to be derived from relatively independent domains within a heterogenous mantle.

The mantle beneath Jeju Island has not been affected by modern subduction-related fluids (Nakamura *et al.*, 1989), however it was metasomatized by fluids related to Quaternary alkali magmatism (Choi *et al.*, 2005) and the resulting hydrous mineralogy consists of amphibole and phlogopite (Tatsumi *et al.*, 2005). Partial

melting in the presence of a hydrous phase likely occurred in the high-Al alkali suite. A marked negative K anomaly in the most primitive samples (Fig. 6.6) as well as Rb depletion with respect to Ba (Fig. 6.5) suggest that phlogopite was a residual phase during partial melting. The same anomalies are generally not observed in the Late Pleistocene to Holocene centres (Fig. 6.6). The large variability in K/Ba and K/Rb in the high-Al alkali suite, as well as Middle Pleistocene centres (Fig. 6.5), contrasts with the relatively restricted range in the Late Pleistocene/Holocene centres and points to melting causing a partial exhaustion of the hydrous phase. Hand specimens do not generally show signs of weathering, and, apart for some variation in the Yongmeori samples, elements such as Ba and Sr are generally well correlated with HFSE, and hence the observed signature is unlikely to be due to post-depositional alteration. In addition, based on composition of spinels in olivine, Tatsumi *et al.* (2005) established that in Jeju magmas (high-Al, low-Al alkali and subalkali), fO_2 is two log units above the fayalite-magnetite-quartz buffer (FMQ+2). We therefore conclude that the magmatic system started with hydrous partial melting in the Early Pleistocene and continued with drier melting due to exhaustion of hydrous phases in the Late Pleistocene/Holocene.

Brenna *et al.* (2010) modelled the likely source lithology and concluded that at Udo both alkali and subalkali magmas were derived from garnet peridotite at c. 3 to 3.5 GPa and 2.5 GPa respectively. Trace element concentrations and ratios for the low-Al alkali basalts introduced here are broadly similar to those of Udo (Figs. 6.4, 6.5), and given the similar chemical evolution, they are likely to have been derived from a similar mantle source region and depth as the Udo alkali magma.

Early Pleistocene, high-Al alkali centres instead show slightly different trace element characteristics (Fig. 6.5). They have comparable La/Yb but lower Tb/Yb, implying a lesser depletion of HREEs compared to low-Al alkali centres (Fig. 6.5). Given the overall similarity of trace element characteristics, it is likely that the source for all centres consists of peridotite with residual garnet (Brenna *et al.*, 2010). A partial melting model (Fig. 6.12) based on La, Tb and Yb K_D for olivine, clinopyroxene, orthopyroxene, garnet (Adam & Green, 2006), spinel (Elkins *et al.*, 2008), amphibole and mica (Adam & Green, 2011) determined at pressures ranging from 2 to 3.5 GPa and primitive mantle (McDonough & Sun, 1995) supports this interpretation for a

source material. In addition, the lesser depletion of HREEs in the high-Al alkali suite suggest a source with less garnet, possibly on the garnet-spinel transition, although not just spinel peridotite, which would require unreasonably low degrees of partial melting (Fig. 6.12). Lower TiO_2/Yb in the Early Pleistocene centres (Fig. 6.5) further supports the interpretation that these were derived from a shallower portion of the mantle with lesser garnet (Pearce, 2008). We prefer this explanation to a model involving larger degrees of partial melting, due to the alkali nature of the Early Pleistocene magmas, and the enriched trace element pattern (Fig. 6.6) indicating very low degrees of melting.

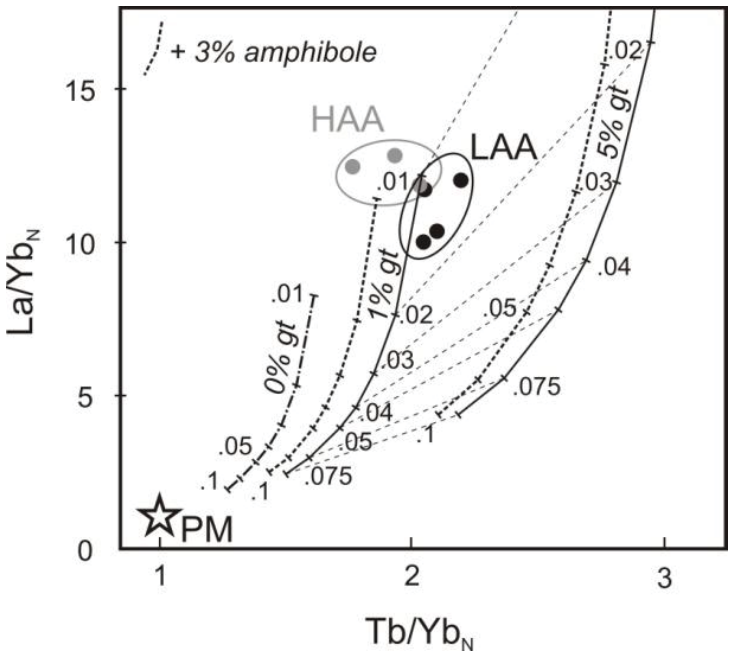

Figure 6.12: *Partial melting model using K_D and primitive mantle (PM) compositions as discussed in the text. HAA is high-Al alkali, LAA is low-Al alkali. Melting paths of peridotite with 5, 1 and 0% residual garnet. Addition of 3% amphibole decreases HREE depletion (shift of melting path to left). Spinel and mica K_Ds are very small and hence their effect is negligible.*

A shallower source with residual amphibole for the high-Al alkali basalt, compared to the low-Al alkali basalt, was previously proposed in the model of Tatsumi *et al.* (2005). However, they did not have any time-control on the occurrence of high- and low-Al alkali magmas and had attributed the variability to sourcing of the high-Al alkali magma from a more metasomatised region of the mantle compared to the low-Al alkali magma. Given that the high-Al alkali magma occurs only in the Early

Pleistocene centres, it is likely that the occurrence is related to the evolution of the field, rather than to contemporaneous tapping of variably metasomatised sources.

6.7.2.2 High-Al alkali primary magma source depth

Estimation of the depth of partial melting can be done based on the major element composition estimated earlier for primary magmas of the high-Al alkali suite (Table 6.6). A basaltic primary magma in equilibrium with mantle peridotite is generally accepted to have Mg# 70 (Ulmer, 1989). We modelled a composition with Mg# 70 ($ADD_{23.5}$) by addition of 23.5% equilibrium olivine (Roeder & Emslie, 1970) in 5% steps to the most primitive (high MgO) sample (SBS04). Another phase which likely fractionated with olivine is Cr-spinel, given that SBS04 contains only c. 250 ppm Cr, which is too low for a primary magma. However, minor amounts (<1%) of Cr-spinel are needed to reduce the Cr concentration to the one measured in SBS04, and hence this would not have significantly affected other major elements for the purpose of our model. Ti-spinel or Al-spinel are not likely to have crystallized due to Ti and Al enrichment at this stage.

As discussed above, melting in the Early Pleistocene occurred in partially hydrous conditions. Low degrees of partial melting of peridotite under hydrous conditions generate primitive melts with Mg# as low as 60 (Kushiro *et al.*, 1968, Mysen & Boettcher, 1975). Qualitative models with pMELTS (Ghiorso *et al.*, 2002) tend to support a relatively low Mg#, as well as relatively low SiO_2 for low (<2%) degrees of melting of hydrous peridotite (<0.5 wt% H_2O). Low Mg# and SiO_2 of a low degree partial melt are also in agreement with the experiments of Kushiro (1996), and hence composition $ADD_{23.5}$, which has Mg# 70, may not be the best approximation of a primary magma. Additionally, modelling of the Ni concentration taking the Ni K_D between olivine and liquid as 9.4 (McKenzie & O'Nions, 1991), results in Ni concentrations of c. 346 and c. 819 ppm for the ADD_{15} and $ADD_{23.5}$ primitive melts respectively (Table 6.6). The Ni concentration in a primitive melt is generally in the range 240-390 ppm (Sato, 1977), which is similar to composition ADD_{15}. Moreover, the Fo# of olivine in equilibrium with low degrees melts (<5%) is c. 87 (Kushiro, 1996). We therefore prefer composition ADD_{15} (addition of 15% olivine to SBS04; Table 6.6) as a primary magma for the high-Al alkali suite.

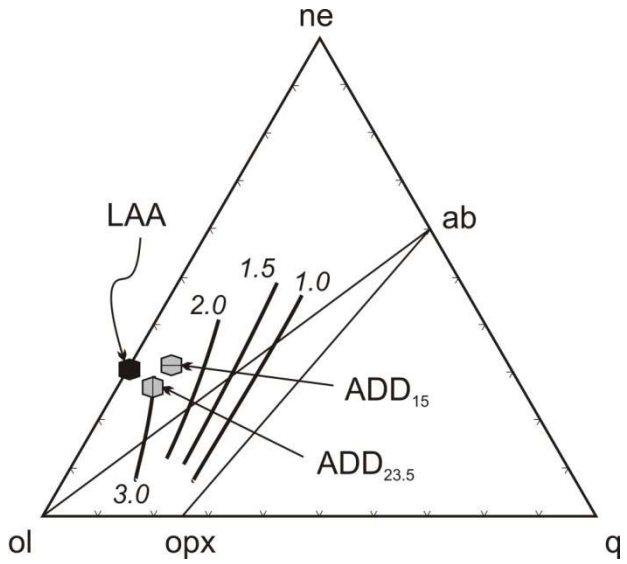

Figure 6.13: *Primitive magma pressure determination based on normative composition and the work of Hirose & Kushiro (1993), with isobars of 3.0, 2.0, 1.5 and 1.0 GPa. LAA is the primitive magma of Udo alkali calculated by Brenna et al. (2010; Chapter 4). Note that both high-Al alkali modeled primitive magma compositions (ADD_{15} and $ADD_{23.5}$) result shallower than the low-Al alkali parent melt of Brenna et al. (2010; Chapter 4).*

Both ADD_{15} and $ADD_{23.5}$ compositions were plotted on the *ne-ol-q* normative diagram of Hirose & Kushiro (1993), together with the previously determined primitive magma composition for the low-Al alkali magma (Brenna *et al.*, 2010; Chapter 4) shown for comparison (Fig. 6.13). Considering composition ADD_{15}, the high-Al alkali magma was generated at a shallower level (c. 2.5 GPa), approximately at the spinel to garnet transition (Robinson & Wood, 1998, Walter, 1998) compared to the low-Al alkali magma at >3 GPa (Brenna *et al.*, 2010).

ADD_{15} has a relatively low SiO_2 concentration (Table 6.6), characteristic of melts derived from greater depths, but with relatively low MgO, in agreement with our estimates of a 2.5 GPa source. The compositions of very low-degree melts can be highly variable and are dependent on the phases being consumed during melting. Given a similar peridotite source, lower degrees of melt result in SiO_2 poor basalts (Frey *et al.*, 1978, Green, 1973). The high-Al alkali magma is trace element-enriched compared to the low-Al alkali magma (Fig. 6.6). This feature may indicate a smaller degree of melting of the former from an overall similar source (Fig. 6.12). An

additional factor contributing to a SiO_2-poor parental melt may be the presence of amphibole or phlogopite in the source (Francis & Ludden, 1995).

The highly variable chemical composition of amphibole has been shown to be a function of pressure and temperature (Foley, 1991, Green, 1973, Millhollen *et al.*, 1974). For richterite the temperature of the stability field decreases with decreasing pressure (Foley, 1991). This may result in breakdown of the hydrous phase as the mantle source is being adiabatically decompressed. The breakdown of amphibole would lower the solidus (Green, 1973), resulting in partial melting. In addition, breakdown of phlogopite to amphibole, which accommodates less H_2O in its crystal structure than the former (Deer *et al.*, 1992) would cause flux melting of peridotite. The absence of a K-depletion in the low-Al alkali suite may suggest that these rocks were the product of greater degrees of melting (Fig. 6.12), without residual hydrous phase, or that it was derived from a drier, less metasomatised source.

An estimation of the mantle temperature conditions of partial melting can be made using the thermobarometers of Putirka (2008) and the primitive magma major element compositions. Calculations were performed using the Excel spreadsheets "RiM69_Ch03_ol-glass_T". Using equations 14 and 15 (Puirka, 2008) we gain temperatures of 1410 ± 51 ºC and 1430 ± 60 ºC respectively for the ADD_{15} composition (dry) and 1386 ± 51 ºC and 1457 ± 60 ºC respectively for the low-Al alkali primitive magma of Brenna *et al.* (2010). These estimates are within error of each other, and may be overestimates given that addition of H_2O reduces T. The models indicate that partial melting occurred between c. 1350 ºC and c. 1500 ºC. However, given that melting in the Early Pleistocene was shallower and at hydrous conditions compared to melting in the Late Pleistocene/Holocene, it likely occurred at comparatively lower temperature to the latter.

6.7.3 Integration of volcano- and field-scale models

We have presented data suggesting that single volcanoes in a monogenetic volcanic field have overall similar, but independent, source chemical signatures and evolutionary characteristics, even within single eruptions. Chemical variability within

single eruptive episodes in a field is controlled by short time-scale crystallization, and/or by mixing of variably sourced and/or variably evolved magma batches. The chemical heterogeneity over longer time scales, such as the lifespan of the volcanic field, records the changing physical dynamics during magma ascent, which result from different magma sources and crystallization/fractionation histories.

The genetic and evolutionary parameters modelled above for the Jeju magmas give rise to a model of four-dimensional (space + time) evolution of a monogenetic, small-volume volcanic field. Melting was initiated in the Early Pleistocene close to the garnet to spinel transition (c. 2.5 GPa) generating high-Al alkali magma (Fig. 6.14). Even earlier very low degrees of partial melting may have caused metasomatism of the mantle peridotite, promoting later melting. Rise of initial, small-volume magma pockets was hindered, possibly due to an immature, relatively cold and coherent mantle, or to low tectonic strain rates (Valentine & Perry, 2007). As a result considerable olivine fractionation occurred, depleting magmas in MgO, Ni and Cr and enriching them in Al_2O_3 and incompatible elements. Further fractionation during ascent may have occurred on dyke walls at shallow levels (lower P, T) in the crust, promoting some plagioclase removal and Al_2O_3 depletion.

As magmatic activity continued, the melting locus started to deepen (>3 GPa) pushing melting into previously unmetasomatised peridotite, and the degree of melting increased slightly, producing low-Al alkali magma. Concurrently the degree of melting at shallow depth increased to generate subalkali magma (Fig. 6.14). Fractionation became deeper with predominantly clinopyroxene removal, accompanied by increased magma ascent rates, precluding the development of a shallow (plagioclase) signature in the erupted products. Nevertheless, in some eruptions (e.g. Songaksan), shallow crystallization and fractionation may have temporarily affected ascending magmas, possibly due to early-injected dykes stalling (due to too low volumes?), before being reactivated by later (larger volume?) injections of magma. This style of activity continued into the Late Pleistocene and Holocene.

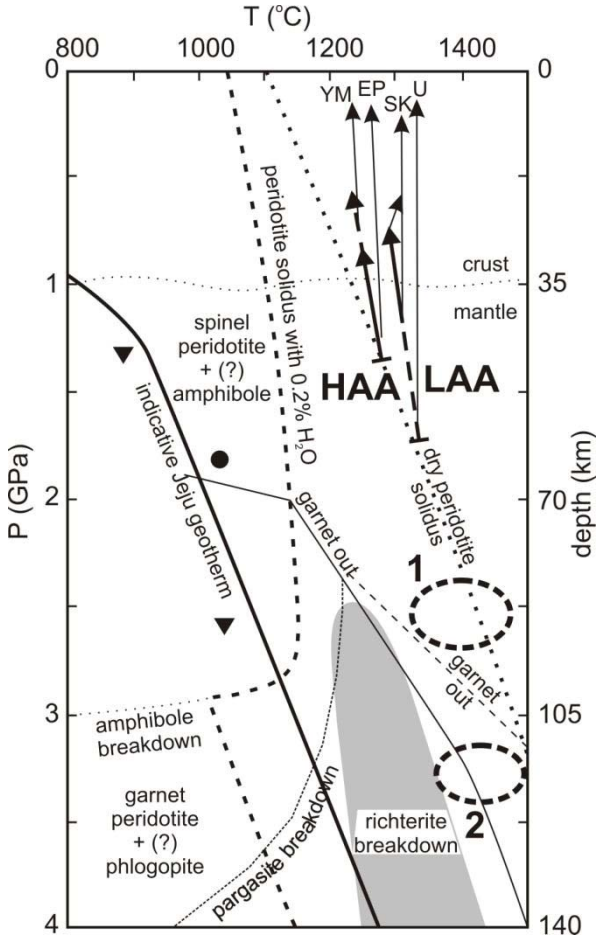

Figure 6.14: *Pressure-Temperature plot with peridotite solidi and mineralogy after Green (1973). Also included are the garnet-spinel transition boundary (dashed) after Robinson & Wood (1998) and the pargasite and the richterite breakdown fields after Foley (1991). The indicative Jeju geotherm is based on Choi et al. (2001; inverted triangles) and Yun et al. (1998; circle). The field marked 1 is the indicative condition of initial melting to form high-Al alkali magma, and Late Pleistocene subalkali magma due to larger degrees partial melting. The field marked 2 is the indicative conditions of melting to form low-Al alkali magma. Magma ascent paths for the Udo (U, Brenna et al., 2010; Chapter 4) and Songaksan (SK) eruptions of the low-Al alkali suite (LAA) and for tuff in deep core (EP) and Yongmeori (YM) eruptions of the high-Al alkali suite (HAA) are representative of fractionation occurring at various depths, but generally deeper in the LAA, and of possible magma mixing in dyke complexes.*

The lack of high-Al alkali magmas after the Early Pleistocene stage of activity reflects the increased degree of melting within the shallower portion of the source zone. This may also partly be due to an increased heat flux resulting from fluid and magma injections derived from a deeper part of the source zone.

Evidence for two-stage chemical evolution through fractionation, and magma mixing suggests that magma ascent occurred in a variety of styles and that the plumbing system of the field as a whole is a complex network of dykes within the mantle and lower crust, further affecting local stress fields and plumbing modes (Brenna *et al.*, 2011; Chapter 5).

Small-volume volcanic centres occur right from the onset of volcanic activity on Jeju Island and over the lifetime of the field. They represent three distinct chemical suites that can be linked to genetic processes in the mantle. This interpretation supports the perspective of Sohn & Park (2004) on the continuous small-volume activity during the development of the field, rather than a stage-development of the volcanic system with a final "scoria cone" (small-volume) stage (Lee, 1982). This has implications for the driving mechanism and genetic model of Jeju Island.

6.7.3.1 Domainal mantle uplift

Our modelled P-T conditions of melting to form the Jeju magmas are above the estimated geotherm for the mantle beneath Jeju Island, where garnet-free spinel peridotite is present to at least c. 2.6 GPa (Fig. 6.14; Choi *et al.*, 2001, Yun *et al.*, 1998). The results of this study suggest melting took place in the presence of residual garnet at a similar pressure (Fig. 6.12, 6.13). Alkali volcanism occurred in two main pulses, culminating in trachytic magmatism, and resulted in eruption in spatially distinct parts of Jeju Island (Chang *et al.*, 2006, Koh *et al.*, 2008, Koh & Park, 2010a, Koh & Park, 2010b). These observations have important implications for our understanding of the driving mechanism behind intraplate volcanism on Jeju Island. A classical "mantle plume" model (Fitton *et al.*, 1997, Takahashi & Nakajima, 2002, Watson & McKenzie, 1991) does not seem to be applicable given the relatively low geothermal gradient, as well as the presence of the subducted Pacific Plate under northeast Asia (Lei & Zhao, 2005), forming a mechanical boundary between upper and lower mantle.

However, localized mantle upwelling driven by tectonic plate movement (Anderson, 2001) could place deep and shallow mantle domains in juxtaposition, leading to

mantle decompression in the upwelled, deeper domains. This may imply that the source region is laterally (and vertically?) heterogeneous with sheared zones separating distinct domains. Sheared mantle with mylonitized lherzolite exist under Jeju Island at the depth (35-80 km) of mantle xenolith entrainment (Yang *et al.*, 2010, Yu *et al.*, 2010), and are likely to extend at depth to the source region. Instead of a classical diapir-like, uniform-upwelling model of mantle plume for Jeju (Tatsumi *et al.*, 2005), we propose that decompression melting was promoted by vertical movement of mantle lenses bound on two sides and "lubricated" by the shear zones (Downes, 1990; Fig. 6.15a). When garnet (gt) peridotite is uplifted into the spinel (sp) peridotite stability field it reaches disequilibrium between c. 3 and 2 GPa and starts melting by reacting cpx + ol + gt to generate liquid (Kinzler, 1997, Walter & Presnall, 1994). This process both initiates and is more efficient at shallow levels where garnet and clinopyroxene are more susceptible to melting than at greater depth (Walter, 1998), and where decomposition of hydrous phases focused in shear zones (Downes, 1990) may contribute by introducing fluids to the mantle peridotite (Fig. 6.14).

Intraplate volcanism in Arabia and Jordan was also interpreted to have evolved from an initial shallower mantle source to a deeper one as the life of the field progressed (Shaw *et al.*, 2003). There too the authors preferred a tectonically driven genetic model not involving a mantle plume.

6.7.3.2 Why Jeju?

A fundamental question remains, as to why Jeju occurs where it is? Here we attempt to explain its location based on tectonic mechanisms that confined volcanism to Jeju Island only, rather than generating a series of distributed volcanic centres throughout the East China Sea.

The Sea of Japan rifted between c. 25 and 15 Ma ago (Jolivet & Tamaki, 1992) and southwestern Honshu rotated by 37 degrees with an Euler pole situated to the south of the Korean Peninsula, near the present location of Jeju Island (Otofuji, 1996).

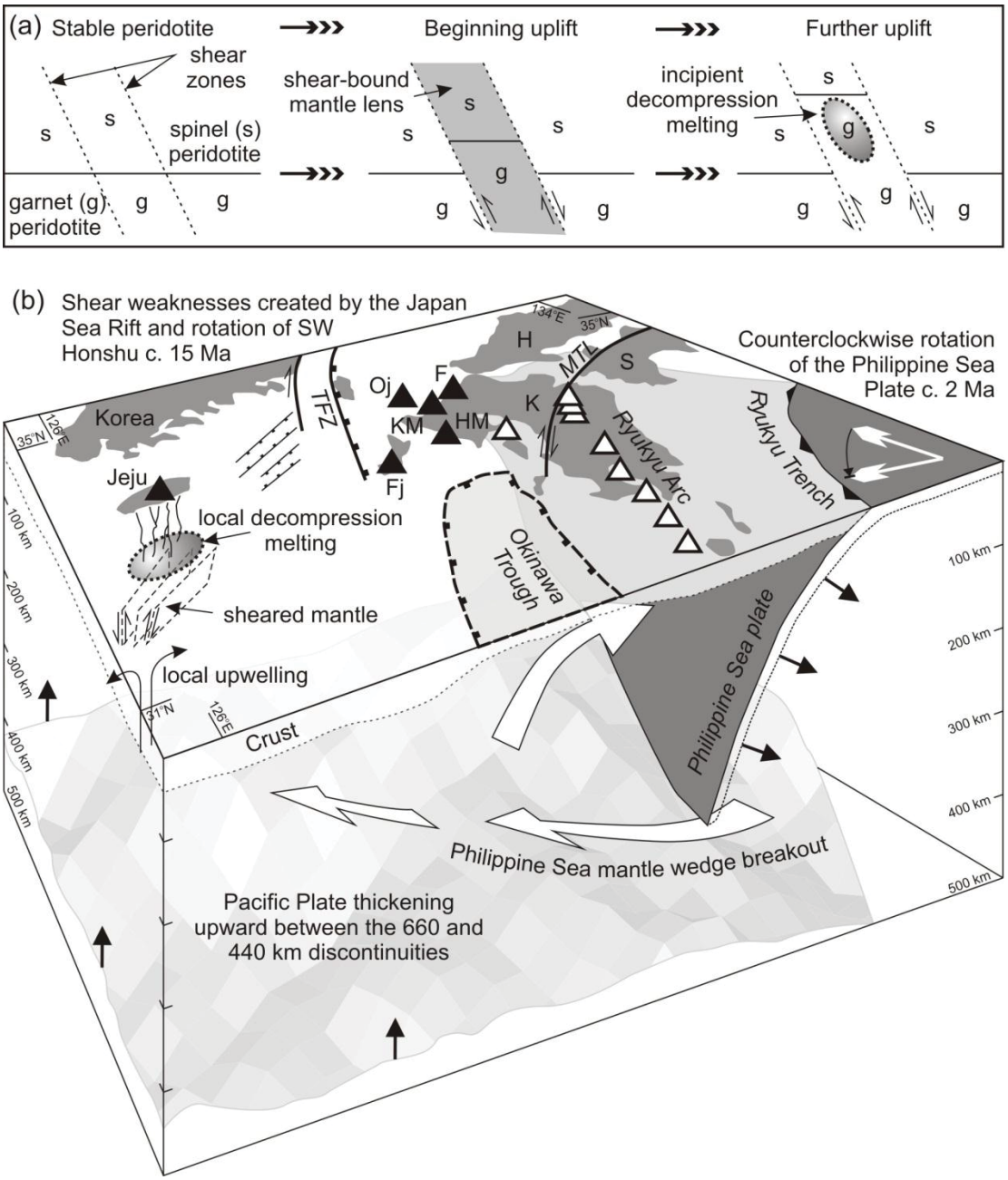

Figure 6.15: *a) Schematic mantle lens uplift model. Shear zones cause differential displacement of the garnet-spinel transition boundary, inducing melting in the uplifted garnet peridotite. b) Tectonic model explaining the focusing of magmatism under Jeju Island. Refer to the text for discussion. H: Honshu, S: Shikoku, K: Kyushu. Volcanic fields in NW Kyushu: F: Fukuoka, Oj: Ojika-jima, KM: Kita Matsuura, HM: Higashi Matsuura, Fj: Fukue-jima. Tectonic structures after Jolivet & Tamaki (1992), TFZ: Tsushima Fault System, MTL: Median Tectonic Line. Position of Philippine Sea Plate after Gudmundsson & Sambridge (1998) and Shiomi et al. (2004).*

This movement was accommodated between Korea and Kyushu along the Tsushima Fault system, including splay faults in the platform to the south of Korea (Fig. 6.15b; Jolivet & Tamaki, 1992). Such tectonic movement is also likely to have generated shear zones and weaknesses deeper in the mantle beneath Jeju Island (Yang *et al.*, 2010) as the elongation of Jeju Island is roughly en-echelon with these extensional structures (Fig. 6.15b). Rifting and subsidence also affected the East China Sea platform from Late Cretaceous to Late Miocene (Cukur *et al.*, 2011). These tectonic movements created a framework of weaker structures in the region.

The Philippine Sea Plate has been subducting beneath Kyushu for several million years (Hall *et al.*, 1995, Seno & Maruyama, 1984), and at around 2 Ma it rotated from northward, oblique, to northwestward, normal subduction (Kamata & Kodama, 1999, Kodama *et al.*, 1995). The resulting anticlockwise motion formed the Median Tectonic Line in central and southwestern Japan, and enhanced extension in the Okinawa Trough (Kamata & Kodama, 1999; Fig. 6.15b). Meanwhile, the subducted Pacific Plate thickened between the 440-660 km discontinuities beneath NE China and Korea, causing localized upward displacement of mantle of up to 0.8 cm/year (Lei & Zhao, 2005, Zou *et al.*, 2008), comparable to upwelling rates attributed to localized mantle convection rather than mantle plume activity (Demidjuk *et al.*, 2007, McGee *et al.*, 2011). Extrusion of the mantle wedge trapped between the Philippine Sea Plate and the Pacific Plate also likely occurs from beneath the edge of the subducted Philippine Sea Plate, and is responsible for anomalously hot mantle domains behind Kyushu and beneath the East China Sea (Sadeghi *et al.*, 2000, Toh & Honma, 2008, Yoshizawa *et al.*, 2010). The rotational movement of the subducting Philippine Sea Plate possibly triggered the reactivation of pre-weakened mantle beneath Jeju. Sheared zones may have acted as lubricated planes, facilitating upwelling of deeper mantle lenses and resulting in partial melting. Melt segregation was subsequently enhanced at the garnet-spinel transition (Asimow *et al.*, 1995), where initial magmatic activity in the Early Pleistocene was sourced.

It is entirely possible that intraplate decompression melting only affects the Jeju area, due to its vicinity to the Euler pole of rotation of SW Japan, which had previously created a mantle weakness. Further to the south, the mantle is possibly more competent and homogeneous, hindering upward shearing. Closer to Kyushu, the roll-

back of the Philippine Sea Plate prevents significant vertical upward shearing in the mantle wedge just above it, but focuses upwelling under the Ryukyu Arc and the Okinawa Trough and its continuation northward to generate the distributed volcanism in NW Kyushu (Fig. 6.15b; Mashima, 2009).

6.8 Conclusions

The relatively distinct chemistry of individual eruptions, and individual pulses feeding eruptions, indicate that the source region beneath the Jeju Island Volcanic Field is heterogeneous on a fine scale. Moreover, magma batches are stored in independent reservoirs (dykes) at depth prior to fractionation and eruption; hence the source region is not likely to be an interconnected partially molten domain.

Based on age relationships, major- and trace-element and isotope geochemistry of small-volume monogenetic volcanoes on Jeju, we have determined a magmatic model for the development of activity in the Field, and integrated this with a tectonic framework. In our model, magmatic activity is centred in the Jeju Island Volcanic Field due to the presence of weaker shear zones in the mantle following tectonic activity related to the opening of the East Sea/Sea of Japan c. 15 Ma ago. The shear zones were reactivated due to rotation of the subducting Philippine Sea Plate c. 2 Ma ago, allowing localized uplift. Mantle lenses or sheets lubricated by shear zones were slid upward causing localized decompression melting, accelerated by the breakdown of hydrous minerals in the mantle peridotite. Early Pleistocene, low degree melts (c. 1%) were derived from relatively shallow upper mantle (c. 2.5 GPa, 90 km), followed by deepening (c. 3.5 GPa, 115 km) of the melting locus and increased extent of melting (<2% alkali and 5-7% subalkali). The small-volume activity derived from a heterogeneous mantle source continued throughout the life of the field rather than representing a final stage in its evolution. In the case of Jeju, mantle heterogeneity on the inferred scale requires shearing of mantle domains only a few kilometres across.

The proposed link between subduction and intraplate activity on Jeju may have implications for future eruptions in the field. A similar type of link has also been presented for the Auckland Volcanic Field, New Zealand (Bebbington & Cronin,

2011). If this is the case, then we also hypothesize that increased tectonic activity at the Ryukyu subduction zone may result in renewed magmatic activity in the field.

6.9 Funding

This output forms part of FRST-IIOF project MAUX0808 “Facing the challenge of Auckland volcanism” and is also supported by a Massey University Vice-Chancellor’s Scholarship to MB, and by a National Research Foundation of Korea (NRF) grant to YKS (No. 2009-0079427).

6.10 Acknowledgements

Chang Woo Kwon and Jeon Yong Mun provided assistance during fieldwork, Ritchie Sims, John Wilmshurst and Ashlea Wainwright helped with analytical work. Discussion with and comments by Károly Németh, Bob Stewart, Richard Price, Georg Zellmer and Ting Wang are appreciated. Reviews by Frank Tepley, John Caulfield and a particularly thoughtful one by George Jenner greatly improved the manuscript.

6.11 Supplementary data

Supplementary data for this paper are available at *Journal of Petrology* online.

Chapter 7:

Integration of Small- and Large-Volume Magmatic Systems

This chapter presents and investigates data from three deep drill cores in the centre of Jeju Island exemplifying large-volume eruptions in the system. Additional samples from trachyte domes and lava flows as well as basaltic lavas at the margins of Jeju Island complete the dataset. The mantle source is analogous to that feeding small-volume eruptions, and hence Jeju consist of a single magmatic system which produced widely variable volumes of melts. These erupted independently and never formed a centralized plumbing system.

7.1 Introduction

The occurrence of distributed scoria and phreatomagmatic cones on the flanks of larger volcanic edifices is a ubiquitous feature of volcanic systems in all tectonic settings. The superposition of small- and large-volume magmatic systems is still enigmatic in various aspects including magma sourcing and ascent. The detailed studies presented in the previous chapters are here integrated with data from the larger volume events in order to develop a comprehensive model for the spatio-temporal development of the Jeju magmatic system.

This chapter consists of the manuscript "*Spatio-temporal evolution of a distributed magmatic system and its implications for volcano growth, Jeju Island Volcanic Field, Korea*" by: Marco Brenna, Shane J. Cronin, Ian E. M. Smith, Young Kwan Sohn and Roland Maas, published in *Lithos* (148, 337-352; DOI 10.1016/j.lithos.2012.06.021). A copy of the article is attached to this thesis as Electronic Appendix J and the supplementary data files are attached as Electronic Appendices K, L and M. This manuscript is devoted to the investigation of large-volume eruptions in the Jeju Island Volcanic Field and the integration with earlier studies of small-volume events. The study reveals the volume-independency of the Jeju magmatic system. Small- and

large- volume events are derived from the same source and underwent similar evolutionary histories, except that large-volume events were affected by greater degrees of chemical evolution. Magma output rates increased twofold c. 400 ka ago concomitant with an increase in volcanic activity in the Ryukyu Arc, suggesting that a tectonic trigger was driving the Jeju system.

The contributions of each author to the study were as follows:

Marco Brenna:	Principal investigator:	
	Carried out:	Field investigations and sampling
		Petrographic observations
		Sample preparation and chemical analysis
		Chemical data interpretation and modelling
		Manuscript preparation and writing
Shane J. Cronin:	Chief advisor:	
	Aided the study by:	Assisting in the field and sampling
		Editing and discussion of the manuscript
Ian E. M. Smith:	Advisor:	
	Aided the study by:	Assisting in the field and sampling
		Provide chemistry data
		Discussion of results and modelling
		Editing and discussion of the manuscript
Young Kwan Sohn:		
	Advisors:	
	Aided the study by:	Assisting in the field and sampling
		Editing and discussion of the manuscript
Roland Maas:	Collaborator:	
	Aided the study by:	Providing Sr-Nd-Pb isotope data
		Editing and discussion of the manuscript

7.2 Spatio-temporal evolution of a distributed magmatic system and its implications for volcano growth, Jeju Island Volcanic Field, Korea

Marco Brenna[1], Shane J. Cronin[1], Ian E. M. Smith[2], Young Kwan Sohn[3], Roland Maas[4],

[1]*Volcanic Risk Solutions, Massey University, Palmerston North, New Zealand*
[2]*School of Environment, University of Auckland, Auckland, New Zealand*
[3]*Department of Earth & Environmental Sciences, Gyeongsang National University, Jinju, South Korea*
[4]*School of Earth Sciences, The University of Melbourne, Parkville, Australia*

7.2.1 Abstract

Jeju Island is the emergent portion of a basaltic volcanic field developed over the last c. 1.8 Ma on continental crust. Initial volcanism comprised dispersed, small-volume (<0.01 km^3) alkali basaltic eruptions that incrementally constructed a tuff pile. Lavas and scoria from continuing small-scaled monogenetic volcanism capped this foundation. From c. 0.4 Ma large-volume (>1 km^3) eruptions began, with lavas building a composite shield. Three magma suites can be recognized: Early Pleistocene high-Al alkali (HAA), and Late Pleistocene to Holocene low-Al alkali (LAA) and subalkali (SA). The chemical similarity between small-volume and primitive large-volume eruptions suggests analogous parent magmas and fractionation histories that are independent of erupted volumes. The large-volume magmas evolved to trachyte, which erupted in two distinct episodes: the HAA Sanbangsan suite at c. 750 ka and the LAA Hallasan suite at c. 25 ka. Sr and Nd isotopes indicate that the early trachytes were contaminated by upper crustal material, whereas the later magmas were not. Both suites bear a Nd isotope signature indicative of lower crustal interaction. Sub-suites transitional between HAA and LAA, and between LAA and SA, indicate that melting occurred in discrete, but adjacent, mantle domains. Throughout the evolution of this volcano, each magma batch erupted separately, and a centralized plumbing system was never created. The Island's central

peak (Mt. Halla 1950 m a.s.l.) is therefore not a *sensu stricto* stratovolcano, but marks the point of peak magma output in a distributed magmatic system. Jeju's shape and topography thus represent the spatial variation of fertility of the mantle below it. An increase in melt production in the Late Pleistocene was related to a deepening of the melting zone due to regional tectonic rearrangements. Temporal coincidences between magmatic pulses on Jeju and large-scale caldera eruptive events along the nearest subduction system in Kyushu, Japan, suggests that tectonic extension and changing strain rates may drive volcanism on a regional basis, influencing the intraplate volcanism of Jeju Island.

7.3 Introduction

Intraplate volcanism is a widespread phenomenon on Earth, occurring in both oceanic and continental settings and ranging in scale between the extremes of small-volume dispersed volcanism, forming monogenetic volcano fields, up to large-volume plume or rift-related volcanoes that can build polygenetic volcanic edifices of considerable size. The mode of magma generation, storage, ascent and eruption in these systems reflects tectonic stress and strain distribution [Brenna *et al.*, 2011 (Chapter 5); Nakamura, 1977; Takada, 1994; Valentine & Hirano, 2010; Valentine & Perry, 2007], the magmatic footprints (Valentine & Perry, 2006) and the degree of partial melting (Frey *et al.*, 1978; Sato *et al.*, 1990), or the sustainability of magma supply (Fedotov, 1981).

Intraplate volcanism is most commonly monogenetic, i.e., magmas are sourced and erupted independently. This contrasts with polygenetic volcanism, in which magmas are interconnected at depth and a repeatedly re-used conduit system develops, resulting in an edifice made up of the products of many thousands of eruptions (Cañón-Tapia & Walker, 2004). Consequences of these systematic differences include low cumulative volumes of commonly primitive compositions in monogenetic eruptions but large volumes and evolved magmas in polygenetic volcanoes. If the two types of system are superposed, distinguishing between them requires a detailed knowledge of chemical variability and eruption chronology.

Small monogenetic volcanic centres can often be sampled throughout their entire eruption sequence, which allows detailed insights into their magmatic origins [Blondes *et al.*, 2008; Brenna *et al.*, 2011 (Chapter 5); Brenna *et al.*, 2010 (Chapter 4); McGee *et al.*, 2011; Smith *et al.*, 2008; Sohn *et al.*, 2012 (Chapter 5); Strong & Wolff, 2003]. These single-volcano studies provide snapshots of the evolution of distributed volcanic fields that may contain many hundreds of monogenetic centres sporadically erupted over hundreds of thousands to millions of years. A similar investigation for a large composite volcano is however hindered by the burial of the majority of early eruption products, which conceal a large part of the volcano development history. Jeju Island, the subaerial part of a volcanic field immediately south of the Korean Peninsula, has been extensively and deeply drilled to explore and exploit groundwater resources (Koh, 2005; Won *et al.*, 2006). This has provided the basis for a thorough understanding of the geological history, age and structural development of the island (Koh & Park, 2010a, b; Koh *et al.*, 2008; Sohn & Park, 2004; Sohn *et al.*, 2008). Drill cores on Jeju also provide a unique opportunity to investigate the evolution of an entire volcanic system, comprising both dispersed, small-volume, monogenetic volcanism and large-volume volcanism that has built a central composite volcanic edifice.

Here we address the relationship between small- and large-volume monogenetic volcanism in focused versus dispersed settings, as exemplified on Jeju Island. Further, we discuss the implications of our model for other intraplate volcanic areas and volcanic edifice building and briefly compare it to the stable magmatic conduit systems established beneath typical andesitic stratovolcanoes (Annen *et al.*, 2006; Turner *et al.*, 2011; Zellmer & Annen, 2008). We present new major and trace element and Sr-Nd-Pb chemical data from both surface samples and three deep cores (400-500m) penetrating the entire lava succession in the central part of Jeju Island. From this we develop a model for the spatio-temporal evolution of the island's magmatic system from its infancy that explains its form and time-varying eruptive behavior. This example provides new insights into how long-lived mantle-fed volcanism operates in continental intraplate areas.

7.4 Geological background and sampling

Jeju Island lies on the continental shelf, south of the Korean Peninsula (Fig. 7.1). It is located c. 600 km behind the subduction front, where the Philippine Sea Plate is being subducted beneath the Eurasian Plate. The subduction gives rise to arc magmatism at the Ryukyu Arc and to backarc extension forming the Okinawa Trough and dispersed volcanism in northwestern Kyushu, Japan (Fig. 7.1; Mashima, 2009; Sibuet *et al.*, 1987).

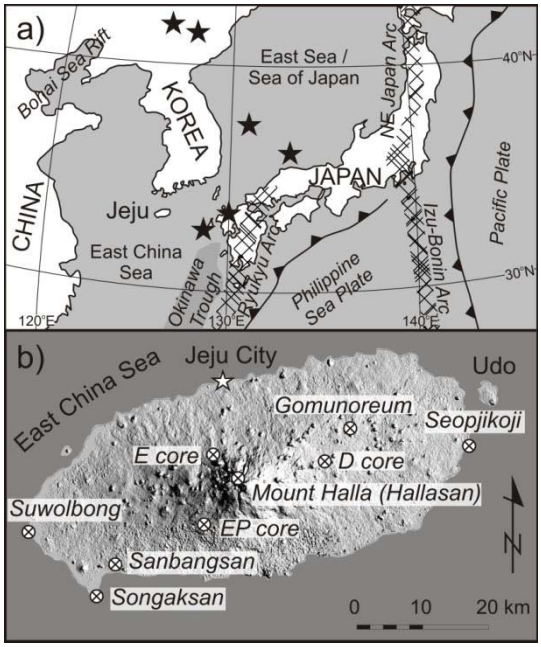

Figure 7.1: *a) Regional geological setting of Jeju Island, Korea, with major tectonic features. Stars indicate other main Quaternary intraplate volcanic areas. b) Digital elevation model of Jeju island with location of sampled sites.*

Jeju Island is a c. 70 x 30 km elliptical and symmetrical island with a central peak rising to 1950 m a.s.l. (Mount Halla; Fig. 7.1b). Morphologically the island is made up of gently sloping, outward dipping lava shields and a central dome/flow complex with steeper flanks. The island is also dotted by at least 300 scoria cones and phreatomagmatic eruptive centres (tuff rings/cones). The earliest evidence for volcanism is represented by the buried Seoguipo Formation, which was formed by phreatomagmatic activity at c. 1.8 Ma, (Kang, 2003; Sohn & Park, 2004; Sohn *et al.*, 2008; Sohn & Yoon, 2010). Volcanic activity has continued into historic times (Lee & Yang, 2006).

7.4.1 Previous work

This contribution follows and is built upon a detailed study of the Udo tuff cone and lava shield [Fig. 7.1b; Brenna *et al.*, 2010 (Chapter 4)] and of an integrated study presented by Brenna *et al.* (2012; Chapter 6) of selected small-volume (<0.1 km^3) eruptive centres throughout Jeju. These studies investigated major and trace element and Sr-Nd-Pb isotopic variation to produce a magmatic model for the development of the small-volume volcanic system that generated dispersed scoria and phreatomagmatic cones from the onset of activity on Jeju. Three distinct chemical suites were described and discussed by Brenna *et al.* (2012; Chapter 6): High-Al alkali (HAA) erupted in the Early Pleistocene, and Low-Al alkali (LAA) and Subalkali (SA) both erupted in the Late Pleistocene to Holocene. The three suites were interpreted to have had chemically distinct parental compositions derived from different depths and degrees of partial melting in the mantle. Studying the small-volume system, which is relatively primitive (SiO_2 < 53wt%) and unaffected by crustal assimilation and contamination, allowed a focused investigation into processes of magma genesis and fractional crystallization in primitive magmas.

7.4.2 New data and sampling

New major and trace element and Sr-Nd-Pb isotope data have been obtained for a suite of samples from the large-volume (> 1 km^3) eruptive units of the Jeju system. The new data are integrated with the model based on data from the small-volume eruptions on Jeju (Brenna *et al.*, 2012; Chapter 6) and an age catalogue compiled from published work. The new dataset extends the chemical range discussed by Brenna *et al.* (2012; Chapter 6), and hence allows the construction of a comprehensive magmatic and volcanic model for the Jeju system.

The majority of samples for this study were collected from three deep cores (400-500 m) in the central part of Jeju Island (Fig. 7.1b). These have intersected several successions of lava flows with interspersed soil horizons and autobreccias (Electronic Appendix K). Contacts between flows are generally highlighted by oxidized, vesiculated or autobrecciated horizons. At least one sample was collected from each

flow for whole rock chemical analysis, or, where flow contacts were not clear, from uninterrupted core sections. Individual flow thicknesses vary from <1 m to c. 30 m. Lava flows could not be directly correlated across cores, because the drill holes were located on three separate flanks of the central volcanic edifice.

Additional samples were collected from and around the Sanbangsan trachyte dome and the summit of Mt. Halla (Fig. 7.1b). These are representative of two trachytic episodes, the Sanbangsan suite (c. 750 ka), and the Hallasan suite (c. 25 ka; Chang *et al.*, 2006; Won *et al.*, 1986). Samples were also collected from lava flows in the lower reaches of the main edifice and in coastal areas (Fig. 7.1b) and these are considered to be representative of the broad, shallow dipping large-volume lava shield forming the outer slopes of Jeju. Samples coordinates are available in Electronic Appendix L.

7.5 Whole rock geochemistry

Clean rock specimens were crushed using a steel crusher and chips free of saw-blade or crusher-plate marks were handpicked and milled in a tungsten carbide ring grinder. Major and minor element (Si, Ti, Al, Fe, Mn, Mg, Ca, Na, K, P,) concentrations were measured by X-ray fluorescence (XRF; Siemens SR3000 spectrometer) at the University of Auckland using standard techniques. In general, precision for each major or minor element is better than ±1% (1sd) of the reported value. Fe was measured as total Fe_2O_3 and analyses were recalculated to 100% volatile free with FeO as total FeO. Trace elements were measured on the XRF glass discs by laser-ablation inductively-coupled-plasma mass-spectrometry (LA-ICPMS) at the Research School of Earth Sciences, Australian National University, using an Excimer LPX120 laser (193 nm) and Agilent 7500 series mass spectrometer. Tests based on 25 repeat analyses of standard BCR-2 (see Electronic Appendix L) indicate precision of <4% (RSD) and accuracy better than 5% at the 95% confidence level for most elements. Representative major and trace element analyses are presented in Table 7.1, and the whole dataset is included in Electronic Appendix L.

Sr-Nd-Pb isotopic compositions were acquired at the University of Melbourne (e.g. Maas *et al.*, 2005). Acid-leached chips (6M HCl, 100^{o}C, 60 min), were dissolved on a

hotplate (2 ml of 3:1 HF-HNO_3 for 2 days at 110 ºC and 6M HCl for 1 day), followed by sequential extraction of Pb, Sr and Nd using a combination of anion exchange and EICHROM RE, LN and SR resin chromatography. Blanks were <100 pg and negligible. Isotopic analyses were completed on a NU Plasma Multicollector-ICPMS. Sr and Nd isotope ratios were normalised to $^{86}Sr/^{88}Sr=0.1194$ and $^{146}Nd/^{145}Nd=2.0719425$ (equivalent to $^{146}Nd/^{144}Nd = 0.7219$, Vance & Thirlwall, 2002), respectively, using the exponential law, and are reported relative to SRM987 = 0.710230 and La Jolla Nd = 0.511860. External precision (2sd) is ≤0.000040 for $^{87}Sr/^{86}Sr$ and ≤0.000020 for $^{143}Nd/^{144}Nd$. The results for secondary standards (BCR-2, BHVO-2, JNd-1) obtained during this study are consistent with TIMS reference ratios. Pb mass bias was corrected using the thallium-doping technique (Woodhead, 2002) which is expected to produce external precisions of 0.025-0.05% (2sd). This is confirmed by the results for 12 runs of SRM981, by duplicate runs for several samples, and by the results for BCR-2 and BHVO-2. Sr-Nd-Pb isotope data and standards measurements are presented in Table 7.2.

Mineral analyses were obtained by electron microprobe at the University of Auckland. The instrument used was a JEOL JXA-840A using LINK systems LZ5 detector, QX2000 pulse processor and ZAF-4/FLS matrix correction software. Standard operating conditions were an accelerating voltage of 15 kV, beam current of 0.5 nA, beam diameter of 5 μm and a live count time of 100 s. Analytical precision was estimated by replicate analyses of mineral standards as (1sd) ≤3% for elements present in abundances >1 wt%. Representative mineral analyses are presented in Table 7.3.

7.5.1 Major and trace elements

Major and trace element variations define discrete chemical suites in time and space, which span a compositional spectrum from basanite to trachyte and from subalkali basalt to basaltic andesite (Figs. 7.2, 7.3). The main suites are hereafter termed high-Al alkali (HAA), low-Al alkali (LAA) and subalkali (SA), with transitional alkali and transitional subalkali suites covering the spectrum of intermediate compositions; this

Table 7.1: *Major and trace elements of selected Jeju large-volume lava samples. The entire dataset complete of sample location is available as Electronic Appendix L.*

Sample	SK01	J-1	J-9	HS02	HS03	E24	E26	E33
Chemical Suite	SA	Trn SA	Trn SA	LAA	LAA	LAA	Trn HAA	HAA
Major elements								
SiO_2	51.69	50.52	51.63	51.01	65.88	47.39	48.34	52.60
TiO_2	2.16	2.20	2.19	2.38	0.28	2.67	3.31	2.06
Al_2O_3	14.43	14.32	15.13	16.72	16.57	13.10	16.78	18.33
FeO	10.77	11.35	11.14	11.07	4.04	11.95	12.03	8.38
MnO	0.15	0.16	0.16	0.17	0.12	0.17	0.17	0.18
MgO	7.85	8.07	6.41	5.68	0.19	10.52	4.87	2.83
CaO	8.96	8.80	8.15	6.97	1.35	9.96	7.96	7.08
Na_2O	2.98	3.11	3.50	3.62	5.95	2.66	3.84	4.59
K_2O	0.72	1.09	1.23	1.71	5.56	1.20	1.88	3.13
P_2O_5	0.29	0.38	0.46	0.67	0.06	0.38	0.82	0.82
Total	100.00	100.00	100.00	100.00	100.00	100.00	100.00	100.00
Mg#	56.49	55.90	50.65	47.79	7.78	61.08	41.90	37.53
Trace elements								
Cs	0.22	0.32	0.36	0.18	0.69	0.27	0.36	0.92
Ba	187.96	279.37	306.90	565.03	762.76	304.27	514.29	848.29
Rb	15.06	24.34	26.94	25.69	125.37	25.89	38.01	77.46
Sr	355.92	409.61	423.45	539.64	67.13	512.45	915.74	1232.92
Pb	10.75	3.33	3.40	6.24	10.21	6.09	5.80	9.76
Th	2.36	3.97	4.71	8.61	18.18	4.18	6.19	14.24
U	0.50	0.74	0.94	1.61	3.61	0.89	1.29	3.15
Zr	136.43	172.12	197.36	330.30	831.82	170.38	248.24	469.50
Nb	19.67	30.70	35.16	62.83	103.95	36.11	55.98	101.46
Hf	3.59	4.29	4.84	7.84	18.40	4.20	5.84	10.41
Ta	1.86	2.09	2.25	4.38	6.98	2.43	3.78	6.72
Y	20.20	22.85	24.39	32.41	34.33	19.78	27.87	31.05
Sc	23.58	24.83	21.57	19.44	8.51	28.74	17.69	9.29
V	206.53	201.14	172.46	114.79	8.08	237.63	188.92	94.78
Cr	357.39	324.51	214.51	143.45	4.59	465.30	28.24	14.26
Co	75.36	51.15	44.10	51.29	18.26	62.69	42.09	21.39
Ni	174.55	168.85	108.30	92.10	4.99	220.62	23.62	13.37
Cu	44.04	41.32	44.04	20.18	7.86	50.85	27.85	14.84
Zn	95.09	97.25	122.09	131.29	129.33	134.42	141.07	150.46
Ga	19.28	19.17	20.13	24.09	28.64	18.19	22.46	25.12
La	15.57	23.42	27.49	50.29	45.71	26.41	43.70	84.52
Ce	33.95	46.70	52.51	91.87	95.97	51.69	85.85	159.84
Pr	4.22	5.79	6.51	11.21	9.59	6.18	10.50	17.92
Nd	19.68	25.52	29.01	47.06	38.36	26.87	45.46	67.61
Sm	5.16	6.00	6.40	9.87	8.18	5.85	9.49	11.90
Eu	1.73	2.01	1.97	2.95	2.16	1.96	3.04	3.67
Gd	5.18	6.34	6.70	9.28	7.78	5.75	8.67	9.63
Tb	0.77	0.94	0.99	1.26	1.14	0.78	1.14	1.23
Dy	4.49	5.13	5.30	7.14	7.19	4.57	6.56	6.88
Ho	0.80	0.95	0.99	1.30	1.40	0.80	1.14	1.23
Er	2.05	2.36	2.59	3.34	4.08	2.01	2.84	3.21
Tm	0.27	0.31	0.33	0.43	0.59	0.26	0.38	0.42
Yb	1.60	1.94	2.08	2.48	3.72	1.50	2.13	2.68
Lu	0.24	0.26	0.29	0.36	0.57	0.20	0.29	0.34
Eu*	10.16	12.08	12.82	18.90	15.74	11.41	17.95	21.48

Table 7.1: *cont.*

Sample	EP-10	EP-22	EP-29	EP-31	D-8	D-25	SBS-01	YM00
Chemical Suite	LAA	Trn HAA	Trn HAA	HAA	LAA	Trn HAA	HAA	HAA
Major elements								
SiO_2	50.29	48.56	51.01	44.64	50.01	58.79	62.20	45.01
TiO_2	2.93	3.15	2.56	3.79	2.91	1.00	0.64	2.98
Al_2O_3	16.72	15.75	17.07	16.20	17.46	17.61	18.57	14.17
FeO	11.64	12.11	10.36	13.11	11.02	7.40	3.87	11.79
MnO	0.16	0.16	0.16	0.19	0.15	0.18	0.24	0.18
MgO	4.16	6.09	4.37	6.88	4.53	1.38	0.49	10.81
CaO	7.06	8.42	7.00	10.37	7.99	3.52	3.25	10.28
Na_2O	4.26	3.56	4.02	3.81	3.92	5.75	6.42	2.71
K_2O	2.07	1.59	2.69	0.56	1.48	3.84	4.19	1.63
P_2O_5	0.71	0.61	0.76	0.45	0.53	0.53	0.13	0.44
Total	100.00	100.00	100.00	100.00	100.00	100.00	100.00	100.00
Mg#	38.93	47.29	42.93	48.34	42.30	24.89	18.52	62.03
Trace elements								
Cs	0.19	0.14	0.45	0.35	0.18	0.31	0.40	0.57
Ba	514.67	426.20	741.38	482.46	405.15	930.14	1097.36	490.79
Rb	44.72	32.89	49.79	57.25	31.06	85.65	99.78	25.30
Sr	688.60	702.28	884.49	702.20	657.08	593.64	763.88	595.98
Pb	5.89	5.06	6.62	5.24	3.65	7.91	11.90	5.36
Th	6.93	5.23	9.94	5.21	5.17	13.79	15.79	5.17
U	1.53	1.13	2.18	1.00	1.16	3.11	3.31	1.12
Zr	285.77	228.77	376.02	222.65	217.27	493.42	690.89	205.34
Nb	59.49	48.06	79.63	50.33	43.54	101.19	125.87	44.05
Hf	6.73	5.55	8.73	5.80	5.20	10.96	14.97	5.19
Ta	3.97	3.24	5.39	3.27	2.88	6.51	10.03	3.08
Y	27.84	24.55	28.54	28.72	23.44	31.26	42.64	23.52
Sc	16.02	20.52	16.16	33.80	17.54	6.74	3.12	
V	163.35	203.39	154.87	369.84	197.33	13.63	11.32	346.46
Cr	7.68	146.55	72.28	57.85	34.05	5.55	5.63	291.01
Co	45.45	56.46	38.88	52.80	42.27	15.12	45.14	65.55
Ni	13.55	79.09	48.08	36.75	43.64	5.29	4.47	140.94
Cu	28.41	35.84	22.09	45.77	19.60	7.97	4.42	43.69
Zn	146.45	129.34	143.87	128.62	132.65	154.13	142.14	80.53
Ga	24.64	22.00	23.85	20.29	23.28	25.74	23.41	17.00
La	43.50	35.56	59.87	37.63	32.03	73.67	94.48	36.23
Ce	86.27	70.91	112.92	74.18	62.28	139.81	178.68	71.75
Pr	10.33	8.65	13.40	9.19	7.47	15.19	19.79	8.45
Nd	43.32	37.55	54.61	39.17	32.55	57.13	73.86	34.94
Sm	9.37	8.03	10.46	8.27	7.13	10.29	12.37	6.94
Eu	2.95	2.69	3.27	2.60	2.40	3.20	3.49	2.17
Gd	8.77	7.46	9.15	8.11	6.98	8.56	10.30	6.42
Tb	1.16	1.01	1.15	1.08	0.97	1.15	1.45	0.90
Dy	6.49	5.72	6.51	6.41	5.44	6.70	8.94	5.24
Ho	1.10	1.00	1.15	1.14	0.95	1.20	1.68	0.93
Er	2.90	2.55	2.90	3.10	2.40	3.26	4.84	2.52
Tm	0.37	0.32	0.37	0.40	0.33	0.48	0.70	0.33
Yb	2.13	1.91	2.17	2.40	1.77	2.83	4.29	2.08
Lu	0.29	0.25	0.30	0.34	0.24	0.38	0.64	0.29
Eu*	17.91	15.29	19.45	16.11	13.89	18.77	22.57	13.19

Total Fe as FeO. Major elements in wt% oxides recalculated to 100% volatile free. SA: Subalkali, Trn SA: Transitional SA, LAA: Low-Al alkali, HAA: High-Al alkali, Trn HAA: Transitional alkali.

terminology follows Brenna *et al.* (2012; Chapter 6) and Tatsumi *et al.* (2005). These suites occur in a specific stratigraphic order: high-Al alkali lavas make up the base of the cores; these are overlain by transitional alkali lavas, which are, in turn, overlain by the low-Al alkali suite at the top (Fig. 7.3i). Subalkali and transitional subalkali compositions are absent from core samples, but occur among the outer flank lavas. The SiO_2 range of the dataset is broader than that known from small-volume Jeju volcanoes (Brenna *et al.*, 2012; Chapter 6). By contrast, the subalkali and transitional subalkali lavas have a restricted compositional range, varying from basalt to basaltic andesites.

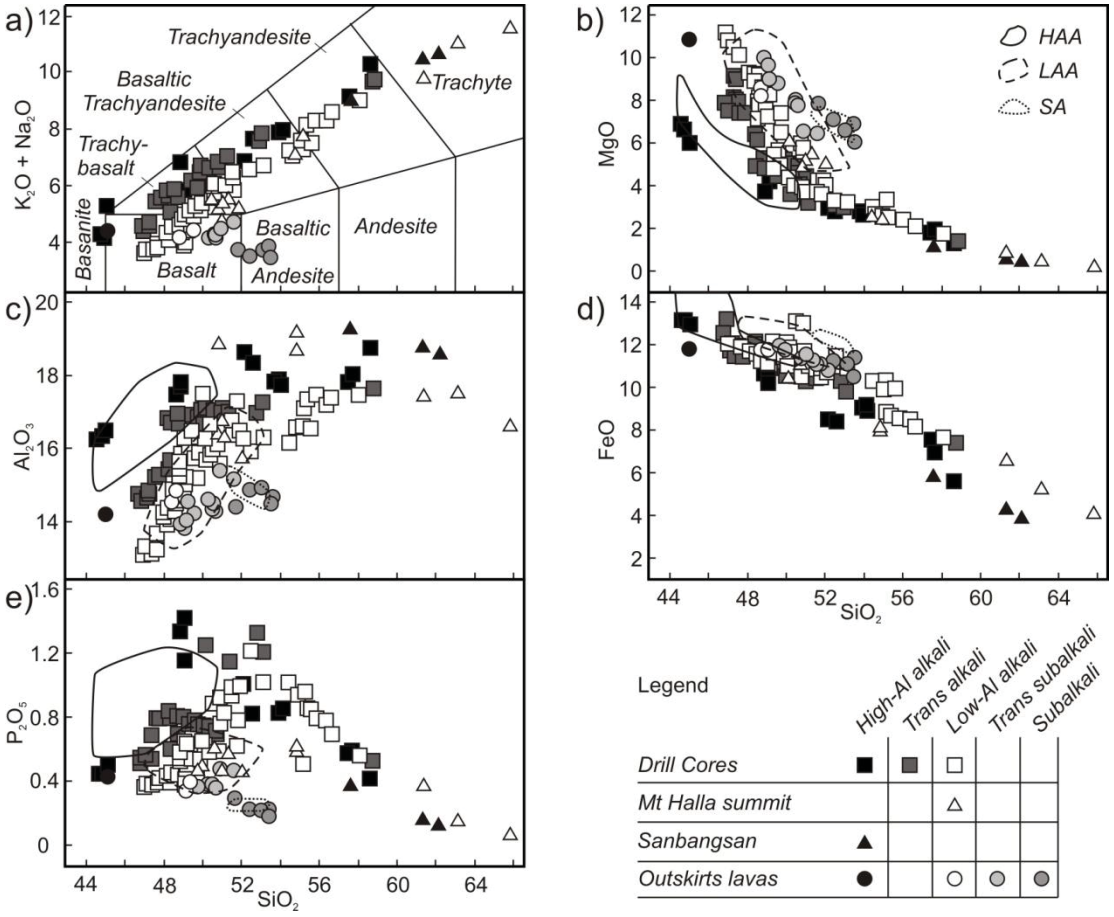

Figure 7.2: *Selected major element variation diagrams for chemical suites identified on Jeju Island. a) Chemical classification after LeBas et al. (1986). HAA, LAA and SA fields are the small-volume high-Al alkali, low-Al alkali and subalkali suites, respectively, of Brenna et al. (2012; Chapter 6). Major oxides in wt%. FeO is total Fe.*

Overall, MgO, FeO_{TOT}, CaO, MnO and TiO_2 abundances generally decrease and Al_2O_3, Na_2O, K_2O and P_2O_5 contents generally increase with increasing SiO_2

abundance up to c. 50 wt%. At higher silica concentrations Al_2O_3 content is constant and P_2O_5 abundance decreases (Figs. 7.2c, e). MnO is more abundant in the high-Al alkali suite (0.17-0.29 wt%) compared to the other suites (0.11-0.18 wt%). Chemical variation in the high-Al alkali suite is not continuous, but rather clusters of samples occur, separated by a SiO_2 gap (Figs. 7.2, 3).

The abundances of trace elements compatible in mafic mineral phases (e.g. Cr, Ni, V, Sc) decrease with increasing SiO_2 content, whereas those of incompatible elements [e.g. rare earth elements (REE), high field strength elements (HFSE) and large ion lithophile elements (LILE)] generally increase (Fig. 7.3). Sr abundance increases up to c. 50 wt% SiO_2, after which it decreases. Sr abundances (and to a lesser extent all other incompatible elements) can be used to discriminate between the three suites, with the high-Al alkali suite being the most enriched in incompatible elements, and the subalkali suite the least enriched (Fig. 7.3). This difference gives rise to sub-parallel chemical evolutionary trends for the different suites on variation diagrams (Figs. 7.2, 7.3).

Normalized diagrams (Figs. 7.3e, g) of the most primitive samples confirm that the high-Al alkali suite is the most incompatible trace element enriched and the subalkali suite is the least incompatible trace element enriched. Additionally, in contrast to the low-Al alkali suite, the high-Al alkali suite shows a negative K anomaly. An extended element diagram of evolved samples (Fig. 7.3f) shows that the low-Al alkali suite has prominent Sr and minor La and Ce negative anomalies with respect to the high-Al alkali suite. Eu shows both positive and negative anomalies (Fig. 7.3h).

7.5.2 Sr-Nd-Pb isotopes

Isotope ratios show overall limited variability within mantle domains (Figs. 7.4a, b; Hart *et al.*, 1992). A detailed discussion of the mantle end members involved is beyond the scope of this contribution, however Choi *et al.* (2005, 2006), Kim *et al.* (2005) and Tatsumi *et al.* (2005) established that the Jeju magmas reflect mixed signatures of both depleted MORB mantle (DMM) and Enriched mantle (EMII).

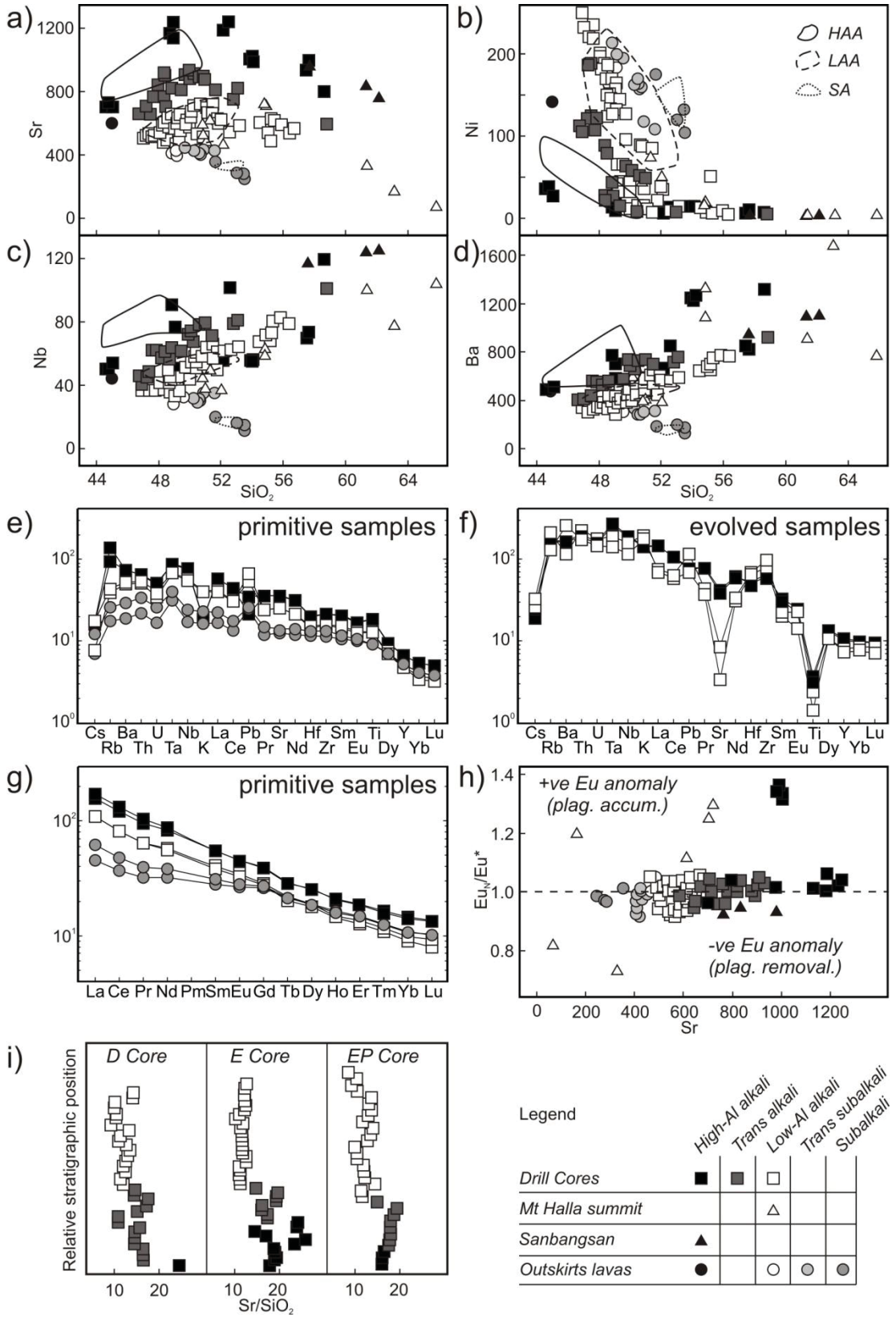

Figure 7.3: *Selected trace element variation diagrams for chemical suites identified on Jeju Island. HAA, LAA and SA fields in a), b), c) and d) are the small-volume high-Al alkali, low-Al alkali and subalkali suites, respectively, of Brenna et al. (2012; Chapter 6). Data shown in the*

extended element e), f), rare earth element g) and Eu anomaly h) diagrams are normalized to primitive mantle (Sun & McDonough, 1989; McDonough 7 Sun, 1995). For clarity in the normalized diagrams (e, g), two samples with the most primitive compositions (low SiO_2) are plotted for each suite and in f) two samples with the most evolved composition (high SiO_2) are plotted for the HAA and LAA suites. Eu is the predicted Eu concentration based on a smooth REE pattern. Note the temporal correlation of the chemical suites in the cores i).*

Table 7.2: *Sr-Nd-Pb isotope data for the Jeju large-volume lavas. F suffix indicate feldspar mineral separate.*

Sample	$^{87}Sr/^{86}Sr \pm 2\sigma$	$^{143}Nd/^{144}Nd \pm 2\sigma$	$^{206}Pb/^{204}Pb$	$^{207}Pb/^{204}Pb$	$^{208}Pb/^{204}Pb$
SA					
SK01	0.705332 ± 12	0.512727 ± 11	18.949	15.694	39.598
S400	0.705251 ± 16	0.512705 ± 15	19.039	15.706	39.681
LAA					
E01	0.704189 ± 17	0.512765 ± 13	19.033	15.639	39.624
E1F	0.704123 ± 17	0.512760 ± 16	19.035	15.639	39.626
E10	0.704414 ± 15	0.512749 ± 13	19.137	15.654	39.780
E24	0.704192 ±16	0.512781 ± 14	19.055	15.621	39.625
EP01	0.704076 ± 18	0.512783 ± 05	19.008	15.645	39.595
EP07	0.704237 ± 17	0.512772 ± 07	19.065	15.633	39.651
D10	0.704177 ± 12	0.512783 ± 14	19.069	15.634	39.662
D17	0.704244 ± 13	0.512785 ± 11	19.034	15.640	39.652
HS03	0.704175 ± 11	0.512798 ± 06	19.034	15.647	39.629
HS3F	0.704176 ± 16	0.512781 ± 09	19.023	15.628	39.567
Trn HAA					
E25	0.704398 ± 15	0.512744 ± 17	19.090	15.640	39.714
EP28	0.704559 ± 19	0.512733 ± 07	19.118	15.663	39.888
D27	0.704429 ± 14	0.512761 ± 08	19.171	15.657	39.878
D33	0.704449 ± 16	0.512746 ± 10	19.162	15.656	39.880
HAA					
E33	0.704642 ± 15	0.512709 ± 09	19.195	15.676	40.006
E36	0.704899 ± 17	0.512711 ± 12	18.817	15.641	39.237
E43	0.704917 ± 17	0.512740 ± 09	18.861	15.649	39.329
D34	0.704641 ± 14	0.512725 ± 08	19.184	15.666	39.995
EP32	0.704147 ± 15	0.512803 ± 07	19.084	15.634	39.591
SB01	0.705011 ± 13	0.512740 ± 09	18.891	15.643	39.354
YM00	0.704256 ± 18	0.512803 ± 08	19.039	15.631	39.612
Standards					
BCR2	0.704974 ± 14		18.764	15.623	38.740
BCR2	0.705013 ± 14				
JNd-1		0.512108 ± 8			

SA, subalkali; LAA, low-Al alkali; Trn HAA, transitional alkali; HAA, high-Al alkali

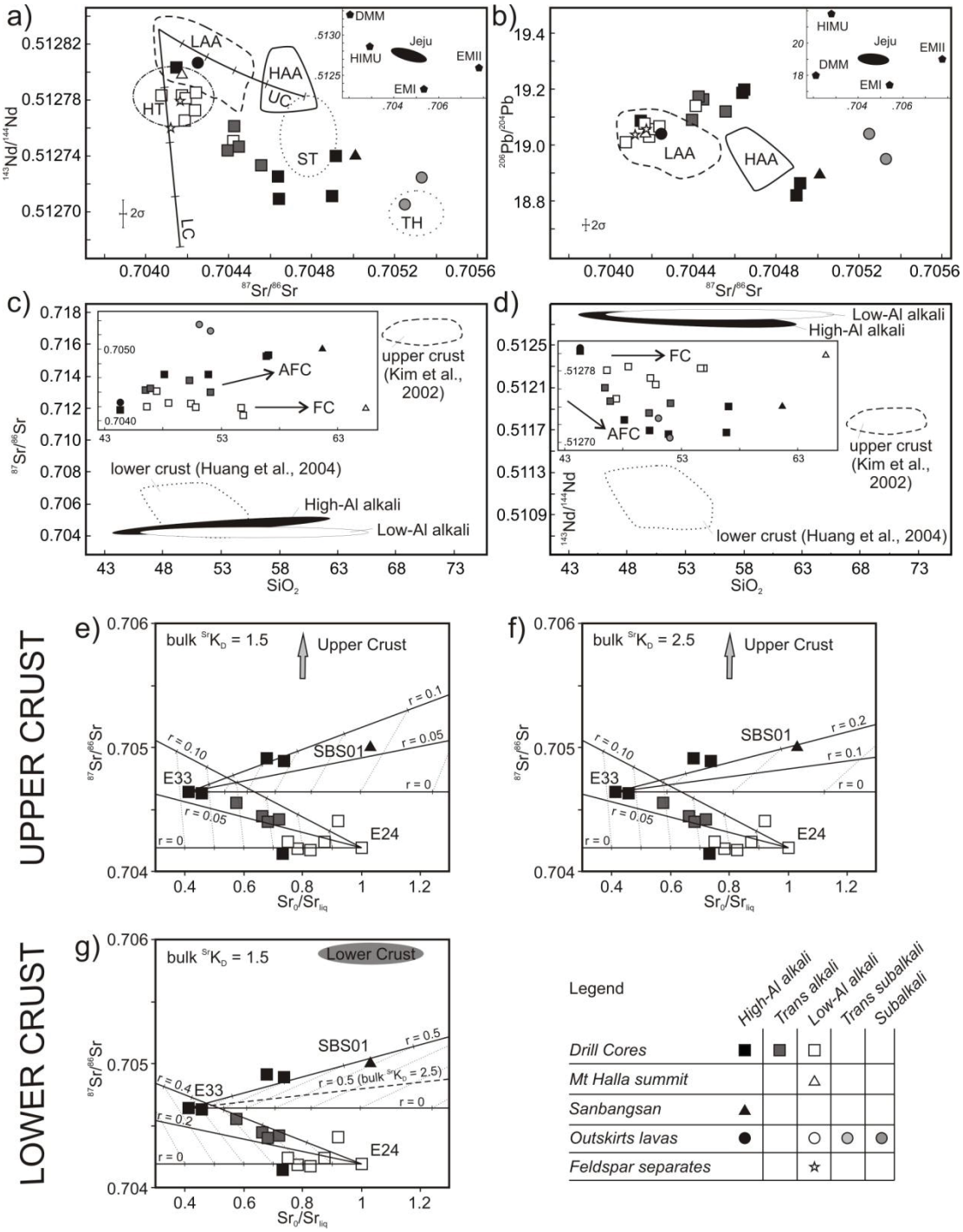

Figure 7.4: *a) and b) Sr, Nd and Pb isotopic characteristics of Jeju rocks. HT: Hallasan Trachyte, ST: Sanbangsan trachyte and TH: Tholeiite fields after Chang et al. (2006). Small-volume LAA: Low-Al alkali and HAA: High-Al alkali fields after Brenna et al. (2012; Chapter 6). Mantle domain end members in the insets are from Hart et al. (1992). Note the overlap between Hallasan Trachyte and low-Al alkali samples, and similarity between Sanbangsan Trachyte and high-Al alkali samples. Note the shift towards lower $^{143}Nd/^{144}Nd$ of the large-volume samples compared to the small-volume samples Jeju (Brenna et al., 2012; Chapter 6). The lines are assimilation fractional crystallization (AFC)*

models (DePaolo, 1981) for lower crust (LC; Huang et al., 2004) and upper crust (UC; Kim et al., 2002) contamination with 10% fraction melt remaining marks. The ratio of assimilation over fractionation volume is taken as 0.1 for both models and $^{Sr}K_D$ and $^{Nd}K_D$ are taken as 0, apart for the UC model with $^{Sr}K_D$ = 1. c) and d) Variation of Sr and Nd isotope with SiO_2 concentration. Note that the low-Al alkali samples have constant Sr and Nd ratios, whereas the high-Al alkali samples have increasing Sr and decreasing Nd isotope ratio. Upper and lower crust fields after Kim et al. (2002) and Huang et al. (2004) respectively. e) and f) Accumulation Fractional Crystallization (AFC) model (Albarède, 1995; DePaolo, 1981) for the high-Al alkali suite. r is the ratio of assimilation and crystallization volumes. Dotted lines represent 10% fractions of removed volume. Data for upper crust are from Kim et al. (2002) and for lower crust from Huang et al. (2004).

Low-Al alkali samples show the lowest $^{87}Sr/^{86}Sr$ and highest $^{143}Nd/^{144}Nd$ ratios, similar to the Hallasan trachyte group (Fig. 7.4a; Chang *et al.*, 2006). Subalkali samples have the highest $^{87}Sr/^{86}Sr$ and the lowest $^{143}Nd/^{144}Nd$. High-Al alkali and transitional alkali lavas plot in an intermediate position, similar to the Sanbangsan trachyte group (Chang *et al.*, 2006). Two relatively primitive high-Al alkali samples have isotopic characteristics similar to low-Al alkali samples (Fig. 7.4a). $^{143}Nd/^{144}Nd$ is shifted towards lower values compared to the samples from small-volume centres of Jeju (Brenna *et al.*, 2012; Chapter 6). Samples from both the small-volume eruptions sampled by Brenna *et al.* (2012; Chapter 6) and those described here were re-analysed, confirming that these differences are greater than those expected from analytical uncertainty.

Both $^{87}Sr/^{86}Sr$ and $^{143}Nd/^{144}Nd$ are constant with increasing SiO_2 concentrations in the low-Al alkali magma suite, whereas the former increases and the latter decreases with increasing SiO_2 content in the high-Al alkali suite (Figs. 7.4c, d). The subalkali samples overlap with the tholeiitic field defined by Chang *et al.* (2006; Fig. 7.4a), and are therefore different from the subalkali samples from the Udo lava shield, which are more akin to the high-Al alkali samples (Brenna *et al.*, 2012; Chapter 6). Feldspar crystal separates from two samples from the low-Al alkali suite have isotope ratios indistinguishable from those of their host whole rock sample (Figs. 7.4a, b).

7.6 Petrography

Lava flows in the cores cover a spectrum of compositions from alkali basalt/basanite to trachyte. At the more primitive end of the spectrum (basalt to trachybasalt), lavas generally consist of phenocrysts of clinopyroxene and olivine in modal abundances <15%, set in a groundmass of plagioclase + olivine + clinopyroxene microlites, with or without dispersed titanomagnetite. More evolved rocks (basaltic trachyandesite) contain plagioclase as a phenocryst phase and alkali feldspar microlites in the groundmass. Trachytes of the Sanbangsan group have plagioclase as a phenocryst phase (<10%) set in a groundmass of alkali feldspar and titanomagnetite with minor plagioclase and trace clinopyroxene. In contrat, the Hallasan trachyte is dominated by phenocrysts of alkali feldspar (10-15%) set in a groundmass of microcrystalline alkali feldspar + clinopyroxene + titanomagnetite. Anhedral amphibole fragments and trace olivine also occur in the Hallasan trachyte. Feldspar phenocrysts are generally uniform or normally zoned. Subalkali basalt and basaltic andesite lava flows at the island margins mainly consist of olivine ± clinopyroxene phenocrysts in an intersertal plagioclase + clinopyroxene groundmass with dispersed trace titanomagnetite.

Table 7.3: *Representative electron microprobe analyses of mineral phases in Jeju rocks. Totals are original totals from microprobe analysis.*

Sample	E01 2863	E01 2871	SBS02 2822	HS11 2766	HS11 2792
Rock	BTA	BTA	T	T	T
Mineral	Plag	Plag	Plag	Kspar	Kspar
Type	Pheno	Gdm	Pheno	Pheno	Gdm
SiO_2	53.96	53.55	55.73	64.47	64.90
TiO_2	-	0.10	-	0.54	0.06
Al_2O_3	27.79	27.64	26.82	19.16	18.22
FeO_{tot}	0.37	0.77	0.59	0.05	0.61
MnO	0.04	-	0.13	0.06	0.04
MgO	-	-	-	-	-
CaO	11.05	11.22	9.68	0.79	0.58
Na_2O	4.81	4.78	5.53	5.77	6.06
K_2O	0.47	0.48	0.58	7.57	7.26
P_2O_5	-	-	-	-	0.14
Total	98.56	98.22	99.00	98.17	97.93
An	54.4	54.9	47.5	3.9	2.9
Ab	42.8	42.3	49.1	51.6	54.3
Or	2.8	2.8	3.4	44.5	42.8

Table 7.3: *cont.*

Sample	E01 2874	E01 2852	SBS02 2845	HS11 2757	SBS02 2838	HS11 2805
Rock	BTA	BTA	T	T	T	T
Mineral	Ol	Cpx	Cpx	Amph	Tmg	Tmg
Type	MPh	Pheno	Gdm	Frag	Gdm	Gdm
SiO_2	36.60	48.62	50.41	40.00	0.22	0.20
TiO_2	0.01	1.64	0.47	6.00	15.48	15.72
Al_2O_3	-	5.52	0.36	13.14	2.07	0.97
FeO_{tot}	37.29	9.27	20.32	13.00	76.67	75.22
MnO	0.63	-	2.77	0.31	2.23	0.87
MgO	27.30	13.62	7.58	12.42	0.59	0.45
CaO	0.25	19.42	17.50	10.77	0.05	0.05
Na_2O	-	0.71	0.56	2.45	-	-
K_2O	-	0.17	0.08	0.85	-	-
P_2O_5	-	0.06	0.22	0.02	-	0.07
Total	101.89	99.30	100.58	99.25	96.82	93.14
Fo	42.3					
En		41.5	24.0			
Fs		15.9	36.1			
Wo		42.6	39.9			

-: not detected
Rock: BTA, basaltic trachyandesite; T, trachyte
Mineral: Plag, plagioclase; Kspar, potassic feldspar; Ol, olivine; Cpx, clinopyroxene; Amph, amphibole; Tmg, titanomagnetite
Type: Pheno, phenocryst; Gdm, groundmass; MPh, microphenocryst; Frag, fragment (xenocryst)

Through the cores, there is no single chemical evolutionary trend with depth, other than the transition from high-Al alkali to transitional alkali to low-Al alkali (Fig. 7.3i). However, the dominant phenocryst assemblages visible in hand specimens vary systematically from olivine and pyroxene-dominated at the base to plagioclase-rich toward the top (Electronic Appendix K). Representative compositions of phenocryst and groundmass minerals used in geochemical modeling are presented in Table 7.3.

7.7 Significance of chemical variability

The discussion on small-volume magmatism on Jeju presented by Brenna *et al.* (2012; Chapter 6) was based on selected monogenetic eruptions. Due to their nature, these are representative of the primitive magma types involved and therefore constrain properties of the mantle source. They nevertheless represented individual points in the evolutionary continuum of Jeju. The new data, including a more complete temporal and chemical spectrum, add to the Brenna *et al.* (2012; Chapter 6)

study by providing new insights into higher-level (including crustal) storage and magma processing.

7.7.1 Chemical classification

The spread of major and trace element compositions defines three evolutionary suites (Figs. 7.2, 7.3). These are well correlated with the high-Al alkali, low-Al alkali and subalkali suites of Tatsumi *et al.* (2005) and Brenna *et al.* (2012; Chapter 6). Each magma type is interpreted to have had a chemically distinct parental melt derived from peridotite with residual garnet [Brenna *et al.*, 2010 (Chapter 4), Brenna *et al.*, 2012 (Chapter 6), Tatsumi *et al.*, 2005]. In addition to these end-member suites, a transitional alkali suite and a transitional subalkali suite were also erupted (Figs. 7.2, 7.3).

These suites are correlated with relative age in the cores, with an eruption sequence of high-Al alkali units and transitional alkali lavas before the low-Al alkali suite. Subalkali and transitional to subalkali samples occur only on the outer flanks of Jeju Island. The suites identified generally exhibit sub-parallel chemical trends, broadly similar to those discussed by Brenna *et al.* (2010; Chapter 4, 2012; Chapter 6; Figs. 7.2, 3). The chemical similarity between primitive small- and large-volume magmas and the continuous chemical spectrum from basalt to trachyte, as well as the isotopic similarity of whole-rock and crystal separates (Figs. 7.4a, b) indicates that the trachytes evolved from a parent alkali basalt. The homogeneous, volume-independent line of descent within each suite suggests similar fractionation conditions for small- and large-volume eruptions at the primitive end of the chemical spectrum. The large volume lavas however evolved to trachyte and crystal assemblages causing chemical variation from intermediate to evolved compositions are investigated in section 5.3.

On Jeju, the presence of a spectrum of compositions from alkali basalt to trachyte indicates that magma underwent evolution in the plumbing system. The long period required to generate a trachyte from a primitive basalt (Hawkesworth *et al.*, 2000), implies that the system may have interacted with, and assimilated its surrounding host rocks. This possibility is investigated first.

7.7.2 Crustal assimilation

In the low-Al alkali magma, constant $^{87}Sr/^{86}Sr$ and $^{143}Nd/^{144}Nd$ occur, independently of the degree of evolution (SiO_2; Figs. 7.4c, d). This, along with plagioclase separates showing isotope ratios indistinguishable from whole-rock values and therefore revealing their magmatic origin, implies that there has not been significant crustal assimilation for the magmas of this suite.

In the high-Al alkali suite, however, increasing $^{87}Sr/^{86}Sr$ and decreasing $^{143}Nd/^{144}Nd$ occurs with increasing SiO_2 content (Figs. 7.4c, d), suggesting the possibility of crustal assimilation. We simulated this process by an Assimilation Fractional Crystallization (AFC) model (Albarède, 1995; DePaolo, 1981), based on Sr concentration and Sr isotope composition (Figs. 7.4a, e, f, g). Sample E24 was chosen as the most primitive and least contaminated sample, because it has the lowest Sr concentration coupled with low $^{87}Sr/^{86}Sr$. Given that Sr abundance shows an inflection at an SiO_2 concentration around 50 wt%, the model has to be calculated in two steps. Brenna *et al.* (2012; Chapter 6) modeled the chemical variation in the high-Al alkali magma up to c. 50 wt% SiO_2 as due to dominantly olivine (± Cr spinel) removal. Given the similar chemical evolutionary paths of small- and large-volume magmas, we assume $^{Sr}K_D = 0$ for the first step of fractionation (McKenzie & O'Nions, 1991). In the second step of fractionation, decreasing Sr abundance indicates a bulk $^{Sr}K_D > 1$. We therefore modeled the AFC process using bulk $^{Sr}K_D = 1.5$ and 2.5, and evaluate the results based on major and trace element evidence.

Figures 7.4e, f and g show the results of the two-step models. In the first step, from primitive (E24) to intermediate (E33) compositions, the models requires assimilation of approximately 30% volume lower crust or <10% volume upper crust, and between 45% (lower crust) and 55% (upper crust) crystal volume removal (fractionation). Increasing the model bulk $^{Sr}K_D$ to >0 but <1 would reduce the amount of assimilation required to reproduce the $^{87}Sr/^{86}Sr$ variation, but would increase the volume of crystal fractionated to 70-80%, which we consider unlikely. Incompatible trace element (Th, Zr, Nb, Hf, Ta, La, Ce) enrichment factors from the most primitive samples to the

intermediate samples are highly variable from 1.4 to 1.8, indicating c. 30-45% crystal volume removal. The large degree of variability does not therefore exclude either contaminant.

The $^{87}Sr/^{86}Sr$ variability in the second step, from intermediate (E33) to evolved (SBS01) samples is modeled with different bulk $^{Sr}K_D$ to reflect uncertain degrees of plagioclase removal. Assuming a relatively low contribution of plagioclase to fractionation (i.e. bulk $^{Sr}K_D$ = 1.5; Figs. 7.4e, g) the model would require approximately 50% volume lower crust, or <10% volume upper crust assimilation and 40% (lower crust) or 60% (upper crust) crystal volume removal (fractionation). If plagioclase was a larger contributor to fractionation (i.e. bulk $^{Sr}K_D$ = 2.5; Fig. 7.4f), the model would require unreasonable high (>100%) lower crustal (not shown), or approximately 20% upper crustal assimilation accompanied by 20-25% crystal volume fractionation. Based on these results we consider that lower crustal material is unlikely to have affected the high-Al alkali magma in the second step of evolution from intermediate to evolved compositions.

Comparison of the isotopic composition of the large-volume samples with data available for the small volume eruptives (Brenna *et al.*, 2012; Chapter 6) indicates that the latter are shifted towards lower $^{143}Nd/^{144}Nd$ at comparable $^{87}Sr/^{86}Sr$ (Fig. 7.4a) suggesting that a slightly different process affected the large-volume magmas compared to their small-volume counterparts. The difference may be due to small- and large-volume magmas originating from different domains within a heterogeneous mantle source. We consider this unlikely due to the systematic lowering of $^{143}Nd/^{144}Nd$ from small- to large-volume datasets and consistency between older and younger magmas.

An alternative explanation for the preferential lowering of the $^{143}Nd/^{144}Nd$ ratio of large-volume magmas is that these assimilated previously underplated mafic material in the subcontinental lithosphere (Hart, 1988). Proterozoic granulite and amphibolite complexes form part of the lower crust in the Korean peninsula (Lee & Cho, 2003). The basement of Jeju Island is considered to be a continuation of the Okcheon Belt in the Korean Peninsula (Kim *et al.*, 2002), which formed during the Paleozoic (Cluzel *et al.*, 1990) and is modeled to be underplated lower crust (Kim *et al.*, 2011). The

boundaries between lower to middle and middle to upper crust are at c. 22 and 8 km depth respectively, and the base of the crust is at c. 33 km depth (Kim *et al.*, 2011). Comparative isotope data for the underplated crust are not available, however, lower crustal granulite in the Sino-Korean Craton has $^{143}Nd/^{144}Nd$ c. 0.5108 to 0.5114, much lower than Jeju basalts, but with comparable $^{87}Sr/^{86}Sr$ ($^{87}Sr/^{86}Sr$ 0.7040-0.7071; Huang *et al.*, 2004; Figs. 7.4c, d). Interaction with such material would result in a preferential shift towards lower $^{143}Nd/^{144}Nd$, as seen in the large-volume Jeju rocks. The influence of upper crustal and lower crustal contaminants on the $^{87}Sr/^{86}Sr$ and $^{143}Nd/^{144}Nd$ ratios is illustrated with the AFC (DePaolo, 1981) model lines in Figure 7.4a. In this model, lower crustal granulite preferentially lowers $^{143}Nd/^{144}Nd$ compared to contamination/assimilation of upper crustal material, which lowers $^{143}Nd/^{144}Nd$ but increases $^{87}Sr/^{86}Sr$.

The isotope data and models suggest that large-volume magma of the high-Al alkali basalt suite evolved to trachyte in the upper crust after some residence at the base of the crust, whereas large-volume magma of the low-Al alkali suite evolved mainly in a sub-crustal to lower crustal environment. The small-volume magmas in contrast erupted directly from the mantle and were unaffected by either lower or upper crust (Brenna *et al.*, 2012; Chapter 6). An upper crustal (<0.35 GPa ≈ 12 km) fractionation environment for the Sanbangsan trachyte, compared to a lower crustal (>0.5 GPa ≈ 18 km) one for the Hallasan trachyte was also proposed based on mineral equilibria (Chang *et al.*, 1999). This may explain the lack of continuity in the high-Al alkali suite chemical spectrum (Figs. 7.2, 7.3). Ponding and evolution at different levels and in independent storage areas (rather than in a single magma chamber) in the crust may have given rise to pockets of individual compositions.

The large-volume subalkali samples described here, forming the low-lying flanks of Jeju Island have the highest $^{87}Sr/^{86}Sr$ and lowest $^{143}Nd/^{144}Nd$ (Fig. 7.4a). They differ from the samples representing subalkali magma erupted at the Udo small-volume volcano located at the outermost eastern edge of Jeju (Fig. 7.1b), which have $^{87}Sr/^{86}Sr$ and $^{143}Nd/^{144}Nd$ similar to the high-Al alkali magma [Brenna *et al.*, 2010 (Chapter 4); Brenna *et al.*, 2012 (Chapter 6)]. However, they have similar major and trace element characteristics (Figs. 7.2, 7.3) indicating that they originated from parent melts derived from similar degrees of mantle partial melting.

The higher $^{87}Sr/^{86}Sr$ and lower $^{143}Nd/^{144}Nd$ of subalkali lavas compared to the alkali ones may suggest some upper crustal contamination/assimilation of the former during crystal fractionation (Fig. 7.4a). The primitive compositions spanning only basalt to basaltic andesite (Fig. 7.2a), however, point towards a short period of crustal residence and chemical evolution through AFC, relative to the alkali suites. The different isotope signatures of the large- and small-volume subalkali lavas also suggest evolution in independent plumbing systems rather than a single magma chamber/storage area.

7.7.3 Fractional crystallization

Brenna *et al.* (2012; Chapter 6) determined that primitive high-Al alkali magma fractionated early olivine followed by later olivine + clinopyroxene + plagioclase + Fe-Ti oxide, whereas the low-Al alkali suite fractionated mainly clinopyroxene + olivine to generate intermediate compositions. Decreasing Al_2O_3 and Sr abundances at SiO_2 > 50 wt%, Sr depletion and Eu positive and negative anomalies (Fig. 7.2, 7.3) indicate that late plagioclase fractionation also affected the latter suite. In addition, lower P_2O_5 abundances in the more evolved magmas (SiO_2 > c. 50 wt%, Fig. 7.2e) indicates that apatite fractionation occurred in both suites. Here we investigate the crystal assemblages responsible for magma evolution from intermediate to evolved compositions.

Based on petrography, the high-Al alkali magma fractionated plagioclase in addition to olivine + clinopyroxene + Fe-Ti oxides. Alkali feldspar is however absent from the phenocryst assemblage, although it forms in the groundmass. Apatite, though not observed, is likely to account for the P_2O_5 depletion. The phenocrysts assemblage responsible for differentiation in the low-Al alkali magma suite is similar, but includes alkali feldspar, which appears as a phenocryst phase. Orthopyroxene is likely to have also been involved in the differentiation process as shown by recent investigation of gabbroic xenoliths in Jeju lavas, which have this phase as part of the crystallizing assemblages in magma storage areas in the middle to lower crust related

Table 7.4: *Results of mass balance calculations. Volume percent of initial magma removed (-) or added (+) phase.*

Plag	Kspar	Ol	Cpx	Opx[a]	Tmg	Apt[b]	Amph	LC[c]	UC[d]	SSR	Tot R
High-Al alkali suite from sample E33 to sample SBS01											
-30.5			-2.9	-7.5	-6.7	-2.6				1.64	50.2
-34.1	-34.7		-7.3	-6.3	-8.2	-2.3				0.35	92.9
-29.5		-5.8	-5.3		-5.2	-2.4				2.04	48.2
-18.9			+0.5	-0.3	-4.4	-1.9	-19.9			0.50	45.4
-24.0			-7.1	-6.1	-5.5	-1.7			+23.1	0.77	44.4
-62.0			-13.3	-15.3	-12.5	-2.6		+83.4		0.21	105.7
-30.9		+8.1	-1.7	-16.1	-8.9	-2.7				1.47	60.3
Low-Al alkali suite from sample EP10 to sample HS03											
-33.4	-30.2	-7.9	-13.5		-9.4	-1.2				1.98	95.6
-35.1	-23.7		-9.0	-10.6	-11.2	-1.8				1.16	91.4
-39.2		+18.1		-32.6	-15.4	-2.9				1.08	90.1
-25.9			-0.8	-3.5	-7.9	-1.5	-23.9			0.15	63.5
-38.6			-7.0	-11.7	-10.1	-1.9			+12.4	1.52	69.3
-71.2			-13.6	-19.4	-15.8	-2.4		+72.5		0.83	122.4
-24.0	+19.6		+4.0	-1.5	-6.3	-1.6	-33.3			0.01	66.7

Plag: plagioclase; Kspar: alkali feldspar; Ol: olivine; Cpx: clinopyroxene; Tmg: titanomagnetite; Amph: amphibole; SSR: sum of the squared residuals; Tot R: total removed relative to initial magma

[a]Opx: orthopyroxene composition from Yang *et al.* (2012)

[b]Apt: apatite composition from Deer *et al.* (1992)

[c]LC: lower crust composition from Huang *et al.* (2004)

[d]UC: uppr crust composition from Kim et al (2002)

to the Quaternary volcanism (Yang *et al.*, 2012). In addition, Yang *et al.* (2012) identified kaersutite megacrysts, which they interpreted as being of magmatic origin. The results of several mass-balance calculations (Petrelli *et al.*, 2005, Stormer & Nicholls 1978) from intermediate to evolved compositions using several combinations of these mineral assemblages and all major oxides are reported in Table 7.4.

These calculations provide a semi-quantitative evaluation of the fractionation assemblages, and can be considered realistic when the sum of the squared residuals (SSR) is < 2 (Stormer & Nicholls, 1978). The results show that a variety of crystal assemblages can reproduce the observed chemical variation and no unique combination can be defined for the chemical evolution from intermediate to evolved compositions in the Jeju magmas. This is probably due to oversimplification of the model, which uses fixed mineral compositions, rather than the more likely probability of changing compositions during the fractionation process. Another source of uncertainty is the composition and magnitude of assimilated crustal material contributing to the chemical signature. With no uniform mineral assemblage accounting for the chemical evolution, it is more likely that this occurred in several separate intrusions/dykes rather than in a homogeneous storage area (magma chamber), i.e. a multistage process under different conditions at different levels in the crust. As mentioned above, this may also explain the clustered chemical variation in the high-Al alkali suite.

The variability from intermediate to evolved samples in the high-Al alkali suite appears to result from c. 45-50 % volume crystal removal, with plagioclase contributing c. 1/3 to 1/2 of it (Table 7.4). Assuming plagioclase $^{Sr}K_D = 2$ (McKenzie & O'Nions, 1991), this supports the AFC model with bulk $^{Sr}K_D = 1.5$ (Fig. 7.4e). The incompatible trace element (Th, Zr, Nb, Hf, Ta, La, Ce) enrichment factors from intermediate to evolved samples in the high-Al alkali suite vary from c. 1.4 to 2, suggesting removal of 30-50 volume % of crystals, consistent with the other major element and isotope models.

7.7.4 Source

The two additional transitional suites (transitional alkali and transitional subalkali) appearing in the large-volume eruption record show that not only is there a spectrum in evolution from basalt to trachyte, but there is also one from high-Al alkali to subalkali magmas. The relative position of each distinct suite within the cores (Fig. 7.3i), as well as the sub-parallel evolutionary (SiO_2 enrichment) trends between suites (Fig. 7.2, 7.3) mean that there was no mixing between suites. The spectrum from basalt to trachyte is mainly generated by initial olivine ± clinopyroxene dominated (Brenna *et al.*, 2012; Chapter 6) and later clinopyroxene + plagioclase ± olivine ± orthopyroxene ± alkali feldspar + Fe-Ti oxide + apatite crystal fractionation processes leading to silica enrichment. The change from high-Al alkali to subalkali is controlled by the parent melt composition, which reflects the P-T conditions and degree of melting (Brenna *et al.*, 2012; Chapter 6). High-Al alkali magma was generated in the Early Pleistocene at c. 2.5 GPa, followed by low-Al alkali and subalkali magmas in the Late Pleistocene generated at c. 3.5 and 2.5 GPa respectively (Brenna *et al.*, 2012; Chapter 6).

The spectrum in parent melt compositions suggests that rather than having distinct magma sources at different levels in the mantle, the Jeju magmas were generated sequentially from a continuous (vertical as well as lateral) section of mantle. In the central part of the island, transitional lavas appear (temporally) only between the high-Al and low-Al alkali suites (Fig. 7.3i). Therefore, this represents a distinctive stage in a progressive evolution, from a source that initially produced high-Al alkali magmas before gradually trending to production of low-Al alkali end members. This transition is a result of the deepening of the source zone from c. 2.5 GPa to c. 3.5 GPa and a slight increase in the degree of partial melting (Brenna *et al.*, 2012; Chapter 6). The appearance of subalkali lavas in the Late Pleistocene, concomitantly with the low-Al alkali magmas indicates that the shallower portion of mantle source had subsequently started to form larger melt volumes by relatively larger degrees of partial melting. The transitional subalkali suite at this stage represents those melts generated in the mantle between (vertically) the deeper low-Al alkali and shallower subalkali magmas. The temporal relationship of the various suites is further investigated below.

7.8 Existing age database

Age determinations on volcanic rocks on Jeju were carried out by the $^{40}Ar/^{39}Ar$ or the K/Ar methods (KIGAM, 1995; Kim *et al.*, 2002; Koh & Park, 2010a, b; Koh *et al.*, 2008; Tamanyu, 1990; Won *et al.*, 1986). We assembled a catalogue of 269 dates from these studies (reported as Electronic Appendix M) and subdivided it into three groups based on chemical composition and degree of chemical evolution: i) alkali basalt + trachybasalt + basaltic trachyandesite, ii) trachyandesite + trachyte, and iii) tholeiitic (subalkali) + transitional (subalkali) basalts + basaltic andesite. Dated

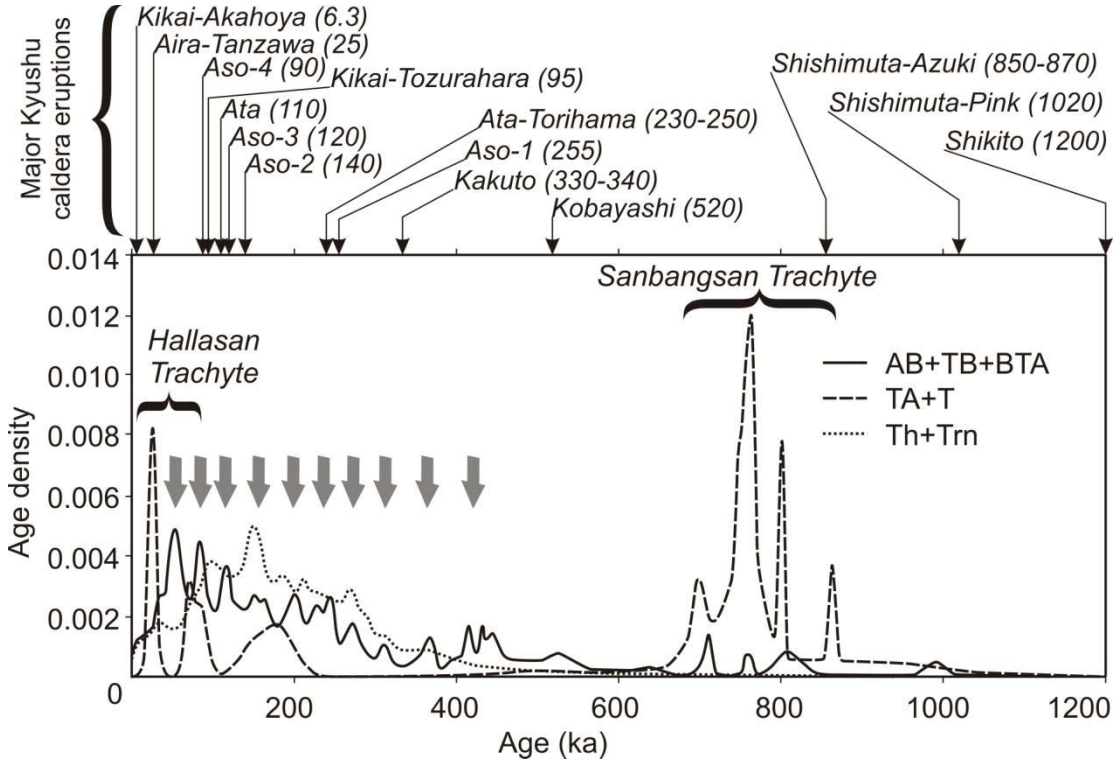

Figure 7.5: *Age density plot of published Jeju Island rock dates. Data from KIGAM (1995), Kim et al. (2002), Koh & Park (2010a, b), Koh et al. (2008), Tamanyu (1990) and Won et al. (1986). AB: alkali basalt, TB: trachybasalt, BTA: basaltic trachyandesite, TA: trachyandesite, T: trachyte, Th: tholeiitic (subalkali) basalt and basaltic andesite, Trn: Transitional basalt, after classification in the source articles. Note that the height of the peaks is not representative of eruptive volumes. The ages (ka in brackets) of caldera volcanism in Kyushu are from the catalogues of Machida (2002) and Mahony et al. (2011). Grey arrows are indicative of the primitive alkali (AB+TB+BTA) age density secondary spikes.*

samples are mainly from lava flows in the lower reaches of the island and from the trachyte suites. The data do not include ages of small-volume monogenetic centres, and do not represent uniform sampling in terms of space and time; the early c. 1 Ma of activity of the field is underrepresented. Also, these data cannot be used to determine eruption frequency distribution, as they are strongly dependent on the number of lava flows dated, several of which may be related to the same eruptive event, and hence not necessarily representative of the frequency of eruptions. They are, however, representative of the chemical variability in the erupted lavas over time.

The age density (Fig. 7.5) shows two main pulses of alkali eruptive activity, each culminating in trachytic episodes (i.e. the Sanbangsan and Hallasan trachytes). Subalkali (tholeiitic) to transitional activity is associated with the second alkali pulse (Fig. 7.5). Minor secondary pulses are also visible in the more primitive end of the alkali magmatism (AB+TB+BTA in Fig. 7.5). Ten such spikes occur in the last c. 450 ka (grey arrows in Fig. 7.5), with the last at about 50 ka.

7.9 Magma volumes

Dispersed monogenetic centres with primitive compositions on Jeju Island were generated by very small-volume eruptions and represent magma batches of mostly <0.01 km^3 (Hasenaka *et al.*, 1997). This includes both recent eruptives, plus the presumed eruptive centres that generated the phreatomagmatic and related sedimentary deposits of the Seoguipo Formation during the Early Pleistocene (Sohn & Park, 2004; Sohn *et al.*, 2008; Sohn & Yoon, 2010). This Formation is generally between 50 m below and 50 m above sea level in the centre of the island and deepens to the level of the seafloor on the eastern and western sides (Won *et al.*, 2006).

The subaerial volume of Jeju Island determined from an ASTER digital elevation model is approximately 500 km^3. This is a minimum estimate of the total output given that Jeju rises from depths of c. 100 m on the continental shelf. Extrapolation of the surface area to the seafloor would add c. 200 km^3 to the volume. Considering the overall porosity of the island, we estimate the total dense rock-equivalent (DRE) magma output to have been between 350 and 500 km^3. There are c. 300 scoria and

phreatomagmatic cones on the surface of Jeju, and at least another 100 are intercalated with lavas, as well as forming the basal Seoguipo Formation (Park *et al.*, 2006). Despite their number, the small-volume dispersed volcanism with primitive basaltic composition represents only a minor (<5%) volumetric contribution to the island. Some of the dispersed eruptive vents are associated with lava flows that are 1 to 2 orders of magnitude larger than the cones (Park *et al.*, 2000). Using an age distribution plot, it canbe argued that alkali lavas evolving to trachybasalt and basaltic trachyandesite built the central edifice in possibly as few as ten large-volume eruption episodes during the last 450 ka (Fig. 7.5). Therefore, each of these episodes was associated with erupted volumes >10 km^3.

Trachytic lava forms domes and extensive, thick flows in the southwestern and central parts of Jeju Island. The southwestern trachytes are generally associated with the Middle Pleistocene Sanbangsan trachyte suite, whereas those in the centre of the island are associated with the Late Pleistocene Hallasan trachyte suite (Chang *et al.*, 2006). Due to poor exposure and burial by subsequent lava flows it is difficult to determine the total erupted volume in each episode, but the known thickness and lateral extent of trachytic lavas (as also seen in drill cores) indicate that each trachytic episode was associated with a >1 km^3 lava extrusion.

Subalkali and transitional lava flows form a large part of the eastern and western outer flanks of Jeju Island and were erupted mainly within the last 300 ka (Koh *et al.*, 2008). With a total erupted volume of 10-100 km^3, each eruptive episode is likely to have involved magma batches of >1 km^3.

7.10 Time-composition-volume evolution

The most significant aspect of the Jeju magmatic system is the similarity in magma generation and subsequent evolutionary paths shown by both the small-volume centres (Brenna *et al.*, 2012; Chapter 6) and the large-volume centres described here. This is valid for both high-Al and low-Al alkali magma suites. Small-volume events were fed by relatively primitive alkali basalt magma. The bulk volume of Jeju Island was, however, built by larger individual lava eruptions of more evolved compositions,

although minor primitive alkali basalts were also erupted during these events. Subalkali lavas erupted later, at the edges of the system, and they also occur as larger volume flows, which are generally relatively primitive, spanning only subalkali basalt to basaltic andesite compositions.

It is evident from the age density plot (Fig. 7.5) that the magma output and hence the production rate changed from the initiation of the system c. 1.8 Ma to the latest c. 400 ka activity on Jeju. From extensive drill core survey data, the products of over 100 monogenetic events are hidden in the subsurface of Jeju and form part of the Seoguipo Formation (Park *et al.*, 2006). These, in addition to some trachyte domes and lavas of the Sanbangsan suite, form the initial, high-Al alkali magmatic phase. Assuming an average volume of 0.01 km^3 for each magma batch feeding single small-volume, monogenetic eruptions (Allen & Smith, 1994; Hasenaka *et al.*, 1997; Kereszturi & Németh, 2012), and c. 10 km^3 for the Sanbangsan trachyte suite, gives a total of c. 11 km^3 of magma erupted over c. 1.4 Ma. This corresponds to an average eruption rate of c. 8 km^3 Ma^{-1}. The c. 500 km^3 of the emergent island is mainly composed of the low-Al alkali and subalkali magmas, which were erupted over the last 400 ka, resulting in a substantially higher average eruption rate of c. 1250 km^3 Ma^{-1}.

Eruption rate of small-volume volcanoes in intraplate settings has been linked to tectonic strain accommodation (Valentine & Perry, 2007); to apply this to Jeju may imply that the tectonic strain rate increased suddenly from c. 450 ka, when the largest volume eruptions began. The extension rate of the Okinawa Backarc Basin (Trough), which is situated c. 240 km southeast of Jeju, increased from c. 4 km Ma^{-1} in the Early Pleistocene to c. 10 km Ma^{-1} in the Late Pleistocene to Holocene (Sibuet *et al.* 1995). Increased caldera eruptive activity in the Ryukyu Arc during the same time (Machida, 2002; Mahony *et al.*, 2011; Fig. 7.5) indicates that an increased extensional period also occurred there, and potentially generated a greater requirement for strain accommodation at Jeju. This is coupled with an increasing magma production rate due to continued mantle uplift and decompression (Brenna *et al.*, 2012; Chapter 6), also potentially linked to the changing regional tectonics in the Late Pleistocene.

Trachyte erupted both before and after the change in tectonic stress in the Late Pleistocene (Fig. 7.5). These evolved magmas are derived from chemical evolution of primitive alkali basalts on Jeju. Therefore, throughout the evolution of Jeju, more magma was fed from the source region into the plumbing system than what was strictly necessary to accommodate tectonic strain and release tectonic stress. The relatively primitive (small volume) volcanism is an indication of the continuing accommodation of low rates of deformation. The greater volume of the Hallasan trachyte compared to the Sanbangsan trachyte is a reflection of the larger magma generation rates after the Late Pleistocene tectonic reorganization.

Given the c. 300 ka duration and relatively primitive composition of subalkali magmatism, it is unlikely that this magma type evolved in a single magma chamber. Moreover, subalkali magma was erupted at the two extremities of the field; a magma chamber feeding such eruptions should have the spatial extent of the field at the surface, and be interrupted in the centre. We consider this unfeasible. It is more likely that individual magma batches ascended and evolved independently.

The subalkali flank lavas (Koh *et al.,* 2008) are individually more voluminous than the batch forming the Udo lava shield at the eastern edge of Jeju (Brenna *et al.,* 2010; Chapter 4). Smaller magma volumes are generated at the edges and larger magma amonuts are available in the core of the source zone, independenlty of the degree of melting. This suggests that magma availability in the source decreases with distance from its centre to a point where individual magma pockets are too small and dispersed to create interconnectivity and assemble a magma volume larger than the minimum threshold to initiate magma ascent. This region of the mantle is mirrored at the surface by absence of eruptions, i.e. the edge of the volcanic field.

7.11 Model of magmatic system evolution

Mantle plume activity is generally invoked as the driver of intraplate volcanic activity, and was proposed for the Jeju system by Tatsumi *et al.* (2005). At Jeju, however, activity has been spatially located within a confined, approximately elliptical area from the onset of activity in the Early Pleistocene. The absence of a plume path

forming a volcanic chain, and the presence of the subducted Pacific Plate at c. 440 km depth forming a mechanical boundary between lower and upper mantle (Lei & Zhao, 2005), count against the existence of a plume beneath Jeju.

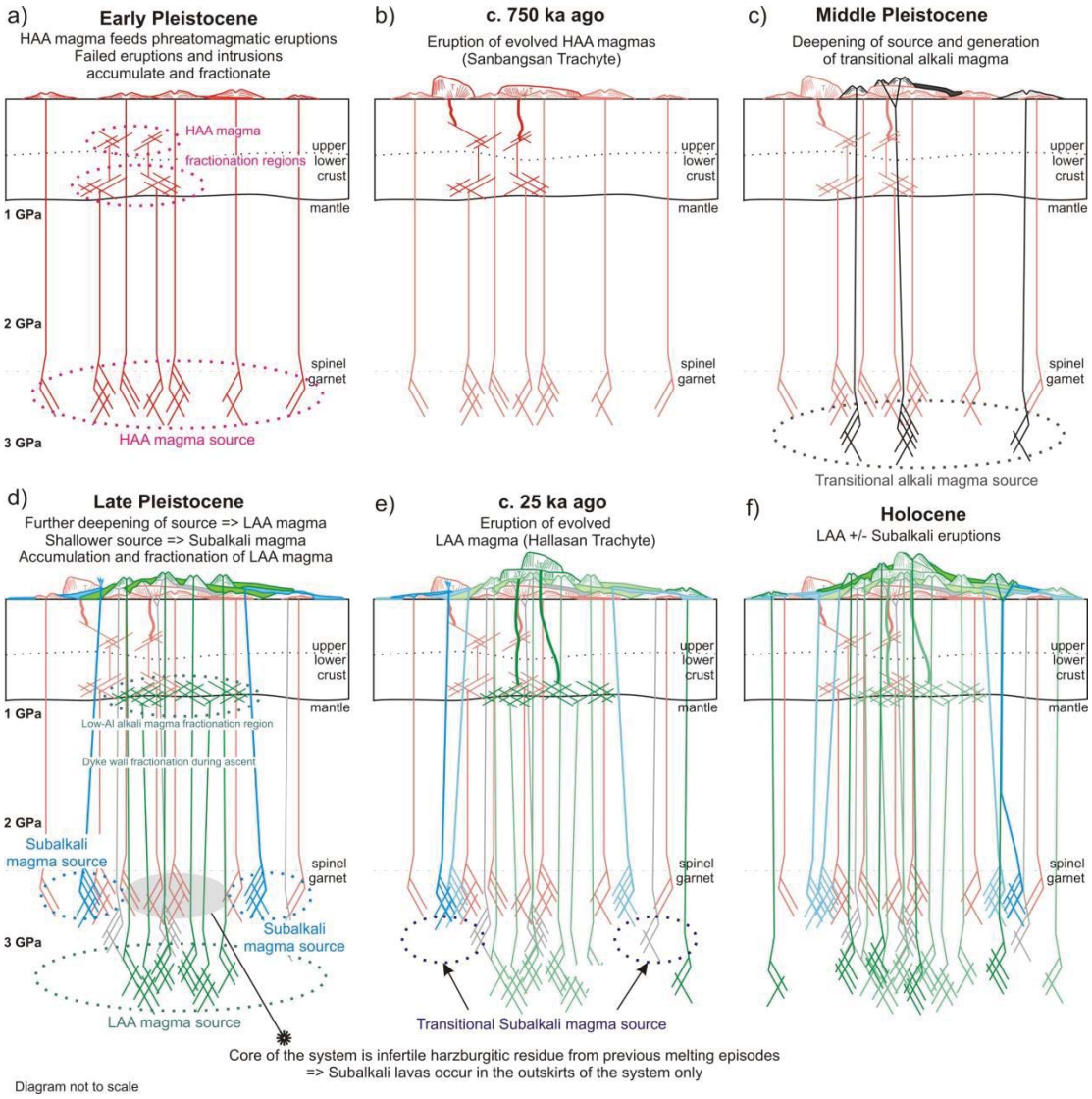

Figure 7.6: *Conceptual model for the spatio-temporal evolution of Jeju Island. Note that the system did not evolve to produce a central, focused conduit, but rather remained dispersed throughout the activity. The construction of a central edifice was due to the accumulation and superposition of sequential monogenetic eruptions from the central most-productive region of the source. HAA is high-Al alkali and LAA is low-Al alkali.*

Alternative models have been proposed for igneous activity in intraplate settings. These include subduction triggered magmatic pulses (Faccenna *et al.*, 2010) and mantle wedge convection (Lei & Zhao, 2005), as well as plate tectonic driven

upwelling (Anderson, 2001; Zou *et al.*, 2008) focused by peridotite shear zones to facilitate decompression melting (Brenna *et al.*, 2012; Chapter 6). Given the features of the Jeju magmatic system, we prefer a non-plume related mechanism, and our proposed evolutionary model is presented in Figure 7.6.

The Jeju volcanic system initiated at c. 1.8 Ma, after a tectonic reorganization of the Philippine Sea Plate, which lead to enhanced extension of the Okinawa Trough (Kamata & Kodama, 1999, Kodama *et al.*, 1995). The system continued for around 1.4 Ma with very low degrees of partial melting at low melting rates, generating small-volume, dispersed, high-Al alkali magma batches (Fig. 7.6a). These were erupted sporadically as dispersed monogenetic events, accommodating tectonic strain (c.f. the "tectoniccally controlled" model of Valentine & Perry, 2007). If not enough tectonic strain built up to be accommodated by magmatic injections, magma accumulated and evolved to trachyte in sub-crustal and crustal reservoirs/dyke complexes. This trachyte magma erupted in a series of separated event c. 750 ka to form the Sanbangsan suite (Fig. 7.6b), which consists of dispersed domes and short lava flows.

At c. 450 ka ago, due to a change in the regional tectonic regime (Sibuet *et al.*, 1995) melting extended to greater depth (Fig. 7.6c). The degree of melting increased slightly in the lower parts of the source to form low-Al alkali magma, and also increased considerably in the shallower parts of the system to form subalkali magma (Fig. 7.6d). The absence of subalkali lavas in the centre of the island can be ascribed to the refractory harzburgitic nature of the mantle source after partial melting in the first phase of activity in the Early to Middle Pleistocene (Fig. 7.6d). Dispersed monogenetic activity continued, but larger volume lava outpourings became more prevalent. Eruption recurrence therefore became increasingly a response to magma pressure buildup (c.f. the "magmatically controlled" model of Valentine & Perry, 2007). The presence of both primitive and evolved lava flows, however, points to some tectonic control, occasionally hindering magma ascent and promoting evolution through fractional crystallization in a sub-crustal environment. The relatively primitive character of the subalkali lavas indicates that these spent only short periods in the plumbing system. The uppermost part of the island consists of the Hallasan trachyte erupted c. 25 ka ago (Fig. 7.6e), which is exposed at few localities (Park *et*

al., 2000). More primitive, individual basaltic eruptions have subsequently covered the trachyte domes and flows (Koh *et al.*, 2003) and smoothed the surface of the volcanic edifice (Fig. 7.6f).

Due to the relatively direct ascent from mantle depths of the small-volume monogenetic magmas, the lateral extent and distribution of these eruptive centres is likely to be an indication of their individual magma footprints (Valentine & Perry, 2006), that is, the spatial extent of the source zone in the mantle. The large volume accumulation of eruptive products in the core of the system in central Jeju reflects the locus of greatest magma productivity in the source. However, these were not erupted from a central conduit, i.e. the summit of Mt. Halla, but from dispersed vents, similar to all other eruptions in the field. Therefore, rather than being a classical strato-type polygenetic volcano, Jeju Island is a construct of accumulated dispersed or monogenetic eruptions, each fed by independent magma batches. We conclude that no central plumbing system has formed under Jeju Island.

7.11.1 Significance for other volcanic areas

Intraplate volcanic fields mostly erupt relatively primitive basaltic magmas at dispersed vents (e.g. Blondes *et al.*, 2008; Jung & Masberg, 1998; Zhang *et al.*, 1995). Some fields also produce more evolved compositions, such as trachyte and phonolite (e.g. Camp & Roobol, 1989; Lynch *et al.*, 1993; Wörner *et al.*, 1985), others may even produce composite edifices erupting evolved compositions (e.g. Ablay *et al.*, 1998; Wei *et al.*, 2007). Within the spectrum of compositions and volumes erupted from intraplate areas, Jeju represents an intermediate point, with both a dispersed (monogenetic) component evident from the scattered vents across the island (Fig. 7.1b), but also a core where magma supply was sufficient to build a high volcanic edifice consisting of stacked evolved lavas. This may also apply to the Pinacate Volcanic Field, Mexico, where trachyte erupted in the centre of the system (Santa Clara shield) is considered to be unrelated to the dispersed basaltic field (Lynch *et al.*, 1993).

We propose that the ratio between magma input from the source and the accommodation of tectonic strain through magma injections in the crust controls the extent of chemical evolution (AFC) in the system. Therefore, we hypothesize that the control on volcanic field morphological development is a function of these two factors. If the build up in tectonic stress is too low to be accommodated by magmatic injection, then larger magma supply rates in the centre of a field could have resulted in magma stalling in the crust and evolving through AFC processes. In other, more stable tectonic areas (further away from plate boundaries), e.g. Changbaishan/Baekdusan on the China/N. Korea border, magma input dominates and a focused plumbing system is more likely to result.

In a dispersed monogenetic field, the eruption site is likely to reflect the site of melting in the mantle (Takada, 1994). Our data suggest that individual magma batches on Jeju evolved independently. This is different from arc-type andesitic volcanoes, where magmatic evolution involves one or a series of magma reservoirs that are repeatedly replenished, and feed eruptions through a stable central conduit, to form a composite edifice with conical morphology (Devine *et al.*, 2003; Watanabe *et al.*, 2006; Zellmer & Annen, 2008). The site of magma evolution in such volcanic systems can also be a complex network of dykes and sills (Price *et al.*, 2010). This network may extend to the lower crust, forming a “hot zone” where magmas initially stall and evolve as well as interact with the surroundings host rocks (Annen *et al.*, 2006).

We envisage that a similar hot zone has developed in the lower crust of the Jeju system, where mantle derived magmas, in excess of that required for accommodating crustal strain release, have stalled and started to chemically evolve. At Jeju, the hot zone does not consist of an interconnected reservoir or networked magma body (such as a magma chamber). Instead, the temporally and spatially dispersed nature of the volcanic system, coupled with the independent evolution of different magma batches suggests that it consists of separated dyke and sill complexes each located above a discrete mantle source. From there, magmas rise and erupt independently of other batches. The fundamental difference between this and a typical arc stratovolcano plumbing system is the lack of a single upper conduit connected to shallow magma chambers.

This Jeju example provides insights into the nature of dispersed volcanism. Monogenetic cones on the flanks of stratovolcanoes have generally been interpreted as parasitic or satellite vents connected to the central feeding system of the main volcano (Ablay *et al.*, 1998; Corazzato & Tibaldi, 2006; Wilson & Head III, 1988). Primitive alkali basalt monogenetic magmas at Jeju have instead erupted directly from their mantle source and accumulation region, independently of the crustal hot zone. Therefore, the volcano morphology is a mirror of the thermal condition, extent and fertility of the mantle source.

7.12 Conclusions

We have introduced a model for the formation and evolution of the Jeju Island intraplate volcanic field based on geochemical and tectonic constraints. The implication of this model is that the volume, proportion, depth and lateral extent (the magma footprints) of magma produced in the mantle are the dominant factors in determining the course of magmatic and surface volcanic activity. Each magma batch acts as a monogenetic entity feeding an independent, spatially distinct eruption. Therefore Mount Halla is not a classical polygenetic volcano but rather an accumulation of volcanic products, and Jeju Island itself, a "cumulative volcanic field" that reflects the lateral extent and fertility of the source zone.

Activity in the field is modulated by the tectonic stress release through strain accommodation by magmatic injections. Magma production and effusion rates increased by two orders of magnitude c. 450 ka ago, penecontemporaneously to increased caldera eruptive activity in the Japan volcanic arc, and after a regional tectonic stress regime rearrangement lead to increased extension.

At Jeju, decompression melting appears to have been greater in the core of the system, giving rise to an accumulation of larger-volume alkali monogenetic eruptions creating the central composite shield and domes. Lower rates in distal parts of the field are reflected by continued smaller-volume monogenetic volcanism. These results imply that alkali eruptions situated in the centre of long-lived monogenetic fields are more

likely to produce larger volume, potentially more evolved and explosive lava outpourings, compared to those at the outer margins, and that eruptive activity in the field may be related to distal plate subduction activity.

7.13 Acknowledgements

Chang Woo Kwon and Jeon Yong Mun provided assistance during fieldwork; Ritchie Sims, John Wilmshurst and Ashlea Wainwright helped with analytical work. Gábor Kereszturi provided ASTER DEM volume of Jeju. Discussion with and comments by Károly Németh, Bob Stewart, Richard Price, Gert Lube, Georg Zellmer and Ting Wang are appreciated. Critical reviews by Richard Price and Madalyn Blondes greatly improved the manuscript. Nelson Eby is thanked for editorial handling. SJC and IEMS are grateful for support from NZ Ministry of Science and Innovation (formerly FRST) project MAUX0808 “Facing the challenge of Auckland volcanism”. MB is also supported by a Massey University Vice-Chancellor’s Doctoral Scholarship, and YKS by a National Research Foundation of Korea (NRF) grant (No. 2009-0079427).

Chapter 8:

Summary, Conclusions and Avenues of Future Research

Here I summarize and integrate the findings presented as chapters in this thesis, before discussing their implications for models of intraplate volcanism that are applicable to other global settings. Lastly I present integrated conclusions and highlight the areas where these may lead to further research questions.

8.1 Summary of the study

The motivation for investigating the monogenetic volcanoes of Jeju Island was to further our understanding of the factors controlling the development and evolution of intraplate basaltic activity. Jeju was chosen as an "older sister" analogue volcano to the Auckland Volcanic Field in order to gain insights into possible future volcanic activity of the New Zealand system. Jeju was also an attractive research target for this study due to the range of compositions and volumes erupted from the field, the excellent coastal exposures into several eruptive sequences, and the unique availability of continuous deep rock cores collected in several locations through the volcanic pile.

This research project was based upon: (1) detailed, stratigraphically ordered, chemical sampling of several individual monogenetic volcanoes in the Jeju Island Volcanic Field, as well as (2) a similar suite of samples from deep cores penetrating the lava succession that makes up the central higher-elevation portion of the Island, along with (3) sampling of further outer-flank lava flows, cones and trachyte domes, including those that make up the current summit area (Mount Halla). The stratigraphic ordering allowed invaluable insights to be made into the temporal evolution of magmatic processes from the very inception of volcanism on Jeju. The spatial examination of individual monogenetic centres also provided a snapshot into both short-term

temporal controls on magma production and eruption as well as the spatial variability and evolution of the magmatic source in the mantle below Jeju.

Small-volume, primitive basaltic eruption centres formed an ideal basis for the investigation of the dynamics of mantle melting and the mechanisms of magma ascent. Their compositions and petrology indicate rapid ascent rates and limited interaction with the surrounding country rock (mantle, lower crust or upper crust), and hence the chemical variation detected could be used to understand the parameters of deep magma evolution. The Udo tuff cone and lava shield was an example investigated in detail in Chapter 4, and the interpretation provided information on the depth of generation of alkali and subalkali magmas, as well as the crystal assemblages responsible for the chemical variation observed within each suite.

Extending from the dynamics of magma generation and rise in a single setting, a detailed chemical and chronological/stratigraphic knowledge of the eruptive products of a range of eruption centres with variable geometries was used to investigate the plumbing system geometry of small-volume monogenetic volcanoes. The transition between distinct feeding batches or the inception of new eruptive phases is coincidently recorded in both the geochemical and stratigraphic records of an eruption. Oscillating and stepped chemostratigraphic signatures indicate that there were compositional transitions between magmas. In the eruptive deposits, these transitions coincide with marker horizons such as breccias or local truncation and erosional surfaces, or vent shifts. The variation patterns in four contrasting monogenetic centres reported in Chapter 5 suggests several diverse modes of magma ascent. The plumbing of monogenetic volcanoes was shown to be a very complex and eruption-specific system, rather than a uniform feature of these eruption centres. In a volcanic field as old as Jeju Island and with several hundred individual eruptive sites, the underlying basement (crust and upper mantle) is thus likely to be riddled with a network of intrusive units. Earlier dykes and sills likely affect the geometry and rise of subsequent intruding bodies, by modifying stress fields, or contributing resident magmas to mix and erupt with later rising magmas.

Knowledge of the chronology of the chemical data can not only improve our understanding of intra-eruptive dynamics, but can help us understand the evolution of

a whole monogenetic volcanic system, provided data from all stages of volcanic activity are available. In Chapter 6 the data from a sample set representative of the full history of monogenetic centres on Jeju were integrated together to investigate the evolution of the whole distributed magmatic system. The model of the fractionation conditions in two magmatic suites developed in Chapter 4 was extended to include a third (and earlier) suite. Coupled with data from the tectonic evolution of the region, the magmatic model was used to develop an hypothesis for the initiation and evolution of volcanism at Jeju. It was proposed that physical mantle modification, due to regional tectonic events several millions of years prior to the onset of volcanism, generated favourable conditions for later localized decompression melting facilitated by shear sliding. The data also supported Chapter 5's conclusion that the volcanic field's plumbing system consisted of a network of intruded magma bodies, some of which were able, at any time, to interact with subsequently ascending magmas.

A further significant feature of the Jeju Island Volcanic Field is that the largest volume eruptives of the system have been concentrated in the central portion of the Island, building stacked lava flows and a large shield-like edifice, with a central volcanic peak, consisting of trachytic domes and lavas. The relationship of this central, possibly polygenetic volcanism with the broader surrounding monogenetic volcanic field with small-volume eruptive centres was investigated in Chapter 7. A new collection of samples from deep cores through the entire lava pile and examination of their chemical variation over time, demonstrate that the two parts (large-volume and small-volume) of the Jeju volcanic system reflect the development of the same complex magmatic continuum, which has evolved over space and time. The specific magmatic suites identified in the small-volume magmatic system, and investigated in Chapters 4, 5 and 6, are also represented in the large-volume system, but the central large-volume lavas represent a more-mature (chemically evolved) phase of volcanism. This maturity is a function of the balance between magma generation rates and tectonic strain accommodation by magmatic intrusions. Surplus magma to that required for accommodating tectonic strain stalled in the plumbing system and evolved to generate trachytes.

8.2 Significance for other volcanic areas

The models developed in this study have considerable implications for our understanding of intraplate volcanic activity in other areas worldwide. Pleistocene to Holocene intraplate volcanism also occurs in northeast China and the East Sea/Sea of Japan (the largest volcano there being Ulleung Island). One of the more significant intraplate volcanoes in the region is Baegdusan (Changbaishan), located on the border between China and North Korea. This has produced large explosive eruptions that have blanketed northern Japan with tephra in historic times (Machida & Arai, 1983, Wei *et al.*, 2007). This volcano has recently come under the spotlight (Stone, 2010) due to anomalous seismic activity between 2002 and 2004, although this may have returned to background levels (Wu *et al.*, 2007). Baegdusan is part of a group of similar volcanoes, including Wangtian'e, an older volcano just to its south, active between c. 3 and 2 Ma ago (Fan *et al.*, 1999). Recent distributed volcanic activity has also occured in northeast China at the Longgang and Jingbo volcanic fields (Wei *et al.*, 2003). Further to the east, alkalic distributed volcanism was reported in the Sikhote-Alin Ranges (Russia), although very limited information is available for this (Whitford-Stark, 1983). Earlier volcanism in the region was also related to opening of the East Sea/Sea of Japan (Liu *et al.*, 2001, Okamura *et al.*, 2005). All of these volcanic areas possibly share a common source structure, where mantle convection is promoted by localized weaknesses, such as sheared domains formed during the tectonic reorganization that lead to the formation of the East Sea. The period and type of eruption (distributed v. central) may subsequently be controlled by local and distal tectonic stress distribution and strain release.

The Auckland Volcanic Field of New Zealand was the original comparator that inspired this study at Jeju. This much smaller system is similarly located in a region that was relatively recently affected by a tectonic reorganization. Although the exact direction of subduction is debated, the northwestern part of North Island, New Zealand, was the site of subduction termination and plate breakoff c. 20 Ma ago (Schellart, 2007). The area of modern intraplate volcanic activity is also distally related to a rifting environment, with the active Taupo Volcanic Zone located 160 km to the southeast. Additionally, the Hauraki basin, a Quaternary extensional structure (Brothers & Delaloye, 1982, Hodder, 1984) is located just to the east of it. Activity in

the field appears to be correlated with extension in the Taupo Volcanic Zone, as epitomized by the timing of large caldera eruptions. The majority of eruptions at Auckland occurred between 40 and 10 ka (Bebbington & Cronin, 2011), penecontemporaneously to the Taupo and Okataina caldera eruptions (Houghton *et al.*, 1995). The sinking of the detached subducting plate may have left behind a physically modified mantle, facilitating later localized upwelling promoted by the extensional tectonics, leading to decompression melting and eruption by strain accommodation.

A similar scenario may be envisioned for the South Auckland, Ngatutura and Alexandra Volcanic Fields, which lie to the south of the Auckland Volcanic Field alongside the Hauraki Basin. The northward progression of volcanism from the Late Pliocene onwards (Briggs *et al.*, 1989, Briggs *et al.*, 1994) ending at the active Auckland Volcanic Field is not coupled with a similar temporal trend in activity in volcanic fields in the Northland Peninsula (Smith *et al.*, 1993). This precludes a fixed source (i.e. a plume) as a source of activity, and suggests instead a link to subduction processes (Briggs *et al.*, 1994).

The Auckland Volcanic Field and its related fields to the south also bear magmatic similarities with the Jeju Island system. They also erupted a spectrum of alkali and subalkali lavas (Cook *et al.*, 2005, Needham *et al.*, 2011) from continuous melting of a heterogeneously metasomatised mantle column (McGee *et al.*, 2012) although in the AVF there does not seem to have been a temporal progression of chemical evolution (Le Corvec *et al.*, 2012). Also, no evolved (trachyte) lavas were erupted in the New Zealand systems. This may potentially be due to the greater proximity of these fields to the subduction zone and backarc rift(s) (Taupo Volcanic Zone/Hauraki Basin) resulting in greater strain rates and ease of magma ascent. Alternatively lower magma generation rates feeding smaller magma volumes into the plumbing system of the New Zealand fields (Kereszturi *et al.*, 2012) may also have resulted in fewer intrusions and magma accumulation at subcrustal/crustal depths.

Further afield, intraplate volcanic areas in a setting similar to that of Jeju Island, and potentially controlled and driven by analogous mechanisms may include the Pinacate Volcanic Field (Mexico) near the Gulf of California rift (Lynch *et al.*, 1993). At this

site, volcanic activity has occurred since the Miocene, evolving from subduction-related calc-alkalic to intraplate alkali volcanism suggesting the breaking up and opening of a window in the subducted Farallon Plate (Vidal-Solano *et al.*, 2008). These tectonic adjustments likely generated shear weaknesses in the mantle, and a subsequent extensional stress regime, also causing lithospheric thinning (Vidal-Solano *et al.*, 2008), generating convective decompression and distributed volcanism.

A common thread that links all of these intraplate volcanic areas together is the occurrence of relatively recent (last few million years) tectonic reorganization, which potentially created shear weaknesses in the mantle. The presence of proximal to distal extensional structures suggesting tensional stress regimes is another common characteristic. A further link between all of these volcanic areas is clearly mantle upwelling leading to local decompression melting. Therefore, in a similar way to the "combustion triangle" having heat, fuel and an oxidising agent at its apexes, an "intraplate field volcano triangle" would need (1) sheared mantle weak zones or planes (created through prior tectonic movements), (2) magma supply (generated through decompression melting) and (3) space for intrusions (caused by extensional strain accommodation).

8.3 Conclusions

Despite the Plate Tectonics and Plume Theories, several genetic features and the locations of many intraplate volcanic fields remain enigmatic. Through the study of the syn-eruptive chemical variation in single monogenetic events, and of the evolution of compositions over the lifetime in the Jeju Island Volcanic Field, Korea, models have been presented to account for genetic and dynamic mechanisms.

Magmas of small-volume distributed volcanic field eruptions are generally derived directly from the mantle and erupt as primitive alkali basalt. They may also stall at various levels, evolve to trachybasalt and mix with later injected primitive magma batches, leading to eruptions of mixed-magmas recorded in the stratigraphy of volcanic deposits as oscillating and stepped chemical trends. The mode of ascent and possible mixing are likely to be a function of the batch volume and of the strain rate

and stress field distribution at the time of eruption. This process results in distinctive features and markers in the eruption deposits, such as inconspicuous local truncations and erosional surfaces indicating short periods of quiescence, or breccias and slump horizons indicative of vent shifts and edifice destabilization. The plumbing system of intraplate volcanic areas is consequently likely to be an array of frozen remanents of dykes throughout the mantle and crust above their mantle source, and the spatial distribution of volcanoes and magma types at the surface thus mirrors the geometry of the source region.

The initiation of mantle decompression and partial melting at Jeju c. 1.8 Ma ago occurred thanks to favourable preconditioning during the opening of the East Sea/Sea of Japan c. 15 Ma earlier. Shear zones facilitated uplift of mantle domains and circulation of magmatic metasomatic fluids that fertilized the source c. 2 Ma ago, during a tectonic reorganization. These conditions led to the initial small-volume primitive magmas feeding phreatomagmatic eruptions on the continental shelf and accommodating low rates of tectonic strain. Surplus magma accumulated and evolved up to trachyte at different levels in the crust before erupting (Sanbangsan trachyte), potentially due to magma pressure build-up in the system.

The deepening of the melting region resulted in the tapping of a renewed magma supply after the initial c. 1.4 Ma of activity, leading to greater magma generation rates and eruptions that built the central pile of large-volume lavas in the last 0.4 Ma. A greater supply of magma resulted in larger volumes of magma accumulating at crustal depths and evolving to trachyte. Although the increase in caldera volcanism in the Kyushu volcanic arc is suggestive of heightened strain in the region, the magma fed into the Jeju system was in excess of that required to accommodate tectonic strain. The later eruption of evolved large-volume magmas (including the Hallasan trachyte) was therefore driven by magma pressure build-up in the storage area. Therefore Jeju Island changed from early tectonically controlled volcanic field to a late magmatically dominated one. The downward development of the source over the life of the field, coupled with the bimodal age distribution of trachytic volcanic activity penecontemporaneous to caldera activity in the Kyushu arc, and the lack of a spatial progression of the locus of magmatism, points towards a tectonic control of the field rather than a mantle plume driving the system.

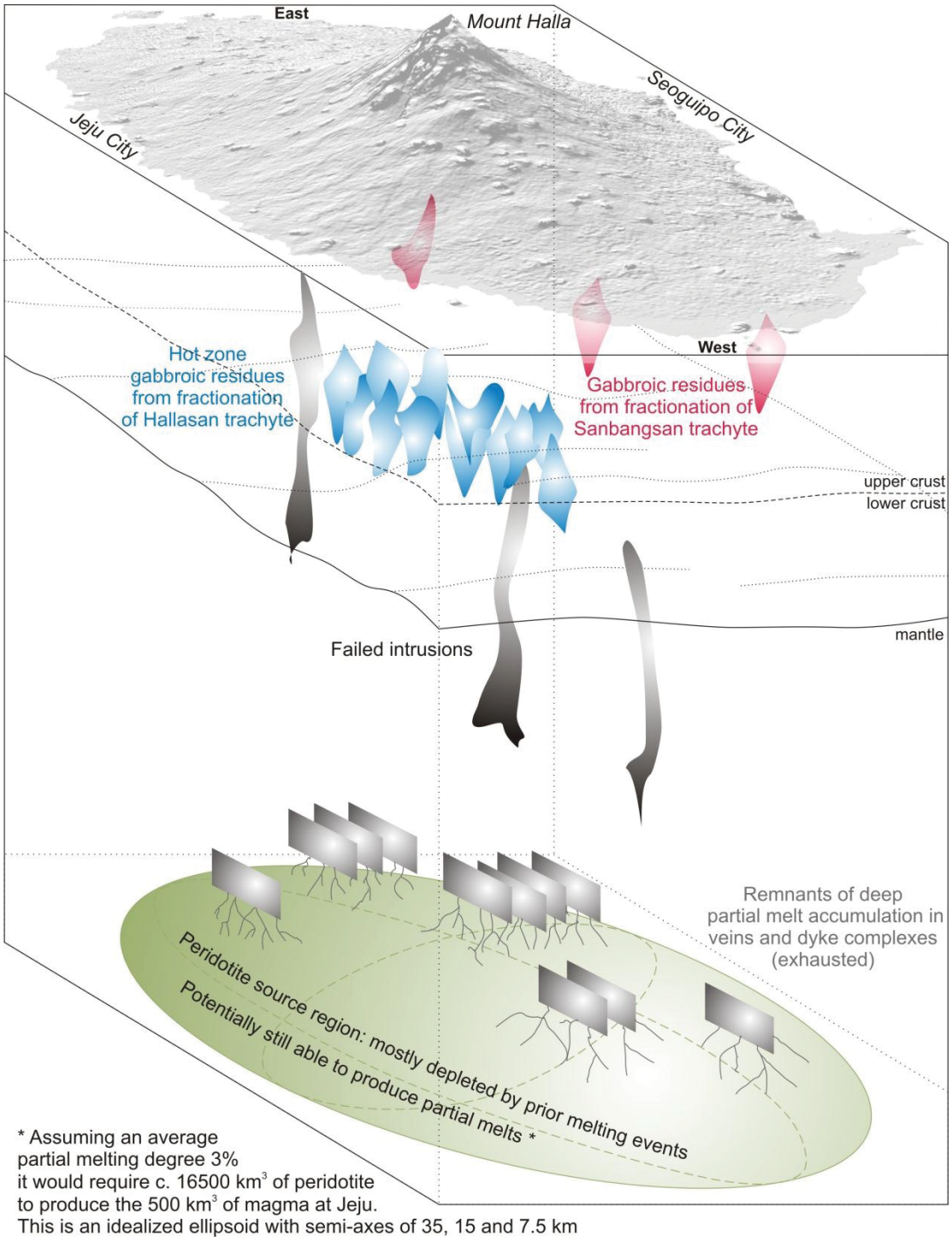

Figure 8.1: *Conceptualized current state of the Jeju magmatic system. The diagram is not to scale.*

Importantly, the spatial distribution of vents on the surface together with the greater volumes erupted in the core of the Island compared to its outskirts suggest that the surface expression and morphology of the volcanic field is a mirror image of the mantle source. The centre of the source region is where a volumetrically larger

portion of peridotite was available to generate primitive melts, and hence larger magma volumes resulted, compared to near the margins of the system. The larger volume of subalkali magmas near the western and eastern margins of the Island were a result of the larger degree of partial melting, but the volumetric portion of mantle available to generate such melts also decreases with distance from the core of the magmatic system. Once partial melts are generated in the mantle, they are accumulated near the source and later ascend independently of surrounding stored magmas. This coincides with a new view of intraplate composite magmatic systems. Namely, this model involves the independent accumulation, rise and eruption of monogenetic magma batches without the development of a centralized plumbing system.

Finally, at present the Jeju system is in a mature state, having already produced several episodes of large-volume magmatism (Fig. 8.1), the last of which terminated c. 25 ka ago. Given the degrees of partial melting required to generate alkali magma (1-2%) and subalkali magma (5-10), 3% bulk partial melting of the Jeju source can be approximated. Assuming the total magma generation to correspond to 500 km^3, and assuming the that surface distribution is an indicator of the source spatial extent, this requires an idealized peridotite source region in the shape of an ellipsoid with semi-axes of 35 km (east-west) and 15 km (north-south) given by the surface area of the field, and 7.5 km (vertical). Melting occurred over a c. 1 GPa vertical pressure variation, corresponding to c. 33 km. It is, therefore, likely that future eruptions may occur in the field above deep pockets of remaining melts. Increased tectonic activity, correlated with volcanic/seismic activity in the Kyushu Arc region may serve as an ascent trigger for such magma pockets at Jeju.

8.4 Avenues of Future Reseach

The excellent three-dimensional knowledge of the geology of Jeju Island and its ease of access makes it a unique natural laboratory for the study of intraplate volcanic systems.

A still perplexing aspect of its history is the presence of voluminous trachyte lava flows and domes, and yet the absence of any indicators of large explosive eruptions, such as thick tephra sequences or pyroclastic deposits, other than those of a phreatomagmatic nature associated with small-volume basaltic eruptions. A detailed study of the petrology and mineralogy of the trachyte suites, and a comparison of these with trachytes erupted explosively in other settings could therefore reveal insights into the controlling factors leading to explosivity in intraplate trachytic activity.

The volatile content of alkali and subalkali magmas is another aspect of volcanism that is as yet poorly understood and warrants further investigation. The Udo eruption discussed in detail in Chapter 4 is a good example of an eruption fed by these two contrasting magma types, with the alkali batch erupting explosively and subalkali magma erupting effusively. The eruption of Songaksan on the other hand presents a prime example to investigate an alkali magma that erupted first explosively and subsequently effusively.

The proposition that the spatial distribution of volcanism at the surface mirrors the source of the magma batch feeding a particular eruption could be pursued in order to develop spatiotemporal volumetric forecast models. The chemical signature of erupted magmas can be used to infer partial melting degree. This, coupled with estimates of the erupted and non-erupted volumes could be used to infer a likely volume of mantle required to generate the batch feeding a particular eruption. Such a model, calculated for all eruptions in the field could give an indication of the mantle areas that have not been tapped yet, and are hence more likely to feed a future eruption.

The relationship between increased activity in the field and caldera type volcanism in the Kyushu volcanic arc also deserves further attention, as such relationships have been observed and proposed for other similar settings. An investigation of this would need to draw on aspects of tectonics and paleoseismology, for ultimately, caldera activity may be related to subduction rates reflected in earthquake recurrence.

This subsequently leads to the physical controls on the triggering mechanisms that lead to magma ascent and eruptions. Recent earthquakes have highlighted the near surface effects (i.e. liquefaction) of seismic waves passing through a liquid-filled porous medium. Analogous experiments conducted in a hot, high-pressure environment may reveal whether such a process also affects partially molten peridotite, hence leading to the accumulation of partial melts in veins and ultimately deep dyke complexes.

References

ABLAY G. J., CARROLL M. R., PALMER M. R., MARTÍ J. & SPARKS R. S. J. 1998. Basanite–phonolite lineages of the Teide–Pico Viejo Volcanic Complex, Tenerife, Canary Islands. *Journal of Petrology*, **39**, 905-936.

ADAM J. & GREEN T. 2006. Trace element partitioning between mica- and amphibole-bearing garnet lherzolite and hydrous basanitic melt: 1. Experimental results and the investigation of controls on partitioning behaviour. *Contributions to Mineralogy and Petrology*, **152**, 1-17.

ADAM J. & GREEN T. 2011. Trace element partitioning between mica- and amphibole-bearing garnet lherzolite and hydrous basanitic melt: 2. Tasmanian Cainozoic basalt and the origins of intraplate basaltic magmas. *Contributions to Mineralogy and Petrology*, **161**, 883-899.

ALBARÈDE F. 1995. *Introduction to Geochemical Modeling.* Cambridge University Press, Cambridge UK, 538 pp.

ALLEN S. R. & SMITH I. E. M. 1994. Eruption styles and volcanic hazard in the Auckland Volcanic Field, New Zealand. *Geoscience reports of Shizuoka University*, **20**, 5-14.

ANDERSON D. L. 2001. Top-down tectonics? *Science*, **293**, 2016-2018.

ANDERSON JR. T. A., SWIHART G. H., ARTIOLI G. & GEIGER C. A. 1984. Segregation vesicles, gas filter-pressing, and igneous differentiation. *The Journal of Geology*, **92**, 55-72.

ANNEN C., BLUNDY J. D. & SPARKS R. S. J. 2006. The genesis of intermediate and silicic magmas in deep crustal hot zones. *Journal of Petrology*, **47**, 505-539.

AOKI K. I. & KUSHIRO I. 1968. Some clinopyroxenes from ultramafic inclusions in Dreiser Weiher, Eifel. *Contributions to Mineralogy and Petrology*, **18**, 326-337.

ASIMOW P. D., HIRSCHMANN M. M., GHIORSO M. S., O'HARA M. J. & STOLPER E. M. 1995. The effect of pressure-induced solid-solid phase transitions and decompression melting of the mantle. *Geochimica et Cosmochimica Acta*, **59**, 4489-4506.

BACON C. R. 1990. Calc-alkaline, Shoshonitic, and Primitive Tholeiitic Lavas from Monogenetic Volcanoes near Crater Lake, Oregon. *Journal of Petrology*, **31**, 135-166.

BAKER J., PEATE D., WAIGHT T. & MEYZEN C. 2004. Pb isotopic analysis of standards and samples using a ^{207}Pb–^{204}Pb double spike and thallium to correct for mass bias with a double-focussing MC-ICP-MS. *Chemical Geology*, **211**, 275-303.

BARTELS K. S., KINZLER R. J. & GROVE T. L. 1991. High pressure phase relations of primitive high-alumina basalts from Medicine Lake volcano, northern California. *Contributions to Mineralogy and Petrology*, **108**, 253-270.

BEATTIE P., FORD C. & RUSSELL D. 1991. Partition coefficients for olivine-melt and orthopyroxene-melt systems. *Contributions to Mineralogy and Petrology*, **109**, 212-224.

BEBBINGTON M. S. & CRONIN S. J. 2011. Spatio-temporal hazard estimation in the Auckland Volcanic Field, New Zealand, with a new event-rder model. *Bulletin of Volcanology*, **73**, 55-72.

BLONDES M. S., REINERS P. W., DUCEA M. N., SINGER B. S. & CHESLEY J. 2008. Temporal-compositional trends over short and long time-scales in basalts of the Big Pine Volcanic Field, California. *Earth and Planetary Science Letters*, **269**, 140-154.

BONS P. D., ARNOLD J., ELBURG M. A., KALDA J., SOESOO A. & VAN MILLIGEN B. P. 2004. Melt extraction and accumulation from partially molten rocks. *Lithos*, **78**, 25-42.

BRADSHAW T. K. & SMITH E. I. 1994. Polygenetic Quaternary volcanism at Crater Flat, Nevada. *Journal of Volcanology and Geothermal Research*, **63**, 165-182.

BRENNA M., CRONIN S. J., NÉMETH K., SMITH I. E. M. & SOHN Y. K. 2011. The influence of magma plumbing complexity on monogenetic eruptions, Jeju Island, Korea. *Terra Nova*, **23**, 70-75.

BRENNA M., CRONIN S. J., SMITH I. E. M., SOHN Y. K. & MAAS R. 2012. How small-volume basaltic magmatic systems develop: a case study from the Jeju Island Volcanic Field, Korea. *Journal of Petrology*, **53**, 985-1018.

BRENNA M., CRONIN S. J., SMITH I. E. M., SOHN Y. K. & NÉMETH K. 2010. Mechanisms driving polymagmatic activity at a monogenetic volcano, Udo, Jeju Island, South Korea. *Contributions to Mineralogy and Petrology*, **160**, 931-950.

BRIGGS R. M., ITAYA T., LOWE D. J. & KEANE A. J. 1989. Ages of the Pliocene-Pleistocene Alexandra and Ngatutura Volcanics, western North Island, New Zealand, and some geological implications. *New Zealand Journal of Geology and Geophysics*, **32**, 417-427.

BRIGGS R. M., OKADA T., ITAYA T., SHIBUYA H. & SMITH I. E. M. 1994. K-Ar ages, paleomagnetism, and geochemistry of the South Auckland volcanic field, North Island, New Zealand. *New Zealand Journal of Geology and Geophysics*, **37**, 143-153.

BROTHERS R. N. & DELALOYE M. 1982. Obducted ophiolite of North Island, New Zealand: origin, age, emplacement and tectonic implications for Tertiary and Quaternary volcanicity. *New Zealand Journal of Geology and Geophysics*, **25**, 257-274.

BULTITUDE R. J. & GREEN D. H. 1971. Experimental study of crystal-liquid relationships at high pressure in olivine nephelinite and basanite compositions. *Journal of Petrology*, **12**, 121-147.

CAMP V. E. & ROOBOL M. J. 1989. The Arabian continental alkali basalt province: Part I. Evolution of Harrat Rahat, Kingdom of Saudi Arabia. *Geological Society of America Bulletin*, **101**, 71-95.

CAMP V. E., HOOPER P. R., ROOBOL M. J. & WHITE D. L. 1987. The Medinah eruption, Saudi Arabia: Magma mixing and simultaneous extrusion of three basaltic chemical types. *Bulletin of Volcanology*, **49**, 489-508.

CAÑÓN-TAPIA E. & WALKER G. P. L. 2004. Global aspects of volcanism: the perspectives of "plate tectonics" and "volcanic systems". *Earth-Science Reviews*, **66**, 163-182.

CARMICHAEL G. R., HONG M. S., UEDA H., CHEN L. L., MURANO K., PARK J. K., LEE H., KIM Y., KANG C. & SHIN S. 1997. Aerosol composition at Cheju Island, Korea. *Journal of Geophysical Research*, **102**, 6047-6061.

CARN S. A. & PYLE D. M. 2001. Petrology and geochemistry of the Lamongan Volcanic Field, East Java, Indonesia: Primitive Sunda Arc Magmas in an extensional tectonic setting? *Journal of Petrology*, **42**, 1643-1683.

CARRACEDO J. C. & RODRIGUEZ BADIOLA E. 1993. Evolución geológica y magmática de la isla de Lanzarote (Islas Canarias). *Revista de la Academia Canaria de Ciencias*, **5**, 25-58.

CARRACEDO J. C., RODRIGUEZ BADIOLA E. & SOLER V. 1992. The 1730-1736 eruption of Lanzarote, Canary Islands: a long, high-magnitude basaltic fissure eruption. *Journal of Volcanology and Geothermal Research*, **53**, 239-250.

CARRASCO-NÚÑEZ G., RIGHTER K., CHESLEY J., SIEBERT L. & ARANDA-GÓMEZ J. 2005. Contemporaneous eruption of calc-alkaline and alkaline lavas in a continental arc (Eastern Mexican Volcanic Belt): chemically heterogeneous but isotopically homogeneous source. *Contributions to Mineralogy and Petrology*, **150**, 423-440.

CHANG K. H., PARK J. B. & KWON S. T. 1999. Petrography and mineral chemistry of trachytes in Cheju Volcanic Island, Korea. *Journal of the Geological Society of Korea*, **35**, 15-34.

CHANG K. H., PARK J. B. & KWON S. T. 2006. Geochemical Characteristics of Trachytes in Jeju Island. *Journal of the Geological Society of Korea*, **42**, 235-252.

CHEN Y., ZHANG Y., GRAHAM D., SU S. & DENG J. 2007. Geochemistry of Cenozoic basalts and mantle xenoliths in Northeast China. *Lithos*, **96**, 108-126.

CHEONG C. S., CHOI J. H., SOHN Y. K., KIM J. C. & JEONG G. Y. 2007. Optical dating of hydromagmatic volcanoes on the southwestern coast of Jeju Island, Korea. *Quaternary Geochronology*, **2**, 266-271.

CHEONG C. S., CHOI M. S., KHIM B. K., SOHN Y. K. & KWON S. T. 2006. $^{230}Th/^{234}U$ dating of Holocene mollusk shells from Jeju Island, Korea, by multiple collectors inductively coupled plasma mass spectrometry. *Geosciences Journal*, **20**.

CHOI S. H., JWA Y. J. & LEE H. Y. 2001. Geothermal gradient of the upper mantle beneath Jeju Island, Korea: Evidence from mantle xenoliths. *The Island Arc*, **10**, 175-193.

CHOI S. H., KWON S. T., MUKASA S. B. & SAGONG H. 2005. Sr-Nd-Pb isotope and trace element systematics of mantle xenoliths from Late Cenozoic alkaline lavas, South Korea. *Chemical Geology*, **221**, 40-64.

CHOI S. H., LEE J. I., PARK C. H. & MOUTTE J. 2002. Geochemistry of peridotite xenoliths in alkali basalts from Jeju Island, Korea. *The Island Arc*, **11**, 221-235.

CHOI S. H., MUKASA S. B., KWON S. T. & ANDRONIKOV A. V. 2006. Sr, Nd, Pb and Hf isotopic compositions of late Cenozoic alkali basalts in South Korea: Evidence for mixing between the two dominant asthenospheric mantle domains beneath East Asia. *Chemical Geology*, **232**, 134-151.

CHOUGH S. K., KWON S. T., REE J. H. & CHOI D. K. 2000a. Tectonic and sedimentary evolution of the Korean peninsula: a review and new view. *Earth-Science Reviews*, **52**, 175-235.

CHOUGH S. K., LEE H. J. & YOON S. H. 2000b. *Marine Geology of Korean Seas*. (2nd edition). Elsevier Science, Amsterdam, 328 pp.

CHOUGH S. K. & SOHN Y. K. 1990. Depositional mechanics and sequences of base surges, Songaksan tuff ring, Cheju Island, Korea. *Sedimentology*, **37**, 1115-1135.

CLAGUE D. A. & FREY F. A. 1982. Petrology and Trace Element Geochemistry of the Honolulu Volcanics, Oahu: Implications for the Oceanic Mantle below Hawaii. *Journal of Petrology*, **23**, 447-504.

CLUZEL D., CADET J.-P. & LAPIERRE H. 1990. Geodynamics of the Ogcheon Belt (South Korea). *Tectonophysics*, **183**, 41-56.

CONDIT C. D. & CONNOR C. B. 1996. Recurrence rates of volcanism in basaltic volcanic fields: An example from the Spingerville volcanic field, Arizona. *Geological Society of America Bulletin*, **108**, 1225-1241.

CONNOR C. B. & CONWAY F. M. 2000. Basaltic Volcanic Fields. *In*: Sigurdsson H. (ed.) *Encyclopedia of Volcanoes*. pp. 331-343. Academic Press, San Diego.

CONWAY F. M., CONNOR C. B., HILL B. E., CONDIT C. D., MULLANEY K. & HALL C. M. 1998. Recurrence rates of basaltic volcanism in SP cluster, San Francisco volcanic field, Arizona. *Geology*, **26**, 655-658.

COOK C., BRIGGS R. M., SMITH I. E. M. & MAAS R. 2005. Petrology and geochemistry of intraplate basalts in the South Auckland Volcanic Field, New Zealand: Evidence for two coeval magma suites from distinct sources. *Journal of Petrology*, **46**, 473-503.

CORAZZATO C. & TIBALDI A. 2006. Fracture control on type, morphology and distribution of parasitic volcanic cones: An example from Mt. Etna, Italy. *Journal of Volcanology and Geothermal Research*, **158**, 177-194.

CRISCI G. M., DI GREGORIO S., RONGO R., SCARPELLI M., SPATARO W. & CALVARI S. 2003. Revisiting the 1669 Etnean eruptive crisis using a cellular automata model and implications for volcanic hazard in the Catania area. *Journal of Volcanology and Geothermal Research*, **123**, 211-230.

CRONIN S. J., GAYLORD D. R., CHARLEY D., ALLOWAY B. V., WALLEZ S. & ESAU J. W. 2004. Participatory methods of incorporating scientific with traditional knowledge for volcanic hazard management on Ambae Island, Vanuatu. *Bulletin of Volcanology*, **66**, 652-668.

CRONIN S. J. & NEALL V. E. 2000. Impacts of volcanism on pre-European inhabitants of Taveuni, Fiji. *Bulletin of Volcanology*, **62**, 199-213.

CUKUR D., HOROZAL S., KIM D. C. & HAN H. C. 2011. Seismic stratigraphy and structural analysis of the northern East China Sea Shelf Basin interpreted from multi-channel seismic reflection data and cross-section restoration. *Marine and Petroleum Geology*, **28**, 1003-1022.

DEER W. A., HOWIE R. A. & ZUSSMAN J. 1992. *An Introduction to the Rock-Forming Minerals.* Longman, Harlow, England, 696 pp.

DEMIDJUK Z., TURNER S., SANDIFORD M., GEORGE R., FODEN J. & ETHERIDGE M. 2007. U-series isotope and geodynamic constraints on mantle melting processes beneath the Newer Volcanic Province in South Australia. *Earth and Planetary Science Letters*, **261**, 517-533.

DEMOUCHY S., JACOBSEN S. D., GAILLARD F. & STERN C. R. 2006. Rapid magma ascent recorded by water diffusion profiles in mantle olivine. *Geology*, **34**, 429-432.

DEPAOLO D. J. 1981. Trace element and isotopic effects of combined wallrock assimilation and fractional crystallization. *Earth and Planetary Science Letters*, **53**, 189-202.

DEVINE J. D., RUTHERFORD M. J., NORTON G. E. & YOUNG S. R. 2003. Magma storage region processes inferred from geochemistry of Fe–Ti oxides in andesitic magma, Soufrière Hills Volcano, Montserrat, W.I. *Journal of Petrology*, **44**, 1375-1400.

DIEZ M., CONNOR C. B., KRUSE S. E., CONNOR L. & SAVOV I. P. 2009. Evidence of small-volume igneous diapirism in the shallow crust of the Colorado Plateau, San Rafael Desert, Utah. *Lithosphere*, **1**, 328-336.

DORENDORF F., CHURIKOVA T., KOLOSKOV A. & WÖRNER G. 2000. Late Pleistocene to Holocene activity at Bakening volcano and surrounding monogenetic centres (Kamchatka): volcanic geology and geochemical evolution. *Journal of Volcanology and Geothermal Research*, **104**, 131-151.

DOWNES H. 1990. Shear zones in the upper mantle--Relation between geochemical enrichment and deformation in mantle peridotites. *Geology*, **18**, 374-377.

DUDA A. & SCHMINCKE H.-U. 1985. Polybaric differentiation of alkali basaltic magmas: evidence from green-core clinopyroxenes (Eifel, FRG). *Contributions to Mineralogy and Petrology*, **91**, 340-353.

EGGINS S. M., RUDNICK R. L. & MCDONOUGH W. F. 1998. The composition of peridotites and their minerals: a laser-ablation ICP–MS study. *Earth and Planetary Science Letters*, **154**, 53-71.

ELBURG M. A., VROON P., VAN DER WAGT B. & TCHALIKIAN A. 2005. Sr and Pb isotopic composition of five USGS glasses (BHVO-2G, BIR-1G, TB-1G, NKT-1G). *Chemical Geology*, **223**, 196-207.

ELKINS L. J., GAETANI G. A. & SIMS K. W. W. 2008. Partitioning of U and Th during garnet pyroxenite partial melting: Constraints on the source of alkaline ocean island basalts. *Earth and Planetary Science Letters*, **265**, 270-286.

ELTHON D. & SCARFE C. M. 1984. High-pressure phase equilibria of high-magnesia basalt and the genesis of primary oceanic basalts. *American Mineralogist*, **69**, 1-15.

EOM Y., YANG K. H., NAM B., HWANG B. H. & KIM J. 2007. Gabbroic xenoliths in alkaline basalts from Jeju Island. *Journal of the Mineralogical Society of Korea*, **20**, 103-114.

ERLUND E. J., CASHMAN K. V., WALLACE P. J., PIOLI L., ROSI M., JOHNSON E. & GRANADOS H. D. 2010. Compositional evolution of magma from Parícutin Volcano, Mexico: The tephra record. *Journal of Volcanology and Geothermal Research*, **197**, 167-187.

FACCENNA C., BECKER T. W., LALLEMAND S., LAGABRIELLE Y., FUNICIELLO F. & PIROMALLO C. 2010. Subduction-triggered magmatic pulses: A new class of plumes? *Earth and Planetary Science Letters*, **299**, 54-68.

FAN Q., LIU R., LI D. & LI Q. 1999. Significance of K-Ar age of bimodal volcanic rocks at Wangtian'e volcano, Changbaishan area. *Chinese Science Bulletin*, **44**, 660-664.

FEDOTOV S. A. 1981. Magma rates in feeding conduits of different volcanic centres. *Journal of Volcanology and Geothermal Research*, **9**, 379-394.

FERRUCCI M., PERTUSATI S., SULPIZIO R., ZANCHETTA G., PARESCHI M. T. & SANTACROCE R. 2005. Volcaniclastic debris flows at La Fossa Volcano (Vulcano Island, southern Italy): Insights for erosion behavior of loose

pyroclastic material on steep slopes. *Journal of Volcanology and Geothermal Research*, **145**, 173-191.

FISHER R. V. & SCHMINCKE H.-U. 1984. *Pyroclastic Rocks.* Springer Verlag, Berlin, 472 pp.

FITTON J. G., SAUNDERS A. D., NORRY M. J., HARDARSON B. S. & TAYLOR R. N. 1997. Thermal and chemical structure of the Iceland plume. *Earth and Planetary Science Letters*, **153**, 197-208.

FLECK R. J., TURRIN B. D., SAWYER D. A., WARREN R. G., CHAMPION D. E., HUDSON M. R. & MINOR S. A. 1996. Age and character of basaltic rocks of the Yucca Mountain region, southern Nevada. *Journal of Geophysical Research*, **101**, 8205-8227.

FOLEY S. 1991. High-pressure stability of the fluor- and hydroxy-endmembers of pargasite and K-richterite. *Geochimica et Cosmochimica Acta*, **55**, 2689-2694.

FOSHAG W. F. & GONZÁLES J. R. 1956. Birth and development of Parícutin volcano Mexico. *USGS Bulletin*, **965-D**, 355-489.

FRANCIS D. & LUDDEN J. 1995. The Signature of Amphibole in Mafic Alkaline Lavas, a Study in the Northern Canadian Cordillera. *Journal of Petrology*, **36**, 1171-1191.

FREY F. A., GREEN D. H. & ROY S. D. 1978. Integrated models of basalt petrogenesis: A study of quartz tholeiites to olivine melilitites from South Eastern Australia utilizing geochemical and experimental petrological data. *Journal of Petrology*, **19**, 463-513.

FUJIMAKI H., TATSUMOTO M. & AOKI K. I. 1983. Partition coefficients of Hf, Zr, and REE between phenocrysts and groundmasses. *Journal of Geophysical Research, Supplement*, **89**, B662-B672.

GHIORSO M. S., HIRSCHMANN M. M., REINERS P. W. & KRESS V. C. I. 2002. The pMELTS: A revision of MELTS aimed at improving calculation of phase relations and major element partitioning involved in partial melting of the mantle at pressures to 3 GPa. *Geochemistry, Geophysics, Geosystems (G3)*, **3**.

GRAY C. M. & MCDOUGALL I. 2009. K-Ar geochronology of basalt petrogenesis, Newer Volcanic Province, Victoria. *Australian Journal of Earth Sciences*, **56**, 245-258.

GREEN D. H. 1973. Experimental melting studies of a model upper mantle composition at high pressure under water-saturated and water undersaturated conditions. *Earth and Planetary Science Letters*, **19**, 37-53.

GUDMUNDSSON O. & SAMBRIDGE M. 1998. A regionalized upper mantle (RMU) seismic model. *Journal of Geophysical Research*, **103**, 7121-7136.

HALL R., ALI J. R., ANDERSON C. D. & BAKER S. J. 1995. Origine and motion history of the Philippine Sea Plate. *Tectonophysics*, **251**, 229-250.

HALLIDAY A. N., LEE D.-C., TOMMASINI S., DAVIES G. R., PASLICK C. R., GODFREY FITTON J. & JAMES D. E. 1995. Incompatible trace elements in OIB and MORB and source enrichment in the sub-oceanic mantle. *Earth and Planetary Science Letters*, **133**, 379-395.

HAMDY A. M., PARK P. H. & LIM H. C. 2005. Horizontal deformation in South Korea from permanent GPS network data, 2000-2003. *Earth Planets Space*, **57**, 77-82.

HAMDY A. M., PARK P. H., LIM H. C. & PARK K. D. 2004. Present-day relative displacement between the Jeju Island and the Korean peninsula as seen from GPS observations. *Earth Planets Space*, **56**, 927-931.

HARE A. G., CAS R. A. F., MUSGRAVE R. & PHILLIPS D. 2005. Magnetic and chemical stratigraphy for the Warribee Plains basaltic lava flow-field, Newer Volcanics Province, southeast Australia: implications for eruption frequency. *Australian Journal of Earth Sciences*, **52**, 41-57.

HART S. R. 1988. Heterogeneous mantle domains: signatures, genesis and mixing chronologies. *Earth and Planetary Science Letters*, **90**, 273-296.

HART S. R., HAURI E. H., OSCHMANN L. A. & WHITEHEAD J. A. 1992. Mantle Plumes and Entrainment: Isotopic Evidence. *Science*, **256**, 517-520.

HASEBE N., FUKUTANI A., SUDO M. & TAGAMI T. 2001. Transition of eruptive style in an arc-arc collision zone: K-Ar dating of Quaternary monogenetic and polygenetic volcanoes in the Higashi-Izu region, Izu peninsula, Japan. *Bulletin of Volcanology*, **63**, 377-386.

HASENAKA T. & CARMICHAEL I. S. E. 1985. The cinder cones of Michoacán-Guanajuato, central Mexico: their age, volume and distribution, and magma discharge rate. *Journal of Volcanology and Geothermal Research*, **25**, 105-124.

HASENAKA T., LEE M. W., TANIGUCHI H., KITAKAZE A., MIYAMOTO T. & FUJIMAKI H. 1997. Catalogue of the Volcanoes from the Cheju Monogenetic Volcano Group, Korea. *Northeast Asian Studies*. pp. 41-74. Center for Northeast Asian Studies, Tohoku University.

HAWKESWORTH C. J., BLAKE S., EVANS P., HUGHES R., MACDONALD R., THOMAS L. E., TURNER S. P. & ZELLMER G. 2000. Time scale of crystal fractionation in magma chambers-Integrating physical, isotopic and geochemical perspectives. *Journal of Petrology*, **41**, 991-1006.

HERZBERG C. 1995. Generation of plume magmas through time: An experimental perspective. *Chemical Geology*, **126**, 1-16.

HIROSE K. & KUSHIRO I. 1993. Partial melting of dry peridotites at high pressures: Determination of compositions of melts segregated from peridotite using aggregates of diamond. *Earth and Planetary Science Letters*, **114**, 477-489.

HODDER A. P. W. 1984. Late Cenozoic rift development and intra-plate volcanism in northern New Zealand inferred from geochemical discrimination diagrams. *Tectonophysics*, **101**, 293-318.

HOERNLE K., WHITE J. D. L., VAN DEN BOGAARD P., HAUFF F., COOMBS D. S., WERNER R., TIMM C., GARBE-SCHÖNBERG D., REAY A. & COOPER A. F. 2006. Cenozoic intraplate volcanism on New Zealand: Upwelling induced by lithospheric removal. *Earth and Planetary Science Letters*, **248**, 350-367.

HOFMANN A. W., JOCHUM K. P., SEUFERT M. & WHITE W. M. 1986. Nb and Pb in oceanic basalts: new constraints on mantle evolution. *Earth and Planetary Science Letters*, **79**, 33-45.

HOLLOWAY J. R. & BLANK J. G. 1994. Application of experimental results to C-O-H species in natural melts. *In*: Carroll M. R. & Holloway J. R. (eds). *Volatiles in Magmas.* pp. 187-230. Mineralogical Society of America, Washington D.C.

HOUGHTON B. F. & SMITH R. T. 1993. Recycling of magmatic clasts during explosive eruptions: estimating the true juvenile content of phreatomagmatic volcanic deposits. *Bulletin of Volcanology*, **55**, 414-420.

HOUGHTON B. F., WILSON C. J. N., MCWILLIAMS M. O., LANPHERE M. A., WEAVER S. D., BRIGGS R. M. & PRINGLE M. S. 1995. Chronology and dynamics of a large silicic magmatic system: Central Taupo Volcanic Zone, New Zealand. *Geology*, **23**, 13-16.

HUANG X. L., XU Y. G. & LIU D. Y. 2004. Geochronology, petrology and geochemistry of the granulite xenoliths from Nushan, east China: implication for a heterogeneous lower crust beneath the Sino-Korean Craton. *Geochimica et Cosmochimica Acta*, **68**, 127-149.

HULBERT H. B. 1962. *Hulbert's History of Korea.* Routledge & Kegan Paul, London.

HUNTER A. G. 1998. Intracrustal Controls on the Coexistence of Tholeiitic and Calc-alkaline Magma Series at Aso Volcano, SW Japan. *Journal of Petrology*, **39**, 1255-1284.

HWANG J. H., LEE B. J. & SONG K. Y. 1994. Quaternary tectonic movement on Cheju Island. *Economic and Environmental Geology*, **27**, 209-212.

IAEA 1967. In the isle of three manies, three noughts. *IAEA Bulletin*, **9**, 11-16.

IRVING A. J. 1980. Petrology and geochemistry of composite ultramafic xenoliths in alkalic basalts and implications for magmatic processes within the mantle. *In*: Irving A. J. & Dungan M. A. (eds). *The Jackson Volume. American Journal of Science.* pp. 389-426.

ITO G. & MARTEL S. J. 2002. Focusing of magma in the upper mantle through dike interaction. *Journal of Geophysical Research*, **107**, 2223.

JENNER G. A., LONGERICH H. P., JACKSON S. E. & FRYER B. J. 1990. ICP-MS – A powerful tool for high-precision trace-element analysis in Earth sciences:

Evidence from analysis of selected U.S.G.S. reference samples. *Chemical Geology*, **83**, 133-148.

JIN S., LI Z. C. & PARK P. H. 2006. Seismicity and GPS constraints on crustal deformation in the southern part of the Korean Peninsula. *Geosciences Journal*, **10**, 491-497.

JIN S., PARK P. H. & ZHU W. 2007. Micro-plate tectonics and kinematics in Northeast Asia inferred from a dense set of GPS observations. *Earth and Planetary Science Letters*, **257**, 486-496.

JOHNSON E. R., WALLACE P. J., CASHMAN K. V., GRANADOS H. D. & KENT A. J. R. 2008. Magmatic volatile contents and degassing-induced crystallization at Volcán Jorullo, Mexico: Implications for melt evolution and the plumbing systems of monogenetic volcanoes. *Earth and Planetary Science Letters*, **269**, 478-487.

JOLIVET L. & TAMAKI K. 1992. 82. Neogene kinematics in the Japan Sea region and volcanic activity of the northeast Japan arc. *In*: Tamaki K., Suyehiro K., Allan J., McWilliams M. & al. e. (eds). *Proceedings of the Ocean Drilling Program, Scientific Results.* pp. 1311-1331.

JUNG C., JUNG S., HOFFER E. & BERNDT J. 2006. Petrogenesis of tertiary mafic alkaline magmas in the Hocheifel, Germany. *Journal of Petrology*, **47**, 1637-1671.

JUNG S. & MASBERG P. 1998. Major- and trace-element systematics and isotope geochemistry of Cenozoic mafic volcanic rocks from the Vogelsberg (central Germany): Constraints on the origin of continental alkaline and tholeiitic basalts and their mantle sources. *Journal of Volcanology and Geothermal Research*, **86**, 151-177.

KAMATA H. & KODAMA K. 1999. Volcanic history and tectonics of the Southwest Japan Arc. *The Island Arc*, **8**, 393-403.

KAMBER B. S. & COLLERSON K. D. 2000. Zr/Nb systematics of ocean island basalts reassessed-the case for binary mixing. *Journal of Petrology*, **41**, 1007-1021.

KANG S. 2003. Benthic foraminiferal biostratigraphy and paleoenvironments of the Seogwipo Formation, Jeju Island, Korea. *Journal of the Paleontological Society of Korea*, **19**, 63-153.

KERESZTURI G. & NÉMETH K. 2012. Structural and morphometric irregularities of eroded Pliocene scoria cones at the Bakony-Balaton Highland Volcanic Field, Hungary. *Geomorphology*, **136**, 45-58.

KERESZTURI G., NÉMETH K., BEBBINGTON M. S., CRONIN S. J., AUGUSTÍN-FLORES J., PROCTER J. & LINDSAY J. 2012. Magma-output rates of the Auckland Volcanic Field (New Zealand). *In*: Arentsen K., Németh K. & Smid E. (eds). *Abstract Volume of the Fourth International Maar Conference: A Multidisciplinary Congress on Monogenetic Volcanism. Auckland, New*

Zealand 20-24 February 2012. Geoscience Society of New Zealand Miscellaneous Publication 131A: p. 47-48.

KIENLE J., KYLE P. R., SELF S., MOTYKA R. J. & LORENZ V. 1980. Ukinrek Maars, Alaska, I. April 1977 eruption sequence, petrology and tectonic setting. *Journal of Volcanology and Geothermal Research*, **7**, 11-37.

KIGAM 1995 Isotope age map of volcanic rocks in Korea. Institute of Geology, Mining and Materials, Korea.

KIL Y. W., SHIN H. J., YUN S. H., KOH J. S. & AHN U. S. 2008. Geochemical characteristics of mineral phases in the mantle xenoliths from Sunheul-ri, Jeju Island. *Journal of the Mineralogical Society of Korea*, **21**, 373-382.

KIM I. S. & LEE D. 2000. Magnetostratigrphy and AMS of the Seoguipo Formation and Seoguipo Trachyte of Jeju Island. *Journal of the Geological Society of Korea*, **36**, 163-180.

KIM K. H., NAGAO K., TANAKA T., SUMINO H., NAKAMURA T., OKUNO M., LOCK J.-B., YOUN J. S. & SONG J. 2005. He-Ar and Nd-Sr isotopic compositions of ultramafic xenoliths and host basalts from the Korean peninsula. *Geochemical Journal*, **39**, 341-356.

KIM K. H., TANAKA T., NAKAMURA T., NAGAO K., YOUN J. S., KIM K. R. & YUN M. Y. 1999. Palaeoclimatic and chronostratigraphic interpretations from strontium, carbon and oxygen isotopic ratios in molluscan fossils of Quaternary Seoguipo and Shinyangri Formations, Cheju Island, Korea. *Palaeogeography, Palaeoclimatology, Palaeoecology*, **154**, 219-235.

KIM K. H., TANAKA T., SUZUKI K., NAGAO K. & PARK E. J. 2002. Evidence of the presence of old continental basement in Cheju volcanic Island, South Korea, revealed by radiometric ages and Nd-Sr isotopes of granitic rocks. *Geochemical Journal*, **36**, 421-441.

KIM K. Y., SEONG H., KIM T., PARK K. H., WOO N. C., PARK Y. S., KOH G. W. & PARK W. B. 2006. Tidal effects on variations of fresh-saltwater interface and groundwater flow in a multilayered coastal aquifer on a volcanic island (Jeju Island, Korea). *Journal of Hydrology*, **330**, 525-542.

KIM S., RHIE J. & KIM G. 2011. Forward waveform modelling procedure for 1-D crustal velocity structure and its application to the southern Korean Peninsula. *Geophysical Journal International*, **185**, 453-468.

KINZLER R. J. 1997. Melting of mantle peridotite at pressures approaching the spinel to garnet transition: Application to mid-ocean ridge basalt petrogenesis. *Journal of Geophysical Research*, **102**, 853-874.

KLEMME S., BLUNDY J. D. & WOOD B. J. 2002. Experimental constraints on major and trace element partitioning during partial melting of eclogite. *Geochimica et Cosmochimica Acta*, **66**, 3109-3123.

KODAMA K., TASHIRO H. & TAKEUCHI T. 1995. Quaternary counterclockwise rotation of south Kyushu, shouthwest Japan. *Geology*, **23**, 823-826.

KOH G. W. 2005 Hydrogeology, Groundwater Occurrences and Management Systems of Jeju. pp. 93. Jeju, Korea: Institute of Environmental Resources Research, Jeju Self-Governing Province.

KOH G. W. & PARK J. B. 2010a. The study of geology and volcanism in Jeju Island (II): Petrochemistry and $^{40}Ar/^{39}Ar$ absolute ages of the volcanic rocks in Gapado-Marado, Jeju Island. *Economic and Environmental Geology*, **43**, 53-66.

KOH G. W. & PARK J. B. 2010b. The study on geology and volcanism in Jeju Island (III): Early lava effusion rocords in Jeju Island on the basis of $^{40}Ar/^{39}Ar$ absolute ages of lava samples. *Economic and Environmental Geology*, **43**, 163-176.

KOH G. W., PARK J. B. & PARK Y. S. 2008. The study on geology and volcanism in Jeju Island (I): petrochemistry and $^{40}Ar/^{39}Ar$ absolute ages of the subsurface volcanic rock cores from boreholes in the eastern lowland of Jeju Island. *Economic and Environmental Geology*, **41**, 93-113.

KOH J. S., YUN S. H., HYEON G. B., LEE M. W. & GIL Y. W. 2005. Petrology of the basalt in the Udo monogenetic volcano, Jeju Island. *Journal of the Petrological Society of Korea*, **14**, 45-60.

KOH J. S., YUN S. H. & JEONG E. J. 2007. Petrology of the basalts in the Seongsan-Ilchulbong area, Jeju Island. *Journal of the Korean Earth Science Society*, **28**, 324-342.

KOH J. S., YUN S. H. & KANG S. S. 2003. Petrology of the volcanic rocks in the Paekrogdam Crater area, Mt. Halla, Jeju Island. *Journal of the Petrological Society of Korea*, **12**, 1-15.

KOKELAAR B. P. 1983. The mechanism of Surtseyan volcanism. *Journal of the Geological Society*, **140**, 939-944.

KUBO A. & FUKUYAMA E. 2003. Stress field along the Ryukyu Arc and the Okinawa Trough inferred from moment tensors of shallow earthquakes. *Earth and Planetary Science Letters*, **210**, 305-316.

KUSHIRO I. 1996. Partial melting of a fertile mantle peridotite at high pressures: An experimental study using aggregates of diamond. *In*: Basu A. & Hart S. (eds). *Earth Processes: Reading the Isotopic Code.* pp. 109-122. American Geophysical Union Monograph 95.

KUSHIRO I., SYONO Y. & AKIMOTO S.-I. 1968. Melting of a peridotite nodule at high pressures and high water pressures. *Journal of Geophysical Research*, **73**, 6023-6029.

LANGMUIR C. H. 1989. Geochemical consequences of *in situ* crystallization. *Nature*, **340**, 199-205.

LE CORVEC N., BEBBINGTON M. S., HAYWARD B. W., LINDSAY J. M. & ROWLAND J. V. 2012. The Auckland Volcanic Field - a basaltic field showing random behaviour? *In*: Arentsen K., Németh K. & Smid E. (eds). *Abstract Volume of the Fourth International Maar Conference: A Multidisciplinary Congress on Monogenetic Volcanism. Auckland, New Zealand 20-24 February 2012.* Geoscience Society of New Zealand Miscellaneous Publication 131A: p. 51-53.

LEBAS M. J., LEMAITRE R. W., STRECKEISEN A. & ZANETTIN B. 1986. A chemical classification of volcanic rocks based on the total alkali-silica diagram. *Journal of Petrology*, **27**, 745-750.

LEE C. W., KIM S. W., CHANG C. H., KIM W. S., SHIN W. C., MIN G. H., PARK Y. S., LEE H. Y., JIN J. H., KIM S. P. & KIM J. K. 1997. *Marine geological and geophysical study of the continental shelf off southern part of Cheju Island, Korea.* KIGAM.

LEE K. & YANG W. S. 2006. Historical seismicity of Korea. *Bulletin of the Seismological Society of America*, **96**, 846-855.

LEE M. W. 1982. Petrology and geochemistry of Jeju volcanic island, Korea. *The Science Reports of the Tohoku University: Third Series; Mineralogy, Petrology, Economic Geology*, **315**, 177-256.

LEE M. W., WON C. K., LEE D. Y., PARK G. H. & KIM M. S. 1994. Stratigraphy and petrology of volcanic rocks in southern Cheju Island, Korea. *Journal of the Geological Society of Korea*, **30**, 521-541.

LEE S. H., LEE Y. I., YOON H. I. & YOO K. C. 2008. East Asian monsoon variation and climate changes in Jeju Island, Korea, during the latest Pleistocene to early Holocene. *Quaternary Research*, **70**, 265-274.

LEE S. R. & CHO M. 2003. Metamorphic and tectonic evolution of the Hwacheon Granulite Complex, Central Korea: Composite P-T path resulting from two distinct crustal-thickening events. *Journal of Petrology*, **44**, 197-225.

LEE T. J., NAM M. J., LEE S. K., SONG Y. & UCHIDA T. 2009. The Jeju dataset: Three-dimensional interpretation of MT data from mid-mountain area of Jeju Island, Korea. *Journal of Applied Geophysics*, **68**, 171-181.

LEEMAN W. P. & HARRY D. L. 1993. A Binary Source Model for Extension-Related Magmatism in the Great Basin, Western North America. *Science*, **262**, 1550-1554.

LEI J. & ZHAO D. 2005. P-wave tomography and origin of the Changbai intraplate volcano in Northeast Asia. *Tectonophysics*, **397**, 281-295.

LI B., PARK B. K., KIM D. & WOO H. J. 1999. The geological age and paleoenvironment of the lower Seogwipo Formation, Cheju Island, Korea. *Geosciences Journal*, **3**, 181-190.

LI X., SOBOLEV S. V., KIND R., YUAN X. & ESTABROOK C. 2000. A detailed receiver function image of the upper mantle discontinuities in the Japan subduction zone. *Earth and Planetary Science Letters*, **183**, 527-541.

LIU G. 1987. The Cenozoic rift system of the North China Plain and the deep internal process. *Tectonophysics*, **133**, 277-285.

LIU J., HAN J. & FYFE W. S. 2001. Cenozoic episodic volcanism and continental rifting in northeast China and possible link to Japan Sea development as revealed from K-Ar geochronology. *Tectonophysics*, **339**, 385-401.

LIU M., CUI X. & LIU F. 2004. Cenozoic rifting and volcanism in eastern China: a mantle dynamic link to the Indo-Asian collision? *Tectonophysics*, **393**, 29-42.

LORENZ V. 1986. On the growth of maars and diatremes and its relevance to the formation of tuff rings. *Bulletin of Volcanology*, **48**, 265-274.

LORENZ V. 1987. Phreatomagmatism and its relevance. *Chemical Geology*, **62**, 149-156.

LUHR J. F. 2001. Glass inclusions and melt volatile contents at Parícutin Volcano, Mexico. *Contributions to Mineralogy and Petrology*, **142**, 261-283.

LUHR J. F. & CARMICHAEL I. S. E. 1985. Jorullo Volcano, Michoacán, Mexico (1759-1774): The earliest stage of fractionation in calc-alkaline magmas. *Contributions to Mineralogy and Petrology*, **90**, 142-161.

LYNCH D. J., MUSSELMAN T. E., GUTMANN J. T. & PATCHETT P. J. 1993. Isotopic evidence for the origin of Cenozoic volcanic rocks in the Pinacate volcanic field, northwestern Mexico. *Lithos*, **29**, 295-302.

MAAS R., KAMENETSKY M. B., SOBOLEV A. V., KAMENETSKY V. S. & SOBOLEV N. V. 2005. Sr-Nd-Pb isotopic evidence for a mantle origin of alkali chlorides and carbonates in the Udachnaya kimberlite, Siberia. *Geology*, **35**, 549-552.

MACHIDA H. 2002. Volcanoes and tephras in the Japan area. *Global Environmental Research*, **6**, 19-28.

MACHIDA H. & ARAI F. 1983. Extensive ash falls in and around the sea of Japan from large Late Quaternary eruptions. *Journal of Volcanology and Geothermal Research*, **18**, 151-164.

MAHONY S. H., WALLACE L. M., MIYOSHI M., VILLAMOR P., SPARKS R. S. J. & HASENAKA T. 2011. Volcano-tectonic interactions during rapid plate-boundary evolution in the Kyushu region, SW Japan. *Geological Society of America Bulletin*, **123**, 2201-2223.

MANHES G., MINSTER J. F. & ALLÈGRE C. J. 1978. Comparative uranium-thorium-lead and rubidium-strontium study of the Saint Sèverin amphoterite: consequence for early solar system chronology. *Earth and Planetary Science Letters*, **39**, 14-24.

MASHIMA H. 2009. A melting anomaly in Northwest Kyushu, Southwest Japan: A consequence of the tectonic evolution of NW Kyushu and the origin of a pseudo hot spot in a convergent zone. *Journal of Volcanology and Geothermal Research*, **186**, 195-209.

MAZZARINI F. & D'ORAZIO M. 2003. Spatial distribution of cones and satellite-detected lineaments in the Pali Aike Volcanic Field (southernmost Patagonia): insights into the tectonic setting of a Neogene rift system. *Journal of Volcanology and Geothermal Research*, **125**, 291-305.

MCARTHUR J. M., RIO D. MASSARI D., CASTRADORI F., BAILEY T. R., THIRLWALL M. & HOUGHTON S. 2006. A revised Pliocene record for maring-$^{87}Sr/^{86}Sr$ used to date an interglacial event recorded in the Cockburn Island Formation, Antarctic Peninsula. *Palaeogeography, Palaeoclimatology, Palaeoecology*, **242**, 126-136.

MCBIRNEY A. R., TAYLOR H. P. & ARMSTRONG R. L. 1987. Paricutin re-examined: a classic example of crustal assimilation in calc-alkaline magma. *Contributions to Mineralogy and Petrology*, **95**, 4-20.

MCDONOUGH W. F. & SUN S. S. 1995. The composition of the Earth. *Chemical Geology*, **120**, 223-253.

MCGEE L. E., BEIER C., SMITH I. E. M. & TURNER S. P. 2011. Dynamics of melting beneath a small-scale basaltic system: a U-Th-Ra study from Rangitoto volcano, Auckland volcanic field, New Zealand. *Contributions to Mineralogy and Petrology*, **162**, 547-563.

MCGEE L. E., SMITH I. E. M., MILLET M.-A., BEIER C., LINDSAY J. M. & HENDLEY H. 2012. Fine scale mantle heterogeneity revealed in monogenetic eruptions in the Auckland Volcanic Field. *In*: Arentsen K., Németh K. & Smid E. (eds). *Abstract Volume of the Fourth International Maar Conference: A Multidisciplinary Congress on Monogenetic Volcanism. Auckland, New Zealand 20-24 February 2012.* Geoscience Society of New Zealand Miscellaneous Publication 131A: p. 66-67.

MCKENZIE D. & O'NIONS R. K. 1991. Partial melt distributions from inversion of rare Earth element concentrations. *Journal of Petrology*, **32**, 1021-1091.

MERTES H. & SCHMINCKE H.-U. 1985. Mafic potassic lavas of the Quaternary West Eifel volcanic field. *Contributions to Mineralogy and Petrology*, **89**, 330-345.

MILLHOLLEN G. L., IRVING A. J. & WYLLIE P. J. 1974. Melting interval of peridotite with 5.7 per cent water to 30 kilobars. *The Journal of Geology*, **82**, 575-587.

MIYASHIRO A. 1978. Nature of alkalic volcanic rock series. *Contributions to Mineralogy and Petrology*, **66**, 91-104.

MOORE J. G. 1970. Water content of basalt erupted on the ocean floor. *Contributions to Mineralogy and Petrology*, **28**, 272-279.

MORDICK B. & GLAZNER A. 2006. Clinopyroxene thermobarometry of basalts from the Coso and Big Pine volcanic fields, California. *Contributions to Mineralogy and Petrology*, **152**, 111-124.

MYSEN B. O. & BOETTCHER A. L. 1975. Melting of a hydrous mantle: II. Geochemistry of crystals and liquids formed by anatexis of mantle peridotite at high pressures and high temperatures as a function of controlled activities of water, hydrogen, and carbon dioxide. *Journal of Petrology*, **16**, 549-593.

NAKAMURA E., CAMPBELL I. H., MCCULLOCH M. T. & SUN S.-S. 1989. Chemical Geodynamics in a Back Arc Region Around the Sea of Japan: Implications for the Genesis of Alkaline Basalts in Japan, Korea, and China. *Journal of Geophysical Research*, **94**, 4634-4654.

NAKAMURA K. 1977. Volcanoes as possible indicators of tectonic stress orientation - principle and proposal. *Journal of Volcanology and Geothermal Research*, **2**, 1-16.

NEEDHAM A. J., LINDSAY J. M., SMITH I. E. M., AUGUSTINUS P. & SHANE P. A. 2011. Sequential eruption of alkaline and sub-alkaline magmas from a small monogenetic volcano in the Auckland Volcanic Field, New Zealand. *Journal of Volcanology and Geothermal Research*, **201**, 126-142.

NÉMETH K. & CRONIN S. J. 2007. Syn- and post-eruptive erosion, gully formation, and morphological evolution of a tephra ring in tropical climate erupted in 1913 in West Ambrym, Vanuatu. *Geomorphology*, **86**, 115-130.

NÉMETH K., CRONIN S. J., CHARLEY D., HARRISON M. & GARAE E. 2006. Exploding lakes in Vanuatu - "Surtseyan-style" eruptions witnessed on Ambae Island. *Episodes*, **29**, 87-93.

NÉMETH K., WHITE J. D. L., REAY A. & MARTIN U. 2003. Compositional variation during monogenetic volcano growth and its implications for magma supply to continental volcanic fields. *Journal of the Geological Society*, **160**, 523-530.

NICHOLSON H., CONDOMINES M., FITTON J. G., FALLICK A. E., GRÖNVOLD K. & ROGERS G. 1991. Geochemical and isotopic evidence for crustal assimilation beneath Krafla, Iceland. *Journal of Petrology*, **32**, 1005-1020.

NORRISH K. & HUTTON J. T. 1969. An accurate X-ray spectrographic method for the analysis of a wide range of geological samples. *Geochimica et Cosmochimica Acta*, **33**, 431-453.

OGAWA T. 1982 On lava caves in Japan and vicinity. In Halliday W. R. (ed.) Third International Symposium on Vulcanospeleology. pp. 56-73. Bend, Oregon: International Speleological Foundation.

OKADA Y. & YAMAMOTO E. 1991. Dyke intrusion model for the 1989 seismovolcanic activity off Ito, central Japan. *Journal of Geophysical Research*, **96**, 10361-10376.

OKAMURA S., ARCULUS R. J. & MARTYNOV Y. A. 2005. Cenozoic magmatism of the north-eastern Eurasian margin: The role of lithosphere versus asthenosphere. *Journal of Petrology*, **46**, 221-253.

OTOFUJI Y. 1996. Large tectonic movement of the Japan Arc in late Cenozoic times inferred from paleomagnetism: Review and synthesis. *The Island Arc*, **5**, 229-249.

OVIATT C. G. & NASH W. P. 1989. Late Pleistocene basaltic ash and volcanic eruptions in the Bonneville basin, Utah. *Geological Society of America Bulletin*, **101**, 292-303.

PARK J. B. & KWON S. T. 1993a. Geochemical evolution of the Cheju Volcanic Island (II): Trace element chemistry of volcanic rocks from the northern part of Cheju Island. *Journal of the Geological Society of Korea*, **29**, 477-492.

PARK J. B. & KWON S. T. 1993b. Geochemical evolution of the Cheju Volcanic Island: Petrography and major element chemistry for stratigraphically-controlled lavas from the northern part of Cheju Island. *Journal of the Geological Society of Korea*, **29**, 39-60.

PARK J. B. & KWON S. T. 1993c. Mineral chemistry of the volcanic rocks from the northern part of Cheju Island. *Journal of the Petrological Society of Korea*, **2**, 139-155.

PARK J. B. & KWON S. T. 1996. Tholeiitic volcanism in Cheju Island, Korea. *Journal of the Petrological Society of Korea*, **5**, 66-83.

PARK J. B., PARK K. H., CHO D. L. & KOH G. W. 1999. Petrochemical classification of the Quaternary volcanic rocks in Cheju Island, Korea. *Journal of the Geological Society of Korea*, **35**, 253-264.

PARK K. H., AHN J. S., KEE W. S. & PARK W. B. 2006. *Guidebook for a Geological Tour of Jeju Island.* KIGAM, Taejon, 283 pp.

PARK K. H., CHO D. L., KIM Y. B., KIM J. C., CHO B. W., JANG Y. N., LEE B. J., LEE S. R., SON B. K., CHEON H. Y., LEE H. Y. & KIM Y. U. 2000 Geological Report of the Seogwipo-Hahyori Sheet (1:50,000). pp. 163. Jeju: Jeju Provincial Government.

PARK P. H., CHWAE U., AHN Y. W. & CHOI K. H. 2001. Preliminary GPS results and a possible neotectonic interpretation for South Korea. *Earth Planets Space*, **53**, 937-941.

PARRA E. & CEPEDA H. 1990. Volcanic hazard maps of the Nevado del Ruiz volcano, Colombia. *Journal of Volcanology and Geothermal Research*, **42**, 117-127.

PEARCE J. A. 2008. Geochemical fingerprinting of oceanic basalts with applications to ophiolite classification and the search for Archean oceanic crust. *Lithos*, **100**, 14-48.

PEARCE J. A. & PEATE D. W. 1995. Tectonic implications of the composition of volcanic arc magmas. *Annual Review of Earth and Planetary Sciences*, **23**, 251-285.

PERRY F. V., BALDRIDGE W. S. & DEPAOLO D. J. 1988. Chemical and isotopic evidence for lithospheric thinning beneath the Rio Grande rift. *Nature*, **332**, 432-434.

PETRELLI M., POLI G., PERUGINI D. & PECCERILLO A. 2005. PetroGraph: A new software to visualize, model, and present geochemical data in igneous petrology. *Geochemistry, Geophysics, Geosystems (G^3)*, **6**, Q07011.

PIOLI L., ERLUND E., JOHNSON E., CASHMAN K., WALLACE P., ROSI M. & DELGADO GRANADOS H. 2008. Explosive dynamics of violent Strombolian eruptions: The eruption of Parícutin Volcano 1943-1952 (Mexico). *Earth and Planetary Science Letters*, **271**, 359-368.

PIN C. & SANTOS-ZALDUEGUI J. F. 1997. Sequential separation of light rare-earth elements, thorium and uranium by miniaturized extraction chromatography: application to isotopic analyses of silicate rocks. *Analytica et Chimica Acta* **339**, 79-89.

PIN C., BRIOT D., BASSIN C. & POITRASSON F. 1994. Concomitant separation of strontium and samarium-neodymium for isotopic analysis in silicate samples, based on specific extraction chromatography. *Analytica et Chimica Acta*, **298**, 209-217.

PORTER S. C. 1972. Distribution, morphology, and size frequency of cinder cones on Mauna Kea Volcano, Hawaii. *Geological Society of America Bulletin*, **83**, 3607-3612.

POUCLET A., LEE J.-S., VIDAL P., COUSENS B. & BELLON H. 1995. Cretaceous to Cenozoic volcanism in South Korea and in the Sea of Japan: magmatic constraints on the opening of the back-arc basin. *In*: Smellie J. L. (ed.) *Volcanism Associated with Extension at Consuming Plate Margins.* pp. 169-191.

PRICE R. C., TURNER S., COOK C., HOBDEN B., SMITH I. E. M., GAMBLE J. A., HANDLEY H., MAAS R. & MÖBIS A. 2010. Crustal and mantle influences and U–Th–Ra disequilibrium in andesitic lavas of Ngauruhoe volcano, New Zealand. *Chemical Geology*, **277**, 355-373.

PUTIRKA K. D. 2008. Thermometers and barometers for volcanic systems. *Reviews in Mineralogy & Geochemistry*, **69**, 61-120.

PUTIRKA K. D., KUNTZ M. A., UNRUH D. M. & VAID N. 2009. Magma evolution and ascent at the Craters of the Moon and neighboring volcanic fields, Southern Idaho, USA: Implications for the evolution of polygenetic and monogenetic volcanic fields. *Journal of Petrology*, **50**, 1639-1665.

RACZEK I., JOCHUM K. P. & HOFMANN A. W. 2003. Neodymium and strontium isotope data for USGS reference materials BCR-1, BCR-2, BHVO-1, BHVO-

2, AGV-1, AGV-2, GSP-1, GSP-2 and eight MPI-DING reference glasses. *Geostandards Newsletter*, **27**, 173-179.

REINERS P. W. 2002. Temporal-compositional trends in intraplate basalt eruptions: Implications for mantle heterogeneity and melting processes. *Geochemistry, Geophysics, Geosystems (G^3)*, **3**.

RIGGS N. R. & DUFFIELD W. A. 2008. Record of complex scoria cone eruptive activity at Red Mountain, Arizona, USA, and implications for monogenetic mafic volcanoes. *Journal of Volcanology and Geothermal Research*, **178**, 763-776.

RITTER J. R. R., JORDAN M., CHRISTENSEN U. R. & ACHAUER U. 2001. A mantle plume below the Eifel volcanic fields, Germany. *Earth and Planetary Science Letters*, **186**, 7-14.

ROBINSON J. A. C. & WOOD B. J. 1998. The depth of the spinel to garnet transition at the peridotite solidus. *Earth and Planetary Science Letters*, **164**, 277-284.

ROEDER P. L. & EMSLIE R. F. 1970. Olivine-liquid equilibrium. *Contributions to Mineralogy and Petrology*, **29**, 275-289.

ROGGENSACK K., HERVIG R. L., MCKNIGHT S. B. & WILLIAMS S. N. 1997. Explosive Basaltic Volcanism from Cerro Negro Volcano: Influence of Volatiles on Eruptive Style. *Science*, **277**, 1639-1642.

ROLLINSON H. R. 1993. *Using Geochemical Data: Evaluation, Presentation, Interpretation.* Longman Group, Singapore, 352 pp.

RUBIN A. M. 1995. Propagation of magma-filled cracks. *Annual Review of Earth and Planetary Sciences*, **23**, 287-336.

RUTHERFORD M. J. 2008. Magma ascent rates. *Reviews in Mineralogy & Geochemistry*, **69**, 241-271.

SADEGHI H., SUZUKI S. & TAKENAKA H. 2000. Tomographic low-velocity anomalies in the uppermost mantle around the northeastern edge of Okinawa trough, the backarc of Kyushu. *Geophysical Research Letters*, **27**, 277-280.

SAKUYAMA T., OZAWA K., SUMINO H. & NAGAO K. 2009. Progressive melt extraction from upwelling mantle constrained by the Kita-Matsuura basalts in NW Kyushu, SW Japan. *Journal of Petrology*, **50**, 725-779.

SALTERS V. J. M. & LONGHI J. 1999. Trace element partitioning during the initial stages of melting beneath mid-ocean ridges. *Earth and Planetary Science Letters*, **166**, 15-30.

SATO H. 1977. Nickel content of basaltic magmas: identification of primary magmas and a measure of the degree of olivine fractionation. *Lithos*, **10**, 113-120.

SATO H., ARAMAKI S., KUSAKABE M., HIRABAYASHI J.-I., SANO Y., NOJIRI Y. & TCHOUA F. 1990. Geochemical difference of basalts between polygenetic and

monogenetic volcanoes in the central part of the Cameroon volcanic line. *Geochemical Journal*, **24**, 357-370.

SCHAAF P., STIMAC J., SIEBE C. & MACÍAS J. L. 2005. Geochemical evidence for mantle origin and crustal processes in volcanic rocks from Popocatépetl and surrounding monogenetic volcanoes, central Mexico. *Journal of Petrology*, **46**, 1243-1282.

SCHELLART W. P. 2007. North-eastward subduction followed by slab detachment to explain ophiolite obduction and Early Miocene volcanism in Northland, New Zealand. *Terra Nova*, **19**, 211-218.

SCHMINCKE H.-U. 2004. *Volcanism.* Springer, Berlin ; New York, 324 pp.

SENO T. & MARUYAMA S. 1984. Paleogeographic reconstruction and origin of the Philippine Sea. *Tectonophysics*, **102**, 53-84.

SHAW J. E., BAKER J. A., MENZIES M. A., THIRLWALL M. F. & IBRAHIM K. M. 2003. Petrogenesis of the Largest Intraplate Volcanic Field on the Arabian Plate (Jordan): a Mixed Lithosphere–Asthenosphere Source Activated by Lithospheric Extension. *Journal of Petrology*, **44**, 1657-1679.

SHIOMI K., SATO H., OBARA K. & OHTAKE M. 2004. Configuration of subducting Philippine Sea plate beneath southwest Japan revealed from receiver function analysis based on the multivariate autoregressive model. *Journal of Geophysical Research*, **109**, B04308.

SIBUET J.-C., HSU S. K., SHYU C. T. & LIU C. S. 1995. Structural and kinematic evolution of the Okinawa Trough Backarc Basin. *In:* Taylor B. (ed.). *Backarc Basins: Tectonics and Magmatism*. pp. 343-378. Plenum Press, New York.

SIBUET J.-C., LETOUZEY J., BARBIER F., CHARVET J., FOUCHER J.-P., HILDE T. W. C., KIMURA M., LING-YUN C., MARSSET B., MULLER C. & STÉPHAN J.-F. 1987. Back arc extension in the Okinawa Trough. *Journal of Geophysical Research*, **92**, 14041-14063.

SIEBE C., RODRÍGUEZ-LARA V., SCHAAF P. & ABRAMS M. 2004. Geochemistry, Sr-Nd isotope composition, and tectonic setting of Holocene Pelado, Guespalapa and Chichinautzin scoria cones, south of Mexico City. *Journal of Volcanology and Geothermal Research*, **130**, 197-226.

SINIGOI S., COMIN-CHIARAMONTI P., DEMARCHI G. & SIENA F. 1983. Differentiation of partial melts in the mantle: Evidence from the Balmuccia peridotite, Italy. *Contributions to Mineralogy and Petrology*, **82**, 351-359.

SMITH I. E. M., BLAKE S., WILSON C. J. N. & HOUGHTON B. F. 2008. Deep-seated fractionation during the rise of a small-volume basalt magma batch: Crater Hill, Auckland, New Zealand. *Contributions to Mineralogy and Petrology*, **155**, 511-527.

SMITH I. E. M., OKADA T., ITAYA T. & BLACK P. M. 1993. Age relationship and tectonic implications of the Cenozoic basaltic volcanism in Northland, New Zealand. *New Zealand Journal of Geology and Geophysics*, **36**, 385-393.

SOHN Y. K. 1996. Hydrovolcanic processes forming basaltic tuff rings and cones on Cheju Island, Korea. *Geological Society of America Bulletin*, **108**, 1199-1211.

SOHN Y. K. & CHOUGH S. K. 1989. Depositional processes of the Suwolbong tuff ring, Cheju Island (Korea). *Sedimentology*, **36**, 837-855.

SOHN Y. K. & CHOUGH S. K. 1992. The Ilchulbong tuff cone, Cheju Island, South Korea: depositional processes and evolution of an emergent, Surtseyan-type tuff cone. *Sedimentology*, **39**, 523-544.

SOHN Y. K. & CHOUGH S. K. 1993. The Udo tuff cone, Cheju Island, South Korea: transformation of pyroclastic fall into debris fall and grain flow on a steep volcanic cone slope. *Sedimentology*, **40**, 769-786.

SOHN Y. K., CRONIN S. J., BRENNA M., SMITH I. E. M., NÉMETH K., WHITE J. D. L., MURTAGH R. M., JEON Y. M. & KWON C. W. 2012. Ilchulbong tuff cone, Jeju Island, Korea, revisited: A compound monogenetic volcano involving multiple magma pulses, shifting vents, and discrete eruptive phases. *Geological Society of America Bulletin*, **124**, 259-274.

SOHN Y. K., PARK J. B., KHIM B. K., PARK K. H. & KOH G. W. 2002. Stratigraphy, petrochemistry and Quaternary depositional record of the Songaksan tuff ring, Jeju Island, Korea. *Journal of Volcanology and Geothermal Research*, **119**, 1-20.

SOHN Y. K. & PARK K. H. 2004. Early-stage volcanism and sedimentation of Jeju Island revealed by the Sagye borehole, SW Jeju Island, Korea. *Geosciences Journal*, **8**, 73-84.

SOHN Y. K. & PARK K. H. 2005. Composite tuff ring/cone complexes in Jeju Island, Korea: possible consequence of substrate collapse and vent migration. *Journal of Volcanology and Geothermal Research*, **141**, 157-175.

SOHN Y. K. & PARK K. H. 2007. *Phreatomagmatic volcanoes of Jeju Island, Korea. IAVCEI-CEV-CVS Field Workshop, Jeju Island, Korea, November 13-17, 2007*. Jeju Special Self-Governing Province, Jeju, Korea.

SOHN Y. K., PARK K. H. & YOON S. H. 2008. Primary versus secondary and subaerial versus submarine hydrovolcanic deposits in the subsurface of Jeju Island, Korea. *Sedimentology*, **55**, 899-924.

SOHN Y. K. & YOON S. H. 2010. Shallow-marine records of pyroclastic surges and fallouts over water in Jeju Island, Korea, and their stratigraphic implications. *Geology*, **38**, 763-766.

SPERA F. J. 1984. Carbon dioxide in petrogenesis III: role of volatiles in the ascent of alkaline magma with special reference to xenolith-bearing mafic lavas. *Contributions to Mineralogy and Petrology*, **88**, 217-232.

STONE R. 2010. Is China's riskiest volcano stirring or merely bidding its time? *Science*, **329**, 498-499.

STORMER J. C. J. & NICHOLLS J. 1978. XLFRAC: a program for the interactive testing of magmatic differentiation models. *Computers & Geosciences*, **4**, 143-159.

STRONG M. & WOLFF J. 2003. Compositional variations within scoria cones. *Geology*, **31**, 143-146.

SUDO M., UTO K., TATSUMI Y. & MATSUI K. 1998. K-Ar geochronology of a Quaternary monogenetic volcano group in Ojika Jima District, Southwest Japan. *Bulletin of Volcanology*, **60**, 171-186.

SUK B. C. 1989. Sedimentology and history of sea level changes in the East China Sea and adjacent seas. *In*: Taira A. & Masuda F. (eds). *Sedimentary Facies in the Active Plate Margin.* pp. 215-231. TERRAPUB, Tokyo.

SUN S. S. & MCDONOUGH W. F. 1989. Chemical and isotopic systematics of oceanic basalts: implications for mantle composition and processes. *In*: Saunders A. D. & Norry M. J. (eds). *Magmatism in the Ocean Basins.* pp. 313-345. Geological Society, London.

TAKADA A. 1994. The influence of regional stress and magmatic input on styles of monogenetic and polygenetic volcanism. *Journal of Geophysical Research*, **99**, 13563-13573.

TAKAHASHI E. & KUSHIRO I. 1983. Melting of a dry peridotite at high pressures and basalt magma genesis. *American Mineralogist*, **68**, 859-879.

TAKAHASHI E. & NAKAJIMA K. 2002. Melting process in the Hawaiian plume: an experimental study. *In*: Takahashi E. & Garcia M. (eds). *Hawaiian Volcanoes: Deep Underwater Perspectives.* pp. 403-418. American Geophysical Union.

TAMANYU S. 1990. The K-Ar ages and their stratigraphic interpretation of the Cheju Island volcanics, Korea. *Bulletin of the Geological Survey of Japan*, **41**, 527-537.

TANAKA T., TOGASHI S., KAMIOKA H., AMAKAWA H., KAGAMI H., HAMAMOTO T., YUHARA M., ORIHASHI Y., YONEDA S., SHIMIZU H., KUNIMARU T., TAKAHASHI K., YANAGI T., NAKANO T., FUJIMAKI H., SHINJO R., ASAHARA Y., TANIMIZU M. & DRAGUSANU C. 2000. JNdi-1: a neodymium isotopic reference in consistency with LaJolla neodymium. *Chemical Geology*, **168**, 279-281.

TATSUMI Y., SHUKUNO H., YOSHIKAWA M., CHANG Q., SATO K. & LEE M. W. 2005. The petrology and geochemistry of volcanic rocks on Jeju Island: plume magmatism along the Asian continental margin. *Journal of Petrology*, **46**, 523-553.

TIEPOLO M., BOTTAZZI P., FOLEY S. F., OBERTI R., VANNUCCI R. & ZANETTI A. 2001. Fractionation of Nb and Ta from Zr and Hf at mantle depths: the role of titanian pargasite and kaersutite. *Journal of Petrology*, **42**, 221-232.

TIMM C., HOERNLE K., WERNER R., HAUFF F., DEN BOGAARD P. V., WHITE J., MORTIMER N. & GARBE-SCHÖNBERG D. 2010. Temporal and geochemical evolution of the Cenozoic intraplate volcanism of Zealandia. *Earth-Science Reviews*, **98**, 38-64.

TOH H. & HONMA S. 2008. Mantle upwelling revealed by genetic algorithm inversion of the magnetovariational anomaly around Kyushu island, Japan. *Journal of Geophysical Research*, **113**, B10103.

TURNER M. B., CRONIN S. J., BEBBINGTON M. S., SMITH I. E. M. & STEWART R. B. 2011. Relating magma composition to eruption variability at andesitic volcanoes: A case study from Mount Taranaki, New Zealand. *Geological Society of America Bulletin*, **123**, 2005-2015.

UKAWA M. & TSUKAHARA H. 1996. Earthquake swarms and dike intrusions off the east coast of Izu Peninsula, central Japan. *Tectonophysics*, **253**, 285-303.

ULMER P. 1989. The dependence of the Fe^{2+}-Mg cation-partitioning between olivine and basaltic liquid on pressure, temperature and composition. *Contributions to Mineralogy and Petrology*, **101**, 261-273.

ULRICH B. & SCHMINCKE H.-U. 1990. Evolution of the Quaternary melilite-nephelinite Herchenberg volcano (East Eifel). *Bulletin of Volcanology*, **52**, 426-444.

VALENTINE G. A. & GREGG T. K. P. 2008. Continental basaltic volcanoes - Processes and problems. *Journal of Volcanology and Geothermal Research*, **177**, 857-873.

VALENTINE G. A. & HIRANO N. 2010. Mechanisms of low-flux intraplate volcanic fields-Basin and Range (North America) and northwest Pacific Ocean. *Geology*, **38**, 55-58.

VALENTINE G. A., KRIER D., PERRY F. V. & HEIKEN G. 2005. Scoria cone construction mechanisms, Lathrop Wells volcano, southern Nevada, USA. *Geology*, **33**, 629-632.

VALENTINE G. A., KRIER D. J., PERRY F. V. & HEIKEN G. 2007. Eruptive and geomorphic processes at the Lathrop Wells scoria cone volcano. *Journal of Volcanology and Geothermal Research*, **161**, 57-80.

VALENTINE G. A. & KROGH K. E. C. 2006. Emplacement of shallow dikes and sills beneath a small basaltic volcanic center - the role of pre-existing structure (Paiute Ridge, southern Nevada, USA). *Earth and Planetary Science Letters*, **246**, 217-230.

VALENTINE G. A. & PERRY F. V. 2006. Decreasing magmatic footprints of individual volcanoes in a waning basaltic field. *Geophysical Research Letters*, **33**, L14305.

VALENTINE G. A. & PERRY F. V. 2007. Tectonically controlled, time-predictable basaltic volcanism from a lithospheric mantle source (central Basin and Range Province, USA). *Earth and Planetary Science Letters*, **261**, 201-216.

VALENTINE G. A., PERRY F. V., KRIER D., KEATING G. N., KELLEY R. E. & COGBILL A. H. 2006. Small-volume basaltic volcanoes: Eruptive products and processes, and posteruptive geomorphic evolution in Crater Flat (Pleistocene), southern Nevada. *Geological Society of America Bulletin*, **118**, 1313-1330.

VANCE D. & THIRLWALL M. F. 2002. An assessment of mass discrimination in MC-ICPMS using Nd isotopes. *Chemical Geology*, **185**, 227-240.

VERNON R. H. 2004. *A practical guide to rock microstructure.* Cambridge University Press, New York, 594 pp.

VERWOERD W. J. & CHEVALLIER L. 1987. Contrasting types of surtseyan tuff cones on Marion and Prince Edward islands, southwest Indian Ocean. *Bulletin of Volcanology*, **49**, 399-417.

VIDAL-SOLANO J. R., DEMANT A., MORENO F. A. P., LAPIERRE H., ORTEGA-RIVERA M. A. & LEE J. K. W. 2008. Insights into the tectonomagmatic evolution of NW Mexico: Geochronology and geochemistry of the Miocene volcanic rocks from the Pinacate area, Sonora. *Geological Society of America Bulletin*, **120**, 691-708.

WALKER G. P. L. 1993. Basaltic-volcano systems. *In*: Prichard H. M., Alabaster T., Harris N. B. W. & Neary C. R. (eds). *Magmatic Processes and Plate Tectonics.* pp. 3-38. Geological Society, London.

WALTER M. J. 1998. Melting of garnet peridotite and the origin of komatiite and depleted lithosphere. *Journal of Petrology*, **39**, 29-60.

WALTER M. J. & PRESNALL D. C. 1994. Melting behavior of simplified lherzolite in the system CaO-MgO-Al_2O_3-SiO_2-Na_2O from 7 to 35 kbar. *Journal of Petrology*, **35**, 329-359.

WANG K., PLANK T., WALKER J. D. & SMITH E. I. 2002. A mantle melting profile across the Basin and Range, SW USA. *Journal of Geophysical Research*, **107**.

WATANABE S., WIDOM E., UI T., MIYAJI N. & ROBERTS A. M. 2006. The evolution of a chemically zoned magma chamber: The 1707 eruption of Fuji volcano, Japan. *Journal of Volcanology and Geothermal Research*, **152**, 1-19.

WATSON S. & MCKENZIE D. A. N. 1991. Melt Generation by Plumes: A Study of Hawaiian Volcanism. *Journal of Petrology*, **32**, 501-537.

WEAVER B. L. 1991. Trace element evidence for the origin of ocean-island basalts. *Geology*, **19**, 123-126.

WEI H., SPARKS R. S. J., LIU R., FAN Q., WANG Y., HONG H., ZHANG H., CHEN H., JIANG C., DONG J., ZHENG Y. & PAN Y. 2003. Three active volcanoes in China and their hazards. *Journal of Asian Earth Sciences*, **21**, 515-526.

WEI H., WANG Y., JIN J., GAO L., YUN S. H. & JIN B. 2007. Timescale and evolution of the intracontinental Tianchi volcanic shield and ignimbrite-forming eruptions, Changbaishan, Northeast China. *Lithos*, **96**, 315-324.

WEIS D., KIEFFER B., MAERSCHALK C., BARLING J., DE JONG J., WILLIAMS G. A., HANANO D., PRETORIUS W., MATTIELLI N., SCOATES J. S., GOOLAERTS A., FRIEDMAN R. M. & MAHONEY J. B. 2006. High-precision isotopic characterization of USGS reference materials by TIMS and MC-ICP-MS. *Geochemistry, Geophysics, Geosystems (G3)*, **7**, Q08006.

WHITE J. D. L. 1991. The depositional record of small, monogenetic volcanoes within terrestrial basins. *In*: Fisher R. V. & Smith G. A. (eds). *Sedimentation in Volcanic Settings*. pp. 155-171. Society for Sedimentary Geology, Tulsa USA.

WHITFORD-STARK J. L. 1983. Cenozoic volcanic and petrochemical provinces of mainland Asia. *Journal of Volcanology and Geothermal Research*, **19**, 193-222.

WILSON L. & HEAD III J. W. 1988. Nature of local magma storage zones and geometry of conduit systems below basaltic eruption sites: Pu'u 'O'o, Kilauea East Rift, Hawaii, Example. *Journal of Geophysical Research*, **93**, 14785-14792.

WILSON S.A. 1997. The collection, preparation, and testing of USGS reference material BCR-2, Columbia River, Basalt. *U.S. Geological Survey Open-File Report 98-xxx*.

WON J. H., LEE J. Y., KIM J. W. & KOH G. W. 2006. Groundwater occurrence on Jeju Island, Korea. *Hydrogeology Journal*, **14**, 532-547.

WON J. K., MATSUDA J.-I., NAGAO K., KIM K. H. & LEE M. W. 1986. Paleomagnetism and radiometric age of trachytes in Jeju Island, Korea. *Journal of the Korean Institute of Mining Geology*, **19**, 25-33.

WOO K. S. & KIM J. K. 2005. The age and constituents of the carbonate sand dunes in Hyeopjae area, Jeju Island: Implication for late Holocene sea level change. *Journal of the Geological Society of Korea*, **41**, 499-510.

WOOD B. J. 2004. Melting of fertile peridotite with variable amounts of H_2O. *Geophysical Monograph*, **150**, 69-80.

WOOD C. A. 1979 Monogenetic volcanoes of the terrestrial planets. Proceedings of the 10th Lunar Planetary Science Conference. pp. 2815-2840.

WOODHEAD J. D. 2002. A simple method for obtaining highly accurate Pb isotope data by MC-ICP-MS. *Journal of Analytical Atomic Spectroscopy*, **17**, 1-6.

WOODHEAD J. D. & HERGT J. M. 1997. Application of the 'double spike' technique to Pb-isotope geochronology. *Chemical Geology*, **138**, 311-321.

WÖRNER G., STAUDIGEL H. & ZINDLER A., 1985. Isotopic constraints on open system evolution of the Laacher See magma chamber (Eifel, West Germany). *Earth and Planetary Science Letters* **75**, 37-49.

WU J. P., MING Y. H., ZHANG H. R., LIU G. M., FANG L. H., SU W. & WANG W. L. 2007. Earthquake swarm activity in Changbaishan Tianchi volcano. *Chinese Journal of Geophysics*, **50**, 938-946.

XIE S. P., HAFNER J., TANIMOTO Y., LIU W. T., TOKINAGA H. & XU H. 2002. Bathymetric effect on the winter sea surface temperature and climate of the Yellow and East China Seas. *Geophysical Research Letters*, **29**.

XU W. L., GAO S., YANG D. B., PEI F. P. & WANG Q. H. 2009. Geochemistry of eclogite xenoliths in Mesozoic adakitic rocks from Xuzhou-Suzhou area in central China and their tectonic implications. *Lithos*, **107**, 269-280.

YAMAMOTO T., SOYA T., SUTO S., UTO K., TAKADA A., SAKAGUCHI K. & ONO K. 1991. The 1989 submarine eruption off eastern Izu Peninsula, Japan: ejecta and eruption mechanisms. *Bulletin of Volcanology*, **53**, 301-308.

YANG K. H. 2004. Fluid inclusions trapped in xenoliths from the lower crust/upper mantle beneath Jeju Island (I): A preliminary study. *Journal of the Petrological Society of Korea*, **13**, 34-45.

YANG K., ARAI S., YU J. E., YUN S. H., KIM J. S. & HWANG J. Y., 2012. Gabbroic xenoliths and megacrysts in the Pleisto-Holocene alkali basalts from Jeju Island, South Korea: The implications for metasomatism of the lower continental crust. *Lithos*, **142-143**, 201-215.

YANG K., HIDAS K., FALUS G., SZABÓ C., NAM B., KOVÁCS I. & HWANG B. 2010. Relation between mantle shear zone deformation and metasomatism in spinel peridotite xenoliths of Jeju Island (South Korea): Evidence from olivine CPO and trace elements. *Journal of Geodynamics*, **50**, 424-440.

YI S., YUN H. & YOON S. 1998. Calcareous nannoplankton from the Seoguipo Formation of Cheju Island, Korea and its paleoceanographic implications. *Paleontological Research*, **2**, 253-265.

YOKOYAMA I. & DE LA CRUZ-REYNA S. 1990. Precursory earthquakes of the 1943 eruption of Paricutin volcano, Michoacan, Mexico. *Journal of Volcanology and Geothermal Research*, **44**, 265-281.

YOO H. J., HERRMANN R. B., CHO K. H. & LEE K. 2007. Imaging the three-dimensional crust of the Korean Peninsula by joint inversion of surface-wave dispersion and teleseismic receiver functions. *Bulletin of the Seismological Society of America*, **97**, 1002-1011.

YOON S. H., LEE B. G. & SOHN Y. K. 2006. Geomorphic and geological characteristics and eruption process of the Hanon volcano, Jeju Island. *Journal of the Geological Society of Korea*, **42**, 19-30.

YOSHIZAWA K., MIYAKE K. & YOMOGIDA K. 2010. 3D mantle sstructure beneath Japan and its surrounding region from inter-station dispersion measurements of surface waves. *Physics of the Earth and Planetary Interiors*, **183**, 4-19.

YU J., YANG K., HWANG B. & LEE S. 2009. Textural and geochemical implications of spinel-peridotite xenoliths(Type I) in basaltic rocks from Jeju Island, South Korea. *Eos Transactions AGU, Fall Meeting Supplement*, **90(52)**, Abstract V13A-1998.

YU J., YANG K. & KIM J. 2010. Textural and geochemical characteristics and their relation of spinel peridotite xenoliths from Jeju Island. *Journal of the Petrological Society of Korea*, **19**, 227-244.

YUN S. H., KOH J. S. & ANH J. Y. 1998. A study of the spinel-lherzolite xenolith in the alkali basalt from eastern Cheju Island, Korea. *Economic and Environmental Geology*, **31**, 447-458.

ZELLMER G. F. & ANNEN C. 2008. An introduction to magma dynamics. *In*: Annen C. & Zellmer G. F. (eds). *Dynamics of Crustal Magma Transfer, Storage and Differentiation.* pp. 1-13. Geological Society Special Publications 304, London.

ZENG L., LIANG F., CHEN Z., LIU F. & XU Z. 2009. Metamorphic garnet pyroxenite from the 540-600 m main borehole of the Chinese Continental Scientific Drilling (CCSD) project. *Tectonophysics*, **475**, 396-412.

ZHAO D. 2004. Global tomographic images of mantle plumes and subducting slabs: insight into deep Earth dynamics. *Physics of the Earth and Planetary Interiors*, **146**, 3-34.

ZHANG M., SUDDABY P., THOMPSON R. N., THIRLWALL M. F. & MENZIES M. A. 1995. Potassic volcanic rocks in NE China: Geochemical constraints on mantle source and magma genesis. *Journal of Petrology*, **36**, 1275-1303.

ZHI X., SONG Y., FREY F. A., FENG J. & ZHAI M. 1990. Geochemistry of Hannuoba basalts, eastern China: Constraints on the origin of continental alkalic and tholeiitic basalt. *Chemical Geology*, **88**, 1-33.

ZINDLER A. & HART S. R. 1986. Chemical geodynamics. *Annual Review of Earth and Planetary Sciences*, **14**, 493-571.

ZONENSHAIN L. P. & SAVOSTIN L. A. 1981. Geodynamics of the Baikal rift zone and plate tectonics of Asia. *Tectonophysics*, **76**, 1-45.

ZOU H., FAN Q. & YAO Y. 2008. U-Th systematics of dispersed young volcanoes in NE China: Asthenosphere upwelling caused by piling up and upward thickening of stagnant Pacific slab. *Chemical Geology*, **255**, 134-142.

List of Appendices

Electronic Appendices (on CD)

Chapter 3

Appendix A: Article "Brenna *et al.* (2010), Contributions to Mineralogy and Petrology 160, 931-950."

Appendix B: Supplementary Data File to article "Brenna *et al.* (2010), Contributions to Mineralogy and Petrology 160, 931-950."

Chapter 4

Appendix C: Article "Brenna *et al.* (2011), Terra Nova 23, 70-75."

Appendix D: Supplementary Data File to article "Brenna *et al.* (2011), Terra Nova 23, 70-75."

Appendix E: Article "Sohn *et al.* (2012), GSA Bulletin 124, 259-274."

Appendix F: Whole rock selected major and trace elements and detailed location of sampled sites for the Songaksan, Suwolbong and Ilchulbong eruptions.

Chapter 5

Appendix G: Article "Brenna *et al.* (2012), Journal of Petrology 53, 985-1018."

Appendix H: Supplementary Data File to article "Brenna *et al.* (2012), Journal of Petrology 53, 985-1018." Sample locations.

Appendix I: Supplementary Data File to article "Brenna *et al.* (2012), Journal of Petrology 53, 985-1018." Whole rock major and trace element compositions.

Chapter 6

Appendix J: Article "Brenna *et al.* (2012), Lithos 148, 337-352."

Appendix K: Supplementary Data File to article "Brenna *et al.* (2012), Lithos 148, 337-352." Core locations, descriptions and sampling depths.

Appendix L: Supplementary Data File to article "Brenna *et al.* (2012), Lithos 148, 337-352." Whole rock major and trace element compositions.

Appendix M: Supplementary Data File to article "Brenna *et al.* (2012), Lithos 148, 337-352." Dates dataset.

Appendix N: Electron Microprobe mineral data.

Appendix O: XRF raw data